Sodium channels and plasticity in cerebellar networks

Markus Martijn de Ruiter

Printed by PrintPartners Ipskamp BV, Enschede.

The cover shows an elephant fish (*Gnathonemus petersii*) swimming between the dendrites of central lobe Purkinje cells in the mormyrid cerebellum.

Sodium channels and plasticity in cerebellar networks

Natriumkanalen en plasticiteit in cerebellaire netwerken

Proefschrift

ter verkrijging van de graad van doctor aan de
Erasmus Universiteit Rotterdam
op gezag van de rector magnificus
Prof.dr. S.W.J. Lamberts
en volgens besluit van het College voor Promoties

De openbare verdediging zal plaatsvinden op
woensdag 29 maart 2006 om 15:45 uur

door

Markus Martijn de Ruiter

geboren te ’s-Gravenzande

Promotiecommissie

Promotor:	Prof.dr. C.I. de Zeeuw
Overige leden:	Prof.dr. P.A.E. Sillevis Smitt Prof.dr. M.A. Frens Dr. T.J.H. Ruigrok
Copromotor:	Dr. C.R.W. Hansel

Luister naar raad,
laat je onderwijzen,
uiteindelijk maakt het je wijs.

Spreuken 19, vers 20

Heer ik kom tot U,
neem mijn hart, verander mij,
als ik U ontmoet vind ik rust bij U.

Opwekking 488

Voor Ralda en Meine

Table of contents

Chapter 1

General introduction

1.1 General role of the cerebellum

The general structure of the cerebellum - the inputs it receives, its output, and the important role the cerebellum plays in fine-tuning movements and posture - have fascinated investigators for centuries. The first accurate drawings of cerebellar gross anatomy were made by Vieussens in 1684. The first book devoted solely to the cerebellum was published in 1776 by M.V.G. Malacarne, and the principal cell type was named by Jan Purkyne in 1837. Our current knowledge suggests that the cerebellum controls the motor system by analyzing differences between intention and action, and by adjusting the actions of motor centers in the spinal cord and cerebral cortex accordingly. The oculomotor system, which is under cerebellar control, comprises an example of a system that works according to these principles. Lesion studies, performed on the cerebella of different species, have been shown to cause inaccuracy of movement in space and time, balance problems, reduced muscle tone and impaired motor learning (Luciani, 1915; Perrett et al., 1993; Rolando, 1809; Rolando, 1823), but sensory threshold, and strength of muscle contraction, remain unaffected, indicating that the cerebellum modulates rather than generates movements.

Structurally, the cerebellum is highly organized, with its cortex consisting of repeating units that form basic circuit modules, with similar functions, throughout the mammalian cerebellar cortex (Eccles, 1967). Even though the entire cerebellar cortex computes information in a similar way (Marr, 1969), the cerebellum can be divided into several distinct regions that receive projections from different portions of the brain and spinal cord, and then project to different motor systems (Groenewegen and Voogd, 1977; Groenewegen et al., 1979; Voogd et al., 1981). Taking the role of the cerebellum in producing accurate and smooth movements into account, it has been suggested that the cerebellum is capable of learning (Flourens, 1842; Luciano, 1891). Further understanding of cerebellar connectivity allowed researchers to begin pinpointing the circuitry and mechanisms underlying cerebellar learning. There are strong indications for a role of the cerebellum in the recalibration and adaptive adjustment of movements, learning of motor skills and associative learning (Houk et al., 1996; Raymond et al., 1996; Thach, 1996). These forms of motor learning are possible through modifications in the strength of synaptic transmission in the cerebellar circuit modules, providing the neuronal basis for information storage (Carey and Lisberger, 2002; Ito, 2001; Raymond et al., 1996). More recent discoveries, however, also implicate the cerebellum in the planning of movements and even non-motor cognitive functions (Petrosini et al., 2003; Schmahmann, 1998; Thach, 1996).

Diseases of the human cerebellum fall into three main categories: hypotonia, ataxia and intention tremors. Hypotonia refers to a diminished resistance to passive limb displacements. An example of hypotonia is seen in testing the knee reflex of cerebellar patients where the legs often oscillate multiple times before coming to rest. Ataxia is described as an abnormality in the execution of a voluntary movement, resulting in a delay in the initiation of the movement and overshooting the target at the end of the movement. Intention tremors are tremors that become exaggerated when the limb is directed towards a particular target. Therefore, cerebellar diseases do not necessarily result in paralysis, as often seen after lesions in other motor systems, but rather in difficulties in fine tuning and timing of movements.

1.2 Anatomy of cerebellar and cerebellum-like structures

1.2.1 Rat cerebellum

The mammalian cerebellum occupies about one tenth of the cranial cavity. At first glance the large degree of folding of the cerebellar cortex is striking (Bijlani et al., 1980; Henery and Mayhew, 1989; Korneliussen, 1968; Voogd, 1967). Transverse folds in the cerebellar cortex are formed by two deep and numerous shallower fissures, subdividing the cerebellum into lobes, lobules and folia (Armstrong et al., 1973). Most of the Purkinje cells in the cortex contact three deep cerebellar nuclei (DCN) which are subdivided in the fastigial, the interposed and the dentate nuclei. While most of the cerebellar output flows through these nuclei, the Purkinje cell axons leaving the flocculonodular lobe, and some vermal Purkinje cell axons, are an exception, as these axons contact the vestibular nuclei in the brainstem directly. A single Purkinje cell is thought to contact about 30-50 deep cerebellar nucleus cells and one DCN cell receives input from 20-30 Purkinje neurons (Chan-Palay, 1977). The deep cerebellar and the vestibular nuclei in turn project to motor areas in the cerebral cortex, and the brainstem (Rand, 1954; Sastry et al., 1997).

The cerebellum can be grossly divided into three, functionally-distinct, regions. The spinocerebellum, consisting of the vermis (due to its worm-like appearance), the intermediate hemispheres and the cerebellar lateral hemispheres (the cerebrocerebellum), and the phylogenically oldest part of the cerebellum, the vestibulocerebellum or flocculonodular lobe (Gravel and Hawkes, 1990; Groenewegen and Voogd, 1977; Groenewegen et al., 1979; Voogd and Glickstein, 1998). These areas all project to different deep nuclei and from there to distinct descending systems. The spinocerebellum, for instance, projects to the fastigial nucleus and from there to the cortical and brainstem regions, giving rise to the medial descending systems, controlling proximal muscles. Regulating body and limb movements is the primary task of the spinocerebellum and its input originates mainly from somatosensory receptors. The spinocerebellum was first shown to contain two inverted somatotopic maps of the body in the early 1940s by Adrian and Snider (Adrian, 1943; Snider and Stowell, 1944). The lateral part of both hemispheres, or cerebrocerebellum, projects to motor and premotor areas of the cerebral cortex involved in planning of voluntary movements. The vestibulocerebellum is involved in regulating balance and eye movements. It receives input from the vestibular sensory organs and the visual system. The vestibulocerebellum mainly controls the axial muscles and limb extensors controlling balance and to the vestibular nucleus that controls eye movements. From this division, and on the basis of cerebellar phylogeny it is clear that the vermis is involved in basic cerebellar functions seen in many species whereas the processing of “higher” cerebellar functions such as planning of movement is done in the later evolved, and in humans relatively large, hemispheres (Brooks and Thach, 1981; Gilman, 1985; Keele and Ivry, 1990; Thach, 1996; Thach et al., 1992).

Despite its relatively small size, the cerebellum contains more neurons than the whole cerebral cortex (Korbo et al., 1993). Of the seven cell types found in the mammalian cerebellar cortex (i.e. Purkinje cells, granule cells, brush cells, Golgi cells, stellate cells, basket cells and Lugaro cells) granule cells are the most abundant, estimated at about one trillion cells (10^{11}). The cerebellar cortex, which

contains the somata of all these neurons, is a relatively simple three-layered structure (Figure 1). The axons of the granule cells, the Purkinje cell dendrites and the basket and stellate cells together form the outer layer, known as molecular layer. The Purkinje cell somata form the second layer, and the third layer is called the granule cell layer, containing all the small somata of the granule cells. These layers together form the gray matter. The collateral forming axons of the sole cortical output, the Purkinje cells, leave the gray matter of the cortex to form, together with the climbing fiber and mossy fiber axons, the cerebellar white matter (for review see Ghez and Thach, 2000).

The Purkinje neurons in the rat cerebellar cortex have large (25-30 μm) somata that are arranged in a single layer (Figure 1) (Marr et al., 1969). Their extensively branched dendritic trees are completely flat (6 μm) in the sagittal plane but in the transverse plane they have a span of 250 μm. The spiny dendrites extend into the molecular layer up to the pial surface. Their inhibitory axons synapse onto the deep cerebellar and vestibular nuclei and use γ-aminobutyric acid (GABA) as neurotransmitter (Ito, 1984).

The activity of the Purkinje neurons is affected by two excitatory afferent inputs coming from outside the cerebellum and by the cerebellar inhibitory interneurons. The two excitatory inputs come from the climbing fibers arising from the inferior olive, and from mossy fibers, coming from several nuclei in the brainstem and from neurons in the spinal cord. The mossy fibers do not contact the Purkinje neurons directly but through synapses with granule cells (Bower and Woolston, 1983; Jaeger and Bower, 1994; Gundappa-Sulur et al., 1999; Shinoda et al., 2000). One climbing fiber contacts about 10 Purkinje cells but each Purkinje cell (in the adult animal) is only contacted by one climbing fiber. The climbing fiber innervates the primary dendrites of Purkinje neurons but climbing fibers have been reported to run along the primary dendrite quite far into the molecular layer, overlapping to a large degree with the parallel fiber input that runs throughout the molecular layer in the transverse plane (Figure 1). Climbing fibers give rise to collaterals that contact Golgi cells in the granular layer. Parallel fibers arise from the granule cell axon. The granule cell axon is initially called the ascending axon. The ascending axon may contact the dendrites of the overlying Purkinje cell numerous times, before it bifurcates into opposite directions in the molecular layer. From the bifurcation onward the granule cell axons are called parallel fibers. Parallel fibers make contact with 300 - 1000 Purkinje neurons as they travel for several millimeters through the transverse plane of the cerebellar cortex. Each Purkinje cell is contacted by approximately 200,000 parallel fibers. Each parallel fiber makes only one or two synaptic contacts with an individual Purkinje cell, however; each granule cell in turn collects information from multiple mossy fiber rosettes. The terminals of the climbing fibers (Ruigrok 2003, Voogd et al., 1996) and the Purkinje cell axons (Chan-Palay, 1977; De Zeeuw et al., 1994) are arranged topographically, which is in contrast to the large convergence and divergence found in the mossy fiber - granule cell system.

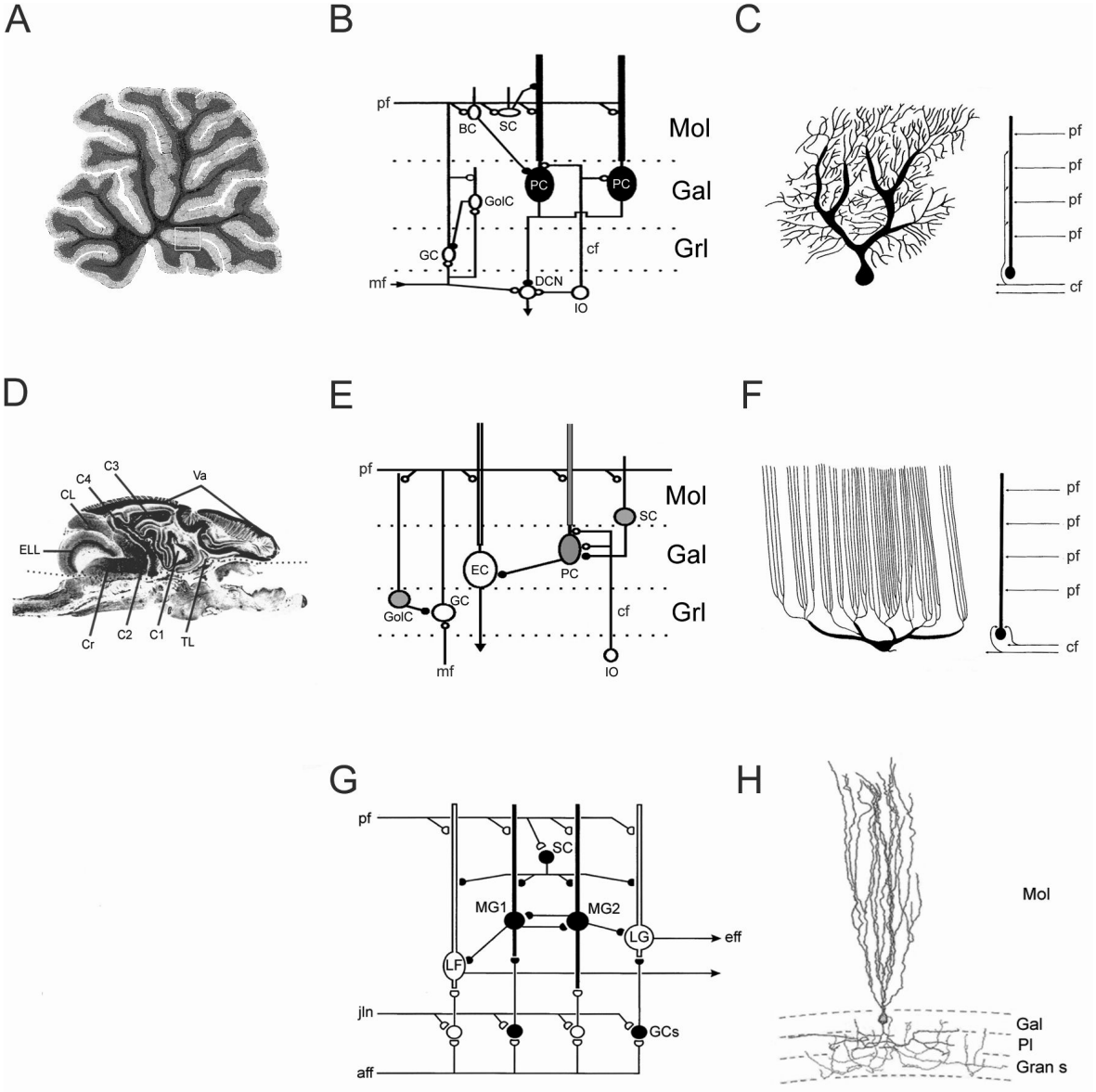

Figure 1: Anatomy of the mammalian cerebellum, the mormyrid central lobes and the mormyrid ELL. **A:** Sagittal slice through the vermis of the rat cerebellum. **B:** Organization of the mammalian cerebellar cortex. **C:** Mammalian Purkinje neuron with in thick black the innervation pattern of the climbing fiber. The diagram depicts the innervation patterns of the climbing fiber and parallel fibers. Note the large overlap of these fibers in the mammalian cerebellum. **D:** Sagittal slice through roughly the midline of the brain of *Gnathonemus petersii*. **E:** Organization of the mormyrid central lobes. **F:** Mormyrid central lobe Purkinje neuron with in thick black the innervation pattern of the climbing fiber. The diagram depicts the innervation patterns of the climbing fiber and parallel fibers. Note the larger distance between these innervations compared to panel C and the long parallel dendrites. **G:** Organization of the mormyrid ELL. **H:** MG cell in the mormyrid ELL. Note the extensive axonal branching and the long straight dendrites. pf: parallel fiber, mf: mossy fiber, cf: climbing fiber, GC: granule cell, BC: basket cell, SC: stellate cell, GolC: Golgi cell, PC: Purkinje cell, DCN: deep cerebellar nucleus, IO: inferior olive, Mol: molecular layer, Gal: ganglionic layer, Grl: granular layer, ELL: electrosensory lateral line lobe, C1-C4: central lobe zones 1-4, Va: valvula, Cr: crista cerebellaris, TL: lobus transitorius, CL: caudal lobe, EC: efferent cell, LF: large fusiform cell, MG: medium ganglionic cell, LG: large ganglionic cell, eff: efferent fibers, aff: afferent fibers, jnl: juxtalobar nucleus, PL: plexiform layer, Gran s: superficial granular layer. *(Adapted from: Meek, 1992 (panels C and F); Nieuwenhuys and Nicholson, 1967(panel D); Han et al., 1999 (panels G and H); Han and Bell, 2003 (panel E)).*

The inhibitory input to Purkinje neurons is exerted by three types of inhibitory interneurons, namely stellate, basket and Golgi cells. Stellate and basket cells receive excitatory inputs from parallel fiber bundles. The short axons of the stellate cells contact nearby Purkinje cell dendrites whereas the much longer axons of the basket cells contact Purkinje neurons some distance away from the active parallel fiber bundle. This system is designed to inhibit the Purkinje neurons around the active parallel fiber bundle. Golgi cells, with their large dendritic trees in the molecular layer, receive input from parallel fibers, and shorten the duration of bursts in the parallel fiber system by innervating the granule cell dendrites directly at the mossy fiber glomeruli (for review see Ghez and Thach, 2000).

1.2.2 Mormyrid cerebellar central lobes

The mormyrid cerebellum differs strikingly from the mammalian cerebellum in several ways. It is phylogenetically also much older. The mormyrid brain was first described by Szabo in 1959 (Szabo, 1959) in the mormyrid fish Gymnarchus niloticus. The family of mormyroidea consists of a large group of freshwater fishes endemic to Africa. This large family comprises more than 200 species placed in 19 genera. Mormyrid fish belong to the ancient teleost order of osteoglossiformes. They all have electric organs, electroreceptors and a greatly enlarged cerebellum. In general, they are found in river systems throughout the African continent, but are most diverse in the river systems of Central and West-Africa. The subspecies that we studied, *Gnathonemus petersii*, is mostly found in the Central African Republic and was first described in 1862 by Gill and Günther. The discovery that these fish produce and sense weak electric signals was made in 1951. Mormyrids are often used as models for electrogenesis, electroreception and electrocommunication (Sullivan et. al., 2000). The mormyrid cerebellum is the relatively largest cerebellum found in vertebrate animals. The whole mormyrid brain has a brain to body weight ratio of 1:50, comparable with the human brain. Whereas the mammalian cerebellum encompasses about 10% of the total brain mass, the mormyrid cerebellum encompasses about 55% of the brain (Bell and Szabo, 1986; Meek et al., 1986b; Szabo, 1983).

The mormyrid cerebellum can be divided into two regions, the corpus cerebelli (or central lobes) and the valvula cerebelli (Figure 1). The valvula cerebelli can be divided further into the valvula cerebelli lobus lateralis and the valvula cerebelli lobus intermedius (Nieuwenhuys and Nicholson, 1967). The valvula cerebelli is not found in other vertebrates, and consist of a cerebellar protrusion in the midbrain ventricle (Finger, 1983; Nieuwenhuys, 1967). The size of the cerebellar valvula differs greatly among different members of the mormyrid family. The size of the central lobes, on the other hand, is rather consistent within this family. The central lobes more closely resemble the mammalian cerebellum and are differentiated into four lobes numbered C1-C4 (Meek et al., 1986a; Meek and Nieuwenhuys, 1991; Nieuwenhuys and Nicholson, 1969 Nieuwenhuys et al., 1974). Even though some parts of the valvula and central lobes are involved in electroreceptive and electromotor function (Finger et al., 1981) most parts are not and therefore the functional significance of the mormyrid “gigantocerebellum” is still largely unknown (Meek and Nieuwenhuys, 1991; Nieuwenhuys and Nicholson, 1969).

The mormyrid cerebellum closely resembles the mammalian cerebellum as described above, in that it contains granule cells, Purkinje cells, Golgi cells and stellate cells, mossy fibers, parallel fibers and climbing fibers, all arranged grossly the same way (Brochu et al., 1990; Finger, 1978; Finger, 1983; Kaiserman-Abramof et al., 1969; Nieuwenhuys, 1976; Nieuwenhuys et al., 1974). It also contains several differences: as mentioned above, the mormyrid cerebellum contains valvula which are lacking in mammalian cerebella. Mormyrid fish lack DCN, and project onto so-called eurydendroid cells located within the Purkinje cell layer (Figure 1) (Meek and Nieuwenhuys, 1991). Since the Purkinje neurons do not project outside the cerebellum they are considered to be interneurons with short axons contacting the eurydendroid cells and neighbouring Purkinje cells. Mormyrid Purkinje cells have also been shown to project onto themselves. Teleost fish, in contrast to mammals, possess a precerebellar nucleus lateralis valvula. This nucleus gives rise to massive mossy fiber input to the valvula and the central lobes. The mormyrid Purkinje neurons show a unique pattern of dendritic branching compared to mammalian Purkinje cells (Meek and Nieuwenhuys, 1991). The mormyrids smooth proximal dendrites, running in the ganglionic layer, branch only a few times before sending up their branches straight to the pial surface, without further branching and highly parallel to each other and the dendritic trees of neighboring Purkinje cells (Figure 1). This specialization might serve to receive and integrate parallel fiber input better. The “climbing” fiber inputs to these Purkinje cells do not really climb but are restricted to the smooth proximal dendrites and do not run up the dendritic tree all the way into the molecular layer as seen in mammals (Figure 1). This restriction to the proximal dendrites can also be found in developing mammalian Purkinje cells, suggesting a primitive climbing fiber input to the mormyrid Purkinje cell. Mormyrid Purkinje cells moreover do not receive a single climbing fiber but often receive multiple climbing fiber innervations, similar as found in developing mammalian Purkinje cells.

The larger spatial separation between parallel and climbing fibers thus occurring in the mormyrid cerebellum can have a large impact on signal integration in the Purkinje cell. The length and diameter as well as the number of synaptic contacts of parallel fibers in the mormyrid cerebellum are significantly smaller than in mammals. Also the size of the granule cell somata is smaller. The fact that the integrative properties of the granule cell parallel fiber pathway are smaller than in mammals can be explained by the existence of the precerebellar nucleus lateralis valvula. This large preprocessing station for mossy fiber input is thought to partly take over both convergent and divergent integrative functions from the granule cells (Meek and Nieuwenhuys, 1991). Taken together, Meek and Nieuwenhuys (1991) argued that the mormyrid Purkinje cell is specialized for receiving and integrating parallel fiber input, whereas the mammalian Purkinje cell is specialized to analyze climbing fiber input.

1.2.3 Mormyrid Electrosensory Lateral line Lobe (ELL)

The electrosensory lobe of weakly electric mormyrid fish, such as *Gnathonemus petersii*, is located between the caudal lobe and the crista cerebellaris (Figure 1). It forms a large portion of the caudal third of the mormyrid brain and has a cerebellum-like organization. The ELL receives input from the primary afferent fibers from electroreceptors in the skin and is therefore the first stage in the central processing of

electrosensory information (Bell et al., 2005). The primary afferent fibers carry information in the form of a single spike provoked by each electric organ discharge (EOD) produced by the fish itself or by fish in its proximity (Denizot et al., 1987). EOD signals are altered by nearby objects, creating an electrical image of the world on the body of the fish. Electrosensory localization is used to navigate, find prey and to avoid predators in the dark (Sawtell et al., 2005). Fish can distinguish between their own EODs and information sent by other fish, and from echoes received from objects by blocking afferent electrosensory impulses with concomitantly occurring EODs in the nucleus of the ELL (nELL) (Denizot et al., 1987). The ELL of mormyrid fish has been extensively studied since the late 1970s. It forms an excellent model to study vertebrate sensory system descending input processing, which, to date, remains poorly understood. Descending input allows sensory systems to function flexibly and adaptively by altering neural responses based on sensory contexts, ongoing motor actions and past experience. The study of mormyrid ELL has contributed greatly towards understanding the role of descending inputs in adapting sensory processing (Chacron et al., 2003; Bell et al., 1992a,b; Bell, 2001).

The ELL of *Gnathonemus petersii* is located at the hind part of the fish's brain. It consists of a cortex and a nucleus. The cerebellum-like cortex contains three anatomically and functionally-distinct regions: the medial, dorsolateral and ventrolateral zones. Primary afferent fibers from the electroreceptors in the skin terminate somatotopically in these zones and in the nELL (Bell et al., 2005). The nELL receives input from electroreceptors called knollenorgans. These receptors respond to EODs from other fish. Ampullary receptors are involved in processing low-frequency external voltage sources. They are thus used for passive electrolocation and project to the ventrolateral zone. A third class of electroreceptors found in the skin of mormyrid fish are called mormyromast electroreceptors. These receptors are used during active electrolocation and project to the medial and dorsolateral zone of the ELL's cortex (Bell et al., 2005; Bell and Szabo, 1986; Meek et al., 1999).

The ELL's cortex consists of six distinctive layers: the deep fiber layer, intermediate layer, granular layer, plexiform layer, ganglionic layer and molecular layer (Bell et al., 2005; Bell and Szabo, 1986; Meek et al., 1999). Both afferent (to ELL) and efferent fibers (from ELL to higher centers) can be found in the deep fiber layer. The intermediate layer contains the cell bodies and proximal dendrites of large multipolar interneurons. The granular layer, in which the primary afferents terminate, contains, as the name suggests, many small granular cells as well as some larger cells. The granular layer can be divided into deep and superficial layers. Granular cells in the deep layer are larger and less densely packed than granular cells in the superficial layer. The larger granular cells are the efferent large fusiform cells (Grant et al., 1996), projecting to the mesencephalon and the medium fusiform cells which are GABAergic interneurons (Bell et al., 2005). The plexiform layer contains the cell bodies of superficial large fusiform cells and the ganglionic layer contains the prominent and larger cell bodies of the large ganglion cells, medium ganglion cells, and thick smooth dendrite cells. The medium ganglion cells are Purkinje-like GABAergic cells that terminate locally on the three different types of efferent cells (Figure 1) (Meek et al., 1996; Han et al., 1999). The molecular layer contains the dendritic trees of all cells mentioned above except for those from the large multipolar interneurons and the small granular cells. The major input to the molecular layer is formed by parallel fibers arising from granule cells located in the eminentia granularis

posterior and fibers to the deep molecular layer form the preeminential nucleus. Bell and colleagues (2005) have recently shown four types of cells in the ELL that were previously undiscovered. They found small ganglionic cells located in the ganglionic layer. Small multipolar plexiform cells located in the superficial granular layer and the plexiform layer, small fusiform cells located in the intermediate layer and the deep granular layer and small multipolar granular cells located in the granular layer. They also described the dendritic arborisation of the already known small granular cells (Bell et al., 2005).

1.3 Spike activity

1.3.1 Rat cerebellar Purkinje neurons

As mentioned in paragraph 1.1, the cerebellum plays an important role in fine-tuning movements and posture by analyzing differences between intention and action, and by adjusting the actions of motor centers in the spinal cord and cerebral cortex. The only way the cerebellar cortex can accomplish these tasks is by changing the output of the Purkinje neurons. In this paragraph, the physiology of two characteristic types of cerebellar spikes, namely simple spikes (SS) and complex spikes (CS), will be discussed. These spikes are both generated by the sole output of the cerebellum, the Purkinje cell. The main focus of this paragraph will be on the complex spike.

Simple spikes (Figure 2) are highly regular, synaptically-evoked action potentials, fired by Purkinje cells during parallel fiber stimulation at high frequency (well beyond 200 Hz) (Häusser and Clark, 1997; Raman and Bean, 1999; Roth and Häusser, 2001). Parallel fiber input, and thus simple spike firing patterns, are thought to convey the conditioned stimulus in simple learning paradigms such as eye-blink conditioning. Learning is assumed to take place at the parallel fiber-Purkinje cell synapse. Simple spike firing patterns are not only influenced by excitatory parallel fiber input but also by inhibitory input from basket and stellate interneurons and excitatory climbing fiber input. The firing of simple spikes is mediated by sodium, calcium and potassium currents (Llinas and Sugimori, 1980b; Raman and Bean, 1997). Upon parallel fiber activity vesicles filled with glutamate fuse with the cell membrane of the presynaptic terminal and enter the synaptic cleft. Glutamate then binds to AMPA receptors located at the dendritic spines of Purkinje cells. AMPA receptors are ionotropic glutamate receptors permeable to sodium. The resulting sodium influx depolarizes the cell membrane. Sodium currents flowing through voltage-gated, tetrodotoxin (TTX) sensitive sodium channels further depolarize the Purkinje cell membrane until it reaches spike threshold, leading to the initiation of a simple spike. The high amount of positively-charged ions flowing across the membrane sufficiently depolarizes the Purkinje cell, leading to the activation of voltage-gated potassium channels. High-voltage activated P-type calcium channels also begin to flux calcium currents. Calcium influx activates calcium-sensitive potassium channels. Together with the current flowing through voltage-gated potassium channels, these currents through calcium-sensitive potassium channels repolarize the cell to its resting potential (Jacquin and Gruol, 1999).

Subtreshold parallel fiber stimulation in voltage-clamp mode enables us to record so-called AMPA receptor-mediated excitatory postsynaptic currents (EPSCs). Parallel

fiber EPSCs, when evoked within a short time interval (10-100 ms), show paired-pulse facilitation (PPF). PPF can be explained by the fact that residual calcium ions left in the presynaptic terminal after the first EPSC has been evoked, facilitates more glutamate release upon the second PF stimulation. The postsynaptic AMPA receptors are not easily saturated and thus show a larger response to the large amount of glutamate released upon the second stimulation (Eccles et al., 1967; Konnerth et al., 1990). Alternatively, PPF can be explained by the recruitment of more parallel fiber terminals upon the second stimulus. An increase in the parallel fiber $[Ca^{2+}]_i$ after the second stimulus on top of the subthreshold $[Ca^{2+}]_i$ increase after the first stimulus can reach the threshold for glutamate release and thus recruits more fibers.

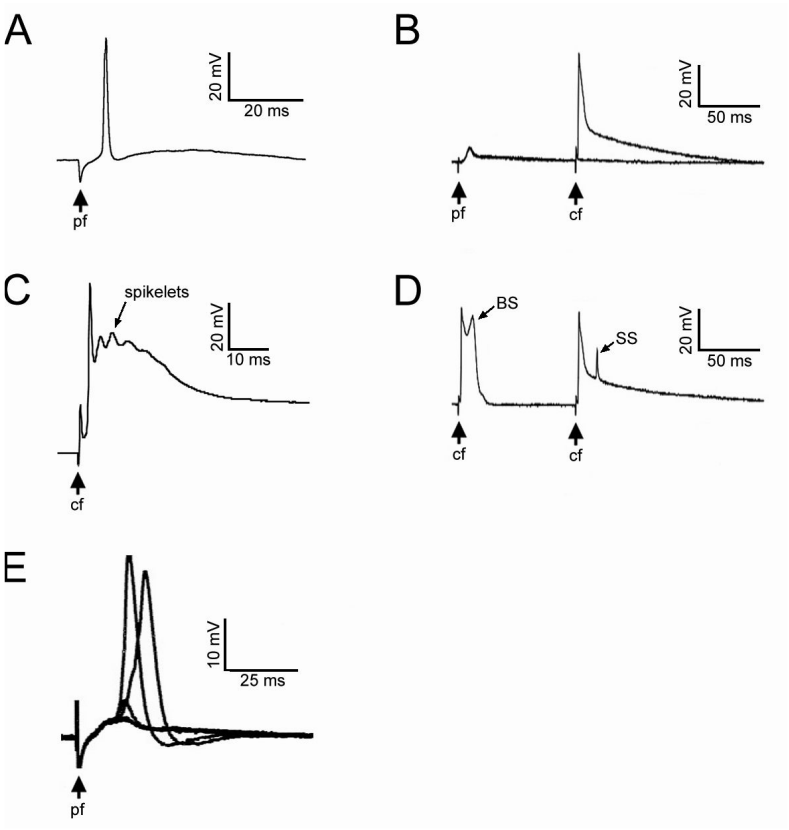

Figure 2: Spike forms elicited after parallel or climbing fiber stimulation in the rat cerebellum, mormyrid central lobes, and mormyrid ELL. **A:** Simple spike elicited by parallel fiber stimulation in a rat Purkinje neuron. **B:** Parallel fiber response and climbing fiber response as recorded from a mormyrid central lobe Purkinje cell. **C:** Climbing fiber stimulation elicits a complex spike in rat cerebellar Purkinje cells. Note the small spikelets on top of the depolarization plateau. **D:** Two additional climbing fiber response patterns that can be recorded from mormyrid central lobe Purkinje cells. On top of the climbing fiber EPSP shown in panel B the left climbing fiber response in panel D shows a secondary spike at the top of the primary EPSP. This climbing fiber response is named broad spike (BS). The right climbing fiber response in panel D shows an EPSP as in panel B but in the repolarization phase an additional small spike (SS) is fired. Sometimes there are multiple small spikes following the initial EPSP. **E:** Several broad spikes elicited in medium ganglion cells from the mormyrid ELL during parallel fiber stimulation have been overlaid *(Adapted from: Han and Bell, 2003 (panels B and D); Grant et al., 1998 (panel E)).*

Complex spikes (Figure 2) (Thach, 1967) are multi-component spikes typically fired by Purkinje neurons upon olivary neuron / climbing fiber activation. Complex spikes are initiated by a large spike, followed by a plateau potential with multiple spikelets riding on top of the plateau. The climbing fiber input, and thus complex spike firing patterns, is thought to convey the unconditioned stimulus (error signal) in simple learning paradigms such as eye-blink conditioning and is often assumed to play a teaching role in learning. As previously mentioned, although each Purkinje neuron receives input from only one climbing fiber, this single fiber makes around 1500 synaptic contacts (Strata et al., 1997; Dittman and Regehr, 1998). This results in a very powerful synaptic contact which, upon activation, produces an all-or-none electrical event that overrides all other synaptic inputs (Eccles et al., 1964). The average spontaneous firing frequency of inferior olivary neurons, and thus climbing fibers, is around 1 Hz. Climbing fiber activity, however, can reach frequencies of up to 10 Hz for short periods of time (Goossens et al., 2001; Simpson et al., 1996). When a climbing fiber is activated the released glutamate binds to postsynaptic AMPA and metabotropic glutamate receptors. The opening of these ligand-gated ion channels causes local excitatory postsynaptic potentials (EPSPs) to occur in the primary dendrites contacted by the climbing fiber. The large number of simultaneously-activated contacts causes a widespread depolarization of the proximal dendrites. This depolarization reaches the threshold for the activation of voltage-sensitive Ca^{2+} conductances (Llinas and Sugimori, 1980b). Experimental data clearly shows the importance of Ca^{2+} currents flowing through P/Q- and T-type voltage-dependant calcium channels for this stage of complex spike formation (for review see Schmolesky et al., 2002). The large depolarization of the dendritic tree now spreads to the soma of the Purkinje cell. The first complex spike component, the fast sodium spike, is likely to be generated in the axon hillock upon depolarization of the soma (Stuart and Häusser, 1994). The fast sodium spike is conducted by fast-inactivating sodium currents. The nature of the currents underlying the plateau potential that follows the initial spike are harder to determine. It is well accepted that the depolarization plateau is caused by Ca^{2+} and non-inactivating Na^{+} currents but the currents underlying the plateau spikelets are still under debate. Calcium currents seem to be the most likely candidate but resurgent sodium currents have been suggested as well. A combination of both currents cannot be excluded. The afterhyperpolarization following the complex spike is generated by K^{+} conductances. The K^{+} channels responsible for complex spike afterhyperpolarization are still under investigation but slow SK channels form a good candidate (Schmolesky et al., 2002).

The anatomy of the dendritic tree plays a major role in the integration of signals originating from the dendrites. The way dendritic architecture shapes the calcium and sodium conductances making up the complex spike recorded in the soma remains largely unclear. Recent and future developments in computer models of Purkinje cell spike firing may give us a better insight into this complex system (De Schutter and Bower, 1994a,b; Jaeger et al., 1997). Climbing fiber EPSCs recorded in voltage-clamp mode, in contrast to PF EPSCs, show paired-pulse depression (PPD) when stimulation takes place within a short time interval. Depression of the second EPSC compared to the first can be attributed to the fact that the climbing fiber has such a potent release machinery (release probability close to 1). The first stimulation thus leads to a depletion of the releasable vesicle pool. Consequentially, the second stimulation of the CF releases less glutamate from the CF terminal, leading to a smaller EPSC.

1.3.2 Mormyrid central lobe Purkinje neurons

One of the most striking differences between rat and mormyrid Purkinje cells is their dendritic tree morphologies. As previously mentioned, the dendrites of mormyrid Purkinje cells branch very proximally, and then run straight to the pial surface. The integration of dendritic signals will thus be completely different in these fish compared to rats. It is possible that this morphological difference leads to differences in spike characteristics. We cannot assume that the same conductances underlie the spike firing patterns recorded from both mormyrid and rat Purkinje cells. Another remarkable feature of the mormyrid brain is the relatively large distance between climbing fiber and parallel fiber innervation sites and the localization of the climbing fiber input that differs greatly from that found in higher vertebrates. These differences in innervation will also undoubtedly lead to differences in spike properties. Studying the differences and similarities between rat and mormyrid Purkinje cell physiology may lead to a better understanding of cerebellar circuitry in general.

The first electrophysiological recordings from the somata of Purkinje cells in the cerebellar central lobes of *Gnathonemus petersii* showed three distinctive spike types upon current injection: a small, narrow sodium spike; a large, broad sodium spike and a large, broad calcium spike (Han and Bell, 2003). Even though the physiology of the mormyrid central lobes differs substantially from that of the mammalian cerebellum, there are also a lot of similarities. For instance, paired-pulse stimulation of the parallel fibers in voltage-clamp mode leads to PPF of the postsynaptic EPSCs. Paired-pulse stimulation of the CF leads, just like in the mammalian cerebellum to paired-pulse depression (PPD) of the CF EPSCs recorded. The neurotransmitters and receptors involved (glutamate and AMPA) are also identical in both species (Han and Bell, 2003). This suggests that the basic synaptic transmission and presynaptic release properties are similar in both mormyrids and mammals. This leaves the postsynaptic Purkinje cell responsible for most of the physiological differences observed between these species.

Upon parallel fiber stimulation under whole-cell current-clamp mode, mormyrid central lobe Purkinje cells respond with an AMPA-mediated EPSP (Figure 2). Using sharp electrodes, an inhibitory post-synaptic potential (IPSP) can be recorded following the initial EPSP. This IPSP can be blocked using bicuculline, a $GABA_A$ receptor blocker, suggesting that the IPSP originates from either stellate cells or other Purkinje cells (Han and Bell, 2003). The parallel fiber responses recorded in mormyrid Purkinje cells thus closely resemble simple spikes recorded in mammalian Purkinje cells. Climbing fiber stimulation in the mormyrid cerebellum evokes an all-or-none EPSP (Figure 2). This response shows two distinct phases: a large initial phase lasting about 10 ms followed by a second phase that consists of a slow return to baseline lasting around 100 ms (Han and Bell, 2003). Two other variants of the basic climbing fiber response can be recorded from mormyrid Purkinje cells: a so-called “broad spike” which has a second spike component following the peak of the initial large EPSP, and a “small spike” which shows one or more spikelets in the slow return phase of the climbing fiber response. Han and Bell (2003) hypothesized that the slow decay of the climbing fiber response can be due to a slow passive decay of the capacitive charge build-up during the synaptic response in the vast dendritic tree of the mormyrid Purkinje cell. They based this hypothesis on the fact that current

injections showed similar decay kinetics in the mormyrid Purkinje cell (Han and Bell, 2003).

The differences in climbing fiber responses recorded in mammalian and mormyrid Purkinje cells could be caused by the different climbing fiber innervation patterns in these animals. In mormyrids the climbing fiber only innervates the most proximal parts of the primary dendrites whereas in mammals the climbing fiber runs up high in the dendritic tree. It is suggested that the large synaptic current into the soma and proximal dendrites results in a passive charging of the dendritic membranes in the molecular layer not reached by the climbing fiber. In mammals, this large current build-up can be discharged immediately through the synaptic and voltage-gated conductance changes caused by the climbing fiber (Han and Bell, 2003). The role played by the different dendritic branching patterns observed between species in forming the climbing fiber response recorded at the soma is currently unclear. Differences in the expression patterns of sodium and calcium channels in the dendrites and somata of Purkinje cells could also play a significant role in shaping the climbing fiber response.

1.3.3 Mormyrid ELL

Medium Ganglionic (MG) cells, which are the ELL's equivalent of Purkinje cells, show one characteristic spike elicited upon parallel fiber activity. This so-called "broad spike" (Figure 2) consists of a single EPSP that lasts for up to 15 ms in vivo. The location where broad spikes originate from (either the MG soma or the distal dendrites) and their propagation and dendritic integration are still debated. Broad spikes can be evoked in vivo by either corollary discharge input or electrosensory input. Repetitive generation of broad spikes, for instance as might happen when the fish uses high-speed electromotor scanning of the environment, has been associated in vivo with spike timing-dependant plasticity (Gomez et al., 2005).

1.3.4 Dendritic spike propagation in Purkinje-(like) cells

Over a century ago, Ramón y Cajal (1904) speculated on the directional flow of signals in neurites, and the propagation of action potentials within the dendritic tree remains a subject of great interest to many researchers. Under most conditions, the sodium action potential constitutes the main output signal of the neuron, and is generated in the axon and retrogradely invades the dendritic tree. This process is known as backpropagation. Action potentials can also be initiated in the dendrites under intense synaptic stimulation. The spread of these action potentials towards the soma is known as forward propagation. Understanding action potential propagation in dendrites is crucial for the understanding of the integration of synaptic input and the induction of some forms of synaptic gain change. Whereas backpropagation of spikes in mammalian Purkinje cells is very limited and even actively dampened (Martina et al., 2003; Llinas and Sugimori, 1980; Stuart and Häusser, 1994) there is a growing body of evidence from numerous cell types, like the mormyrid ELL MG cells (Gomez et al., 2005), that spikes can backpropagate far into the dendritic tree. In a range from limited, passive backpropagation, to active strengthening of backpropagation this phenomenon is thought to aid in long-term potentiation or

depression of the active synapses involved (Llinas and Nicholson, 1971; Regehr et al., 1992; Stuart and Sakmann, 1994; Golding et al., 2002). Differences in spike propagation between neurons can be explained by differences in the density of dendritic voltage-gated channels. This theory, in which different cell types with different spiking patterns all have a unique “fingerprint” of voltage-gated ion channels expressed in different gradients throughout their dendritic tree, has been investigated in many different cell types (Magee et al., 1998; Stuart et al., 1997). Using a model Häusser and colleagues showed that different cell types with differently shaped dendritic trees continue to backpropagate action potentials differently even when the exact same set of passive and active parameters concerning the ion channels have been inserted for each cell type (Vetter et al., 2001). These experiments show that both the architecture of the dendritic tree and the differential distribution and expression of voltage-gated ion channels can be very important for spike propagation, spike integration, and the induction of synaptic plasticity.

The Purkinje cells and Purkinje-like cells described in this thesis exhibit very different dendritic structures and spike forms. They thus form an interesting basis to study questions regarding spike integration and propagation. One of the questions concerning spike activity addressed here is whether the completely different dendritic branching patterns we observe can explain the differences in the climbing fiber responses described between rat cerebellar and mormyrid central lobe Purkinje cells (chapter 2). Another central question concerns how sodium spikes backpropagate in the mormyrid ELL, and in what way they are shaped by potassium currents (chapter 3). The effects that small differences in climbing fiber responses may have on cerebellar spike output are also addressed (chapter 4 and 6).

1.4 Synaptic plasticity

The cerebellum is involved in motor learning and fine-tuning of the learned motor skills (discussed in paragraph 1.1). Learning something new is impossible without storing the new information. But how do Purkinje neurons store new information? Where do they store it? How do they know what to store and what to neglect? How do they forget the learned skill again when it is no longer necessary? Storage of information in neurons starts with changes in the synaptic connectivity with other neurons. Synapses can be made stronger (potentiated) or weaker (depressed). New synapses can be formed or depressed synapses can be deleted. In this way, the whole network of connections can be altered. In order to understand how the cerebellum accomplishes these feats, we first must look at cerebellar connections, and specifically which connections are plastic and can thus be altered.

At a systems level, the inputs to the cerebellum carry extensive internal feedback information about goals, commands and programming of movement, as well as external feedback information associated with the execution of movement, thereby allowing the cerebellum to compare the intended movement with the reported actual movement. The cerebellar circuitry is essentially composed of a relay station in the deep cerebellar and vestibular nuclei (DCN and VN) and a cortical “side loop”. Cerebellar output to premotor centers originates from the DCN and VN and is driven by direct excitatory input from the mossy fibers. The DCN and VN output is modulated by the inhibitory input from Purkinje cell axons, which convey the

computations and interactions in the Purkinje cell. Two types of excitatory input innervate the Purkinje cells in the cerebellar side loop. They receive input from the mossy fiber/parallel fiber system and from the inferior olivary/climbing fiber system. The Purkinje neuron provides the only output of the cerebellar cortex. The mossy fiber system transmits sensory information from the periphery, and cerebral cortical information, to the DCN and the Purkinje cells. The inferior olive is thought to convey an error signal to the Purkinje cell via the climbing fiber. In this small and simplified circuit there are several synapses between different cell types that all have been shown to be plastic (Ito et al., 1982; Ekerot and Kano, 1985; Bear and Linden, 2000; Hansel et al., 2001). The plasticity of the cerebellar cortex is particularly interesting since it is designed to change the output of the DCN in a way that is analogous to classical conditioning, with the parallel fibers conveying the conditioned stimulus (CS), the climbing fiber an unconditioned stimulus (US) and a depression of the parallel fiber-Purkinje cell synapse giving rise to a conditioned response (CR) via disinhibition of the DCN. In a behavioural context, associative eyeblink conditioning is a perfect example for cerebellar learning. Before training, an airpuff to the eye (US) gives rise to an immediate reflexive blink, which is the unconditioned response (UR). During training, a neutral stimulus such as a tone (CS) is paired with the airpuff stimulation so that the tone onset precedes the airpuff and the two stimuli co-terminate. As the association is acquired, a carefully-timed eyelid response is performed (CR), the onset of which shortly precedes the airpuff. In well-trained animals, populations of cells in the DCN begin to fire during the CS-US interval. This firing is predictive of and correlated with the performance of the CR. The relatively simple wiring of the cerebellar cortex makes it a suitable candidate to study plasticity. This paragraph will therefore focus on the plasticity of parallel fiber-Purkinje cell and climbing fiber-Purkinje cell synapses.

1.4.1 Parallel fiber to Purkinje cell synapse

Modifications of parallel fiber to Purkinje cell synapses (Figure 3) are believed to be crucial for certain forms of cerebellar motor learning (Marr, 1969; Albus, 1971; Ito 1972). One way to study parallel fiber activity-induced Purkinje cell plasticity at a cellular level is to investigate long-term changes in parallel fiber EPSCs induced by tetanic stimulation.

Two forms of postsynaptic plasticity have been described at the parallel fiber-Purkinje cell synapse, namely parallel fiber long-term depression (PF-LTD) and parallel fiber long-term potentiation (PF-LTP). Electrophysiologically, these effects can be recorded as a reduction or increase in the parallel fiber EPSC amplitude recorded under voltage-clamp in whole-cell patch-clamp experiments. In slices or in situ, PF-LTD is typically induced by pairing parallel fiber and climbing fiber stimulation at low frequencies. This paired stimulation results in an attenuation of the parallel fiber-Purkinje cell synapse, typically to about 50-80% of its baseline synaptic strength (Ito et al., 1982; Ekerot and Kano, 1985; Wang et al., 2000). The most appropriate timing interval between parallel fiber and climbing fiber stimulation for the induction of PF-LTD is still under debate (Bear and Linden, 2000; Raymond and Lisberger, 1998; Wang et al., 2000).

Three initial signals are required for PF-LTD induction: activation of AMPA and metabotropic glutamate I receptors (mGluR1) by glutamate released from the parallel fiber, and depolarization of the Purkinje cell by climbing fiber stimulation or intra-somatic current injection. The massive influx of calcium ions upon depolarisation of the Purkinje cell membrane caused by the climbing fiber input, and the additional calcium influx in the dendrites and from intracellular inositol 1,4,5-triphosphate (IP_3)-mediated calcium stores, causes a supralinear calcium influx. This large calcium signal is crucial for PF-LTD induction (Coesmans et al., 2004). The second messenger 1,2-diacylglycerol (DAG), which is produced in a cascade following mGluR1 receptor activation, together with the high calcium concentration reached, activates protein kinase C (PKC), which is thought to underlie the final pathway for expression of PF-LTD. Inhibition of PKC blocks PF-LTD induction, whereas exogenous PKC activation induces PF-LTD (Linden and Connor, 1991). The phosphorylation of AMPA receptor subunits by PKC induces an internalisation cascade. Fewer AMPA receptors are thus available in the parallel fiber-Purkinje cell synapse, and the response of the Purkinje cell to parallel fiber stimulation is reduced (Wang and Linden, 2000).

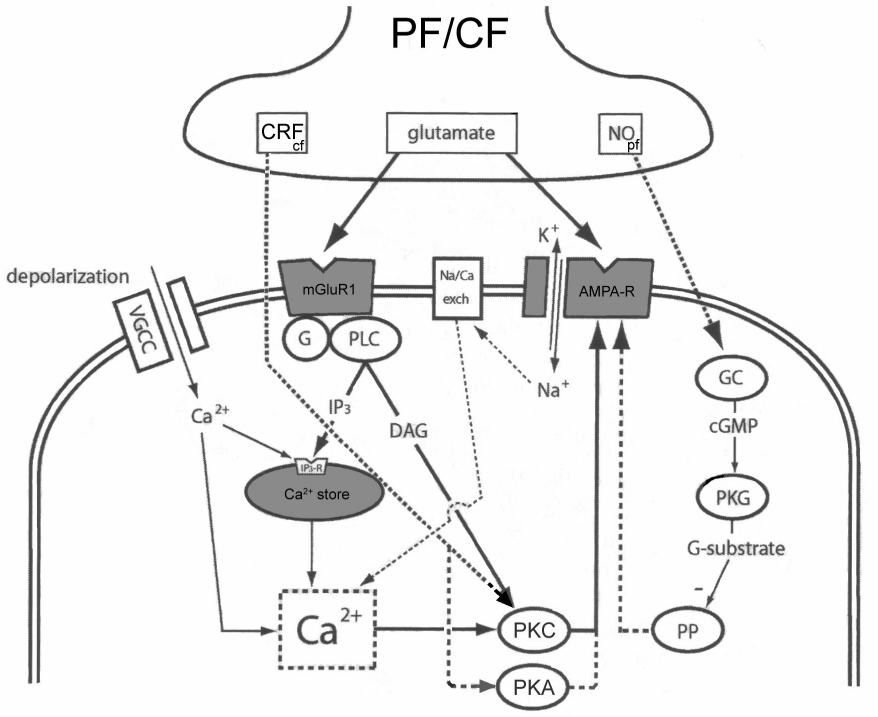

Figure 3: Model of the parallel and climbing fiber to Purkinje cell synapse. Phosphorylation of the AMPA receptor by PKC and its subsequent internalisation leads to a reduction of synaptic strength. Well-established mechanisms are indicated with solid lines whereas other suggested pathways are indicated using dotted lines. CRF: corticotropin releasing factor, NO: nitric oxide, VGCC: voltage-gated sodium channels, mGluR1: metabotropic glutamate receptor type 1, AMPA-R: AMPA receptor, G: G protein, PLC: phospholipase C, IP3: inositol 1,4,5-triphosphate, DAG: 1,2-diacylglycerol, PKC: protein kinase C, PKA: protein kinase A, PKG: protein kinase G, GC: guanylyl cyclase, PP: phosphatase, c-GMP: cyclic guanyl monophosphate, CF: climbing fiber, PF: parallel fiber. *(Adapted from Coesmans, Cerebellar Plasticity in Health and Disease, PhD thesis, Rotterdam 2004).*

Parallel fiber-Purkinje cell synapses cannot only be depressed, but can also be potentiated. The first anecdotal observations of PF-LTP were made during PF-LTD studies (Sakurai, 1987; Crepel and Jaillard, 1991). This form of LTP proved to be presynaptic and can be induced by stimulating the parallel fibers 120 times at 4-8 Hz (Salin et al., 1996). In addition, a more recently discovered postsynaptic form of PF-LTP has been described. This form of LTP is induced by stimulating the parallel fiber alone at low frequency for a prolonged period of time (Lev-Ram et al., 2002; 2003; Coesmans et al., 2004). Although the molecular pathways underlying postsynaptic PF-LTP have been shown to be different from those underlying presynaptic PF-LTP (Lev-Ram et al., 2002), they remain to be characterized in detail. The main difference between PF-LTD and postsynaptic PF-LTP initial phase induction seems to be the large amount of calcium ions entering the cell upon climbing fiber stimulation. Coesmans and colleagues argued that the climbing fiber plays the role of a switch in the induction of parallel fiber postsynaptic plasticity, with a low calcium threshold for LTP and a high calcium threshold for LTD (Coesmans et al., 2004).

In the mormyrid ELL, in vitro pairing of parallel fiber EPSPs with postsynaptic broad action potentials has revealed a spike-timing dependant, anti-Hebbian plasticity rule: when the postsynaptic broad spike occurred within a window up to 60-80 ms following the presynaptic activation, the response to parallel fiber input became depressed, whereas when a postsynaptic spike was evoked at other delays, the synaptic response was frequently potentiated (Bell et al., 1997, 1999; Grant et al., 1996; Han et al., 2000). The underlying mechanism is thought to rely upon backpropagation of the broad spike into the distal dendrites (Grant et al., 1998).

1.4.2 Climbing fiber to Purkinje cell synapse

Until recently, the powerful climbing fiber input to Purkinje cells was thought to be functionally invariant in adult animals. This widespread assumption results from the role of the climbing fiber in coding for the unconditioned stimulus (error signal) in reflex conditioning pathways, the high release probability at climbing fiber terminals, the all-or-none character of the postsynaptic responses, the large postsynaptic depolarisation that accompanies complex spikes, and the firing frequencies that complex spikes can attain (Eccles et al., 1967). Climbing fibers, however, do show a form of developmental plasticity in the first three weeks of postnatal life. After an initial innervation of each Purkinje cell by several climbing fibers, an activity-dependant elimination of surplus climbing fibers occurs until a single Purkinje cell is contacted by a single climbing fiber, typical for the adult cerebellum (Crepel et al., 1976). Interestingly, mutant mice that lack components of an mGluR1 signalling pathway, and transgenic mice which express a PKC inhibitor peptide, show persistent multiple climbing fiber innervation in adult life (Kano et al., 1995; Levenes et al., 1997).

The synapses between a climbing fiber and a Purkinje cell (Figure 3) contain a comparable, and thus potentially modifiable, molecular machinery as seen at the parallel fiber-Purkinje cell synapse. Their synapses also contain AMPA and mGluR1 receptors, voltage-gated calcium channels and PKC. Since the role the climbing fiber plays in the balance between parallel fiber LTD and LTP has been recently elucidated (Lev-Ram et al., 2002; 2003; Coesmans et al., 2004), the modifiability of

synaptic strength at the climbing fiber-Purkinje cell synapse has grown more interesting. Variant climbing fiber synaptic strength immensely increases the range of effects it can have on parallel fiber plasticity. An alternative, but less supported, hypothesis still worth noting is that, in contrast to weakening or strengthening parallel fiber synapses, the climbing fiber is used as a timing device for motor coordination (reviewed by Simpson et al., 1996). Hansel and Linden (2000) found that stimulation of the climbing fiber alone at 5 Hz for 30 seconds leads to climbing fiber long-term depression (CF-LTD) of approximately 20% measured at the climbing fiber EPSC level. They also noted that the later complex spike components, the so-called small spikes, were reduced in size; this finding was especially evident for the second small spike (Hansel and Linden, 2000; Weber et al., 2003). CF-LTD could also be associated with long-term changes in potassium currents. The slow afterhyperpolarizing (AHP) potassium current, which underlies the tail of the complex spike, was shown to be reduced after CF-LTD induction (Schmolesky et al., 2002). Changes in the afterhyperpolarization can be crucial for cerebellar function since they are associated with the complex spike pause in simple spike firing (Schmolesky et al., 2002). It is unclear whether LTD of the EPSCs is the sole factor underlying the alteration of the complex spike. It is possible that tetanization of the climbing fiber also produces sustained alterations in the intrinsic excitability of the Purkinje neuron, as has been previously observed in cerebellar deep nuclear neurons (Hansel and Linden, 2000; Aizenman and Linden, 2000). CF-LTD does not spread to neighbouring parallel fiber synapses, is saturated after repeated tetanization, and does not show a change in paired-pulse ratio, suggesting a postsynaptic expression site (Hansel and Linden, 2000; Shen et al., 2002). Similar to PF-LTD, CF-LTD depends on an increase in postsynaptic calcium concentration, the activation of mGluR1, and PKC (Hansel and Linden, 2000; Weber et al., 2003). CF-LTD might alter the probability of complex spike firing and/or the subsequent climbing fiber pause at the systems level by altering Purkinje neuron throughput. CF-LTD can also influence cerebellar network function through modulation of dendritic integration and heterosynaptic processes. Attenuation of the climbing fiber-evoked calcium transient, an important consequence of CF-LTD, might serve as a neuroprotective mechanism to attenuate calcium-triggered neurodegenerative events. Such a mechanism, as previously suggested for PF-LTD (De Schutter, 1995), is potentially more relevant for the climbing fiber which imposes a much larger calcium load on the Purkinje neuron (Hansel and Linden, 2000).

Besides the long-term depression first decribed by Hansel and Linden, there are also different forms of short-term plasticity expressed at the climbing fiber-Purkinje cell synapse or in the climbing fiber response. For example, activity of the inhibitory interneurons in the cerebellar cortex has been shown to reduce climbing fiber-evoked calcium signals in the dendrites of Purkinje cells by up to 90% (Callaway et al., 1995; Eccles et al., 1966). These reductions in dendritic calcium transients have been noted to reduce late complex spike components in some cases but not in others. The climbing fiber-Purkinje cell synapse has a very high release probability. This high release probability results in PPD of the climbing fiber-evoked EPSC upon repeated stimulation with an interpulse interval of up to 5 s (Konnerth et al., 1990). PPD is a consequence of a reduction in transmitter release. At interpulse intervals of up to 1 s, the second complex spike has been shown to express a reduced number of spikelets (Hashimoto and Kano, 1998). It is thus possible that the complex spike waveform changes continuously as a function of discharge frequency. In addition to AMPA

receptors, mGluRs have been suggested to participate in electrogenesis resulting from synaptic activity. mGluRs have been shown to elicit a transient inward current followed by an outward current (Vranesic et al., 1993). Purkinje cell excitability is transiently increased through activation of phospholipase C after mGluR1 activation (Netzeband et al., 1997). It is now known that mGluR1 activation changes Purkinje cell excitability through actions on transient receptor potential (TRP) family calcium channels. Local dendritic potassium conductances almost certainly influence dendritic complex spike components. Using intracellular and imaging techniques, potassium currents were shown to modify the amplitude of dendritic calcium spikes, as well as the spatial spread of calcium spike-associated calcium increases in the dendrites (Midtgaard et al., 1993).

Recent studies have investigated the effects of diverse neuromodulators on climbing fiber-evoked calcium transients. Whereas carbachol, serotonin, noradrenaline and dopamine had no effect on calcium transients, corticotropin releasing factor (CRF) caused a drastic reduction in the complex spike AHP (Pisani and Ross, 1999; Fox and Gruol, 1993; Miyata et al., 1999). Light and electron microscopy revealed an extremely dense CRF label in inferior olive neurons and climbing fibers (Palkovits et al., 1987; Tian and Bishop, 2003). Evidence suggests that CRF is released by climbing fibers in an activity-dependant manner (Barmack and Young, 1990; Tian and Bishop, 2003) and may alter Purkinje cell spike activity. Climbing fiber-dependant release of CRF is also required for the induction of LTD at the parallel fiber-Purkinje cell synapse (Miyata et al., 1999). In light of their common synaptic machinery, CRF release potentially plays a role in regulating activity and plasticity at the climbing fiber-Purkinje cell synapse as well (Schmolesky et al., 2002).

Aside from fine-tuning plasticity at the parallel fiber-Purkinje cell synapse, CF-LTD can play a direct role in changing the spike output of the Purkinje cell. Changes in the AHP can lead to differences in the complex spike pause, and a reduction in the slow complex spike components can potentially lead to differences in action potential firing patterns (Schmolesky et al., 2002) since it has been shown that the different complex spike components are capable of triggering individual action potentials in the Purkinje cell axon (Ito and Simpson, 1971). The climbing fiber-Purkinje cell synapse is an unusual synapse, as it does not primarily serve to change local synaptic input weight and spike output, but to influence significantly both dendritic calcium signalling and dendritic integration.

This thesis addresses plasticity at the climbing fiber-Purkinje cell synapse, the parallel fiber-MG cell synapse, and plasticity in the oculomotor system. We investigate whether CRF application has an effect on the basic synaptic transmission, and the induction of LTD at the climbing fiber-Purkinje cell synapse. The possible cellular pathways involved are also discussed (chapter 4). Chapter 3 discusses anti-Hebbian plasticity at the parallel fiber-MG cell synapse in the mormyrid ELL. The question here is whether GABA released from the MG cell dendrites is required for the induction of this form of associative plasticity. In chapter 5 we investigate whether the oculomotor system is capable of plastic changes compensating for the loss of gravitational information it normally receives from the otolith organs.

1.5 Sodium conductances in Purkinje-(like) cells

As described above, Purkinje cells of mormyrid fish and rats differ markedly from each other in both their anatomy and physiology. Since our knowledge about the ionic currents underlying the climbing fiber responses in rats and mormyrids is currently limited, it is very difficult to pinpoint these differences to either morphology or to the expression and/or distribution of ion channels and currents. The initial EPSP of the mormyrid climbing fiber response differs in both amplitude and duration from the sodium spike observed after climbing fiber stimulation in the rat cerebellum. Together with the suggestion that the later complex spike components in rat Purkinje cells may have resurgent sodium currents underlying them, and the observation of low amplitude sodium spikes that sometimes follow the climbing fiber response in mormyrid fish, a detailed description of Purkinje cell sodium channel expression and the currents carried by these channels in both species is highly warranted.

1.5.1 Voltage-gated sodium channels

Voltage-gated sodium channels consist of an α-subunit, which has the size of about 260 kDa, and one or more β-subunits (Catterall et al., 2002). The α-subunit forms the channel pore and possesses all the main properties of the channel, such as voltage-dependant gating and sodium selectivity. The β-subunits are capable of changing the channel kinetics as well as the voltage dependence of inactivation (Isom et al., 1995a+b). The α-subunits are organized in four homologous domains (I-IV), which each contain six transmembrane α-helices (S1-S6) and an additional pore loop located between the S5 and S6 segments. The pore loops line the outer, narrow entry to the pore while the S5 and S6 segments line the inner, wider exit from the pore. The S4 segments in each domain contain positively-charged amino acid residues at every third position. These residues serve as gating charges and move across the membrane in order to initiate channel activation in response to depolarization of the membrane. The short intracellular loop connecting homologues domains III and IV serves as the inactivation gate, folding into the channel structure and blocking the pore from the inside during sustained depolarization of the membrane (Catterall et al., 2002). Nine mammalian sodium channel isoforms have been identified so far. They are all more than 50% identical in amino acid sequence in the transmembrane and extracellular domains, where the amino acid sequence is similar enough for clear alignment. All mammalian sodium channels are members of a single family of proteins, in contrast to potassium and calcium channels, in which distinct gene families arose early in evolution. In the adult mammalian cerebellum, three types of sodium channel α-subunits are expressed, namely $\alpha Na_v1.1$, $\alpha Na_v1.2$ and $\alpha Na_v1.6$ (equivalent to rat brain I, rat brain II and Scn8α) (Westenbroek et al., 1989; Vega-Saenz de Miera et al., 1997; Gong et al., 1999). The genes for $\alpha Na_v1.1$ and $\alpha Na_v1.2$ are both located on human chromosome 2q23-24, indicating a common evolutionary origin. The $\alpha Na_v1.6$ gene is located on human chromosome 12q13. These chromosome segments are paralogous segments, generated by whole genome duplication events during early vertebrate evolution. Mammalian Purkinje cells express sodium channel α-subunits $Na_v1.1$ and $Na_v1.6$ in both soma and dendrites (Gong et al., 1999; Schaller and Caldwell, 2003). Reports on the expression of $Na_v1.2$ in Purkinje cells are conflicting (Black et al., 1994; Felts et al.,

1997; but see Brysch et al., 1991; Gong et al., 1999). In addition, two β-subunits (β1, β2) are expressed in the mammalian cerebellum.

1.5.2 Voltage-gated sodium currents

In mammalian Purkinje cells, three TTX-sensitive sodium currents have been described. Fast-inactivating and persistent sodium currents, generating fast spikes and slow plateau potentials, were described in cerebellar organotypic cultures and slices (Llinas and Sugimori, 1980; Gahwiler and Llano, 1989; Kay et al., 1998). Resurgent sodium currents, which can be elicited upon repolarization after a depolarizing step to positive potentials, were first described by Raman and Bean (1997, 2001). The assignment of the different α-subunits expressed in Purkinje cells to particular currents remains unclear. It does seem clear, however, that $Na_v1.1$ channels are responsible for the fast-inactivating currents that initiate the complex spike together with $Na_v1.6$ channels which also mediate resurgent and possibly persistent sodium currents. $Na_v1.2$ sodium channels mediate similar currents as $Na_v1.1$ channels in other parts of the central nervous system. To what extent they contribute to the fast sodium current, or to other slower conductances in Purkinje neurons, assuming the $Na_v1.2$ channel is expressed at all (see above), is yet unknown (Kay et al., 1998; Schaller and Caldwell, 2003). The resurgent current is a component of the sodium current that results from inactivated sodium channels recovering through an open state (Raman and Bean, 1997). The same sodium channel can thus mediate both fast and resurgent current components. Purkinje neurons can fire at high frequencies. Resurgent sodium currents through $Na_v1.6$ channels can play a major role in high-frequency firing by promoting depolarization after their reactivation, inducing additional short latency spikes time and time again. Resurgent sodium currents conducted by $Na_v1.6$ channels are pleomorphic in nature. While in $Na_v1.6$ null-mutant mice resurgent currents are normally absent or very small in Purkinje cells (Grieco and Raman, 2004), subthalamic nucleus neurons from $Na_v1.6$ null-mutants show considerable resurgent sodium currents (37% of wildtype) (Do and Bean, 2004). Another example is provided by the fact that CA3 pyramidal cells and motor neurons, both expressing $Na_v1.6$ channels, lack resurgent sodium currents (Raman and Bean, 1997; Garcia et al., 1998; Pan and Beam, 1999). Purkinje cells from $Na_v1.6$ null-mutant mice show reduced repetitive spike firing (Raman et al., 1997).

The sodium channel distribution, and the currents flowing through by these channels, is largely known for the mammalian cerebellum, as described above. These data are not well known, however, for the mormyrid central lobes and ELL. This thesis therefore investigates sodium channel expression patterns and sodium currents in the mormyrid central lobes and over the somato-dendritic axis in the ELL. In addition to comprising a basic descriptive study, we ask whether sodium channel expression and distribution patterns, or the presence of specific sodium currents, can explain the characteristic spike patterns in the mormyrid Purkinje and MG cells as compared to rat Purkinje cells (chapters 2 and 3).

1.6 Compensatory eye movements

As described in detail above, the highly plastic cerebellum controls the motor system by analyzing differences between intention and action. Until now, this introduction has mainly focused on the cellular aspects of cerebellar anatomy, physiology and learning. Here, we give an in vivo view of cerebellar computation and plasticity. Vision plays an important role in reporting movement errors back to the cerebellum. The output signals of the oculomotor system are, in turn, computed under cerebellar control. The oculomotor system network is relatively simple (Figure 4) but covers the entire conversion from sensory input to the generation of movement. It thus forms an attractive, in vivo model for the study of the cerebellum, and its plasticity and computations. For instance, the oculomotor system allows us to study the importance of individual genes in cerebellar function using transgenic mice.

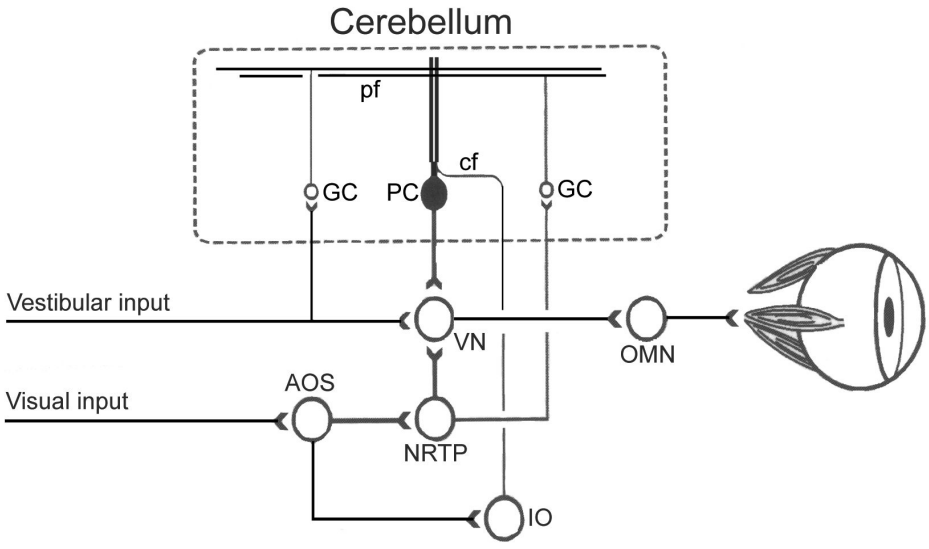

Figure 4: A schematic representation of the compensatory eye movement pathways illustrates the presence of a cerebellar side loop that influences direct oculomotor pathways. Information about linear and angular head acceleration from the labyrinth, and visual information from the retina are both projected to the vestibular nuclei (VN), which relay to the oculomotor nuclei (OMN), forming the direct pathway. The cerebellar flocculus receives visual information and vestibular information via mossy fibers, as well as a 'performance error' signal via the climbing fibers. The Purkinje cells compute these signals and change their input to the vestibular nuclei accordingly. AOS: accessory optic system, IO: inferior olive, NRTP: nucleus reticularis tegmentum pontis, pf: parallel fiber, cf: climbing fiber, GC: granual cell, PC: Purkinje cell *(Adapted from Coesmans, Cerebellar Plasticity in Health and Disease, PhD thesis, Rotterdam 2004).*

One of the cerebellum-controlled tasks of the oculomotor system is to keep the image of the world steady on the retina. In order to compensate for self-generated or imposed head movements, vestibular and visual information is used to generate compensatory eye movements to keep retinal slip to a minimum. The vestibulo-ocular reflex (VOR) generates eye movements in response to head movements, which are detected by the labyrinth. The optokinetic reflex (OKR) generates eye movements in response to movement of images on the retina (retinal slip). Together, these two reflexes form the visually enhanced VOR (VVOR). Information about head

movement and retinal slip signals are sent to the vestibular nuclei (VN) that send their eye movement commands directly to the occulomotor nuclei. The VN are under cerebellar control (Leigh and Zee, 1999). The fast-acting VOR is particularly sensitive to high-frequency head movements. The OKR compensates for the residual slow retinal slip using visual feedback (Collewijn, 1969). Purkinje cells in the flocculus receive visual and vestibular information via mossy fibers and climbing fibers. The floccular Purkinje cells send their axons to the VN. The climbing fibers, which carry retinal error signals (Simpson and Alley, 1974), relay the error signal that is induced by an inadequate VOR, to Purkinje cells in the flocculus. This climbing fiber activity causes LTD of the appropriate “vestibular” parallel fiber inputs to these Purkinje cells, in order to keep the VOR calibrated (Ito, 1982; 1989) and thereby reduce retinal error. *Tilted* mice, which lack otoconia due to a mutation in otopetrin 1, are well-suited as a model to study eye movement plasticity under vestibular deprivation.

Chapter 5 therefore studies the oculomotor system of *tilted* mice. The central question concerns what happens to the VOR and OKR gain and phase lead when vestibular input is lacking, and to what extent the OKR is capable of compensating for the loss of vestibular input.

1.7 Scope of this thesis

Cerebellar plasticity has been a subject of interest for neuroscientists for many decades. Scientists have attempted to unravel how the highly plastic cerebellum combines the information it receives, integrates it, and adjusts its synaptic strength accordingly, from the single cell to the behavioural level. With some exceptions most of the knowledge we have about the cerebellum comes from studying the mammalian cerebellum. The cerebellum, however, is an evolutionary highly conserved structure and some questions that until now remain open may be answered better by comparing what we already know from the mammalian cerebellum with studies in other animal groups, which may have slightly different cerebellar structures. In a large part of this thesis the rat cerebellum will be compared on a morphological and electrophysiological level with that of mormyrid fish. This introduction started with a description of the general role of the cerebellum (paragraph 1.1). Answers to the question, “what does the cerebellum do” can be found there. What the cerebellum looks like in rats and in mormyrid fish, and what differences and similarities have been found between these species, are discussed in paragraph 1.2. Spike physiology of cerebellar Purkinje cells is discussed in paragraph 1.3. What spike types do these cells generate? What are the differences between the spikes elicited in these animals? What ionic currents underlie these spikes? How do spikes propagate and integrate? In paragraph 1.4 an overview is given of what we know about cerebellar synaptic plasticity in these animals. We discuss there how Purkinje cells, parallel fibers and climbing fibers can change their synaptic strength and what this means for the system as a whole. Since the research presented in this thesis will for a large part focus on the role of sodium channels in spike plasticity and propagation paragraph 1.5 discusses the sodium channels expressed in the mammalian cerebellum, their characteristics and the currents they pass. In paragraph 1.6 the oculomotor system is discussed. This system has a cerebellar side loop, is highly plastic and makes an in vivo study of cerebellar plasticity feasible.

In **chapter 2** cerebellar voltage-gated sodium channels are investigated. This chapter studies the expression and localisation patterns of sodium channel α-subunits, the currents carried by these channels and the role dendritic tree architecture plays in shaping sodium currents upon climbing fiber stimulation in rat and mormyrid fish cerebellum. The focus of chapter 2 is on $Na_V1.6$ sodium channels. $Na_V1.6$ sodium channels carry resurgent sodium currents in Purkinje neurons, and allow fast recovery from inactivation, thus supporting the Purkinje neurons unique capability to fire spikes at high frequency. Differences in climbing fiber responses observed between rat and mormyrid fish cerebellar slices can potentially broaden our understanding of how changing climbing fiber-evoked spikes can influence Purkinje neuron output.

Chapter 3 investigates backpropagation of spikes in interneurons of the mormyrid electrosensory lateral line lobe (ELL). This chapter, like chapter 2, studies voltage-gated sodium channels. The focus of chapter 3, however, is on backpropagating spikes in the dendritic arborisation of the ELL interneurons. Chapter 3 also discusses sculpting of these backpropagating sodium spikes by potassium transients and the possible role of GABA as a retrograde messenger in the formation of anti-Hebbian plasticity. Anti-Hebbian plasticity in the ELL depends on the generation of backpropagating spikes. While the focus of chapters 2 and 3 is on sodium currents, which underlie a wide variety of spikes observed in Purkinje neurons and interneurons of the mormyrid and rat cerebellum or cerebellum-like structures, **chapter 4** studies another intracellular factor involved in cerebellar plasticity. This chapter focuses on the role of CRF in regulating excitatory transmission and LTD at the climbing fiber-Purkinje cell synapse of rat cerebellar slices.

Chapter 5 studies cerebellar plasticity at the in vivo level in mice that have been genetically deprived of vestibular input. In **chapter 6** the experimental data presented in chapters 2, 3, 4, 5 are summarised and discussed. An attempt is made in this chapter to put the data presented in this thesis into a broader context and to suggest future research directions towards a better understanding of spike morphology, propagation, integration and plasticity in the cerebellum.

Adrian ED. 1943. Afferent areas in the cerebellum connected with the limbs. Brain 66:289-315.

Aizenman C, Linden DJ. 2000. Rapid, synaptically-driven increases in the intrinsic excitability of cerebellar deep nuclear neurons. Nat Neurosci 3:109-111.

Albus JS. 1971. A theory of cerebellar function. Math Biosci 10:25-61.

Armstrong DM, Harvey RJ, Schild RF. 1973. Branching of inferior olivary axons to terminate in different folia, lobules or lobes of the cerebellum. Brain Res 54:365-371.

Barmack NH, Young WS. 1990. Optokinetic stimulation increases corticotrophin releasing factor mRNA in inferior olivary neurons of rabbits. J Neurosci 10:631-640.

Bear MF, Linden DJ. 2000. The mechanisms and meaning of long-term synaptic depression in the mammalian brain. In: Synapses, ed Cowan WM, Sudhof TC, Stevens CF. Baltimore: John Hopkins University Press 455-517.

Bell CC. 2001. Memory-based expectations in electrosensory systems. Curr Opin Neurobiol 11:481-487.

Bell CC, Grant K, Serrier J. 1992a. Corollary discharge effects and sensory processing in the mormyrid electrosensory lobe. I. Field potentials and cellular activity in associated structures. J Neurophysiol 68:843-858.

Bell CC, Grant K. 1992b. Corollary discharge effects and sensory processing in the mormyromast regions of the mormyrid electrosensory lobe. II. Cell types and corollary discharge plasticity. J Neurophysiol 68:859-875.

Bell CC, Han VZ, Sugawara Y, Grant K. 1997. Synaptic plasticity in a cerebellum-like structure depends on temporal order. Nature 387: 278-281.

Bell CC, Han VZ, Sugawara Y, Grant K. 1999. Synaptic plasticity in the mormyrid electrosensory lobe. J Exp Biol 202: 1339-1347.

Bell CC, Meek J, Yang JY. 2005. Immunocytochemical identification of cell types in the mormyrid electrosensory lobe. J Comp Neurol 483:124-142.

Bell CC, Szabo T. 1986. Electroreception in mormyrid fish: central anatomy. In T.H. Bullock and W. Heiligenberg (eds): Electroreception. New York: John Wiley & sons, pp. 375-421.

Bijlani V, Grewal MS, Rao K. 1980. Birth weight and development of cerebellar cortex. J Anat 130(4):769-775.

Black JA, Yokoyama S, Higashida H, Ransom BR, Waxman SG. 1994. Sodium channel mRNAs I, II and III in the CNS: cell-specific expression. Brain Res Mol Brain Res 22:275-289.

Bower JM, Woolston DC. 1983. Congruence of spatial organization of tactile projections to granule cell and Purkinje cell layers of cerebellar hemispheres of the albino rat: vertical organization of cerebellar cortex. J Neurophysiol 49:745-766.

Brochu G, Maler L, Hawkes R. 1990. Zebrin II: A polypeptide antigen expressed selectively by Purkinje cells reveals compartments in rat and fish cerebellum. J Comp Neurol 291: 538-552.

Brooks VB, Thach WT. 1981. Cerebellar control of posture and movement. In: VB Brooks (ed). Handbook of physiology. Section 1: The nervous system. Vol. 2: Motor Control, Part 2 pp. 877-946. Bethesda, MD: American Physiological Society.

Brysch W, Creutzfeldt OD, Luno K, Schlingensiepen R, Schlingensiepen KH. 1991. Regional and temporal expression of sodium channel messenger RNAs in the brain during development. Exp Brain Res 86:562-567.

Callaway JC, Lasser-Ross N, Ross WN. 1995. IPSPs strongly inhibit climbing fiber activated $[Ca^{2+}]_i$ increases in the dendrites of cerebellar Purkinje neurons. J Neurosci 15:2777-2787.

Carey M, Lisberger S. 2002. Embarrassed, but not depressed: eye opening lessons for cerebellar learning. Neuron 35(2):223-226.

Catterall WA, Goldin AL, Waxman SG. 2002. NC-IUPHAR subcommittee on sodium channels. Int Union of Pharmacology 10-30.

Chacron MJ, Doiron B, Maler L, Longtin A, Bastian J. 2003. Non-classical receptive field mediates switch in a sensory neuron's frequency tuning. Nature 423:77-81.

Chan-Palay V. 1977. Cerebellar dentate nucleus: Springer-Verlag.

Coesmans M, Weber JT, De Zeeuw CI, Hansel C. 2004. Bidirectional parallel fiber plasticity in the cerebellum under climbing fiber control. Neuron 44(4):691-700.

Collewijn H. 1969. Optokinetic eye movements in the rabbit: input-output relations. Vision Res 9:117-132.

Crepel F, Jaillard D. 1991. Pairing of pre- and postsynaptic responses in cerebellar Purkinje cells induces long-term changes in synaptic efficacy in vitro. J Physiol 432:123-141.

Crepel F, Mariani J, Delhaye-Bouchaud N. 1976. Evidence for a multiple innervation of Purkinje cells by climbing fibers in the immature rat cerebellum. J Neurobiol 7:567-578.

De Schutter E. 1995. Cerebellar long-term depression might normalize excitation of Purkinje cells: a hypothesis. Trends Neurosci 18:291-295.

De Schutter E, Bower JM. 1994a. An active model of the cerebellar Purkinje cell I. Stimulation of current-clamps in slices. J Neurophysiol 71:375-400.

De Schutter E, Bower JM. 1994b. An active model of the cerebellar Purkinje cell II. Stimulation of synaptic input. J Neurophysiol 71:401-419.

De Zeeuw CI, Wylie DR, DiGiorgi PL, Simpson JI. 1994. Projections of individual Purkinje cells of identified zones in the flocculus to the vestibular and cerebellar nuclei in the rabbit. J Comp Neurol 349:428-447.

Denizot JP, Clausse S, Elekes K, Geffard M, Grant K, Libouban S, Ravaille-Veron M, Szabo T. 1987. Convergence of electrotonic club endings, GABA- and serotonergic terminals on second order neurons of the electrosensory pathway in mormyrid fish, *Gnathonemus petersii* and Brienomyrus niger (Teleostei). Cell Tissue Res 249:301-309.

Dittman JS, Regehr WG. 1998. Calcium dependence and recovery kinetics of presynaptic depression at the climbing fiber to Purkinje cell synapse. J Neurosci 18:6147-6162.

Do MT, Bean BP. 2004. Sodium currents in subthalamic nucleus neurons from Nav1.6-null mice. J Neurophysiol 92(2):726-733.

Eccles JC, Llinas R, Sasaki K. 1964. Excitation of cerebellar Purkinje cells by the climbing fibers. Nature 203:245-246.

Eccles JC, Llinas R, Sasaki K, Voorhoeve PE. 1966. Interaction experiments on the responses evoked in Purkinje cells by climbing fibers. J Physiol 182:297-315.

Eccles JC, Ito M, Szentagothai J. 1967. The cerebellum as a neuronal machine. Springer Verlag, Berlin-Heidelberg-New York, pp. 335.

Ekerot CF, Kano M. 1985. Long-term depression of parallel fiber synapses following stimulation of climbing fibers. Brain Res 342:357-360.

Felts PA, Yokoyama S, Dib-Haij S, Black JA, Waxman SG. 1997. Sodium channel α-subunit mRNAs I, II, III, NaG, Na6 and hNE (PN1): different expression patterns in developing rat nervous system. Brain Res Mol Brain Res 45:71-82.

Finger TE. 1978. Efferent neurons of the teleost cerebellum. Brain Res 153:608-614.

Finger TE, Bell CC, Russell CJ. 1981. Electrosensory pathways to the valvula cerebelli in mormyrid fish. Exp Brain Res 42:23-33.

Finger TE. 1983. Organization of the teleost cerebellum. In R.G. Northcutt and R.E. Davis (eds): Fish neurobiology. Vol 1: Brainstem and sense organs. Ann Arbor: University of Michigan press, pp. 261-284.

Flourens P. 1842. Recherches experimentales sur les proprietes et les fontions du system nerveux dans les animaux vertebres. Edition 2. Paris: Bailliere.

Fox EA, Gruol DL. 1993. Corticotropin-releasing factor suppresses the afterhyperpolarization in cerebellar Purkinje neurons. Neurosci Lett 149:103-107.

Garcia KD, Sprunger LK, Meisler MH, Beam KG. 1998. The sodium channel Scn8a is the major contributor to the postnatal developmental increase of sodium current density in spinal motoneurons. J Neurosci 18:5234-5239.

Gähwiler BH, Llano I. 1989. Sodium and potassium conductances in somatic membranes of rat Purkinje cells from organotypic cerebellar cultures. J Physiol 417:105-122.

Ghez C, Thach WT. 2000. The cerebellum. In: Kandel ER, Schwartz JH, Jessell TM (eds). Principles of neural science. Fourth edition. chapter 42, pp. 832-852. McGraw-Hill.

Gilman S. 1985. The cerebellum: its role in posture and movement. In: M swah, C Kennard (eds). Scientific basis of clinical neurology, pp. 36-55. New York: Churchill Livingston.

Golding NL, Staff NP, Spruston N. 2002. Dendritic spikes as a mechanism for cooperative long-term potentiation. Nature 418: 326-331.

Gomez L, Kanneworff M, Budelli R, Grant K. 2005. Dendritic spike backpropagation in the electrosensory lobe of *Gnathonemus petersii*. J Exp Bio 208: 141-155.

Gong B, Rhodes KJ, Bekele-Arcuri Z, Trimmer JS. 1999. Type I and type II Na(+)channel α-subunit polypeptides exhibit distinct spatial and temporal patterning, and association with auxiliary subunits in rat brain. J Comp Neurol 412:342-352.

Goossens J, Daniel H, Rancillac A, Van der Steen J, Oberdick J, Crepel F, De Zeeuw CI, Frens MA. 2001. Expression of protein kinase C inhibitor blocks cerebellar long-term depression without affecting Purkinje cell excitability in alert mice. J Neurosci 21:5813-5823.

Gravel C, Hawkes R. 1990. Parasagittal organization of the rat cerebellar cortex: direct comparison of Purkinje cell compartments and the organization of the spinocerebellar projection. J Comp Neurol 291:79-102.

Grant K, Bell CC, Han VZ. 1996. Sensory expectations and anti-Hebbian synaptic plasticity in cerebellum-like structures. J Physiol Paris 90: 233-237.

Grant K, Meek J, Sugawara Y, Veron M, Denizot JP, Hafmans J, Serrier J, Szabo T. 1996. Projection neurons of the mormyrid electrosensory lateral line lobe: morphology , immunocytochemistry and synaptology. J Comp Neurol 375:18-42.

Grant K, Sugawara Y, Gomez L, Han VZ, Bell CC. 1998. The mormyrid electrosensory lobe in vitro: physiology and pharmacology of cells and circuits. J Neurosci 18: 6009-6025.

Grieco TM, Raman IM. 2004. Production of resurgent current in Nav1.6-null Purkinje neurons by slowing sodium channel inactivation with b-pompilidotoxin. J Neurosci 24:35-42.

Groenewegen HJ, Voogd J. 1977. The parasagittal zonation within the olivocerebellar projection. I. Climbing fiber distribution in the vermis of cat cerebellum. J Comp Neurol 174(3):417-488.

Groenewegen HJ, Voogd J, Freedman SL. 1979. The parasagittal zonation within the olivocerebellar projection. II. Climbing fiber distribution in the intermediate and hemispheric parts of cat cerebellum. J Comp Neurol 183(3):551-601.

Gundappa-Sulur G, De Schutter E, Bower JM. 1999. Ascending granule cell axon: an important component of cerebellar cortical circuitry. J Comp Neurol 408:580-596.

Han VZ, Bell CC. 2003. Physiology of cells in the central lobes of the mormyrid cerebellum. J Neurosci 23(35):11147-11157.

Han VZ, Bell CC, Grant K, Sugawara Y. 1999. Mormyrid electrosensory lobe in vitro: morphology of cells and circuits. J Comp Neurol 404:359-374.

Han VZ, Grant K, Bell CC. 2000. Reversible associative depression and non-associative potentiation at a parallel fiber synapse. Neuron 27: 611-622.

Hansel C, Linden DJ. 2000. Long-term depression of the cerebellar climbing fiber-Purkinje neuron synapse. Neuron 26:473-482.

Hansel C, Linden DJ, D'Angelo E. 2001. Beyond parallel fiber LTD: the diversity of synaptic and non-synaptic plasticity in the cerebellum. Nat Neurosci 4:467-475.

Hashimoto K, Kano M. 1998. Presynaptic origin of paired-pulse depression at climbing fiber-Purkinje cell synapses in the rat cerebellum J Physiol 506:391-405.

Häusser M, Clark BA. 1997. Tonic synaptic inhibition modulates neuronal output pattern and spatiotemporal synaptic integration. Neuron 19:665-678.

Henery CC, Mayhew TM. 1989. The cerebrum and cerebellum of the fixed human brain: efficient and unbiased estimates of volumes and cortical surface areas. J Anat 167:167-180.

Houk JC, Buckingham JT, Barto AG. 1996. Models of the cerebellum and motor learning. Behav Brain Sci 19:368-383.

Ito M. 2001. Cerebellar long-term depression: characterization, signal transduction, and functional roles. Physiol Rev 81(3):1143-1195.

Ito M. 1982. Cerebellar control of the vestibulo-ocular reflex around the flocculus hypothesis. Annu Rev Neurosci 5:275-296.

Ito M. 1984. The cerebellum and neural control: Raven Press, New York.

Ito M. 1989. Long-term depression. Annu Rev Neurosci 12:85-102.

Ito M. 1972. Neural design of the cerebellar motor control system. Brain Res 40:81-84.

Ito M, Sakurai M, Tongroach P. 1982. Climbing fiber induced depression of both mossy fiber responsiveness and glutamate sensitivity of cerebellar Purkinje cells.. J Physiol 324:113-134.

Ito M, Simpson JI. 1971. Discharges in Purkinje cell axons during climbing fiber activation. Brain Res 31:215-219.

Jacquin TD, Gruol DL. 1999. Ca2+ regulation of large conductance K+ channel in cultured rat cerebellar Purkinje neurons.. Eur J Neurosci 11:735-739.

Jaeger D, Bower JM. 1994. Prolonged responses in rat cerebellar Purkinje cells following activation of the granule cell layer: an intracellular in vitro and in vivo investigation. Exp Brain Res 100:200-214.

Jaeger D, De Schutter E, Bower JM. 1997. The role of synaptic and voltage-gated currents in the control of Purkinje cell spiking: a modelling study. J Neurosci 17:91-106.

Kaiserman-Abramof IR, Palay SL. 1969. Fine structural studies of the cerebellar cortex in a mormyrid fish. In R.R. Llinas (ed): Neurobiology of cerebellar evolution and development. Chicago: Am Med Ass Educ & Res Found pp. 171-205.

Kano M, Hashimoto K, Chen C, Abeliovich A, Aiba A, Kurihara H, Watanabe M, Inoue Y, Tonegawa S. 1995. Impaired synapse elimination during cerebellar development in PKC gamma mutant mice. Cell 83(7):1223-1231.

Kay AR, Sugimori M, Llinas R. 1998. Kinetic and stochastic properties of a persistent sodium current in mature guinea pig cerebellar Purkinje cells. J Neurophysiol 80:1167-1179.

Keele SW, Ivry R. 1990. Does the cerebellum provide a common computation for diverse tasks? A timing hypothesis. Ann NY Acad Sci 608:179-211.

Konnerth A, Llano I, Armstrong CM. 1990. Synaptic currents in cerebellar Purkinje cells. Proc Natl Acad Sci USA 87:2662-2665.

Korbo L, Andersen BB, Ladefoged O, Moller A. 1993. Total numbers of various cell types in rat cerebellar cortex estimated using an unbiased stereological method. Brain Res 609(1-2):262-268.

Korneliussen HK. 1968. On the ontogenetic development of the cerebellum (nuclei, fissures, and cortex) of the rat, with special reference to regional variations in corticogenesis. J Hirnforsch. 10(5):379-412.

Lev-Ram V, Wong ST, Storm DR, Tsien RY. 2002. A new form of cerebellar long-term potentiation is postsynaptic and depends on nitric oxide but not on cAMP. Proc Natl Acad Sci USA 99:8389-8393.

Lev-Ram V, Mehta SB, Kleinfeld D, Tsien RY. 2003. Reversing cerebellar long-term depression. Proc Natl Acad Sci USA 100:15989-15993.

Levenes C, Daniel H, Jaillard D, Conquet F, Crepel F. 1997. Incomplete regression of multiple climbing fibre innervation of cerebellar Purkinje cells in mGluR1 mutant mice. Neuroreport 8(2):571-574.

Leigh RJ, Zee DS. 1999. The neurology of eye movements, 3rd Edition. Oxford University Press.

Linden DJ, Conner JA. 1991. Participation of postsynaptic PKC in cerebellar long term depression in culture. Science 254:1656-1659.

Luciani L. 1915. The hindbrain. In: Human physiology, trans. F.A. Welby. Macmillan.

Luciano L. 1891. Il cerveletto: Nuovi studi di fisiologia normale e patologica. Firenze: Le Monnier.

Llinas R, Nicholson C. 1971. Electrophysiological properties of dendrites and somata in alligator Purkinje cells. J Neurophysiol 34: 532-551.

Llinas R, Sugimori M. 1980. Electrophysiological properties of in vitro Purkinje cell somata in mammalian cerebellar slices. J Physiol 305:171-195.

Llinas R, Sugimori M. 1980b. Electrophysiological properties of in vitro Purkinje cell somata in mammalian cerebellar slices. J Physiol 305:197-213.

Magee J, Hoffman D, Colbert C, Johnston D. 1998. Electrical and calcium signaling in dendrites of hippocampal pyramidal neurons. Annu Rev Physiol 60:327-346.

Marr D. 1969. A theory of cerebellar cortex. J Physiol 202(2):437-470.

Martina M, Yao GL, Bean BP. 2003. Properties and functional role of voltage-dependant potassium channels in dendrites of rat cerebellar Purkinje neurons. J Neurosci 23(13): 5698-5707.

Meek J. 1992. Comparative aspects of cerebellar organization: from mormyrids to mammals. Eur J Morph 30(1): 37-51.

Meek J, Nieuwenhuys R, Elsevier D. 1986a. Afferent and efferent connections of cerebellar lobe C1 of the mormyrid fish Gnathonemus petersi: An HRP study. J Comp Neurol 245:319-341.

Meek J, Nieuwenhuys R, Elsevier D. 1986b. Afferent and efferent connections of cerebellar lobe C3 of the mormyrid fish Gnathonemus petersi: An HRP study. J Comp Neurol 245:342-358.

Meek J, Nieuwenhuys R. 1991. Palisade pattern of mormyrid Purkinje cells: correlated light and electron microscopic study. J Comp Neurol 306:156-192.

Meek J, Grant K, Sugawara S, Hafmans TGM, Veron M, Denizot JP. 1996. Interneurons of the ganglionic layer in the mormyrid electrosensory lateral line lobe: morphology, immunocytochemistry, and synaptology. J Comp Neurol 375:43-65.

Meek J, Grant K, Bell C. 1999. Structural organization of the mormyrid electrosensory lateral line lobe. J Exp Biol 202:1291-1300.

Midtgaard J, Lasser-Ross N, Ross WN. 1993. Spatial distribution of calcium influx in turtle Purkinje cell dendrites in vitro: role of a transient outward current. J Neurophysiol 70:2455-2469.

Miyata M, Okada D, Hashimoto K et al. 1999. Corticotropin-releasing factor plays a permissive role in cerebellar long-term depression. Neuron 22:763-775.

Netzeband JG, Parsons KL, Sweeney DD, Gruol DL. 1997. Metabotropic glutamate receptor agonists alter neuronal excitability and Ca levels via the phospholipase C transduction pathway in cultured Purkinje neurons. J Neurophysiol 78:63-75.

Nieuwenhuys R. 1967. Comparative anatomy of the cerebellum. In C.A. Fox and R.S. Snider (eds.): Amsterdam: Elsevier, pp. 1-93.

Nieuwenhuys R, Nicholson C. 1967. Cerebellum of Mormyrids. Nature 215: 764-765.

Nieuwenhuys R, Nicholson C. 1969. A survey of the general morphology, the fiber connections, and the possible functional significance of the gigantocerebellum of mormyrid fishes. In: R. Llinas (ed): Neurobiology of cerebellar evolution and development. Chicago: Am Med Ass Educ & Res Found, pp. 107-134.

Nieuwenhuys R, Pouwels E, Smulders-Kersten E. 1974. The neuronal organisation of cerebellar lobe C1 in the mormyrid fish *Gnathonemus petersii* (teleostei) Z Anat Entwickl Gesch 144:315-336.

Nieuwenhuys R. 1976. Aspects of the structural organization of the cerebellum of mormyrid fishes. In O. Creutzfeldt (ed): Afferent and intrinsic organization of laminated structures in the brain. Exp Brain Res Suppl 1:90-95.

Palkovits M, Lernanth C, Gorcs T, Young WS. 1987. Corticotropin releasing factor in the olivocerebellar tract of rats: demonstration by light- and electron- microscopic immunohistochemistry and in situ hybridization histochemistry. Proc Natl Acad Sci USA 84:3911-3915.

Pan F, Beam KG. 1999. The absence of resurgent sodium currents in mouse spinal neurons. Brain Res 849:162-168.

Perrett SP, Ruiz BP, Mauk MD. 1993. Cerebellar cortex lesions disrupt learning-dependant timing of conditioned eyelid responses. J Neurosci 13(4):1708-1718.

Petrosini L, Graziano A, Mandolesi L, Neri P, Molinari M, Leggio MG. 2003. Watch how to do it! New advances in learning by observation. Brain Res Brain Res Rev 42(3):252-264.

Pisani A, Ross WN. 1999. Weak effect of neuromodulators on climbing fiber activated $[Ca^{2+}]_i$ increases in rat cerebellar Purkinje cells. Brain Res 831:113-118.

Rand RW. 1954. An anatomical and experimental study of the cerebellar nuclei and their efferent pathways in the monkey. J Comp Neurol 101(1):167-223.

Raman IM, Bean BP. 1997. Resurgent sodium currents and action potential formation in dissociated cerebellar Purkinje neurons. J Neurosci 17:4517-4526.

Raman IM, Bean BP. 1999. Ionic currents underlying spontaneous action potentials in isolated cerebellar Purkinje neurons. J Neurosci 19:1663-1674.

Raman IM, Bean BP. 2001. Inactivation and recovery of sodium currents in cerebellar Purkinje neurons: evidence for two mechanisms. Biophys J 80:729-737.

Raymond JL, Lisberger SG, Mauk MD. 1996. The cerebellum: a neuronal learning machine? Science 272(5265):1126-1131.

Raymond JL, Lisberger SG. 1998. Neural learning rules for the vestibulo-ocular reflex. J Neurosci 18:9112-9129.

Regehr WG, Konnerth A, Armstrong CM. 1992. Sodium action potentials in the dendrites of cerebellar Purkinje cells. Proc Natl Acad Sci USA 89: 5492-5496.

Rolando L. 1809. Saggio sopra la vera struttura del cervello dell'uomo e degli animali e sopra le funzioni del sistema nervosa. Sassari: Satmperia Da SSRM Privilegiata.

Rolando L. 1823. Experiences sur les fonctions du systeme nerveux. Journal de Physiologie Experimentale 3:95-113.

Roth A, Häusser M. 2001. Compartmental models of rat cerebellar Purkinje cells based on simultaneous somatic and dendritic patch-clamp recordings. J Physiol 535:445-472.

Ruigrok TJ. 2003. Collateralization of climbing and mossy fibers projecting to the nodulus and flocculus of the rat cerebellum. J Comp Neurol 466:278-298.

Sakurai M. 1987. Synaptic modification of parallel fiber-Purkinje cell transmission in in-vitro guinea-pig cerebellar slices. J Physiol 394:463-480.

Salin PA, Malenka RC, Nicoll RA. 1996. Cyclic AMP mediates a presynaptic form of LTP at cerebellar parallel fiber synapses. Neuron 16(4):797-803.

Sastry BR, Morishita W, Yip S, Shew T. 1997. GABA-ergic transmission in deep cerebellar nuclei. Prog Neurobiol 53(2):259-271.

Sawtell NB, Mohr C, Bell CC. 2005. Recurrent feedback in the mormyrid electrosensory system: Cells of the Preeminential and lateral toral nuclei. J Neurophysiol 93: 2090-2103.

Schaller KL, Caldwell JH. 2003. Expression and distribution of voltage-gated sodium channels in the cerebellum. The Cerebellum 2:2-9.

Schmahmann J. 1998. Dysmetria of thought: clinical consequences of cerebellar dysfunction on cognition and affect. Trends Cogn Sci 2:362-371.

Schmolesky MT, Weber JT, De Zeeuw CI, Hansel C. 2002. The making of a complex spike: ionic composition and plasticity. Ann NY Acad Sci 978:359-390.

Shen Y, Hansel C, Linden DJ. 2002. Glutamate release during LTD at cerebellar climbing fiber-Purkinje cell synapses. Nat Neurosci 5:725-726.

Shinoda Y, Sugihara I, Wu HS, Sugiuchi Y. 2000. The entire trajectory of single climbing and mossy fibers in the cerebellar nuclei and cortex. Prog Brain Res 124:173-86.

Simpson JI, Alley KE. 1974. Visual climbing fiber input to rabbit vestibulocerebellum: a source of direction-specific information. Brain Res 82:302-308.

Simpson JI, Wylie DR, De Zeeuw CI. 1996. On climbing fiber signals and their consequence(s). Beh Brain Sciences 19:380-394.

Snider RS, Stowell A. 1944. Receiving areas of the tactile, auditory, and visual systems in the cerebellum. J Neurophysiol 7: 331-357.

Strata P, Tempia F, Zagrebelsky M, Rossi F. 1997. Reciprocal trophic interactions between climbing fibers and Purkinje cells in the rat cerebellum. Prog Brain Res 114:263-282.

Stuart GJ, Häusser M. 1994. Initiation and spread of sodium action potentials in cerebellar Purkinje cells. Neuron 13:703-712.

Stuart GJ, Sakmann B. 1994. Active propagation of somatic action potentials into neocortical pyramidal cell dendrites. Nature: 367 69-72.

Stuart G, Spruston N, Sakmann B, Häusser M. 1997. Action potential initiation and backpropagation in neurons of the mammalian CNS. Trends Neurosci 20:125-131.

Sullivan JP, Lavoue S, Hopkins CD. 2000. Molecular systematics of the African electric fishes (Mormyroidea: teleostei) and a model for the evolution of their electric organs. J Exp Biol 203(Pt 4):665-83.

Szabo T. 1959. Organisation particuliere de la commande nerveuse centrale de la decharge chez un poisson electrique, Gymnarchus niloticus. C R Hebd Seances Acad Sci 248(24):3488-3489.

Szabo T. 1983. Cerebellar pathways in the brain of the mormyrid teleost fish. Acta Morph Hung 31:219-234.

Thach WT. 1967. Somatosensory receptive fields of single units in cat cerebellar cortex. J Neurophysiol 30:675-696.

Thach WT, Goodkin HG, Keating JG. 1992. Cerebellum and the adaptive coordination of movement. Annu Rev Neurosci 15:403-442.

Thach WT. 1996. On the specific role of the cerebellum in motor learning and cognition: clues from PET activation and lesion studies in man. Behav Brain Sci 19:411-431.

Tian JB, Bishop GA. 2003. Frequency-dependant expression of corticotropin releasing factor in the rat's cerebellum. Neuroscience 121:363-377.

Vega-Saenz De Miera E, Rudy B, Sugimori M, Llinas R. 1997. Molecular characterization of the sodium channel subunits expressed in mammalian cerebellar Purkinje cells. Proc Natl Acad Sci USA 94:7059-7064.

Vetter P, Roth A, Häusser M. 2001. Propagation of action potentials in dendrites depends on dendritic morphology. J Neurophysiol 85:926-937.

Voogd J. 1967. Comparative aspects of the structure and fiber connexions of the mammalian cerebellum. Prog Brain Res 25:94-134.

Voogd J, Bigare F, Gerrits NM, Marani E. 1981. Structure and fiber connections of the cerebellum. Prog Clin Biol Res 59A:259-268.

Voogd J, Gerrits NM, Ruigrok TJ. 1996. Organization of the vestibulocerebellum. Ann N Y Acad Sci 781:553-579.

Voogd J, Glickstein M. 1998. The anatomy of the cerebellum. TINS 21:370-375.

Vranesic I, Staub C, Knopfel T. 1993. Activation of metabotropic glutamate receptors induces an outward current which is potentiated by methylxanthines in rat cerebellar Purkinje cells. Neurosci Res 16:209-215.

Wang SSH, Khiroug L, Augustine GJ. 2000. Quantification of spread of cerebellar long-term depression with chemical two-photon uncaging of glutamate. Proc Natl Acad Sci USA 97:8635-8640.

Wang SSH, Denk W, Häusser M. 2000. Coincidence detection in single dendritic spines mediated by calcium release. Nat Neurosci 3(12):1266-1273.

Wang YT, Linden DJ. 2000. Expression of cerebellar long-term depression requires postsynaptic clathrin-mediated endocytosis. Neuron 25:635-647.

Weber JT, De Zeeuw CI, Linden DJ, Hansel C. 2003. Long-term depression of climbing-fiber evoked calcium transients in Purkinje cell dendrites. Proc Natl Acad Sci USA 100:2878-2883.

Westenbroeck RE, Merrick DK, Catterall WA.1989. Differential subcellular localization of the RI and RII Na channel subtypes in central neurons. Neuron 3:695-704.

Chapter 2

Voltage-gated sodium channels in cerebellar Purkinje cells of mormyrid fish

MM de Ruiter, CI De Zeeuw, C Hansel

Abstract

Cerebellar Purkinje cells of mormyrid fish differ in some morphological as well as physiological parameters from their counterparts in other teleost fish or mammals. Morphologically, Purkinje cells of mormyrid fish have larger dendrites that are characterized by a lower degree of branching in the molecular layer. Physiologically, there are differences in electrophysiological response patterns that are related to sodium channel activity: first, sodium spikes in mormyrid Purkinje cells have unusually low amplitudes, typically not exceeding 30 mV. Second, the response to climbing fiber stimulation in mormyrid Purkinje cells does not consist of a complex spike (with an initial fast sodium spike) as in mammals, but instead it consists of an all-or-none excitatory postsynaptic potential, the so-called 'climbing fiber response'. Because of these unique properties, we have begun to characterize mormyrid Purkinje cells electrophysiologically. In this study, we provide a description of voltage-gated Na^+ channels and conductances in Purkinje cells of the mormyrid fish *Gnathonemus petersii*. Various types of Na^+ channel α-subunits, namely $Na_v1.1$, $Na_v1.2$ and $Na_v1.6$, have been described in rodent Purkinje cells. Using immunohistochemical techniques, we found that $Na_v1.1$, $Na_v1.2$ and $Na_v1.6$ subunits are present in Purkinje cells of mormyrid fish as well. To test whether these Na^+ channel subunits can mediate fast-inactivating and resurgent Na^+ currents in *Gnathonemus* Purkinje cells, we conducted patch-clamp recordings in acutely dissociated cells as well as in cerebellar slices. Both types of Na^+ currents could be measured in rat and fish Purkinje cells. These data show that, despite of prominent differences in electrophysiological response characteristics, Purkinje cells of rats and mormyrid fish share the same set of voltage-gated Na^+ conductances.

Introduction

The cerebellum of mormyrid fish has for a long time attracted the attention of neuroanatomists due to its relative size ('gigantocerebellum') and its unique organization (Nieuwenhuys and Nicholson, 1967; 1969; Meek, 1992). At the cellular level, a hallmark of the mormyrid cerebellum is the unusual architecture of the Purkinje cell dendritic tree, which differs substantially from that of mammalian Purkinje cells. Their dendrites show a palisade pattern displaying very different branching characteristics. The smooth proximal dendrites do not protrude into the molecular layer and run parallel to the boundary between the ganglion cell layer (Purkinje cell layer in mammals) and the molecular layer. The proximal dendrites give rise to perpendicularly oriented dendrites, which mostly do not branch any further and run parallel to each other towards the cerebellar surface. The parallel fibers (PFs) selectively contact these distal dendrites, whereas the climbing fiber (CF) input contacts the smooth proximal dendrite. This configuration leads to a far stronger spatial separation between PF and CF synapses than that known from mammalian Purkinje neurons. The axons of mormyrid Purkinje cells are very short. They project in the ganglion cell layer itself onto efferent cells (also called eurydendroid cells) and neighboring Purkinje cells. The efferent cells represent a functional equivalent of the cerebellar nuclei neurons in mammals and provide the sole output of the mormyrid cerebellum (Nieuwenhuys and Nicholson, 1967; 1969; Meek and Nieuwenhuys, 1991; Meek, 1992).

The unusual dendritic tree architecture and synaptic input organization of mormyrid Purkinje cells has motivated us to attempt to characterize these cells electrophysiologically. While the medium ganglion cells (Purkinje-like interneurons) in the mormyrid electrosensory lobe (a cerebellum-like structure) have been characterized with regard to several electrophysiological parameters and with regard to synaptic plasticity (e.g. Bell et al., 1997a+b; Han et al., 2000), the physiological description of cerebellar Purkinje cells of mormyrid fish has only recently begun (Han and Bell, 2003). Our initial recordings focused on synaptic responses of mormyrid Purkinje cells to CF stimulation. In mammalian Purkinje cells, CF activation results in a large all-or-none response, the so-called complex spike, which consists of an initial, fast spike component followed by a series of smaller spikelets riding on top of a plateau (for review see Schmolesky et al., 2002). The fast, initial spike is generated by a somatic Na^+ current. The following slower components have been described to result from the activation of dendritic Ca^{2+} conductances (Llinas and Sugimori, 1980 a+b). More recently, it has been shown that complex spike-like events can be evoked in the soma by intrasomatic depolarization or anode break stimulation (Callaway and Ross, 1997) and can even be elicited in dissociated Purkinje cells (Swensen and Bean, 2003). Thus, it is likely that the complex spike is triggered by dendritic events, but that, at least at the somatic level, the slow complex spike components are mediated by somatic Na^+ and Ca^{2+} currents (for discussion see Schmolesky et al., 2002), which can be activated locally.

In contrast to mammals, stimulation of the CF in the cerebellum of the mormyrid fish *Gnathonemus petersii* does not elicit a complex spike, but rather an all-or-none 'CF response' that lacks obvious spike components (see below). These CF responses can occur in isolation, but they are often followed by series of 'small spikes', which were shown to be Na^+ spikes, probably originating from the axon, reaching amplitudes of $\leq$30 mV (Han and Bell, 2003). The absence of otherwise Purkinje cell-typical complex spikes and the presence of small-amplitude Na^+ spikes, which have not been described in other types of neurons, are the most obvious electrophysiological features that distinguish mormyrid Purkinje cells from their mammalian counterparts. Both, the unique morphological and electrophysiological properties motivated us to attempt to characterize mormyrid Purkinje cells in more detail.

Voltage-gated Na^+ channels consist of an α-subunit and one or more β-subunits. The α-subunit forms the channel pore and possesses all the main properties of the channel such as voltage-dependent gating and Na^+ selectivity. The β-subunits are capable of changing the channel kinetics as well as the voltage dependence of inactivation (Isom et al., 1995a+b). In the adult mammalian cerebellum, three types of Na^+ channel α-subunits are expressed, namely $\alpha Na_v1.1$, $\alpha Na_v1.2$ and $\alpha Na_v1.6$ (equivalent to rat brain I, rat brain II and Scn8a, Westenbroek et al., 1989; Vega-Saenz de Miera et al., 1997; Gong et al., 1999). Na^+ channel α-subunits of teleost fish, the taxonomical group to which mormyrid fish belong, show high homology to Na^+ channel α-subunits of rats. Goldfish $\alpha Na_v1.2$ and $\alpha Na_v1.6$ subunits, for instance, show 77% and 87% homology with $\alpha Na_v1.2$ and $\alpha Na_v1.6$ subunits in rats (Zenisek et al., 2001). In addition, two β-subunits ($\beta1$, $\beta2$) are expressed. The different subunits are heterogeneously distributed in different cell types (for review see Schaller and Caldwell, 2003). Mammalian Purkinje cells express Na^+ channel α-subunits $Na_v1.1$ and $Na_v1.6$ in both soma and dendrites (Gong et al., 1999; Schaller and Caldwell,

2003). Reports on the expression of $Na_v1.2$ in Purkinje cells are conflicting (Black et al., 1994; Felts et al., 1997; but see Brysch et al., 1991; Gong et al., 1999).

Electrophysiologically, three tetrodotoxin (TTX)-sensitive Na^+ conductances were described in mammalian cerebellar Purkinje cells. Recordings from Purkinje cells in slices or organotypic cultures have revealed a fast-inactivating and a persistent Na^+ conductance (Llinas and Sugimori, 1980a; Gähwiler and Llano, 1989; Kay et al., 1998). Additionally, Raman and Bean described a third Na^+ current mediated by $Na_v1.6$ channels, the 'resurgent Na^+ current' (Raman and Bean, 1997, 2001; Raman et al., 1997), which can be elicited upon repolarization after a depolarization to positive potentials. There are uncertainties about the assignment of the different subunit types to particular currents. Recordings from Purkinje cells of $Na_v1.6$ knock-out mice indicate that $Na_v1.6$ channels mediate large parts of the resurgent Na^+ current (Raman et al., 1997). The fast-inactivating Na^+ currents and the persistent Na^+ currents were reduced in those mutant mice as well, but to a lower degree. These observations indicate that $Na_v1.6$ channels participate in all three types of currents, but that $Na_v1.1$ and $Na_v1.2$ channels are involved in the fast-inactivating Na^+ currents and/or the persistent Na^+ currents as well (for discussion see Kay et al., 1998; Schaller and Caldwell, 2003).

$Na_v1.6$ mediated resurgent Na^+ currents are pleomorphic in nature. While in $Na_v1.6$ null-mutant mice resurgent currents are normally absent or very small in Purkinje cells (Grieco and Raman, 2004), subthalamic nucleus neurons from $Na_v1.6$ null-mutants show considerable resurgent Na^+ currents (37% of wildtype) (Do and Bean, 2004). Another example illustrating the pleomorphic nature is provided by CA3 pyramidal neurons and motor neurons, which do express $Na_v1.6$ Na^+ channels but lack resurgent Na^+ currents (Raman and Bean, 1997; Garcia et al., 1998; Pan and Beam, 1999). Resurgent Na^+ currents mediated by $Na_v1.6$ channels can recover from inactivation at relatively depolarized potentials (Raman and Bean, 1997; Khaliq et al., 2003). This feature enables them to accelerate spike firing during bursts. It is therefore likely that resurgent Na^+ currents also contribute to the late complex spike components, which can reach frequencies exceeding 200Hz. Although there are still gaps in our understanding of which conductances are mediated by which types of Na^+ channel α-subunits, it can be shown that alterations in the expression pattern of Na^+ channel α-subunits lead to changes in the firing pattern of Purkinje cells. For example, Purkinje cells from mice lacking $Na_v1.6$ channels do not only show a reduction in resurgent currents, but also diminished repetitive spike firing (Raman et al., 1997). Biolistic introduction of $Na_v1.8$ cDNA into Purkinje cells reduced the number of spikes in conglomerate action potentials evoked by depolarizing current pulses (Renganathan et al., 2003), thus altering a characteristic feature of Purkinje cell electrophysiology. These observations emphasize that the expression profile of voltage-dependent Na^+ channels provides an important component of a complete electrophysiological characterization of neurons, even if the expression of a certain type of subunit does not allow to reliably predict associated conductances.

To characterize the functional expression of Na^+ channel α-subunits, we applied immunohistochemistry to describe their distribution and performed voltage-clamp recordings to test for the presence of various types of voltage-gated Na^+ conductances. All immunohistochemical as well as electrophysiological experiments were not only performed in Purkinje cells of the mormyrid fish *Gnathonemus petersii*,

but also in rats to obtain reference values for comparison and to investigate the debated presence of $Na_v1.2$ Na^+ channels in rat Purkinje cell membranes.

Materials and methods

Animals

Sprague-Dawley rats (Harlan, Netherlands), aged P18-P28 were housed in filtertop cages. Mormyrid fish of the species *Gnathonemus petersii* (obtained from a local fish dealer) were wild-caught and kept in standard aquaria. All experiments described were approved by the Erasmus Medical Center animal care and use committee.

Immunohistochemistry

Mormyrid fish and rats were anaesthetized with 0.20 mmol/l eugenol and 0.2 ml Nembutal, respectively, and perfused with 4% paraformaldehyde in 0.02 M phosphate buffer (PB). Brains were removed, postfixed and rinsed overnight at 4 ^oC in 0.1 M PB, containing 10% sucrose. Embedding of the brains in gelatin was done as described by Groenewegen and Voogd (1977). 40 μm thick sections were cut and collected in 0.1 M PB. Sections were rinsed in Tris-buffered saline (TBS) and pre-incubated for 1 hour at 4 ^oC in 10% normal horse serum (NHS) and 0.5% triton in TBS.

Avidin biotin complex (ABC) staining

Sections were incubated with primary antibody for 48 to 72 hours at 4 ^oC in incubation buffer 1 (IB1) containing: 2% NHS and 0.4% triton in TBS and rinsed (TBS). Secondary antibody was added for 1.5 to 2 hours at room temperature in IB1. Sections were rinsed again, after which the biotin-labeled secondary antibody was conjugated with Avidin from a Vectastain ABC kit (Vector, Burlingame, CA, USA). Sections were rinsed (TBS, Tris) and stained for 15 minutes using diaminobenzidine (DAB). Finally sections were rinsed again (Tris, PB), put on slides, dried and coverslipped.

Fluorescent labeling

Sections were incubated 48 hours with primary antibody at 4 ^oC in incubation buffer 2 (IB2) containing: 1% NHS and 0.4% triton in TBS and rinsed (TBS). Sections were then incubated for 90 minutes with secondary antibody in IB2 and rinsed (TBS). Finally, they were mounted on slides and coverslipped.

Antibodies

Primary antibodies used were: Rabbit anti-brain type I Na^+ channel ($Na_v1.1$) directed against peptide (KY)TAS EHSRE PSAAG RLSD, corresponding to residues 465-481

of rat $Na_v1.1$ intracellular loop between I and II domains (accession P04774), rabbit anti-$Na_v1.2$ directed against peptide (KY)ASA ESRDF SGAGG IGVFS E, corresponding to residues 467-485 of rat $Na_v1.2$ intracellular loop between I and II domains (accession P04775), rabbit anti-Scn8a ($Na_v1.6$) directed against peptide CIANH TGVDI HRNGD FQKNG, corresponding to residues 1042-1061 of rat Scn8α intracellular loop between II and III domains (accession AAC26014) (Alomone labs, Jerusalem, Israel) and rabbit anti-IP_3 receptor subtype I (Calbiochem, Amsterdam, Netherlands). Secondary antibodies used were: Biotinylated goat anti-rabbit (Bio-Gar) (Vector, Burlingame, CA, USA) and fluorescein-isothiocyanate (FITC) labeled donkey anti-rabbit (FITC-Dar) (Jackson, Amsterdam, Netherlands). All other chemicals were purchased from Sigma.

Control experiments for antibody staining

The specificity of the immunohistochemical procedure was examined by performing parallel incubations in which the primary antibody was omitted, or pre-adsorbed. Before pre-adsorption testing we first determined the antibody concentration at which staining was just visible. For all three Na^+ channel primary antibodies used this concentration was 1:100. We then doubled the primary antibody concentration and 1h before incubating the sections, as suggested by Saper and Sawchenko (Saper and Sawchenko, 2003), we added 50 μmol/ml of antigen against which the primary antibody was raised. We used three different control antigens (rat) for the three Na^+ channel primary antibodies (Alomone labs, Jerusalem, Israel).

Western blots

Rats and mormyrid fish were anaesthetized with halothane or 0.20 mmol/l eugenol, respectively, and decapitated, brains were removed and put on ice in 320 mM sucrose with protease inhibitor cocktail (Boehringer-Mannheim). Brains were homogenized and centrifuged at 2000 *g* for 5 minutes. Supernatant was collected and centrifuged at 100, 000 *g* for 1 h at 4^0C after which the pellet was resuspended in 320 mM sucrose with protease inhibitor cocktail to a final concentration of 2000 μg per 10 μl and stored at -80^0C. Samples were mixed with sample buffer and samples plus markers (Biorad) were heated for 10 minutes at 70^0C. 10 μl of sample per lane was applied to a 7% polyacrylamide gel. Gels were run for 1.5 h at 30 mA/gel under standard conditions. After running of the gel was completed, proteins were transferred onto a nitrocellulose membrane for 1.5 h using standard wet-blot techniques at 100 mA per gel. Blots were then blocked with 5% non-fat dry milk in PBS and 0.025% Na-azide for 2 h at room temperature. Blots were incubated with primary antibody (anti-$Na_v1.1$, 1.2 and 1.6, final concentration 1:100, Alomone labs, Jerusalem, Israel) for 2 h at room temperature in blocking solution. Blots were then washed 4 times for 10 minutes with PBS containing 0.1% tween 20. Incubation with secondary antibody (SwaR-HRP (swine anti-rabbit conjugated with horse-radish peroxidase) 1:4000, Dako, Denmark) was done at room temperature for 1 h. After the blot was washed again ECL was performed using a commercial kit (Amersham Bioscience). Film (Kodak) was developed on a Kodak film processor.

Photography

Photographs (Figure 2A and 2B, Figures 3, 4 and 5 panels A-F) were taken using a digital camera (Leica) mounted on a brightfield microscope (Leica). Brightness and contrast were enhanced to comparable levels using the camera's software package (Leica) and microscope settings before the pictures were taken. Fluorescent images (Figures 2C, D) were taken using a confocal microscope (Zeiss). The image in Figure 2D was constructed from a 15 image Z-stack using LSM photo software (Zeiss). Films developed for our Western blot experiments (Figures 3G, 4G and 5G) were scanned using a HP flatbed scanner.

Electrophysiology

The mormyrid cerebellum is subdivided into a valvula, a central corpus and a caudal lobe (see Meek, 1992). The corpus cerebelli consists of four central lobes, C1 to C4. Our recordings from mormyrid Purkinje cells were restricted to these central lobes. In the rat, all experiments were performed using the cerebellar vermis. All recordings were done at room temperature.

Slice recordings (Figure 7): Rats and mormyrid fish were anaesthetized with halothane or 0.20 mmol/l eugenol, respectively, and decapitated. Brains were removed, cut into 200 μm thick sagittal slices and immersed in standard artificial cerebrospinal fluid (ACSF) containing (in mM): 124 NaCl, 5 KCl, 1.25 NaH_2PO_4, 26 $NaHCO_3$, 2 $CaCl_2$, 2 $MgSO_4$ and 10 D-glucose, bubbled with 95% O_2 and 5% CO_2. Following a recovery period of at least 1 hour, slices were placed in a submerged chamber and perfused at a flow rate of 1.6 ml/min with either bubbled ACSF (Figure 1) or rACSF ("resurgent" artificial cerebrospinal fluid) containing (in mM): 122 NaCl, 5 TEA-Cl, 2 KCl, 1.25 NaH_2PO_4, 26 $NaHCO_3$, 2 $CaCl_2$, 2 $MgSO_4$, 10 D-glucose and 0.30 $CdCl_2$ to block most Ca^{2+} and K^+ currents (Figures 6, 7).

Acutely dissociated cells (Figure 6): Slices were prepared as mentioned. Rat cerebellar slices were then treated with 3 mg/ml protease XXIII in dissociation buffer (DB) containing (in mM): 82 Na_2SO_4, 30 K_2SO_4, 5 $MgCl_2$, 10 HEPES and 10 glucose (buffered to pH 7.4 using NaOH) for 7 minutes at 37 degrees with oxygen blown over the surface. Tissue was washed in warm oxygenated DB containing 1mg/ml BSA + 1mg/ml trypsin inhibitor and was allowed to cool to room temperature. The tissue was then triturated in DB and maintained at room temperature with oxygen blown over the surface in Tyrode's solution containing (in mM): 150 NaCl, 4 KCl, 2 $CaCl_2$, 2$MgCl_2$, 10 HEPES and 10 glucose (buffered to pH 7.4 using NaOH). Cells were used within four hours after dissociation (Raman and Bean, 1997). Fish slices were incubated for 15 minutes at room temperature using 40 U/ml Papain in Eagle's MEM incubation buffer (IB) containing (in mM): 10 HEPES, 1 Cysteine, 0.5 EDTA and 5 Na-acetate (pH 7.2). Slices were then washed and triturated in IB, and kept in recording solution in the recording chamber to settle (Afshari et al., 2004).

All recordings from acutely dissociated cells were made in rACSF. Recordings were performed using the visualized whole-cell patch-clamp technique with a Zeiss Axioskop FS and an EPC-9 amplifier (HEKA Electronics, Lambrecht, Germany). Recording electrodes (resistance 3-5 MΩ) were filled with a solution containing (in

mM): 9 KCl, 10 KOH, 120 K^+ gluconate, 3.48 $MgCl_2$, 10 HEPES, 4 NaCl, 4 Na_2ATP, 0.4 Na_3GTP and 17.5 sucrose (Figures 1A-C) or, (in mM): 128 CsOH, 111 gluconic acid, 4 NaOH, 10 CsCl, 2 $MgCl_2$, 10 HEPES, 4 Na_2ATP, 0.4 Na_3GTP and 30 sucrose (Figures 1D-F, Figures 6+ 7; Hansel and Linden, 2000). Both types of internal saline were pH-adjusted (pH 7.25).

Currents were filtered at 3 kHz and digitized at 8 kHz using Pulse software. For extracellular stimulation (Figure 1), standard patch pipettes were filled with external saline. Climbing fibers were stimulated in the granule cell layer. Voltage-step protocols used were either a 20 millisecond depolarizing step from -90 to +30 mV followed by repolarizing steps to potentials between 0 and -60 mV or a depolarizing ramp; 0.1 mV/millisecond from –90 to +30 mV followed by repolarizing steps to between +20 and –60 mV (Raman and Bean, 1997). Traces recorded in rACSF containing 300 nM TTX were subtracted from traces recorded in rACSF alone to isolate TTX-sensitive Na^+ currents from e.g. capacitive and leak currents (Figures 6, 7). Directly after forming a giga-seal the fast capacitance was corrected using the automatic capacitance compensation function embedded in the amplifier window of the HEKA Pulse software package. After brake in (whole cell configuration) the slow capacitance was compensated the same way. All drugs were purchased from Sigma.

Results

Synaptic responses to CF stimulation

In mammalian Purkinje cells, CF activation results in the firing of a complex spike. Figure 1A shows a complex spike recorded from a rat Purkinje cell. The complex spike is characterized by an initial somatic Na^+ spike, followed by a slow plateau potential with small spikelets on top. The plateau potential could result from Ca^{2+} currents and / or non-inactivating Na^+ currents in the Purkinje cell soma and proximal dendrites (Llinas and Sugimori, 1980a+b; for review see Schmolesky et al., 2002). The origin of the small spikelets is still not resolved. While the complex spike is initiated by the activation of dendritic α-amino-3-hydroxy-5-methyl-4-isoxazole propionic acid (AMPA) receptors and subsequent local Ca^{2+} spike activity, it is likely that the spikelets, as recorded in the soma, are mediated by somatic Ca^{2+} and Na^+ currents. Resurgent Na^+ currents might facilitate the high frequency discharge that characterizes the late complex spike components.

The climbing fiber response of mormyrid fish (*Gnathonemus petersii*) differs substantially from its mammalian counterpart in several aspects (Figures 1B, C). The initial component is an all-or-none excitatory postsynaptic potential (EPSP; the all-or-none character is shown in Figure 1B), which is sometimes followed by one or more small spikes which are thought to be axonal Na^+ spikes that do not invade the soma (Han and Bell, 2003). These small spikes may or may not occur (for examples of CF responses without and with small spikes see Figures 1B, C respectively) and thus cannot be considered as a CF response component.

CF evoked excitatory postsynaptic currents (EPSCs) reverse typically around +12 mV in both rat and mormyrid fish Purkinje cells (Figures 1D, E). The amplitudes of mormyrid fish EPSCs are generally smaller than those recorded in rat Purkinje cells

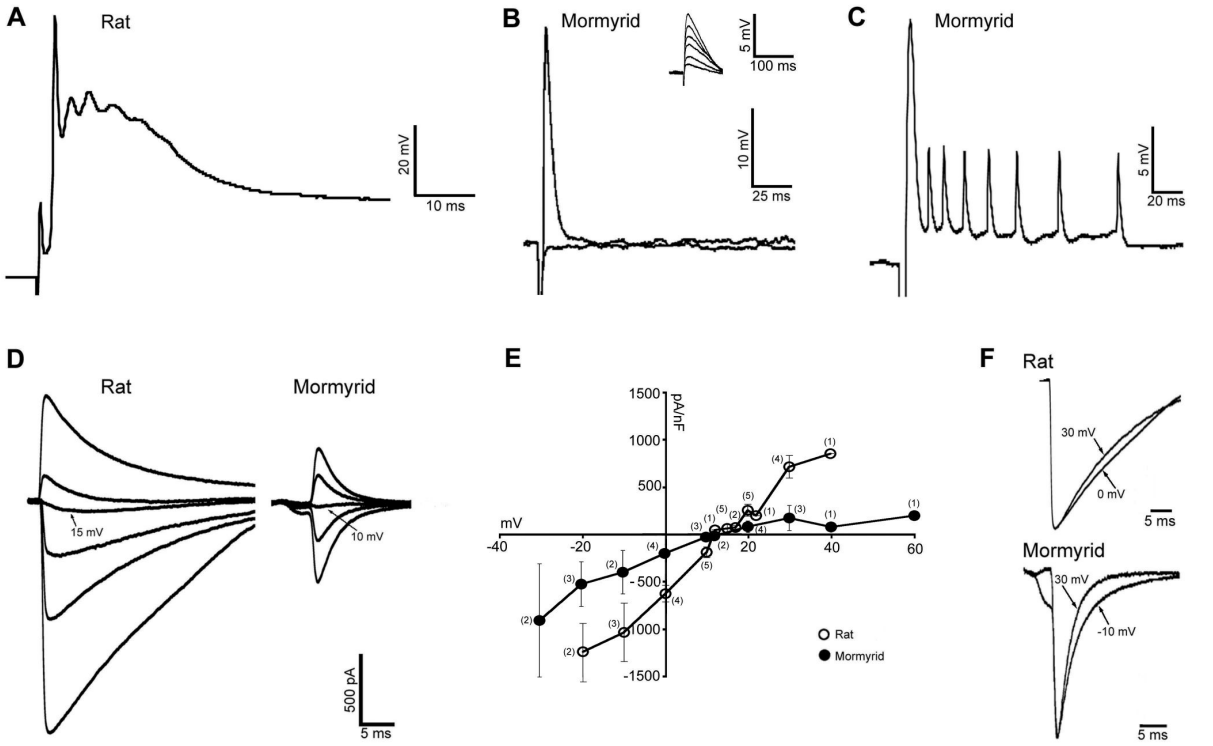

Figure 1: Climbing fiber-evoked electrical responses in Purkinje cells. **A:** Complex spike recorded from a rat Purkinje cell. **B:** All-or-none climbing fiber responses recorded from a *Gnathonemus petersii* Purkinje cell. Responses are shown above and below the threshold for evoking an EPSP. The inset shows a series of parallel fiber EPSPs evoked at increasing stimulus intensities. Note the different time scales of the CF and PF response. **C:** Example of a cell in which the EPSP was followed by small spikes. **D:** Voltage dependence of CF-EPSCs recorded from rat (left) and mormyrid Purkinje cells (right). Voltage steps were to +30, +20, +15, +10, 0 and –10 (in mV) for the rat recording and +30, +20, +10, 0 and –10 (in mV) for the fish recording. **E:** Voltage dependence of CF-EPSCs measured in rat (n = 5) and fish Purkinje cells (n = 4). Not every voltage step was applied to every cell. **F:** CF EPSCs from Figure 1D show comparable rising phase kinetics above and below the reversal potential (the positive currents were reversed and scaled to the same amplitude). Top: currents recorded from a rat Purkinje cell at +30 and 0 mV. Bottom: currents recorded from a fish Purkinje cell at +30 and –10 mV. Current amplitudes differ for the traces shown and amplitude scale bars were therefore omitted. The original traces are shown in Figure 1D.

(Figures 1D, E). CF EPSCs of both species show similar rise time kinetics when traces above and below the reversal potential were scaled to the same amplitude after the positive currents were reversed (Figure 1F).

Since voltage-gated Na^+ channels are critically involved in the generation of complex spikes, and CF responses differ substantially between rat and mormyrid fish, we wanted to determine the expression patterns of the three mammalian Na^+ channel α-subunits in mormyrid fish to better understand the molecular and cellular basis of the unique electrophysiological features of their Purkinje cells.

Immunohistochemistry

In mormyrid fish, cerebellar Purkinje cells can be confused with efferent cells or stellate cells, which have a roughly similar palisade pattern of their dendritic trees in the molecular layer. Reliable criteria for the identification of Purkinje cells are a particularly low degree of dendritic branching and the resulting regularity in appearance, the relative thickness of dendrites, the presence of dendritic spines and the superficial position of the somata within the ganglion cell layer (Meek and Nieuwenhuys, 1991). In addition, IP_3-receptor subtype I is known to be selectively expressed in Purkinje cells (Sharp et al., 1999; Koulen et al., 2000).

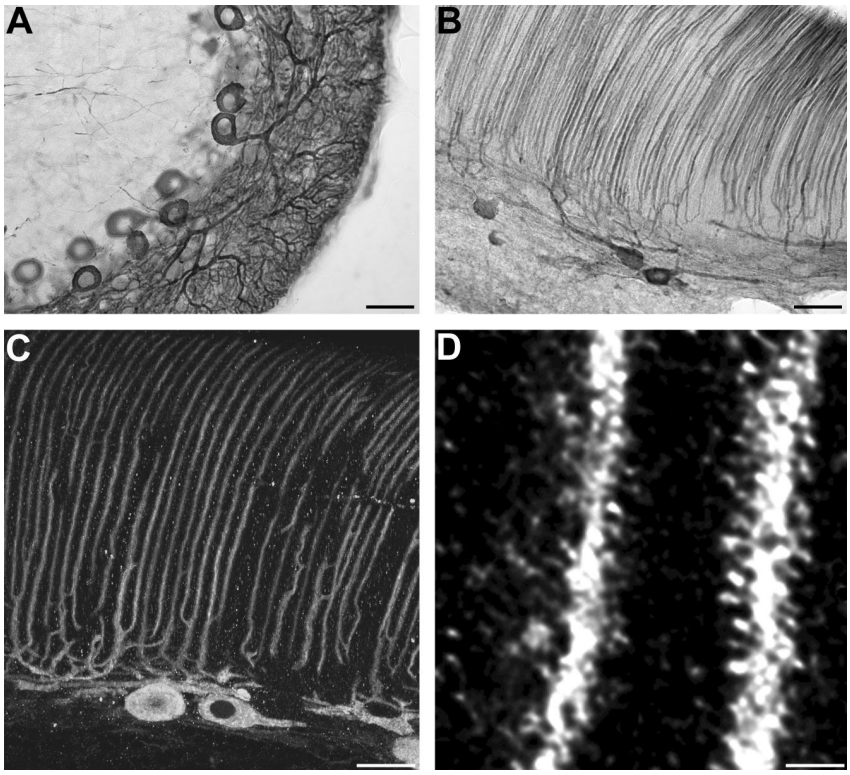

Figure 2: IP_3-receptor subtype I antibody staining **A:** Rat cerebellar section stained with anti-IP_3-receptor subtype I antibodies and DAB. Note the Purkinje cell specificity of the IP_3-receptor in the cerebellum and the evenly dense staining in the somata and dendrites of the Purkinje cells. Top left a few Purkinje cell axons are stained. **B:** Staining as in panel A, but in a section of the mormyrid cerebellum. Note that the staining pattern of IP_3-receptors is very similar between rat and fish (panels A and B), but that the architecture of the Purkinje cell dendrite is different. **C:** Mormyrid cerebellar section stained with anti-IP_3-receptor subtype I antibodies and FITC. Note that the dendrites of mormyrid Purkinje cells branch only a few times very proximally and then run straight to the pial surface. **D:** The dendritic tree of a mormyrid Purkinje cell clearly shows numerous spines that are stained for IP_3-receptors of subtype I (FITC). Scale bars = 12.5 μm in A, B, 20 μm in C and 2 μm in D.

To obtain reference images for the identification of Purkinje cells, we used an antibody against the IP_3-receptor subtype I . The DAB staining pattern for IP_3-receptor subtype I was similar in both rat and mormyrid fish (Figures 2A, B). In rat sections, the Purkinje cells are easily identified by the unique shape of their dendritic

trees. It is obvious from Figure 2A that the staining was selective for Purkinje cells. In sections of mormyrid fish, the identity of the stained cells was confirmed by the presence of spines (Figure 2D), which we could visualize using fluorescent secondary antibodies (Figures 2C, D). The presence of spines allows for an unambiguous identification of these cells as Purkinje cells, because the other two types of neurons with palisade-shaped dendrites are aspiny (Meek and Nieuwenhuys, 1991; Meek, 1992). Thus, in both rat and fish sections the staining for IP_3-receptor subtype I was Purkinje cell-specific.

To characterize the distribution pattern of $Na_v1.1$ channels, we immunostained cerebellar sections obtained from rats (Figures 3A, B) and from mormyrid fish (Figures 3C, D).

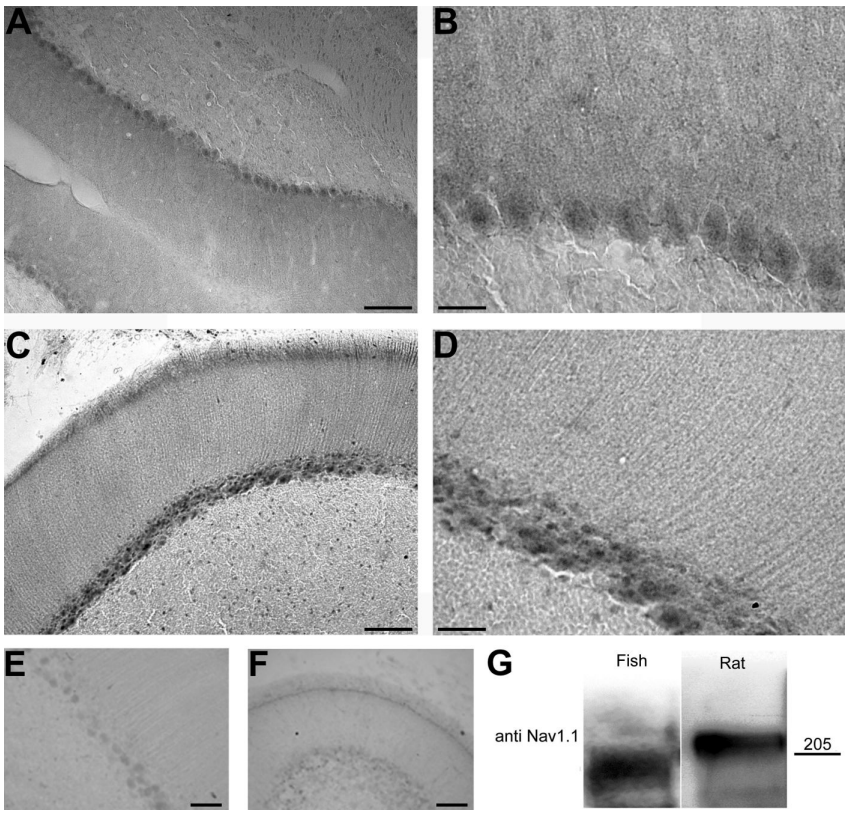

Figure 3: $Na_v1.1$ channel staining. **A:** Anti-$Na_v1.1$ channel antibody and DAB staining. Note the denser staining of $Na_v1.1$ channels in the somata of the rat Purkinje cells versus the weaker staining in the dendrites. **B:** Higher magnification of panel A. **C:** Anti-$Na_v1.1$ channel antibody staining of somata in the ganglion cell layer of mormyrid Purkinje cells. Note the comparable staining pattern between panels A and C. Also note the staining of cells in the granule cell layer (bottom right). **D:** Higher magnification of panel C. Scale bars = 25 μm in A, C and 6 μm in B, D. **E:** Preadsorption control for anti-$Na_v1.1$ antibody on a mormyrid cerebellar section. **F:** Omission of primary antibody shows weak unspecific binding of secondary antibody comparable to that in panel E. Scale bar = 25 μm in E and 6 μm in F. **G:** Western blot analysis shows that anti-$Na_v1.1$ antibodies bind to proteins of the appropriate size in both fish and rat brain membrane preparations.

In rat sections, Purkinje cell somata are stained and there is some staining in the molecular layer that, however, is too weak to identify dendritic structures. In the fish sections, there is a staining of small and larger somata in the ganglion cell layer as well and also a similarly weak staining in the molecular layer. Figures 3C, D show pictures taken from the central lobe C2. In contrast to lobes 3 and 4, lobes 1 and 2 are known to have a layer of stellate cells external to the layer of Purkinje cells (Han and Bell, personal communication). In Figure 3D, smaller, more superficial somata can be distinguished from larger somata. Thus, it is likely that somata of both stellate and Purkinje cells were stained.

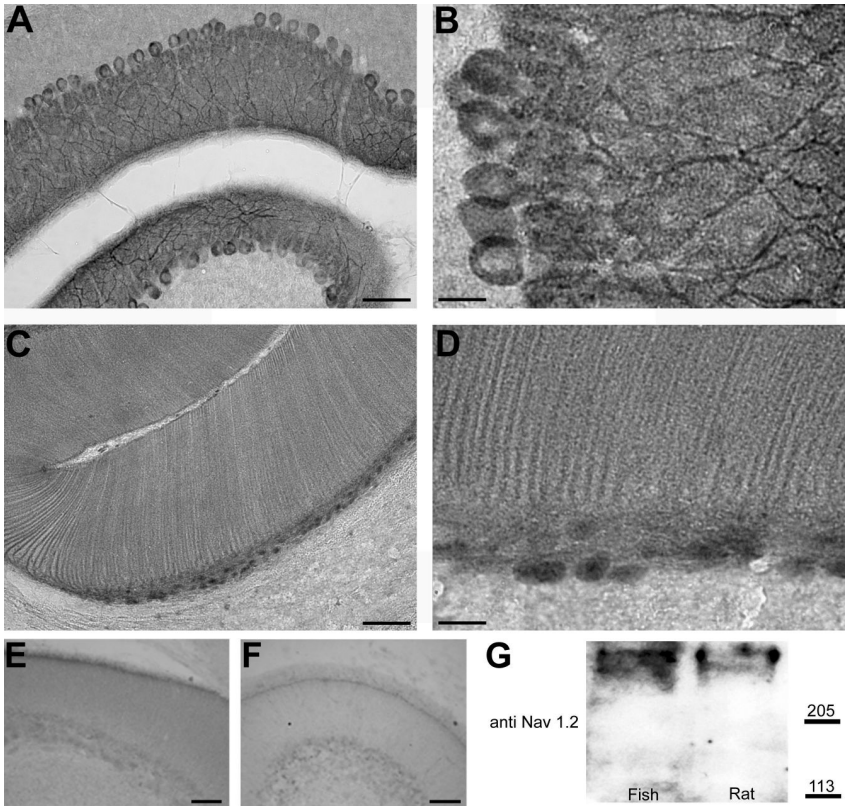

Figure 4: $Na_v1.2$ channel staining. **A:** Anti-$Na_v1.2$ channel antibody and DAB staining. $Na_v1.2$ staining is equally dense in the somata and dendrites of rat Purkinje cells. **B:** Higher magnification of panel A. **C:** Same staining as in panel A but now of mormyrid Purkinje cells. Note that the density of the $Na_v1.2$ staining is comparable between rat and fish Purkinje cells. **D:** Higher magnification of panel C. Scale bars = 25 μm in A, C and 6 μm in B, D. **E:** Preadsorption control for anti-$Na_v1.2$ antibody on a mormyrid cerebellar section. **F:** Omission of primary antibody shows weak unspecific binding of secondary antibody comparable to that in panel E. Scale bars = 25 μm in E, F. **G:** Western blot analysis shows that anti-$Na_v1.2$ antibodies bind to proteins of the appropriate size in both fish and rat brain membrane preparations.

In contrast to the staining for $Na_v1.1$ channels, antibodies against $Na_v1.2$ channels let to a strong staining in rat Purkinje cells in both somata and dendrites (Figures 4A, B). Similarly, somata and dendrites of *Gnathonemus* Purkinje cells were heavily stained (Figures 4C, D). The dendrites could be clearly distinguished and the identification of Purkinje cells was based on the criteria as mentioned above. A very similar staining

pattern emerges from the antibody staining against $Na_v1.6$ channels. In rat sections, there is a strong staining in somata and dendrites of Purkinje cells (Figures 5A, B). A similar distribution can be seen in fish sections, where $Na_v1.6$ channels are also expressed in Purkinje cell somata and dendrites (Figures 5C, D).

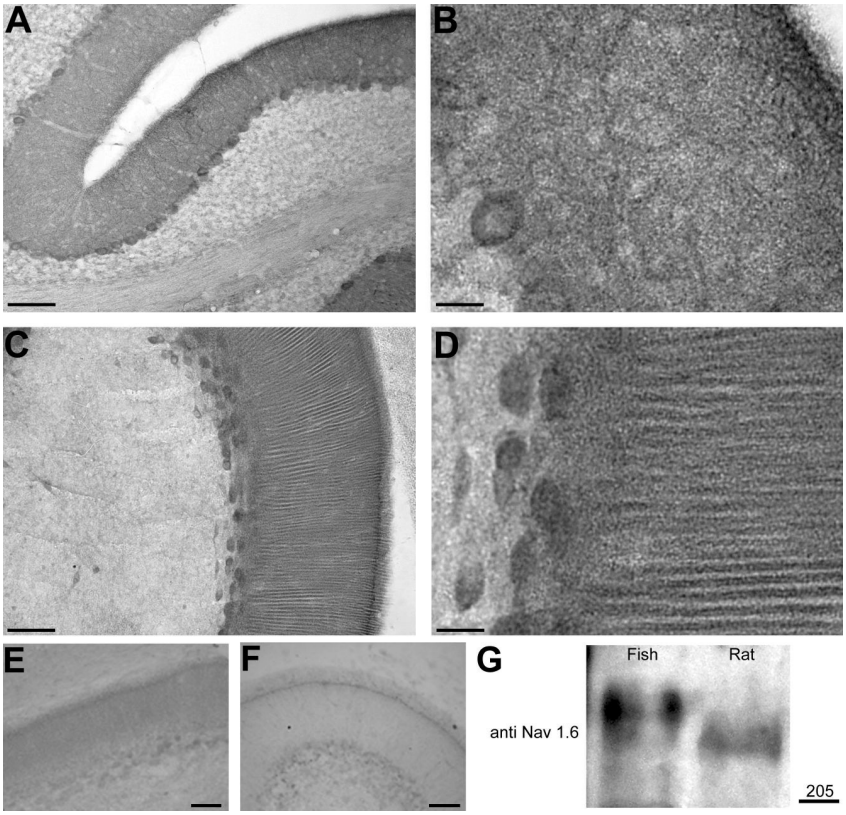

Figure 5: $Na_v1.6$ channel staining. **A:** Anti-$Na_v1.6$ channel antibody and DAB staining. $Na_v1.6$ staining is in the rat present in the somata and in the dendrites. **B:** Higher magnification of panel A. **C:** Same staining as in panel A but now of mormyrid Purkinje cells. Note that the density of the $Na_v1.6$ staining is comparable between rat and fish Purkinje cells. **D:** Higher magnification of panel C. Scale bars = 25 μm in A, C and 6 μm in B, D. **E:** Preadsorption control for anti-$Na_v1.6$ antibody on a mormyrid cerebellar section. **F:** Omission of primary antibody shows weak unspecific binding of secondary antibody comparable to that in panel E. Scale bars = 25 μm in E, F. **G:** Western blot analysis shows that anti-$Na_v1.6$ antibodies bind to proteins of the appropriate size in both fish and rat brain membrane preparations.

These results show that Purkinje cells in rats and mormyrid fish show the same expression pattern of Na^+ channel α-subunits. $Na_v1.1$ channels also appeared to be expressed in somata in the granule cell layer (these could be somata of Golgi cells, unipolar brush cells or a subset of granule cells), whereas $Na_v1.2$ and 1.6 were found to be not, or very lightly, expressed in the granule cell layer (Figures 3, 4, 5). Figures 3, 4 and 5 show, in panel E and F, that when the primary antibody directed against the respective Na^+ channel was adsorbed to the antigen before incubation (panel E) or omitted (panel F), no, or very weak, staining could be detected in mormyrid slices compared to panels C and D of Figures 3, 4 and 5. When we compare panel E and F we can conclude that the very weak staining that is still found after adsorption and

omission of the antibody can be fully attributed to weak unspecific staining of the secondary antibody used. In addition, Western blot analysis (Figures 3, 4, 5 G) shows that antibodies directed against $Na_v1.1$ $Na_v1.2$ and $Na_v1.6$ stain proteins of the expected molecular size in both fish and rat brain membrane preparations.

These results show that the Na^+ channel antibodies used in this study are specific for the antigen they are directed against (Figures 3, 4, 5 E) and that these antibodies react to proteins of the appropriate size in mormyrid fish brain membrane preparations (Figures 3, 4, 5 G). The secondary antibody used does only very weakly stain the cerebellar sections to a degree that does not interfere with the interpretation of our results (Figures 3, 4, 5 F). Purkinje cells of both species express the same subset of Na^+ channels in comparable densities at comparable sites. To examine whether the immunohistochemically characterized Na^+ channels are functional and to compare Na^+ conductances in Purkinje cells of rats and mormyrid fish, we set out to study different types of Na^+ conductances using patch-clamp electrophysiological recordings.

Electrophysiological characterization of Na^+ conductances

We first recorded from dissociated neurons to minimize space-clamp limitations and thus to allow for a characterization of current properties. Voltage steps (20 millisecond depolarizing step from -90 to +30 mV; Figure 6A) resulted in a fast-inactivating TTX-sensitive Na^+ current in dissociated rat Purkinje cells (n = 6, Figures 6B, F). The displayed traces show the TTX-sensitive current components after subtraction of the currents that remained when TTX was bath-applied. In the following, the TTX-sensitive currents remaining after subtraction are labelled as 'TTX-subtracted'. In dissociated mormyrid Purkinje cells, we found a similar fast-inactivating current (n = 6, all TTX-subtracted; Figures 6C, F). Sodium currents were corrected for membrane capacitance (16.6 $\pm$ 1.1 pF ($\pm$SEM) for rat (n = 5) and 9.8 $\pm$ 0.7 pF ($\pm$SEM) for mormyrid (n = 5) Purkinje cells) and plotted as current density on a pA/pF scale. This was done to correct for the smaller size of mormyrid Purkinje cell somata. The fast-inactivating Na^+ current reached 189 $\pm$ 57 pA/pF ($\pm$SEM) with a decay time constant of 0.31 $\pm$ 0.05 ms ($\pm$SEM) in rat Purkinje cells (n = 6, all TTX-subtracted) and 179 $\pm$ 59 pA/pF ($\pm$SEM) with a decay time constant of 0.47 $\pm$ 0.06 ($\pm$SEM) ms in mormyrid Purkinje cells (n = 6, all TTX-subtracted, $p>0.05$, Mann-Whitney U test) (Figures 6H, L). Fast-inactivating current rise times also did not differ between species (0.38 $\pm$ 0.05 ms ($\pm$SEM) for rat and 0.39 $\pm$ 0.01 ms ($\pm$SEM) for mormyrid dissociated cells, $p>0.05$, Mann-Whitney U test) (Figure 6J). Our data from rat dissociated Purkinje cells are very similar to those previously obtained from isolated rat Purkinje cell somata (Raman and Bean, 1997).

To test for the presence of resurgent Na^+ currents in the dissociated cell preparations, the depolarizing voltage steps were followed by repolarizing steps to potentials between 0 and –60 mV (rat n = 6 all TTX-subtracted; fish n = 6; all TTX-subtracted) (Figure 6A). Resurgent Na^+ currents were elicited in mormyrid fish and rat Purkinje cells during repolarization steps (Figures 6 B, C, E), which were very similar to resurgent Na^+ currents previously described in rat and mouse cerebellar Purkinje cells using the same protocol (Raman and Bean, 1997; Raman et al., 1997). In rat Purkinje cells, the amplitude of the resurgent current was, at peak, 30.6 $\pm$ 8.7

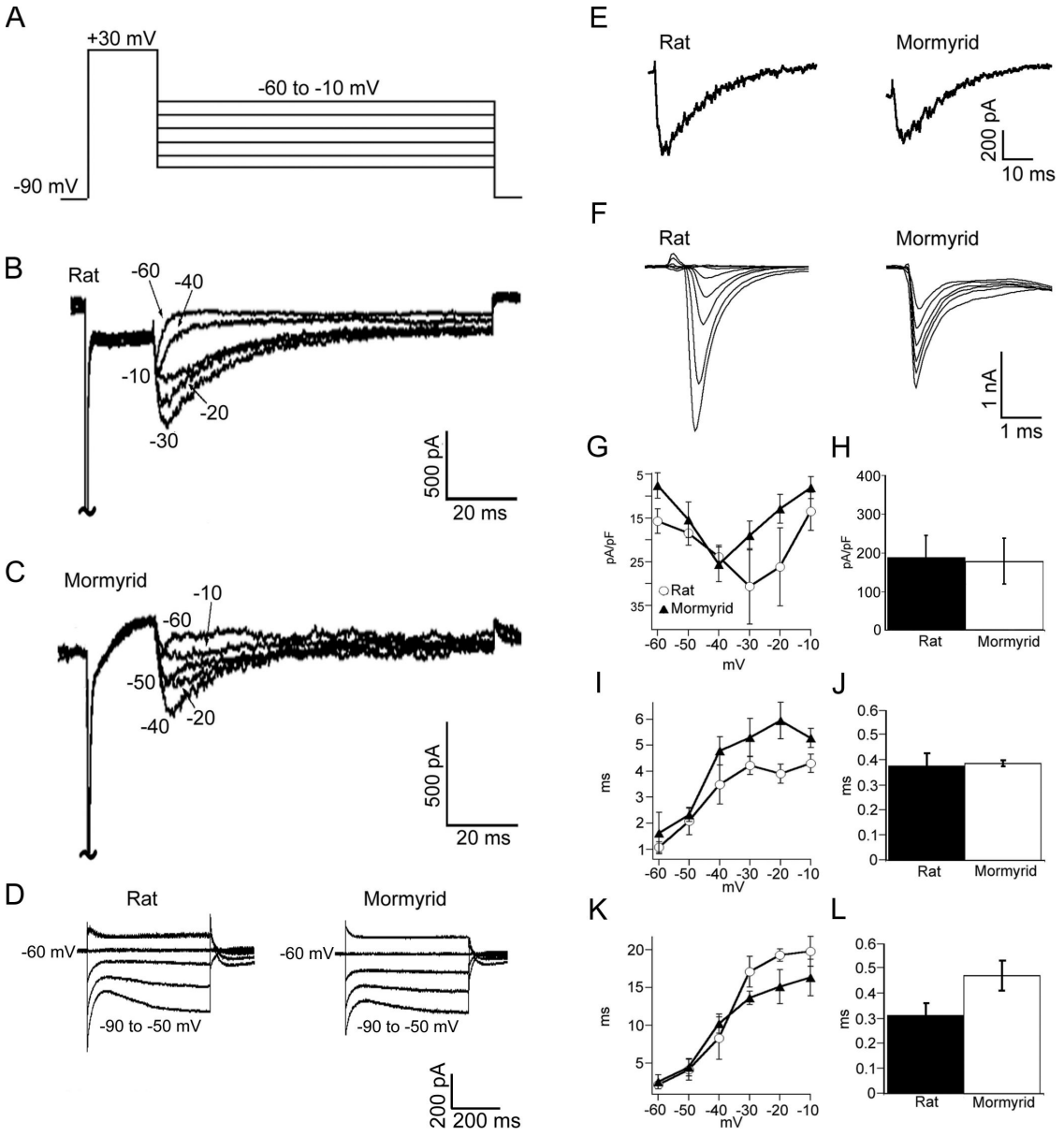

Figure 6: Fast-inactivating and resurgent Na^+ currents recorded from dissociated rat and mormyrid fish Purkinje neurons. **A:** Voltage step protocol used to elicit Na^+ currents. **B:** TTX-subtracted fast-inactivating (+30 mV step) and resurgent Na^+ currents (-60 to –10 mV steps) recorded from rat dissociated Purkinje neurons. **C:** TTX-subtracted fast-inactivating and resurgent Na^+ currents recorded from mormyrid dissociated Purkinje neurons. **D:** Voltage-step protocols were applied to determine the input resistances of rat (left) and fish (right) Purkinje cells. **E:** Enlargement of peak resurgent Na^+ currents recorded **F:** Fast Na^+ currents recorded during wash-in of TTX. **G:** Current-voltage relationship of resurgent Na^+ currents. **H:** Peak fast Na^+ current. **I:** Rise time of resurgent Na^+ currents. **J:** Rise time of fast Na^+ current. **K:** 50% decay time of resurgent Na^+ currents. Measured from peak to 50% decay of the peak current. **L:** 50% decay time of fast Na^+ current. Panels G through L show the average +/- SEM, rat n = 5, mormyrid n = 6.

pA/pF (±SEM) with a rise time of 4.22 ± 0.35 ms (±SEM) and a decay time constant of 17.1 ± 2.0 ms (±SEM) (n = 6, all TTX-subtracted, step protocol, -30 mV) (Figures 6 G, I, K). In mormyrid Purkinje cells, the resurgent Na^+ current reached 25.6 ± 4.0 pA/pF (±SEM) with a rise time of 4.77 ± 0.54 ms (±SEM) and a decay time constant of 10.24 ± 1.29 ms (±SEM) (n = 6, all TTX-subtracted, step protocol, -30 mV)

(Figures 6 G, I, K). Resurgent current peak size, rise and decay times were all not significantly different between rat and mormyrid Purkinje cells at all voltage steps ($p>0.05$, Mann-Whitney U test). There was also no difference in the input resistance (rats: 104.9 ± 13.1 MΩ; n = 5; fish: 97.1 ± 13.3 MΩ; n = 4; $p>0.05$; Mann-Whitney U test; Figure 6D).

Our observations suggest that the types of conductances described here are of somatic origin. This assumption is supported by the immunohistochemical data. A caveat is, however, that the dissociated Purkinje cells often still contain axon and dendrite stumps. Therefore, it is not possible to exclude contributions from these structures to the recorded conductances.

While recordings from dissociated neurons provide the best technical approach to characterize Na^+ currents, they are limited by difficulties to distinguish different types of neurons. This aspect is particularly relevant for the mormyrid cerebellum, because here Purkinje cells and efferent cells are quite similar and are, in fact, indistinguishable after dissociation. Therefore, we performed an additional series of recordings from Purkinje cells in slices to qualitatively confirm the observations described above.

Purkinje cells were identified by the superficial position of their somata in the ganglion cell layer (Meek and Nieuwenhuys, 1991). Voltage steps (20 millisecond depolarizing step from -90 to +30 mV; Figure 7A) resulted in a fast-inactivating TTX-sensitive Na^+ current in rat Purkinje cells (n = 15, of which 3 were TTX-subtracted; Figure 7B). Sodium currents were corrected for membrane capacitance (1013 ± 195 pF (±SEM) for rat (n = 5) and 833 ± 92 pF (±SEM) for mormyrid (n = 5) Purkinje cells) and plotted on a pA/nF scale. The fast current component was followed by a slower, low amplitude current. In mormyrid Purkinje cells, we found a similar biphasic current (n = 10, of which 5 were TTX-subtracted; Figure 7D). The fast-inactivating Na^+ current differed ($p < 0.05$, Mann-Whitney U test), in amplitude, but not in rise or decay time constant ($p > 0.05$, Mann-Whitney U test, measured at 50% decay) between the two species, even after compensation for cell capacitance. This difference might be due to the poor space clamp conditions in intact Purkinje cells which makes a good estimate of cell capacitance virtually impossible. The current reached 3.78 ± 0.71 nA/nF (±SEM) with a decay time constant of 0.80 ± 0.19 ms (±SEM) in rat Purkinje cells (n = 3, all TTX-subtracted) and 1.31 ± 0.62 nA/nF (±SEM) with a decay time constant of 1.02 ± 0.24 ms (±SEM) in mormyrid Purkinje cells (n = 6, all TTX-subtracted) (Figures 7F, G). Rise times were (0.42 ± 0.07 ms (±SEM) in rats and 0.37 ± 0.05 ms (±SEM) in mormyrids) (Figure 7G). As these recordings were obtained from intact Purkinje cells and not from isolated somata, it is possible that inadequate space clamp in some cells allowed for voltage escape during the depolarizing step (for a discussion of the space clamp problem see Häusser, 2003). Despite this technical limitation that makes a reliable quantification difficult to achieve, these data from intact slices are similar to those obtained in our dissociated cell experiments and to those previously obtained from isolated rat Purkinje cell somata (Raman and Bean, 1997). They furthermore strongly resemble fast current recordings recently obtained from intact Purkinje cells in slices (Afshari et al., 2004).

To test for the presence of resurgent Na^+ currents, the depolarizing voltage steps were followed by repolarizing steps to potentials between 0 and –60 mV (rat n = 15 of

which 3 were TTX-subtracted; fish n = 10; 5 TTX-subtracted) (Figure 7A). Alternatively, we used ramp protocols (0.1 mV/millisecond from –90 to +30 mV followed by repolarizing steps between +20 and -60 mV, fish n = 6; rat n = 7; all TTX-subtracted; Figures 7C, E, H). Both protocols elicited resurgent Na^+ currents in mormyrid fish and rat Purkinje cells during repolarization (Figures 7C, E), which were resembling the resurgent Na^+ currents we recorded in dissociated cells and those previously described in rat and mouse dissociated cerebellar Purkinje cells using the same protocol (Raman and Bean, 1997; Raman et al., 1997).

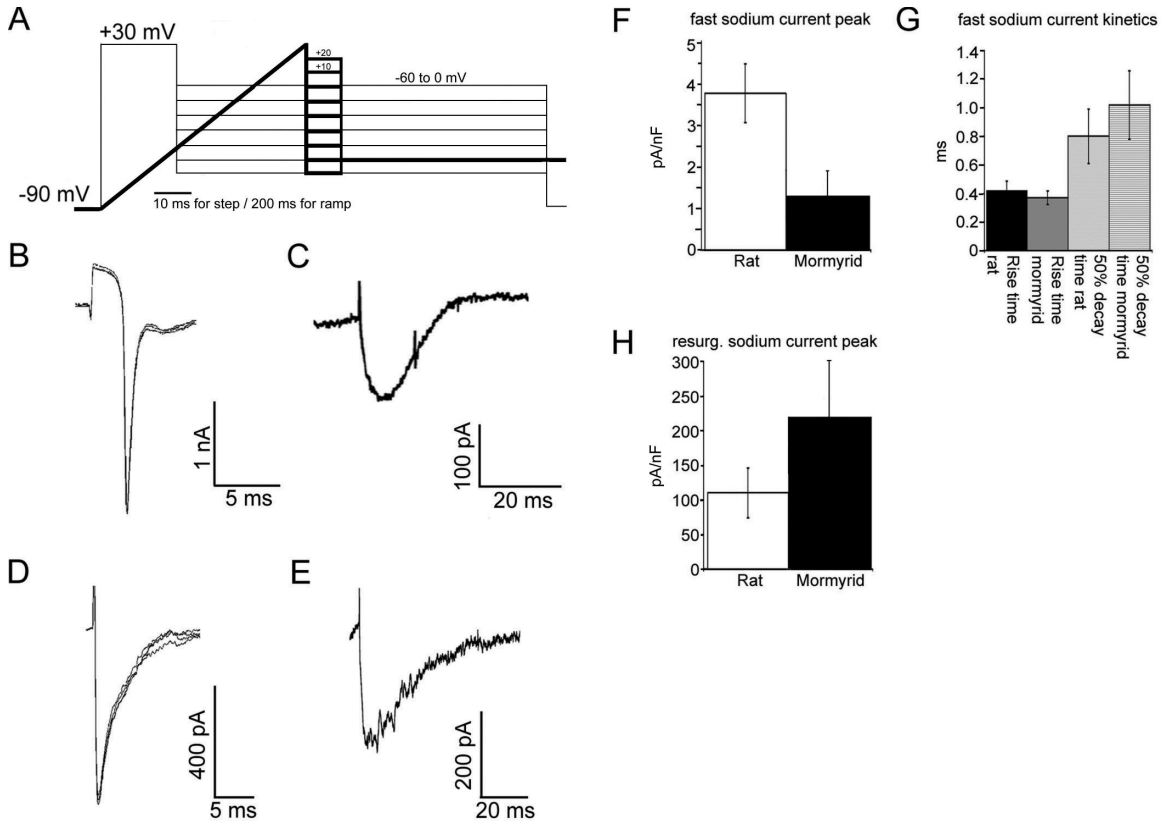

Figure 7: Fast-inactivating and resurgent Na^+ currents recorded from rat and mormyrid fish cerebellar Purkinje neurons in slices. **A:** Voltage step and voltage ramp protocols used to elicit Na^+ currents. Note the different time scales. **B:** Three consecutive TTX-subtracted fast Na^+ current traces recorded 20 seconds apart during voltage steps from –90 to +30 mV from a rat Purkinje cell. **C:** TTX-subtracted resurgent Na^+ current recorded from a rat Purkinje cell during a step from +30 to –30 mV. **D:** Same as in B but from mormyrid Purkinje cell. **E:** Same as in C but from mormyrid Purkinje cell. **F:** Peak fast Na^+ current recorded from rat (average +/- SEM, n = 3) and mormyrid (average +/- SEM, n = 5) Purkinje cells in slices. **G:** Fast Na^+ current kinetics recorded from rat (average +/- SEM, n = 3) and mormyrid (average +/- SEM, n = 5) Purkinje cells in slices. **H:** Peak resurgent Na^+ current recorded from rat (average +/- SEM, n = 7) and mormyrid (average +/- SEM, n = 6) Purkinje cells in slices.

The resemblance between our slice data and previously published work on slices (Afshari et al., 2004) is again striking. In rat Purkinje cells, the amplitude of the resurgent current was 110.32 ± 36.19 pA/nF (±SEM) (n = 4, all TTX-subtracted, ramp protocol, -30 mV) (Figure 7H). In mormyrid Purkinje cells, the resurgent Na^+ current reached 219.30 ± 82.33 pA/nF (±SEM) (n = 4, all TTX-subtracted, ramp protocol, -30

mV) (Figure 7H) ($p > 0.05$, Mann-Whitney U test). No attempt was made to quantify the voltage dependence, or kinetics, of the resurgent currents in slices because the voltage at which the peak amplitude was measured, and the kinetics of the resurgent current, varied from cell to cell probably due to space clamp problems. In all recordings, however, the voltage-dependence of the resurgent current was clearly seen. There was no difference in the input resistance between rat and mormyrid Purkinje cells in slices (rat: 84.8 $\pm$ 18.5 MΩ; n = 5; fish: 81.3 $\pm$ 13.1 MΩ; n = 5; $p > 0.05$, Mann-Whitney U test; data not shown).

Discussion

The dendritic tree architecture of Purkinje cells and their electrophysiological characteristics differ substantially between mormyrid fish and mammals. These differences motivated us to better characterize Purkinje cells of the mormyrid fish *Gnathonemus petersii* using immunohistochemical as well as electrophysiological approaches. In this initial study, we focused on Na^+ currents, because the most striking electrophysiological differences are related to Na^+ spike activity, namely a) unusually low Na^+ spike amplitudes and b) the absence of complex spikes, including their fast, initial Na^+ spike component.

Our immunohistochemical experiments show that the Na^+ channel α-subunits $Na_v1.1$, 1.2 and 1.6 are present in comparable densities and locations in the mormyrid and rat cerebellum (Figures 3, 4, 5). $Na_v1.1$ is expressed in Purkinje cell somata, but the staining in the molecular layer is weak and does not allow to resolve dendrites. In mammalian Purkinje cells, Na^+ action potentials do not backpropagate into the dendrite, which is partially due to a low dendritic Na^+ channel density (Stuart and Häusser, 1994). Our observations raise the question whether or not $Na_v1.1$ channels need to be present at a certain density to allow action potentials to backpropagate into the dendrites. Of the three types of Na^+ channel α-subunits, only $Na_v1.1$ is also expressed in somata in the granule cell layer of both species. In contrast to the $Na_v1.1$ subunits, $Na_v1.2$ and 1.6 were found to be densely expressed in somata of both rat and mormyrid Purkinje cells as well as in the molecular layer. We cannot rule out the possibility that the staining in the molecular layer reflects the expression of these Na^+ channel α-subunits in PF terminals. This, however, is unlikely as no staining was found in somata or axons of granule cells. The expression of $Na_v1.2$ in mammalian Purkinje cells has been debated (Black et al., 1994; Felts et al., 1997; but see Brysch et al., 1991; Gong et al., 1999; for review see Schaller and Caldwell, 2003). Our data indicate that $Na_v1.2$ is expressed in somata and dendrites of rat Purkinje cells and thus support the findings of Waxman and colleagues (Black et al., 1994; Felts et al., 1997). $Na_v1.6$ channels were strongly expressed in somata and dendrites of rat and fish Purkinje cells as well. So far, the resurgent Na^+ current, which is attributed to $Na_v1.6$ channels, has been described on the basis of somatic patch-clamp recordings (Raman and Bean, 1997, 2001). Our data suggest that this current exists in the dendrites as well.

Next, we conducted voltage-clamp experiments to investigate whether the Na^+ channels found to be expressed in the mormyrid cerebellum could mediate the same set of voltage-gated conductances as the Na^+ channels expressed in rat Purkinje cells. The present results show that a depolarizing voltage step activates a TTX-

sensitive, fast-inactivating Na^+ current in dissociated Purkinje cells of both rats and mormyrid fish, which is followed by a low amplitude tail component in slice recordings. While the fast-inactivating current was clearly present in both preparations, it reached higher amplitudes in rat than in mormyrid Purkinje cells in slices. Using a voltage step (dissociated cells and slices) or a ramp (slices only) protocol, we could demonstrate a TTX-sensitive resurgent Na^+ current in both rats and fish, which strongly resembled the resurgent Na^+ current described earlier (Raman and Bean, 1997; Afshari et al., 2004). The resurgent currents had indistinguishable amplitudes in rat dissociated cells compared to mormyrid cells after capacitance compensation ($p > 0.05$, Mann-Whitney U rank test) and these amplitudes were well in the range of data published earlier (Raman and Bean, 1997; Afshari et al., 2004) Rise and decay time constant ranges in the two species were overlapping and were also similar to what has been published before (Raman and Bean, 1997; Afshari et al., 2004). The recordings in slices were added to demonstrate that the resurgent currents are indeed present in Purkinje cells (as they cannot be distinguished with certainty from similar cells once being dissociated) under more physiological conditions (without their dendrites being cut). Resurgent Na^+ currents have so far been described in only a limited number of different types of neurons. In the cerebellum, they were described in Purkinje cells (Raman and Bean, 1997), unipolar brush cells (Mossadeghi and Slater, 1998; Afshari et al., 2004), deep cerebellar nuclei cells (Afshari et al., 2004) and granule cells (D'Angelo et al., 2001; Afshari et al., 2004). Our results show that mormyrid Purkinje cells, which otherwise differ in several morphological and physiological parameters from their mammalian counterparts, can be added to the list.

We have performed all immunohistochemical and electrophysiological experiments in slices or dissociated neurons from both rats and mormyrid fish to allow for a direct comparison. While there are obvious differences in electrophysiological response characteristics, we did not detect differences in the expression pattern of $Na_v1.1$, $Na_v1.2$ or $Na_v1.6$ subunits, or in fast-inactivating or resurgent Na^+ currents. While these observations allow us to conclude that the different electrophysiology is not due to differences in the functional expression pattern of these three types of Na channel α-subunits, they do not allow any conclusion what other parameters are causing these differences instead. Possible candidates are differences in the expression pattern of voltage-gated K^+ or Ca^{2+} channels, or the different dendrite morphologies (see also Mainen and Seijnowski, 1996; Vetter et al., 2001).

Two types of electrophysiological differences were of particular interest to us, namely the absence of complex spikes in mormyrid Purkinje cells and their low-amplitude Na^+ spikes. The complex spike received attention following recent demonstrations of synaptic plasticity at the CF synapses, involving long-term changes of slow complex spike components (Hansel and Linden, 2000; Hansel et al., 2001; Weber et al., 2003). These results stimulated some interest in the ionic composition of the slow complex spike components (for a discussion see Schmolesky et al., 2002). It has been suggested that resurgent Na^+ currents might be characteristic for types of rapidly firing neurons (Afshari et al., 2004) and might allow Purkinje cells to generate the high-frequency spikelets that make up the late complex spike components (Raman et al., 1997; Schmolesky et al., 2002). Our results show that, while mormyrid Purkinje cells do not fire complex spikes, they still show resurgent Na^+ currents. What other parameters might then cause the absence of complex spikes in mormyrid

Purkinje cells? As we argued above, the unique dendrite morphology might be involved, but at this point we simply do not understand the impact of this parameter on spike patterns sufficiently well to argue what specific features of mormyrid Purkinje cell dendrites would prevent complex spike firing. Moreover, burst firing (as in complex spikes) can also be evoked in dissociated Purkinje cells (Swensen and Bean, 2003). This observation does not exclude an impact of the dendrite morphology on the occurrence or waveform of complex spikes, but it shows that this characteristic all-or-none response of mammalian Purkinje cells can be evoked in isolated somata. The observed difference in the CF EPSC amplitude (Figure 1D) could also play a role in the different response patterns. Our recordings of CF responses of different amplitudes and at different membrane potentials allow us, however, to exclude the possibility that this phenomenon is solely related to the spike threshold.

Interestingly, the initial complex spike component, attributed to a somatic Na^+ spike, is completely absent in mormyrid Purkinje cells. Na^+ spikes can be recorded in these neurons, but they do not reach the amplitudes seen in other types of neurons and typically stay below 30 mV. While qualitatively the same types of Na^+ conductances were present in Purkinje cells of rat and mormyrid fish, the fast-inactivating current was smaller in slices obtained from mormyrid fish than in rat slices. The smaller amplitude of the fast-inactivating Na^+ conductances in mormyrid fish could explain the absence of full-scale Na^+-spikes. We consider this unlikely, however, as our dissociated cell recordings (which are quantitatively more accurate) indicate that the amplitudes of the fast-inactivating currents did not differ and still reach amplitudes in the range of 180 pA/pF in mormyrid Purkinje cells, whereas the spike height was often <10 mV. Therefore, we consider it more likely that the difference in Na^+ spike amplitudes has morphological causes. For example, the thin, unmyelinated axons of mormyrid Purkinje cells might reduce axonal spike propagation from the axonal spike initiation zone towards the soma (see also Han and Bell, 2003), where the spikes were recorded.

Purkinje cells of mormyrid fish are very interesting for reasons that go beyond the described differences in synaptic responses and in Na^+ spike activity. They are, for example, optimally suited to study the impact of dendritic tree architecture (e.g. degree of dendritic branching) on dendritic integration and spike propagation (see Vetter et al., 2001). Further studies on the expression profiles of voltage-dependent ion channels will be necessary to better understand what electrophysiological or morphological parameters critically contribute to the unique response features of mormyrid Purkinje cells.

Acknowledgements

We are grateful to P. French, E.D. Haasdijk, A. Vlug and E. Teuling for their excellent technical assistance and we thank Drs. C.C. Bell, V.Z. Han and D. Jaarsma for helpful discussions and comments on the manuscript. This work was supported by grants from the Netherlands Organization for Scientific Research, NWO-MW 903.47.190 (to C.I.D.Z), NWO-ALW 812.07.006 (to C.H.) and the Royal Dutch Academy of Sciences (to C.H.).

Afshari FS, Ptak P, Khaliq ZM, Grieco TM, Slater NT, McCrimmon DR, Raman IM. 2004. Resurgent Na currents in four classes of neurons of the cerebellum. J Neurophysiol 92:2831-2883.

Bell CC, Han VZ, Sugawara Y, Grant K. 1997a. Synaptic plasticity in a cerebellum-like structure depends on temporal order. Nature 387:278-281.

Bell CC, Caputi A, Grant K. 1997b. Physiology and plasticity of morphologically identified cells in the mormyrid electrosensory lobe. J Neurosci 17:6409-6423.

Black JA, Yokoyama S, Higashida H, Ransom BR, Waxman SG. 1994. Sodium channel mRNAs I, II and III in the CNS: cell-specific expression. Brain Res Mol Brain Res 22:275-289.

Brysch W, Creutzfeldt OD, Luno K, Schlingensiepen R, Schlingensiepen KH. 1991. Regional and temporal expression of sodium channel messenger RNAs in the brain during development. Exp Brain Res 86:562-567.

Callaway JC, Ross WN. 1997. Spatial distribution of synaptically activated sodium concentration changes in cerebellar Purkinje neurons. J Neurophysiol 77:145-152.

D'Angelo E, Nieus T, Maffei A, Armano S, Rossi P, Taglietti V, Fontana A, Naldi G. 2001. Theta-frequency bursting and resonance in cerebellar granule cells: experimental evidence and modeling of a slow K^+-dependent mechanism. J Neurosci 21:759-770.

Do MT, Bean BP. 2004. Sodium currents in subthalamic nucleus neurons from $Na_v1.6$-null mice. J Neurophysiol 92(2):726-733.

Felts PA, Yokoyama S, Dib-Haij S, Black JA, Waxman SG. 1997. Sodium channel α-subunit mRNAs I, II, III, NaG, Na6 and hNE (PN1): different expression patterns in developing rat nervous system. Brain Res Mol Brain Res 45:71-82.

Gähwiler BH, Llano I. 1989. Sodium and potassium conductances in somatic membranes of rat Purkinje cells from organotypic cerebellar cultures. J Physiol 417:105-122.

Garcia KD, Sprunger LK, Meisler MH, Beam KG. 1998. The sodium channel Scn8a is the major contributor to the postnatal developmental increase of sodium current density in spinal motoneurons. J Neurosci 18:5234-5239.

Gong B, Rhodes KJ, Bekele-Arcuri Z, Trimmer JS. 1999. Type I and type II Na(+) channel α-subunit polypeptides exhibit distinct spatial and temporal patterning, and association with auxiliary subunits in rat brain. J Comp Neurol 412:342-352.

Grieco TM, Afshari FS, Raman IM. 2002. A role for phosphorylation in the maintenance of resurgent sodium current in cerebellar Purkinje neurons. J Neurosci 22:3100-3107.

Grieco TM, Raman IM. 2004. Production of resurgent current in $Na_v1.6$-null Purkinje neurons by slowing sodium channel inactivation with β-pompilidotoxin. J Neurosci 24:35-42.

Groenewegen HJ, Voogd J. 1977. The parasagittal zonation within the olivo-cerebellar projection. I. Climbing fiber distribution in the vermis of cat cerebellum. J Comp Neurol 174:417-488.

Han VZ, Grant K, Bell CC. 2000. Reversible associative depression and non-associative potentiation at a parallel fiber synapse. Neuron 27:611-622.

Han VZ, Bell CC. 2003. Physiology of cells in the central lobes of the mormyrid cerebelum. J Neurosci 23(35):11147-11157.

Hansel C, Linden DJ. 2000. Long-Term Depression of the Cerebellar Climbing Fiber Purkinje Neuron Synapse. Neuron 26:473-482.

Hansel C, Linden DJ, D'Angelo E. 2001. Beyond parallel fiber LTD: the diversity of synaptic and non-synaptic plasticity in the cerebellum. Nature Neurosci 4:467-475.

Häusser M. 2003. Revealing the properties of dendritic voltage-gated channels: a new approach to the space clamp problem. Biophys J 84:3497-3498.

Isom LL, Ragsdale DS, De Jongh KS, Westenbroek RE, Reber BF, Scheuer T, Catterall WA. 1995a. Structure and function of the beta 2 subunit of brain sodium channels, a transmembrane glycoprotein with a CAM motif. Cell 83:433-442.

Isom LL, Scheuer T, Brownstein AB, Ragsdale DS, Murphy BJ, Catterall WA. 1995b. Functional co-expression of the beta 1 and type IIA α-subunits of sodium channels in a mammalian cell line. J Biol Chem 270:3306-3312.

Kay AR, Sugimori M, Llinas R. 1998. Kinetic and stochastic properties of a persistent sodium current in mature guinea pig cerebellar Purkinje cells. J Neurophysiol 80:1167-1179.

Khaliq ZM, Gouwens NW, Raman IM. 2003. The contribution of resurgent sodium current to high-frequency firing in Purkinje neurons: an experimental and modeling study. J Neurosci 23:4899-4912.

Koulen P, Janowitz T, Johnston LD, Ehrlich BE. 2000. Conservation of localization patterns of IP(3) receptor type 1 in cerebellar Purkinje cells across vertebrate species. J Neurosci Res 61:493-499.

Llinas R, Sugimori M. 1980a. Electrophysiological properties of in vitro Purkinje cell somata in mammalian cerebellar slices. J Physiol 305:171-195.

Llinas R, Sugimori M. 1980b. Electrophysiological properties of in vitro Purkinje cell dendrites in mammalian cerebellar slices. J Physiol 305:197-213.

Mainen ZF, Sejnowski TJ. 1996. Influence of dendritic structure on firing pattern in model neocortical neurons. Nature 382(6589):363-366.

Meek J, Nieuwenhuys R. 1991. Palisade pattern of mormyrid Purkinje cells: a correlated light and electron microscopic study. J Comp Neurol 306:156-192.

Meek J. 1992. Comparative aspects of cerebellar organization. Eur J Morphol 30:37-51.

Mossadeghi B, Slater NT. 1998. Persistent and resurgent sodium currents in cerebellar unipolar brush cells. Soc Neurosci Abstr 24:1078.

Nieuwenhuys R, Nicholson C. 1967. Cerebellum of mormyrids. Nature 215:764-765.

Nieuwenhuys R, Nicholson C. 1969. Aspects of the histology of the cerebellum of mormyrid fishes. In: Neurobiology of Cerebellar Evolution and Development, edited by Llinas R. Am Med Ass Educ & Res Found, Chicago, IL, pp. 135-169.

Pan F, Beam KG. 1999. The absence of resurgent sodium currents in mouse spinal neurons. Brain Res 849:162-168.

Raman IM, Bean BP. 1997. Resurgent Sodium Current and Action Potential Formation in Dissociated Cerebellar Purkinje Neurons. J Neurosci 17:4517-4526.

Raman IM, Sprunger LK, Meisler MH, Bean BP. 1997. Altered subthreshold sodium currents and disrupted firing patterns in Purkinje neurons of Scn8a mutant mice. Neuron 19:881-891.

Raman IM, Bean BP. 2001. Inactivation and recovery of sodium currents in cerebellar Purkinje neurons: evidence for two mechanisms. Biophys J 80:729-737.

Renganathan M, Gelderblom M, Black JA, Waxman SG. 2003. Expression of $Na_v1.8$ sodium channels perturbs the firing patterns of cerebellar Purkinje cells. Brain Res 959:235-242.

Saper CB, Sawchenko PE. 2003. Magic peptides, magic antibodies: guidelines for approriate controls for immunohistochemistry. J Comp Neurol 465:161-163.

Schaller KL, Caldwell JH. 2003. Expression and distribution of voltage-gated sodium channels in the cerebellum. The Cerebellum 2:2-9.

Schmolesky MT, Weber JT, De Zeeuw CI, Hansel C. 2002. The making of a complex spike: ionic composition and plasticity. Ann N Y Acad Sci 978:359-390.

Sharp AH, Nucifora FC Jr, Blondel O, Sheppard CA, Zhang C, Snyder SH, Russell JT, Ryugo DK, Ross CA. 1999. Differential cellular expression of isoforms of inositol 1,4,5-triphosphate receptors in neurons and glia in brain. J Comp Neurol 406:207-220.

Stuart G, Häusser M. 1994. Initiation and spread of sodium action potentials in cerebellar Purkinje cells. Neuron 13:703-712.

Swensen AM, Bean BP. 2003. Ionic mechanisms of burst firing in dissociated Purkinje neurons. J. Neurosci. 23:9650-9663.

Vega-Saenz De Miera E, Rudy B, Sugimori M, Llinas R. 1997. Molecular characterization of the sodium channel subunits expressed in mammalian cerebellar Purkinje cells. Proc Natl Acad Sci USA 94:7059-7064.

Vetter P, Roth A, Häusser M. 2001. Propagation of action potentials in dendrites depends on dendritic morphology. J Neurophys 85:926-937.

Weber JT, De Zeeuw CI, Linden DJ, Hansel C. 2003. Long-term depression of climbing fiber-evoked calcium transients in Purkinje cell dendrites. Proc Natl Acad Sci USA 100:2878-2883.

Westenbroeck RE, Merrick DK, Catterall WA. 1989. Differential subcellular localization of the RI and RII Na channel subtypes in central neurons. Neuron 3:695-704.

Zenisek D, Henry D, Studholme K, Yazulla S, Matthews G. 2001. Voltage-dependent sodium channels are expressed in nonspiking retinal bipolar neurons. J Neurosci 21(13):4543-4550.

Chapter 3

Analysis of backpropagation and plasticity in interneurons of the mormyrid ELL

J Engelmann, E van den Burg, J Bacelo, MM de Ruiter, C Hansel, K Grant, Y Sugawara

Abstract

Immunocytochemical and electrophysiological techniques were used to localize TTX-sensitive voltage-gated sodium channels (VGSCs) over the soma-dendritic axis of cells in the electrosensory lateral line lobe (ELL) of weakly electric fish (*Gnathonemus petersii*). Dense labelling was detected on the membranes of efferent somata as well as on medium ganglionic cells, GABAergic interneurons of the ELL. VGSC labelling was detected over the entire extent of apical dendrites, with a similar α-subunit distribution as in Purkinje cells of the mammalian cerebellum.

Intracellular recordings from efferent and interneuron cell somata were obtained using an in vitro ELL slice preparation. Tetrodotoxin (TTX)-sensitive potentials were identified by focal pressure ejection of TTX at somatic and/or dendritic levels. These recordings demonstrated the presence of dendritic and somatic action potentials in interneurons of the ELL. Dendritic spikes could propagate both in a retrograde and anterograde fashion. The backpropagation was active over at least the inner half of the molecular layer as determined by the conduction of an antidromic population spike and focal TTX ejections. The sculpting of these backpropagating action potentials by potassium channels was investigated by aid of several blockers and voltage-sensitive dye measurements. The possible role of GABA as a retrograde messenger in the formation of anti-Hebbian plasticity, which depends on the generation of backpropagating spikes, was investigated. The results indicate that, although the dendrites of the interneurons contain high concentration of GABA, dendritic release of GABA following backpropagating events is not essential for the observed plasticity.

Introduction

The electrosensory lobe of *Gnathonemus petersii*, a mormyrid electric fish, is a cerebellum-like sensory structure that removes predictable features of electrosensory input following anti-Hebbian rules (Bell et al., 1997b). Plasticity is mediated by associative depression at synapses between parallel fibers and Purkinje-like interneurons (MG cells) and requires NMDA receptor activation, changes in postsynaptic calcium and especially, the occurrence of a postsynaptic broad action potential (AP) within a few milliseconds following excitatory postsynaptic potential (EPSP) onset as recorded in the soma (Han et al., 2000). Since the site of the plastic changes presumably is in the apical dendrites, where the parallel fiber input reaches the MG cells, it is of importance how the generation of the broad spikes is able to mediate the anti-Hebbian plasticity in these MG cells.

A previous study (Gomez et al., 2005), based on field potential recordings, proposed that the broad spikes actively propagate back into the apical dendritic arbor and thereby link the sensory input arriving at the basal dendrites with the parallel fiber input arriving at the apical dendrites. The time-locked backpropagation of a broad spike in the dendrites following parallel fiber activation would thereby lead to a prolonged depolarization via NMDA-channels in the dendrites, enabling plasticity. However, clear evidence for the backpropagation of broad spikes is still lacking.

Using dendritic recordings, backpropagation has been shown in a variety of neurons. While cerebellar Purkinje cells show only weak, almost passive backpropagation (Stuart and Sakmann, 1994), the dendrites of dopaminergic substantia nigra neurons (Hausser et al., 1995) and mitral cell apical dendrites (Bischofberger and Jonas, 1997) show almost un-attenuated backpropagation. Decremental propagation was found in a variety of neurons, including apical dendrites of L5 pyramidal cells (Kim and Connors, 1993; Stuart and Sakmann, 1994; Williams and Stuart, 2000b), hippocampal CA1 pyramidal cells (Andreasen and Lambert, 1995; Spruston et al., 1995) and thalamocortical neurons (Williams and Stuart, 2000a).

While the above results were all obtained in vitro, the question of the relevance of backpropagation in vivo is presently unsettled. For example, Steriade (Steriade, 2001) argued that synaptic input to dendrites in vivo would abolish backpropagation. Initial in vivo studies concluded that backpropagation was passive in neocortical layer 2/3 pyramidal neurons (Helmchen et al., 1999; Svoboda et al., 1999). Yet, these results are contrasted by other studies concluding that backpropagation occurs despite background synaptic activity in vivo (Buzsaki and Kandel, 1998; Helmchen et al., 1996; Waters et al., 2003).

The conditions which promote backpropagation have been investigated at the ionic basis in a variety of cell types (Reyes, 2001). The major conductances found in almost all cells with active backpropagation are dendritic sodium channels and possibly also calcium channels. The role of potassium channels has also been studied. In both CA1 (Hoffman et al., 1997) and neocortical L5 pyramidal neurons (Bekkers, 2000; Korngreen and Sakmann, 2000), A-type channels were shown to be present in the apical dendrites. Pharmacological blockade of these channels in CA1 pyramidal cells promoted backpropagation, demonstrating their importance in limiting dendritic AP propagation. In contrast, the density of A-type channels in L5 pyramidal neurons decreases with distance from the soma, rendering the distal dendrite more excitable than proximal regions.

Backpropagation of somatic action potentials has been attributed to a number of functions, including synaptic plasticity and associated transient increases in dendritic calcium concentrations (Bell et al., 1997a; Golding et al., 2002; Markram et al., 1997), lowering of the threshold for the induction of dendritic regenerative events (Larkum et al., 1999; Schiller et al., 1995; Schiller et al., 1997) and the release of transmitters from dendrites as seen in the olfactory bulb (Margrie et al., 2001; Schoppa and Westbrook, 2001; Urban and Sakmann, 2002).

Hence, in this study, we focused on the role of voltage-activated Na^+ channels, K^+ channels and Ca^+ channels for the properties of the broad AP of MG cells. Using voltage-sensitive dye (VSD) measurements, intracellular recordings, pharmacological procedures and immunohistochemistry we addressed the role of K^+ and voltage-gated Na^+ channels in the propagation of action potentials in the dendritic tree of MG cells.

Materials and methods

A total of 16 *Gnathonemus petersii* were used for the experiments. Their body lengths ranged from 6.8 to 13 cm. The procedures to isolate and slice the ELL were according to Grant et al. 1998 (Grant et al., 1998) with minor modifications. Briefly, the ELL was collected in ice-cold low-sodium artificial CSF, containing (in mM): NaCl 0, KCl 2.5, $NaH_2PO_4.H_2O$ 1.25, $NaHCO_3$ 24, $CaCl_2$ 2, $MgSO_4.7H_2O$ 2, glucose 10, and sucrose 210. The tissue was cut transversally into 300-500 µm thick slices in ice-cold low-sodium aCSF; the cutting plane was tilted 10° from horizontal. The slices were collected in low-sodium aCSF at room temperature (23 - 25°C), and then transferred to an incubation chamber. They were immersed in medium-sodium/high-magnesium solution containing (in mM): NaCl 58, KCl 2.5, $NaH_2PO_4.H_2O$ 1.25, $NaHCO_3$ 24, $CaCl_2$ 2, $MgSO_4.7H_2O$ 2, glucose 10, and sucrose 105. After 20 min the slices were immersed in the same buffer with sucrose being replaced by 116 mM NaCl for 45 min. Then the slices were immersed in normal aCSF which was composed of (in mM): NaCl 116, KCl 2.5, $NaH_2PO_4.H_2O$ 1.25, $NaHCO_3$ 24, $CaCl_2$ 2, $MgSO_4.7H_2O$ 1.2, and glucose 10. All solutions were bubbled with carbogen. The pH was 7.3-7.4 and the osmolarity was ~280 mOsm. Following these steps slices were either transferred into a super fusion chamber for intracellular recordings or into an immersed slice chamber for the voltage-sensitive dye measurements. Perfusion was 1-3 ml/min by gravity flow.

Recording and stimulation

The eminentia granularis posterior (EGp) or molecular layer was stimulated with bipolar (intracellular data) or monopolar (VSD measurements) tungsten electrodes. The tips of these electrodes were slightly scraped to remove insulation, and then plated with gold to minimize polarization. Stimulation strength was 3–20 µA. For field potential recordings and voltage-sensitive dye measurements, the EGp or parallel fibers were stimulated twice with an interval of 30-80 ms every two seconds.

Intracellular recordings (Axoclamp 2B) were made with sharp microelectrodes filled with 2 M potassium methylsulphate (Sigma) containing 2% biocytin (Sigma). The resistance of the microelectrodes ranged from 140-220 MΩ. Input resistance was estimated by injecting hyperpolarizing current pulses and the bridge was balanced at all times.

For the VSD measurements, slices were incubated for two minutes in DiI-4- Anepps (2 mM). Following a washout of accessory dye, slices were transferred to a super fusion chamber under a microscope (Nikon Eclipse E600FN) equipped with an Olympus objective (XL-Flour 4 times, N.A. 0.28) and a sensitive CCD camera (MiCam CCD). Video signals were collected using MiCam software (BrainVision 1.1) in combination with a shutter (Oriel 71445) and an Oriel illumination system with a 510-560 nm excitation filter (Thermo Oriel). The maximal frame rate achievable with this set-up was 1.3 kHz. As a compromise between signal intensity and temporal resolution we used 1 or 2 ms of integration time per frame. The maximum sampling time per stimulus was 254 ms, i.e. 400 frames per trial and for each trial 30 ms pre-stimulus were recorded. The repetition rate for a given stimulus was 0.5 Hz and for each condition 10-40 trials were conducted.

Drug application

Drugs were either applied locally (Picospritzer III, Intracell) (intracellular recordings: TEA, TTX and 4-AP), or bath applied (VSD recordings: TEA, nickel, cadmium). All drugs were bought from Sigma. For bath applications the following concentrations were used: 8 mM TEA, 100 µM cadmium. Local applications of TEA were done with 4-20 mM solutions, 4-AP was applied at a concentration of 20 mM and TTX at a concentration of 5 mM (all diluted in working aCSF).

Immunohistochemistry

To further address the distribution of voltage-activated sodium channels in the ELL, fish were used for immunohistochemistry. Following deep anesthesia with MS-222 (1:10,000), fish were perfused intracardially with 20 ml phosphate buffered saline (PBS), followed by 3% paraformaldehyde (w/v in PBS) and 1% Glutardialdehyde. Brains were postfixed overnight and cut following standard procedures on a vibratome (40-70 µm) or using a cryostat (12 µm). If not noted otherwise, all steps were conducted at room temperature.

Immunofluorescence

After cutting, slices were washed in 0.1 M phosphate buffer (PB) (pH 7.4) and pre-incubated for 1 hour in PB containing 3% bovin serum albumin. Following this step, sections were incubated in blocking medium (1% normal goat serum and 0.3% Triton X-100) for one hour. Sections were incubated with the primary antibody (PAN sodium antibody 1:400 Sigma S 6936, anti-K_v3.3 antibody 1:700, gift from Prof. R. Dunn, see Rashid et al., 2001b; Seybold et al., 1999 for specificity of the antibody) for 3-4 hours at room temperature followed by 20 hours of incubation at 4 degrees in the same blocking solution. Following incubation, sections were washed three times for 15 minutes in PBS. For immunofluorescence processing, sections were incubated for 4-20 hours using Oregon green (1:300, Molecular Probes) diluted in blocking solution. After three more washes in PB, sections were mounted using Vectashield with DAPI.

Immunoperoxidase

Sections were treated identical except for a pre-treatment to block the endogenous peroxidase activity following cutting. For this pre-treatment the sections were immersed in 50% ethanol for 10 minutes, followed by 70% ethanol for 15 minutes and a secondary incubation in 50% ethanol. After this treatment the incubation with the primary antibody was as described for the fluorescent protocol. Following the incubation in the primary antibody, sections were washed three times in the blocking solution and then treated according to previously published protocols (Han et al., 1999).

Data acquisition and analysis

Data obtained using single-cell recordings were stored after amplification (Axoclamp 2B amplifier) using Elphy acquisition software (G. Sadoc, CNRS), and analyzed off-line. Input resistance, membrane potential (Vm) and input-output functions were all analyzed off-line. For the VSD measurements the analysis was done off-line using the commercial software MiCam 1.1 (Brain Vision Inc, Japan). For comparing VSD measurements in the same slice, yet using different drugs, the peak excitation, latency to the stimulus and width at 50% amplitude were measured “on beam” of the stimulating electrode with a fixed distance of 150 μm from the insertion point.

Results

Immunohistochemistry

As active backpropagation greatly depends on voltage-gated sodium channels (VGSCs), we used immunohistochemical methods to study their distribution. Figure 1A shows the distribution of VGSCs in the ELL for a section where VGSCs were visualized using a green fluorescent secondary antibody. A magnification of a similar section treated with the DAB method and counterstained with cresyl-violet to enhance the visibility of the different layers of the ELL is shown in Figure 1E. Using fluorescent staining the molecular layer containing the apical dendrites of the cells in the ganglionic and upper granular layer was stained most strongly. In both fluorescent and DAB-treated material the labeling of the dendrites in the outer region of the molecular layer was stronger than in the inner molecular region. Probably the higher intensity of labeling is due to the higher number of dendrites in this part of the molecular layer, as the dendrites branch just at the border of the inner molecular layer, leading to an increase in membrane area. Another possible explanation could be an actual increase in the density of VGSCs in the outer molecular layer, i.e. in the region where the parallel fibers convey their input. Which of the explanations is accurate was not further investigated here.

The plexiform layer was intensely labeled. This was especially visible in the DAB-stained sections (Figure 1E). This was due to the axons and/or basal dendrites of cells in the ganglionic layer. The somata in the ganglionic layer, containing both MG interneurons and large efferent LG cells were intensely stained using either technique, while the deeper large fusiform (LF) cells were only seen in the fluorescent stained material. LF cells stood out due to positive terminals and fibers surrounding their somata. For LG and MG cells we found apical dendrites extending all through the molecular layer that were strongly labeled, while for the LF cells it was not possible to trace their apical dendritic tree, thus we do not know if their apical dendrites contain VGSCs.

Further analysis with subtype-specific antibodies (Figure 1B-D) revealed that the labeling found in the apical dendrites was specific for the $Na_v1.2$ and 1.6 subtypes, while $Na_v1.1$ was predominantly found in the ganglionic and granular layers. This is comparable to granule cells of the mammalian cerebellum which predominantly express $Na_v1.2$ and $Na_v1.6$, primarily localized in the granule cell parallel fibers. Purkinje cells express $Na_v1.1$ and $Na_v1.6$, the latter mainly in their apical dendrites

(Schaller and Caldwell, 2003). Thus our results show that at least MG and LG cells of the ELL possess VGSCs in their apical dendrites.

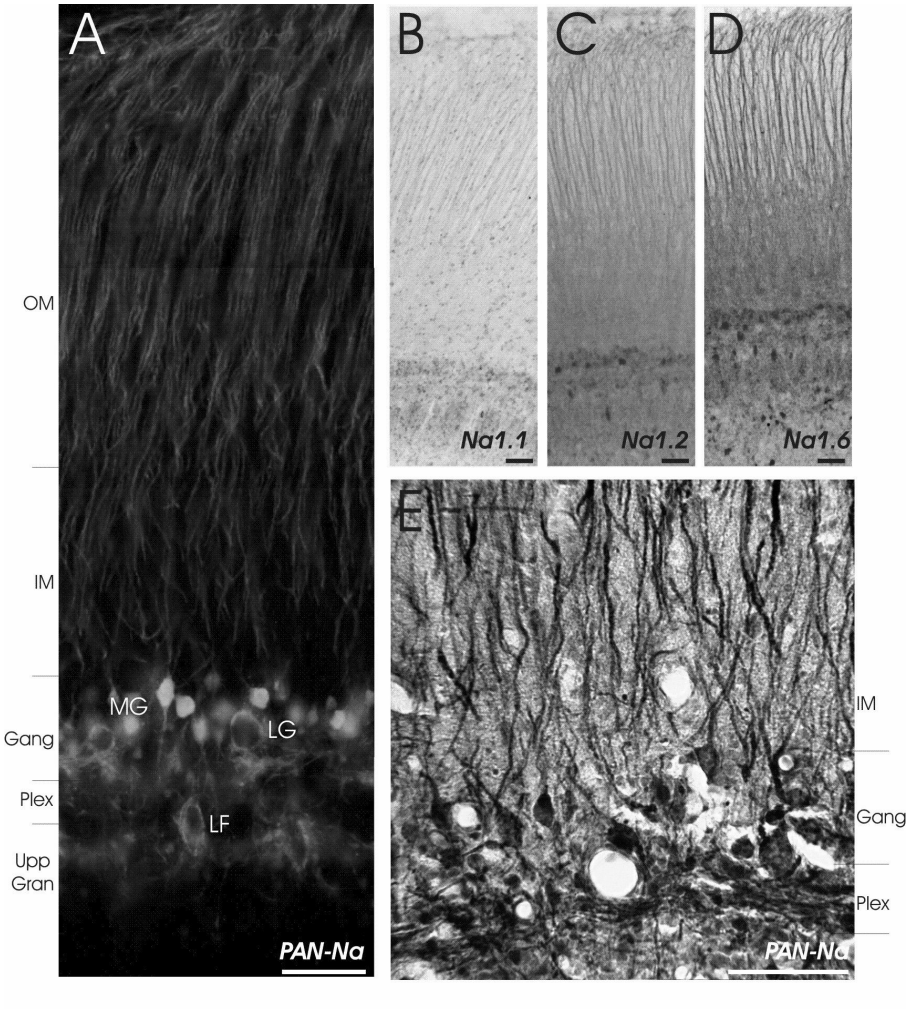

Figure 1: A-E: Immunohistochemistry using a polyclonal anti-voltage-gated sodium channel antibody (**A** and **E**) and subtype-specific voltage-gated sodium antibodies directed against $Na_v1.1$ (**B**), $Na_v1.2$ (**C**) and $Na_v1.6$ (**D**). **A:** Overview of the medial zone of the ELL. Note that the apical dendrites as well as the somata of ganglionic layer cells (MG and LG) are strongly labeled, while the somata of the large fusiform cells (LF) stand out due to synaptic terminations. When viewing the results using the same antibody processed with the ABD-DAB method (**E**), the plexiform layer of the ELL is also clearly stained, revealing the axons of ganglionic layer cells, most probably being MG cell axons. **B:** Using a monoclonal antibody targeted against the $Na_v1.1$ α-subunit of VGSCs results in relatively uniform staining of the granular, plexiform and ganglionic layers with weak staining in the outer molecular layers. $Na_v1.2$ (**C**) and $Na_v1.6$ (**D**) subtypes were strongly expressed in the apical dendrites in the outer molecular layer. Diffuse staining for $Na_v1.2$ was seen in the different cellular layers of the ELL and big somata in the ganglionic layer were strongly stained, probably resembling LG cells. The staining for $Na_v1.6$ also diffusely labeled all layers of ELL and led to additional staining of large fusiform somata in the upper granular layer, as well as different somata in the ganglionic and deep granular layers. Both $Na_v1.2$ and $Na_v1.6$ showed a relatively strong staining in the inner molecular layer, yet in contrast to the polyclonal VGSC antibody (see **A** and **E**) individual dendrites were not stained in this region. Note that neither antibody staining procedure resulted in positive labeling of the parallel fiber axons in the outer molecular layer, while the PAN antibody clearly stained fibers in the tract of the pre-eminential tract just dorsal to the ELL, which also were found in the outer molecular layer (data not shown). The scale bar in all cases has a length of 100 μm.

Notably, no VGSC staining was found in the parallel fibers. While the somata of the cells in the EGp that give rise to the parallel fibers were positive for PAN, $Na_v1.2$ and 1.6, no labeling was found in the parallel fibers running through the ELL (note Figure 1B-C). However, a second fiber tract overlying the ELL, the pre-eminential fibers, showed strong staining with the PAN antibody and individual fibers could be followed through the molecular layer (data not shown). A second major source of input to the granular layer of the ELL, the mormyromast afferents, were also not stained with these antibodies.

Role of VGSCs in MG cells

Based on the above observations we investigated the dependence of the two types of spikes, namely the spikelets and the broad spike on dendritic VGSCs. Earlier studies indicate that the broad spikes are generated in the apical dendrites of MG cells and actively propagate into the apical dendritic arbor (Gomez et al., 2005; Han et al., 2000). This idea is in line with the observation that plasticity at the parallel fiber/MG cell synapses depends on the generation of these broad spikes (Han et al., 2000).

To distinguish if the broad spikes are generated in the apical dendrites or in the basal dendrites/soma of MG cells we used local application of 5 mM TTX either in the molecular layer (n=3) or in the plexiform layer (n=2) while recording the responses of MG cells both to an artificial parallel fiber stimulus and to an intracellular current pulse. Figure 2 shows two examples.

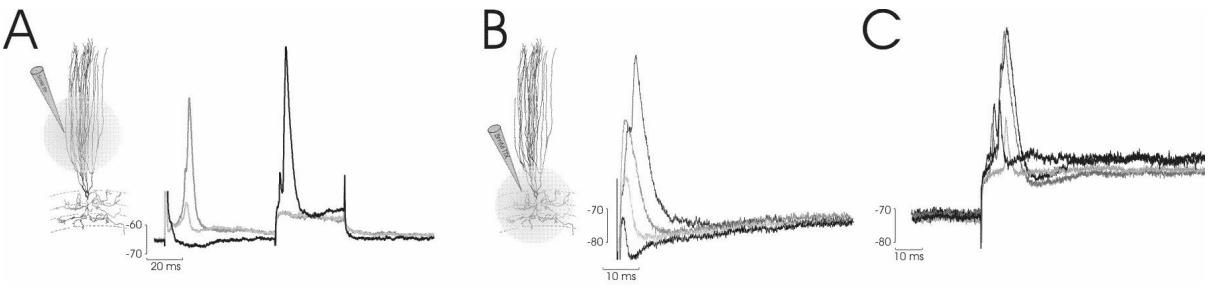

Figure 2: A-C: Effect of local application of tetrodotoxin (TTX) on the responses of MG cells to parallel fiber and current pulse stimulation. **A:** Application of TTX in the medial zone of the molecular layer (see schematic at left side). **B** and **C**. Application of TTX in the plexiform/ganglionic layers (see schematic in **B**).

Application of TTX in the molecular layer initially increased the threshold for evoking broad spikes by current injection, finally leading to a complete failure in evoking broad spikes while spikelets were still elicited. Likewise the response to the parallel fiber stimulus, which initially was a broad spike, turned into an inhibitory postsynaptic potential (IPSP) after the application of TTX. Spikelets in response to the current pulse were only abolished after an additional application of TTX in the plexiform /ganglionic layer. These results show that broad spikes are sodium-dependent, they

further indicate that their initiation site is the apical dendrites. To validate this we applied TTX in the plexiform layer first (Figure 2B,C). Both the broad spikes and the spikelets that initially could be elicited by the current injection could no longer be evoked, independent of current amplitude. In contrast, the response to the parallel fiber stimulus changed from an initial early excitatory postsynaptic potential (EPSP) followed by a long-lasting IPSP into an EPSP with broad spikes after the TTX application. These broad spikes finally decreased in amplitude and duration till only small depolarizing events were recorded. We interpret the change in response to the parallel fiber stimulus as due to the block by TTX of inhibitory input from neighboring cells onto the MG cell recorded. These findings show that the spikelets are sodium-dependent and are generated in the axon/soma. Furthermore, the finding that the broad spike was still elicited by the parallel fiber stimulus when no spikelets or broad spikes could be elicited by the current pulse indicates that broad spikes can be evoked in the apical dendrites and travel towards the soma. We interpret the slow decrease in the amplitude of the broad spike, in response to the parallel fiber stimulus following TTX application in the plexiform layer, as an indication that TTX slowly reached the apical dendrites by diffusion, thus inactivating the VGSCs in the apical dendrites. Consequently the weak EPSP-like event remaining after the blocking of the broad spikes might reflect the dendritic spikes reaching the recording site via electrotonic spread.

Role of K^+ channels

To address the role of K^+ channels in shaping the backpropagating and somatic action potentials of MG cells we applied different K^+ channel blockers while recording intrasomatically or using voltage-sensitive dye recordings.

Bath application of TEA (10 mM) led to a significant increase (Wilcoxon paired-test: $p < 0.03$, n=7) of broad spike width (3.7 ± 1.4 to 6.6 ± 3.8 ms, n=7) and peak amplitudes (54.1 ± 6.1 to 64.8 ± 9.1 mV, n=7). The width of the spikelets also increased (1.1 ± 0.2 to 2.3 ± 1.4 ms; Wilcoxon paired-test: $p = 0.04$, n=7) during TEA application, while spikelet amplitudes were not significantly (Wilcoxon paired-test: $p = 0.47$, n=7) altered by TEA. The longer repolarization times of the spikes, i.e. their increased width, was accompanied by an increase of the input resistance (12.8 ± 7.9 to 15.3 ± 8.4 MΩ, Wilcoxon paired-test: $p = 0.02$; n=7) and a decrease of the membrane potential (-71.6 ± 4.5 to -76.2 ± 3.1 mV, Wilcoxon paired-test: $p = 0.03$; n=7) as measured intra-somatically. Similar results were obtained when TEA was applied in the ganglionic/plexiform layer close to the recorded cells.

Voltage-sensitive dye measurements

To further investigate the signal processing in the apical dendrites in response to parallel fiber and deep fiber stimulation we used voltage-sensitive dye measurements.

Figure 3 shows the responses measured by this technique upon parallel fiber stimulation. Following the stimulus a local excitation spreads mainly horizontally through the molecular layer of the ELL. This excitation has a minimum latency (2 ms

to peak) and maximal amplitude (0.3 %dF) next to the stimulation electrode. It reaches the field potential (FP) recording electrode with about 1 ms latency (see black asterisk in the inset and corresponding black trace in Figure 3B) at a lower amplitude. The timing of this event and the simultaneously recorded FP indicates that the excitation seen in the VSD measurements coincides with the n2 wave of the FP. The n2 FP has been associated with postsynaptic activation and backpropagating events (van den Burg et al. in preparation), while n3 reflects backpropagating activity only (Gomez et al., 2005).

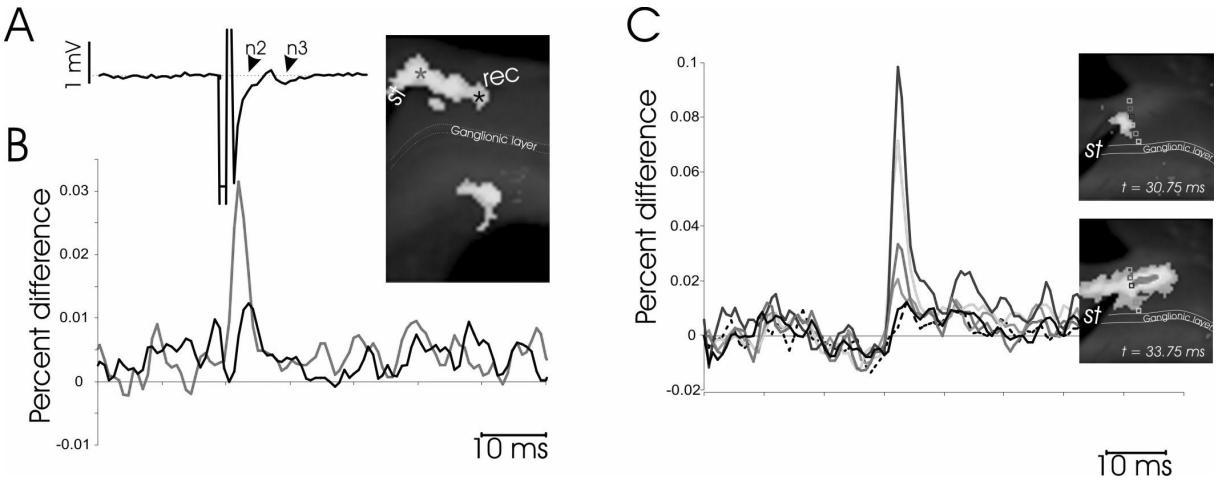

Figure 3: A-C: Example for the voltage-sensitive dye responses obtained with molecular layer stimulation. **A:** Field potential recorded "on beam" of the stimulating electrode in the molecular layer. The relative positions of stimulating and recording electrodes are indicated in the image of the slice on the right. Two events, termed n2 and n3 could be observed, The n3-wave has been attributed to the arrival of backpropagating broad spikes (Gomez et al., 2005). The change in voltage-sensitive dye excitation is shown in **B** for the two measuring windows situated next to the stimulating (gray *) and the recording (black *) electrode. **C:** Temporal and spatial evolution of the excitation following parallel fiber stimulation. The images at the right show the activity in the slice immediately after stimulation (top) and 3 ms after the stimulation (bottom). Note that excitation can be measured at the site of stimulation first and then extends both down towards the ganglionic layer and also laterally in the molecular layer.

Similar results were seen when the stimulating electrode was placed in the EGp instead of the direct stimulation reported above. However, this method needed longer sampling durations and higher stimulus amplitudes and thus all further data was obtained with the stimulating electrode in the molecular layer. The horizontal spread of the VSD-signal shown in Figure 3A was often accompanied by a vertical spread, as shown in Figure 3B. In these cases the signal that could be recorded at the level of the ganglionic layer was usually quite weak.

Deep fiber stimulation resulted either in local inhibition at the ganglionic layers, followed by excitation in the molecular layer (Figure 4), or only showed activation at the level of the molecular layer. The reason for this was not further investigated, but presumably it represents a columnar-like organization of inhibitory and excitatory networks within the ELL.

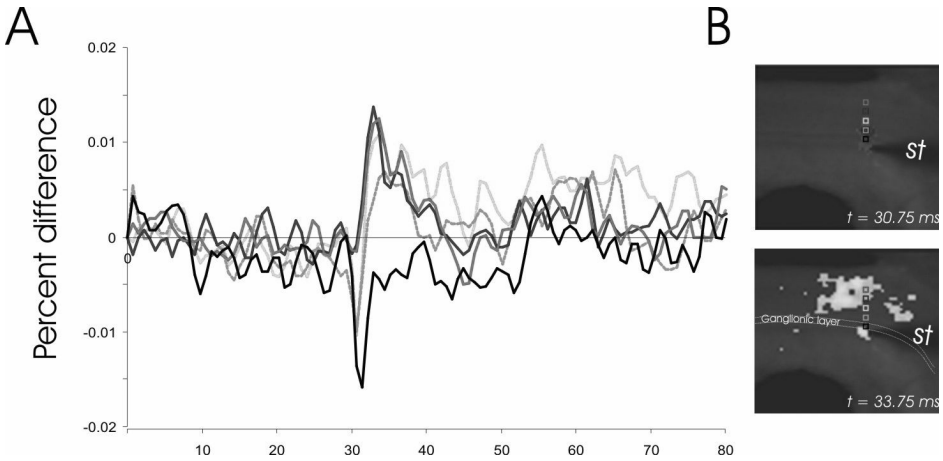

Figure 4: A-B: Example for the voltage-sensitive dye responses obtained with deep fiber stimulation. **A:** Temporal and spatial evolution of the excitation following parallel fiber stimulation. The different shades of gray apply to the positions in the transect through the ELL marked by the squares of the same shade of gray in **B**. **B:** The images show the activity in the slice immediately after stimulation (top) and 3 ms after the stimulation (bottom). Note that a decrease in activity was initially measured at the site of stimulation. This is followed by a spread of excitation that extends to the molecular layer.

For both kinds of stimulation we tested the effect of TEA (5-8mM) and cadmium (0.1 μM) on the extent of the VSD signal propagation and the VSD signal intensity. While single-cell recordings indicate that different types of K^+ channels are involved in shaping the broad spikes of both MG cells and efferent cells, this technique allowed us to estimate to which extent dendritic K^+ channels contribute to signal integration by sculpturing dendritic propagation within the ELL.

Application of TEA leads to an increased efficacy of the spread of the excitation within the molecular layer of ELL following parallel fiber stimulation (Figure 5).

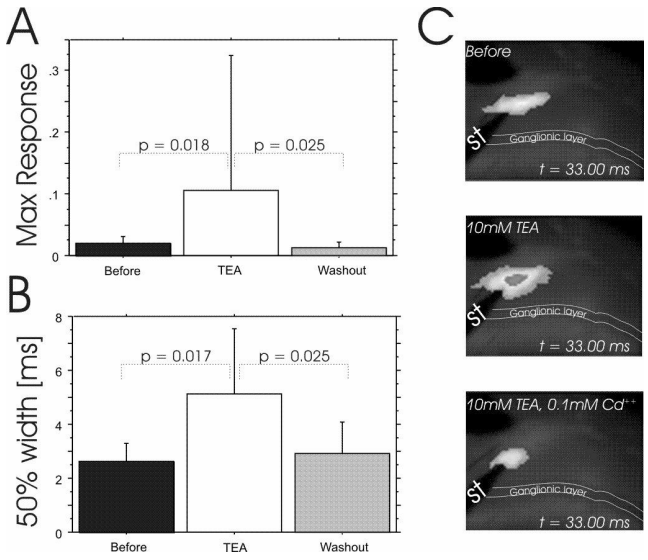

Figure 5: A-C: Results obtained for parallel fiber stimulation using the voltage-sensitive dye. **A** and **B** summary of the effects of bath application of TEA (5-8 mM) on the maximal intensity (**A**) of the VSD

signal and the duration during which the excitation remained above 50% of the maximal excitation. For both **A** and **B**, data was measured at a fixed distance of 150 μm lateral to the stimulating electrode. **C:** Individual examples showing an overlay of the excitation-map over the slice of the ELL. *From top to bottom*: VSD signal measured at a latency of 33 ms (stimulation was at 30 ms) before any drugs were administered, same but after 10 mM TEA was applied to the bath and last graph shows the result obtained after the additional application of 0.1 mM cadmium. In all graphs the molecular layer is indicated by the dotted lines and the stimulating electrode is designated with "st". Note that application of TEA did not only result in an increased VSD-signal (see also **A**), but that excitation occurred over a larger region of the ELL. Both effects were augmented by the application of cadmium, for which a washout could not be obtained.

In all cases (7 slices in 5 fish), the duration and intensity of the VSD-excitation increased significantly (see Figure 5A and B, Wilcoxon, $p < 0.02$, $Z > -2.37$, n=7, n=5). In addition the excitation following the parallel fiber stimulation spreads over a wider area following the block of K^+ channels with TEA. These effects were reversible following a washout with TEA-free ACSF (n=6, see Figure 5A and B), or by adding 100 µM cadmium to the TEA-containing ACSF (n=2, see Figure 5C bottom).

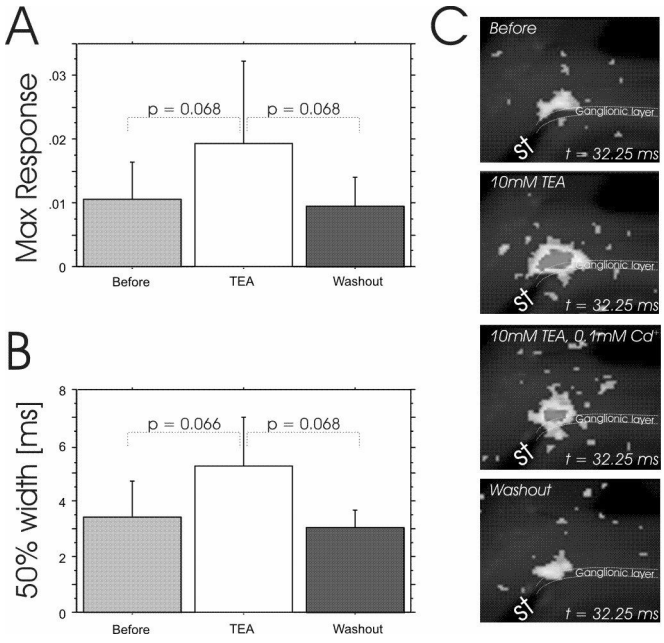

Figure 6: A-C: Results obtained for deep fiber stimulation using the voltage-sensitive dye. **A** and **B** summary of the effects of bath application of TEA (5-8 mM) on the maximal intensity (**A**) of the VSD signal and the duration during which the excitation remained above 50% of the maximal excitation. For both **A** and **B**, data was measured at a fixed distance of 150 μm lateral to the stimulating electrode. **C:** Individual examples showing an overlay of the excitation-map over the slice of the ELL. *From top to bottom*: VSD-signal measured at a latency of 33 ms (stimulation was at 30 ms) before any drugs were administered, same but after 10 mM TEA was applied to the bath and last graph shows the result obtained after the additional application of 0.1 mM cadmium. In all graphs the molecular layer is indicated by the dotted lines and the stimulating electrode is designated with "st". Note that application of TEA did not only result in an increased VSD signal (see also **A**), but that excitation occurred over a larger region of the ELL. Both effects were augmented by the application of cadmium, for which a washout could not be obtained.

The same trend was observed for the deep fiber stimulation, although on average the changes observed remained below the significance criterion (Figure 6, Wilcoxon, $p > 0.068$, $z < 1.82$, n=4, n=3). This indicates that dendritic and/or somatic K^+ channels are involved in regulating the spread of excitation in the apical dendrites following parallel fiber stimulation as well as the spread of action potentials propagating towards the apical dendrites.

One candidate K^+ channel, the $K_v3.3$ subtype was previously shown to have a prominent somato-dendritic expression in the ELL of *Apteronotus leptorhynchus* (Rashid et al., 2001a). These authors showed that $K_v3.3$ is important for determining the switch from tonic to bursting mode in output cells of the ELL by inactivation of the K^+ channel due to backpropagation (Turner et al., 2002). We investigated the distribution of this channel using the same antibody (a gift from Prof. R. Dunn). While some cells in ELL were clearly $K_v3.3$ positive, dendritic expression was weak or absent (Figure 7A).

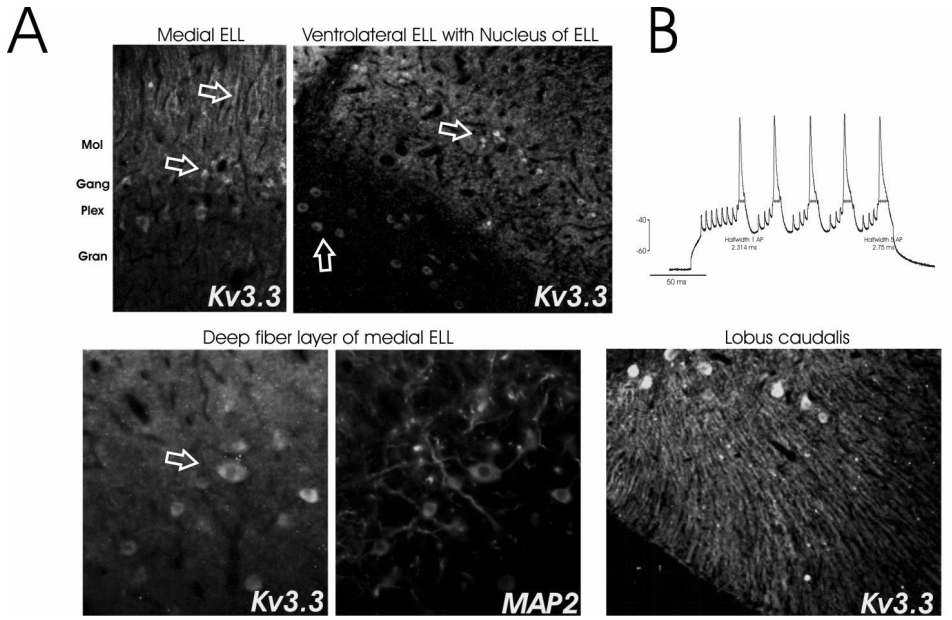

Figure 7: A-B: A: Distribution of $K_v3.3$ in different regions of the ELL and the cerebellum as revealed by a secondary antibody coupled to Oregon green. The distribution of somata and dendrites/axons are further revealed by the double staining with MAP2 shown for the deep layers of the medial ELL. **B:** Example of usage-dependent broad-spike broadening in response to a long depolarizing current pulse.

Strong labeling in the ELL was only seen for the nucleus and in the caudal lobes overlying the ELL, confirming the specificity of the antibody. Thus we conclude that $K_v3.3$ is not of major importance in shaping backpropagation in the ELL of *Gnathonemus,* although broad spikes show a usage-dependent broadening (Figure 7B) that in the case of dendritic spikes in *Apteronotus leptorhynchus* has been attributed to $K_v3.3$. channels.

Role of backpropagation in parallel fiber plasticity

The documented role of broad spikes in the ELL is the generation of long-term depression (LTD). As recent studies indicate that postsynaptic processes are involved in this form of plasticity (Han et al., 2000), we investigated if release of dendritic GABA could be involved as a retrograde messenger. This is based on the finding that the apical dendrites of MG cells contain high quantities of GABA (Meek et al., 1996). Previous experiments on the plasticity of MG cells were carried out in presence of the GABA-A blocker Bicuculline, which did not block LTD in MG cells (Bell et al., 1999). Dendritic GABA release and GABA-B receptors have been shown to be involved in the regulation of synaptic efficacy between bitufted interneurons and pyramidal neurons in rat layer 2/3 of the somatosensory cortex (Zilberter et al., 1999). Thus our hypothesis is that GABA-B receptors on parallel fibers and/or MG cell dendrites are activated by GABA released from MG cell dendrites following the occurrence of backpropagating broad action potentials, which would serve as a retrograde messenger. We investigated the contribution of GABA-B receptors by blocking them using CGP 35348 (1 or 5 µM in aCSF, Sigma) preceding the pairing protocols used by Han et al (2000). To avoid a wash-out of the drug, CGP was re-applied every 30 seconds during the recordings.

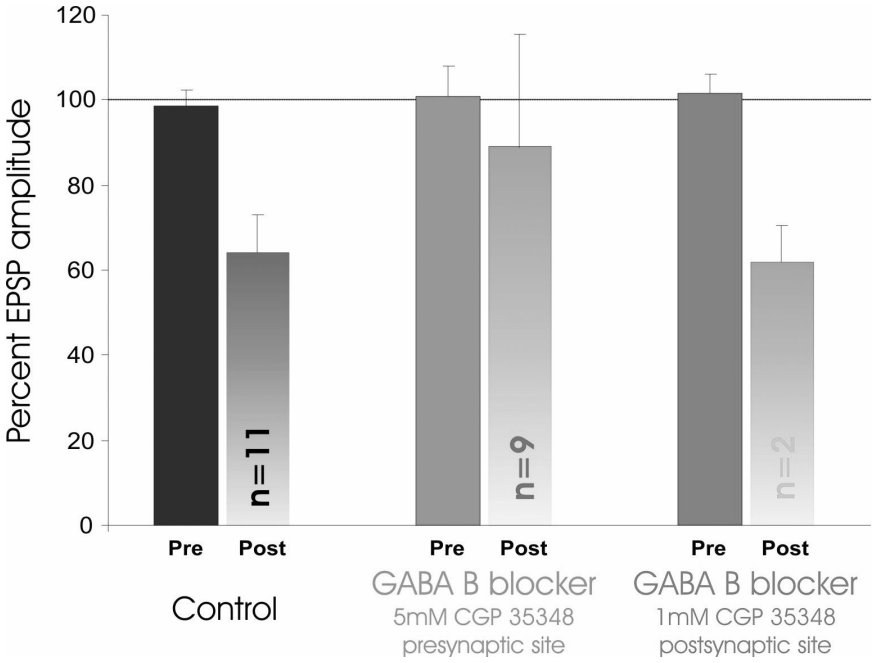

Figure 8: Effect of the pairing between the parallel fiber input and the occurrence of a broad spike following the parallel fiber EPSP within 20 ms. In the absence of any blocker (control bars) the EPSP amplitude was significantly reduced after the 5 min pairing. When the same pairing paradigm was repeated for nine cells in the presence of 5 mM CGP-35348 (middle bars), the decrease of the parallel fiber EPSP was significantly less then in absence of the blocker. For two cells we tested the effect of CGP-35348 at a concentration of 1 mM (right hand bars). Under this condition the pairing was not different from the control condition.

Figure 8 compares the effectiveness of the pairing between the parallel fiber input and the broad spikes for the amplitude of the parallel fiber EPSPs for two conditions, in the presence or absence of CGP. In absence of the drug the EPSP amplitude declined during the pairing and usually remained at a depressed level over 2-3 minutes. In nine cells we were able to repeat the same pairing protocol following the application of 5mM CGP. In these cells, the depression of the parallel fiber EPSP was weaker than before (Wilcoxon test, $p < 0.021$, $Z > -2.366$, n=9, n=4) but depression still occurred. Thus we conclude that liberation of GABA and GABAb receptors might be involved in the formation of LTD, but are not the predominant retrograde messenger in this form of synaptic plasticity.

Discussion

Our immunohistochemical data showed that VGSCs are present in the apical dendrites of MG cells and at least one type of efferent cells of the ELL. Our results are quite different from the only other data available on electric fish. In *Apteronotus* (Turner et al., 1994) TTX sensitive Na^+ channels were found both at the soma and the axon of efferent neurons of the ELL. In addition, positive staining was found in punctuate-like zones over the first 200 µm of the apical dendrites. In these neurons it has been shown that backpropagation occurs and that the backpropagating spike broadens due to $K_v3.3$ potassium channels, with the result that current sources back to the soma (Doiron et al., 2003; Lemon and Turner, 2000; Turner et al., 2002). Depending on the frequency of somatic spikes, the backpropagating spikes can result in a burst at the level of the soma due to the depolarizing current sourcing back to the soma. This burst then is terminated due to different refractory periods of somatic and dendritic spike generation. Thus in these neurons the switch between a bursting and a tonic discharge behavior can be mediated by the backpropagating spikes.

While our results differ in the revealed distribution of VGSCs from those of Turner and colleagues (Turner et al., 1994), they are similar to the results found in the mammalian cerebellum: cells of ELL expressed dendritic VGSCs of the $Na_v1.1$ and $Na_v1.6$ type, the latter mainly in their apical dendrites, as has been documented for Purkinje cells (Schaller and Caldwell, 2003). While Purkinje cells show only weak, almost passive backpropagation (Stuart and Sakmann, 1994), this backpropagation nonetheless depends on the VGSCs.

While our results clearly demonstrate the presence of dendritic VGSCs, some questions remain unsolved. The apparent lack of staining for VGSCs in either the parallel fibers or the mormyromast afferents was unexpected. While up to now no physiological recordings of the parallel fibers in ELL have been made, we speculate that these fibers conduct the action potential actively. The same is known of the mormyromast afferents where Bell and Slesinger (Slesinger and Bell, 1985) showed that both anti- and orthodromic spikes can be recorded at the termination site of these fibers within the ELL. Thus, we expected to see positive staining both for the primary afferents and for the parallel fibers but found no positive staining. It has been shown (Meek et al., 1992) that immunohistochemistry in *Gnathonemus* can have its difficulties, and we speculate that at least in the case of the mormyromast fibers the absence of staining indicates that not all fish-VGSCs are recognized by our PAN-

antibody. Another possibility would be that, although both the mormyromast afferents and the parallel fibers project in rather thick bundles, our method was not sensitive enough to reveal a weak stain. To settle these questions, further studies using electron-microscopy together with immunohistochemistry should be done.

Based on current source-density recordings and the results obtained from experiments on synaptic plasticity in the ELL, various authors have speculated that the two types of spikes occurring in MG cells are of different origin and serve different purposes (Bell et al., 1997c; Gomez et al., 2005; Grant et al., 1998; Han et al., 2000; Sugawara et al., 1999). That both the broad spike and the spikelets are TTX sensitive and thus mainly depend on VGSCs was shown by Sugawara (Sugawara et al., 1999).

Here we show that indeed VGSCs can be found along the apical dendritic arbor of the cells in ELL. Especially the filed-potential recordings of Gomez (Gomez et al., 2005) emphasized the possibility that the broad spikes are generated at the soma and can actively propagate towards the parallel fiber synapses. As field potential recordings are not easy to interpret and always reflect population activity, intracellular confirmation was lacking. Thus our in vitro recordings from MG cells aimed at revealing the site and propagation direction of the different spikes. By applying TTX either in the apical dendrites or at the granular layer we found that broad spikes were the first to fail when TTX was administered in the dendrites. In contrast, when applying TTX in the region of the soma, both the broad and the small spikes could no longer be evoked by intra-somatic current injection. This is in agreement with the idea that spikelets are generated in the axon/soma. However, the finding that the apical TTX application first abolished broad spikes and that the application at the level of the soma could lead to the generation of broad spikes in response to the parallel fiber stimulation following the TTX application indicate, that broad spikes are generated in the apical dendrites close to the soma. That TTX application could change the response to the parallel fiber stimulus in all cases can be explained by its effect on synaptic input from neighboring cells. In the example shown in Figure 2B, the switch from the initial IPSP to the later broad spike most likely reflects the action of TTX on the inhibitory input mediated by cells excited by the parallel fiber input. Once these cells cease firing due to TTX, this inhibition is removed and reveals the net response of this MG cell to the parallel fiber stimulus (and input from neighboring cells), in this case, a broad spike. This indicates that broad spikes are not only generated in the apical dendrites close to the soma, but that they might be propagating from the dendrites towards the soma. Evidence for this kind of propagation was reported by Gomez (Gomez et al., 2005). He found that following parallel fiber stimulation, sometimes active propagation from the dendrites to the soma was observed in current source density recordings. Thus, our interpretation of the current data is that spikelets are generated in the axon/soma of MG cells and that broad spikes can be generated in the primary apical dendrites of these cells. These broad spikes normally, as supported by the current source data, propagate towards the apical region, while, depending on the previous history of the neuron, they might also propagate towards the soma occasionally.

Based on the pharmacological experiments where we blocked K^+ channels we can conclude that the broad spikes are not broad due to the lack of repolarizing potassium channels. In fact, judging the effect of either TEA or 4-AP on the width of

the broad spikes compared to either spikelets or efferent spikes (data not shown) revealed that the relative change is comparable. This might indicate that the expression of repolarizing K^+ channels is equal in MG and efferent cells. Thus, in contrast to the data on *Apteronotus* already discussed above (Doiron et al., 2002; Doiron et al., 2001; Lemon and Turner, 2000; Turner et al., 2002), K^+ channels do not seem to be of major importance in regulating the backpropagation of broad spikes. However, the VSD measurements show that blocking K^+ channels increased the amplitude and effectiveness of signal propagation within the slice. Based on the simultaneous VSD and field potential recordings we conclude that the major component of the signal revealed by the VSD technique in the slice of ELL is due to the postsynaptic activation of the cells in ELL by the parallel fiber stimulus. This postsynaptic activity is reflected in the N2 wave measured on beam with the stimulating electrode and it occurs just at the time that the VSD signal was maximal at that location. This is in line with unpublished data (Sugawara, personal communication) that showed that blocking NMDA and/or metabotropic glutamate receptors resulted in a loss of the VSD signal. However, in some of our recordings the VSD signal seemed to propagate from the ganglionic layer out towards the molecular layer and it is presently unclear if the N2 wave only reflects the postsynaptic activation. Given the fact that stimulation strength was rather high in the VSD experiments, compared to intensities needed to evoke synaptic responses to the parallel fibers in intracellular records, we think that N2 in our experiments reflects not only synaptic activation but also the backpropagation of spikes in the dendrites. This interpretation is further supported by the timing of the VSD signals which peaked at about 3 to 4ms following stimulation. Compared to intracellular data and current source-density recordings this is within the time window published for N2 and N3.

Following this interpretation we suggest that, although the role of K^+ channels in regulating backpropagation is not predominant, the suppression of depolarization significantly increased the efficacy of backpropagation. Given that the apical dendrites of cells in ELL receive vast synaptic input (Bell et al., 2005; Grant et al., 1996; Meek et al., 1996) it is possible to imagine that the feedback arriving form pre-eminentialis might be responsible for regulating the efficacy of broad spike generation/propagation by either shunting or boosting them.

Our experiments on the nature of the retrograde messenger liberated by the interaction between the backpropagating broad spikes and synaptic input (Han et al., 2000) lead to the conclusion that neither GABAa nor GABAb are essential in the formation of the observed plasticity. That GABAa receptors are not involved was known as previous experiments were all conducted in the presence of GABAa blockers. Our experiments point to a contribution mediated by GABAb receptors in the LTP induced by the pairing protocol used. However, some experimental drawbacks prevent us from concluding that it is the only retrograde transmitter involved. The major reason is that we did repetitive pairings in order to evaluate the effect of the drug. Although it has been shown that pairing can be reversed by non associative stimulation, we can not rule out that the initial pairing did already lead to a saturation. In order to prevent this it would be better to independently investigate individual neurons with the same pairing protocol either with or without the blocker present. However, we tried to evaluate the impact of repetitive pairing in absence of any blocker and a following pairing at a low concentration of the blocker in two cells (Figure 8). In these two cells plasticity was the same for both pairings, adding backup

to the data obtained with the drug present, but can not rule out the mentioned problems.

We consequently checked for the presence of GABAb receptors in the terminals of parallel fibers. However, with the antibody used, we were thus far not able to establish unequivocal prove that these receptors are present (Engelmann et al., unpublished data). Thus more data is needed on the nature of the retrograde messenger(s) involved in the observed plasticity, and our present results indicate that more common retrograde messengers like endocannabinoids should be tested.

Acknowledgements

This paper is dedicated to Dr. Yoshiko Sugawara, a pioneer in the in vitro and in vivo work on electric fish and a teacher and friend that will be dearly missed.

Andreasen M, Lambert JD. 1995. Regenerative properties of pyramidal cell dendrites in area CA1 of the rat hippocampus. J Physiol 483(2):421-441.

Bekkers JM. 2000. Distribution of slow AHP channels on hippocampal CA1 pyramidal neurons. J Neurophysiol 83:1756-1759.

Bell C, Bodznick D, Montgomery J, Bastian J. 1997a. The generation and subtraction of sensory expectations within cerebellum-like structures. Brain Behav Evol 50:Suppl 1, 17-31.

Bell CC, Caputi A, Grant K. 1997b. Physiology and plasticity of morphologically identified cells in the mormyrid electrosensory lobe. J Neurosci 17:6409-6423.

Bell CC, Han VZ, Sugawara Y, Grant K. 1997c. Synaptic plasticity in a cerebellum-like structure depends on a temporal order. Nature 387:278-281.

Bell CC, Han VZ, Sugawara Y, Grant K. 1999. Synaptic plasticity in the mormyrid electrosensory lobe. J Exp Biol 202(10):1339-1347.

Bell CC, Meek J, Yang JY. 2005. Immunocytochemical identification of cell types in the mormyrid electrosensory lobe. J Comp Neurol 483:124-142.

Bischofberger J, Jonas P. 1997. Action potential propagation into the presynaptic dendrites of rat mitral cells. J Physiol 504(2):359-365.

Buzsaki G, Kandel A. 1998. Somadendritic backpropagation of action potentials in cortical pyramidal cells of the awake rat. J Neurophysiol 79:1587-1591.

Doiron B, Laing C, Longtin A, Maler L. 2002. Ghostbursting: a novel neuronal burst mechanism. J Comput Neurosci 12:5-25.

Doiron B, Longtin A, Turner RW, Maler L. 2001. Model of gamma frequency burst discharge generated by conditional backpropagation. J Neurophysiol 86:1523-1545.

Doiron B, Noonan L, Lemon N, Turner RW. 2003. Persistent Na^+ current modifies burst discharge by regulating conditional backpropagation of dendritic spikes. J Neurophysiol 89:324-337.

Golding NL, Staff NP, Spruston N. 2002. Dendritic spikes as a mechanism for cooperative long-term potentiation. Nature 418:326-331.

Gomez L, Kannenworf M, Budelli R, Grant K. 2005. Dendritic spike backpropagation in the electrosensory lobe of Gnathonemus petersii. J Exp Biol 208:141-155.

Grant K, Meek J, Sugawara Y, Veron M, Denizot JP, Hafmans TG, Serrier J, Szabo T. 1996. Projection neurons of the mormyrid electrosensory lateral line lobe: morphology, immunohistochemistry, and synaptology. J Comp Neurol 375:18-42.

Grant K, Sugawara Y, Gomez L, Han VZ, Bell CC. 1998. The mormyrid electrosensory lobe in vitro: physiology and pharmacology of cells and circuits. J Neurosci 18:6009-6025.

Han VZ, Bell CC, Grant K, Sugawara Y. 1999. Mormyrid electrosensory lobe in vitro: morphology of cells and circuits. J Comp Neurol 404:359-374.

Han VZ, Grant K, Bell CC. 2000. Reversible associative depression and nonassociative potentiation at a parallel fiber synapse. Neuron 27:611-622.

Hausser M, Stuart G, Racca C, Sakmann B. 1995. Axonal initiation and active dendritic propagation of action potentials in substantia nigra neurons. Neuron 15:637-647.

Helmchen F, Imoto K, Sakmann B. 1996. Ca^{2+} buffering and action potential-evoked Ca^{2+} signaling in dendrites of pyramidal neurons. Biophys J 70:1069-1081.

Helmchen F, Svoboda K, Denk W, Tank DW. 1999. In vivo dendritic calcium dynamics in deep-layer cortical pyramidal neurons. Nat Neurosci 2:989-996.

Hoffman DA, Magee JC, Colbert CM, Johnston D. 1997. K^+ channel regulation of signal propagation in dendrites of hippocampal pyramidal neurons. Nature 387:869-875.

Kim HG, Connors BW. 1993. Apical dendrites of the neocortex: correlation between sodium- and calcium-dependent spiking and pyramidal cell morphology. J Neurosci 13:5301-5311.

Korngreen A, Sakmann B. 2000. Voltage-gated K^+ channels in layer 5 neocortical pyramidal neurons from young rats: subtypes and gradients. J Physiol 525(3):621-639.

Larkum ME, Kaiser KM, Sakmann B. 1999. Calcium electrogenesis in distal apical dendrites of layer 5 pyramidal cells at a critical frequency of back-propagating action potentials. Proc Natl Acad Sci U S A 96:14600-14604.

Lemon N, Turner RW. 2000. Conditional spike backpropagation generates burst discharge in a sensory neuron. J Neurophysiol 84:1519-1530.

Margrie TW, Sakmann B, Urban NN. 2001. Action potential propagation in mitral cell lateral dendrites is decremental and controls recurrent and lateral inhibition in the mammalian olfactory bulb. Proc Natl Acad Sci U S A 98:319-324.

Markram H, Lubke J, Frotscher M, Sakmann B. 1997. Regulation of synaptic efficacy by coincidence of postsynaptic APs and EPSPs. Science 275:213-215.

Meek J, Grant K, Sugawara Y, Hafmans TG, Veron M, Denizot JP. 1996. Interneurons of the ganglionic layer in the mormyrid electrosensory lateral line lobe: morphology, immunohistochemistry, and synaptology. J Comp Neurol 375:43-65.

Meek J, Hafmans TGM, Joosten HWJ. 1992. An intriguing pitfall in chemical neuroanatomy: specific populations of unspecifically immunoreactive neurons in the brain of the mormyrid ?? J. Chem. Neuroanat. 5:181-191.

Rashid AJ, Dunn RJ, Turner RW. 2001a. A prominent soma-dendritic distribution of $K_v3.3$ K^+ channels in electrosensory and cerebellar neurons. J Comp Neurol 441:234-247.

Rashid AJ, Morales E, Turner RW, Dunn RJ. 2001b. The contribution of dendritic K_v3 K^+ channels to burst threshold in a sensory neuron. J Neurosci 21:125-135.

Reyes A. 2001. Influence of dendritic conductances on the input-output properties of neurons. Annu Rev Neurosci 24:653-675.

Schaller KL, Caldwell JH. 2003. Expression and distribution of voltage-gated sodium channels in the cerebellum. Cerebellum 2:2-9.

Schiller J, Helmchen F, Sakmann B. 1995. Spatial profile of dendritic calcium transients evoked by action potentials in rat neocortical pyramidal neurons. J Physiol 487:(3)583-600.

Schiller J, Schiller Y, Stuart G, Sakmann B. 1997. Calcium action potentials restricted to distal apical dendrites of rat neocortical pyramidal neurons. J Physiol 505:(3) 605-616.

Schoppa NE, Westbrook GL. 2001. NMDA receptors turn to another channel for inhibition. Neuron 31:877-879.

Seybold EA, Dunn EJ, Jenis LG, Sweeney CA. 1999. Variation in the posterior vertebral contour line at the level of C-2 on lateral cervical roentgenograms: a method for odontoid fracture detection. Am J Orthop 28:696-701.

Slesinger P, Bell CC. 1985. Primary afferent fibers conduct impulses in both directions under physiological stimulus conditions. J Comp Physiol [A] 157:15-22.

Spruston N, Schiller Y, Stuart G, Sakmann B. 1995. Activity-dependent action potential invasion and calcium influx into hippocampal CA1 dendrites. Science 268:297-300.

Steriade M. 2001. Impact of network activities on neuronal properties in corticothalamic systems. J Neurophysiol 86:1-39.

Stuart GJ, Sakmann B. 1994. Active propagation of somatic action potentials into neocortical pyramidal cell dendrites. Nature 367:69-72.

Sugawara Y, Grant K, Han VZ, Bell CC. 1999. Physiology of electrosensory lateral line lobe neurons in Gnathonemus petersii. J Exp Biol 202(10):1301-1309.

Svoboda K, Helmchen F, Denk W, Tank DW. 1999. Spread of dendritic excitation in layer 2/3 pyramidal neurons in rat barrel cortex in vivo. Nat Neurosci 2:65-73.

Turner RW, Lemon N, Doiron B, Rashid AJ, Morales E, Longtin A, Maler L, Dunn RJ. 2002. Oscillatory burst discharge generated throug conditional backpropagation of dendritic spikes. J. Physiol. (Paris) 96:517-530.

Turner RW, Maler L, Deerinck T, Levinson SR, Ellisman MH. 1994. TTX-sensitive dendritic sodium channels underlie orcillatory discharges in a vertebrate sensory neuron. J. Neurosci. 14:6453-6471.

Urban NN, Sakmann B. 2002. Reciprocal intraglomerular excitation and intra- and interglomerular lateral inhibition between mouse olfactory bulb mitral cells. J Physiol 542:355-367.

Waters J, Larkum M, Sakmann B, Helmchen F. 2003. Supralinear Ca^{2+} influx into dendritic tufts of layer 2/3 neocortical pyramidal neurons in vitro and in vivo. J Neurosci 23:8558-8567.

Williams SR, Stuart GJ. 2000a. Action potential backpropagation and somato-dendritic distribution of ion channels in thalamocortical neurons. J Neurosci 20:1307-1317.

Williams SR, Stuart GJ. 2000b. Backpropagation of physiological spike trains in neocortical pyramidal neurons: implications for temporal coding in dendrites. J Neurosci 20:8238-8246.

Zilberter Y, Kaiser KM, Sakmann B. 1999. Dendritic GABA release depresses excitatory transmission between layer 2/3 pyramidal and bitufted neurons in rat neocortex. Neuron 24:979-988.

Chapter 4

The neuropeptide corticotropin releasing factor regulates transmission and plasticity at the climbing fiber-Purkinje cell synapse

MT Schmolesky, MM de Ruiter, CI De Zeeuw, C Hansel

Abstract

The climbing fiber (CF) input onto cerebellar Purkinje cells (PCs) controls PC activity as well as synaptic plasticity at parallel fiber (PF)-PC synapses. Under high activity conditions, CFs release not only glutamate, but also corticotropin releasing factor (CRF). Brief periods of such high CF activity can lead to the induction of long-term depression (LTD) at CF-PC synapses. Thus, we have examined the role of CRF in regulating both excitatory transmission and long-term plasticity at this synapse. Exogenous application of CRF alone transiently mimics CF-LTD causing a reduction in the CF-evoked excitatory postsynaptic potential (EPSC), complex spike second component, and complex spike afterhyperpolarisation. The complex spike first component was unaffected by CF-LTD induction and is similarly unaffected by CRF. Application of CRF receptor antagonists had little or no effect on CF-EPSCs, but blocked the effects of exogenous CRF. Application of these antagonists reduced the expression amplitude and induction probability of CF-LTD monitored at the EPSC level. The reduction of CF-EPSCs by CRF may be substantiated through kinase signalling pathways as inhibition of either protein kinase A or protein kinase C attenuated the CRF effects. In summary, these results suggest that, under certain sensorimotor conditions, co-release of CRF could downregulate transmission and facilitate LTD induction at CF-PC synapses.

Introduction

Purkinje cells are the only output neurons of the cerebellar cortex and play a central role in both motor control and the acquisition or modification of motor skills. PCs receive two forms of excitatory input: the climbing fiber (CF) projection from the inferior olive and the parallel fiber (PF) projections from granule cells. Each PC in the adult rat receives input from only one CF (Crepel et al., 1976) that is, nevertheless, potent because the CF forms ~1500 synapses upon the primary dendrite (Strata and Rossi, 1998). The PC response to CF stimulation is an all-or-none event, registered as an excitatory postsynaptic current (EPSC; in voltage-clamp) or a complex spike (in current-clamp)(see Figure 1; Schmolesky et al., 2002; 2005). The CF maintains a unique heterosynaptic control of bidirectional synaptic plasticity at the PF input, by providing large dendritic calcium transients that favour LTD over LTP induction at PF synapses (Coesmans et al., 2004).

Both PF and CF terminals release glutamate but CFs also contain the neuropeptide corticotropin releasing factor (CRF). In fact, light and electron immunomicroscopy reveal a dense CRF label in inferior olive neurons, their axonal projections and the CF terminals (Palkovits et al., 1987; Tian and Bishop, 2003). Evidence suggests that CRF is released by CFs in an activity-dependent manner (Barmack and Young, 1990; Tian and Bishop, 2003) and may alter PC spike activity (Bishop, 1990; Bishop and King, 1992). CRF also impairs the PC slow afterhyperpolarisation (AHP) following somatic current injection or complex spikes (Fox and Gruol, 1993; Miyata et al., 1999). Finally, CF-dependent release of CRF is required for the induction of long-term depression (LTD) at the PF-PC synapse (Miyata et al., 1999). Despite these various reports on CRF actions, little is yet known about the role of CRF in modulating synaptic activity or plasticity at the CF-PC synapse itself.

Recently, we have demonstrated that tetanic stimulation of the climbing fiber alone leads to long-term depression of the CF-PC synapse (Hansel and Linden, 2000). Climbing fiber LTD is expressed as a ~20% reduction in the CF-evoked EPSC, dendritic calcium transient, complex spike second component and AHP (Hansel and Linden, 2000; Weber et al., 2003; Schmolesky et al., 2005). CF-LTD is a postsynaptic phenomenon (Shen et al., 2002), whose induction is dependent upon activation of type 1 metabotropic glutamate receptors (mGluRs), a rise in cytosolic Ca^{2+}, and PKC activation (Hansel and Linden, 2000).

In this study we recorded from Purkinje cells in the *in vitro* cerebellar slice preparation to test the hypothesis that CRF plays a role in regulating activity and/or plasticity at the CF-PC synapse.

Materials and methods

Slice preparation and electrophysiology

Parasagittal slices of the cerebellar vermis (200 μm thick) were prepared from P16-28 Sprague-Dawley rats. Rats were anaesthetized with isoflurane and decapitated in conformity with animal care protocols approved by the Erasmus Medical Centre. Dissection and slicing were conducted in ice cold artificial cerebrospinal fluid (ACSF) containing (in mM): 124 NaCl, 5 KCl, 1.25 Na_2HPO_4, 2 $MgSO_4$, 2 $CaCl_2$, 26 $NaHCO_3$, and 10 D-glucose bubbled with 95% O_2/5% CO_2. Slices were perfused with room-temperature ACSF supplemented with 20 μM picrotoxin to block γ-aminobutyric acid type A receptors (flow rate 1-3 ml/min). Whole-cell patch-clamp recordings were conducted using a Zeiss Axioskop FS and EPC-9 amplifier (HEKA Electonics, Lambrecht/Pfalz, Germany). For current-clamp recordings, patch pipettes were filled with (in mM): 9 KCl, 10 KOH, 120 mM K-gluconate, 3.48 $MgCl_2$, 10 HEPES, 4 NaCl, 4 Na_2-ATP, 0.4 mM Na_3-GTP, and 17.5 sucrose (pH adjusted to 7.25). This same solution was used for LTD induction experiments (Figure 3) where EPSC recordings were conducted in voltage-clamp mode and the 5 Hz, 30 sec tetanus was delivered in current-clamp mode. For all other voltage-clamp experiments the pipette solution contained (in mM): 128 CsOH, 111 gluconic acid, 4 NaOH, 10 CsCl, 2 $MgCl_2$, 10 HEPES, 4 Na_2-ATP, 0.4 mM Na_3-GTP, and 30 sucrose (pH adjusted to 7.25). Currents were filtered at 3 kHz, digitized at 8 kHz and acquired using PULSE software. The climbing fiber was stimulated using a stimulus isolation unit attached to a standard pipette filled with ACSF and placed in the molecular layer. Test responses were evoked at 0.05 Hz with ~3.0 μA pulses of 0.5 ms duration. In voltage-clamp experiments, stimuli were delivered in pairs with a 50 ms separation to measure the paired pulse depression (PPD) ratio (EPSC2 amplitude / EPSC1 amplitude). Only cells that were innervated by a single CF, as indicated by a single step in the CF input-output relation, were used. All drugs were purchased from Sigma, except CRF and αH-CRF (Calbiochem), astressin (Bachem), and KT5720 (Tocris). Drugs were administered using a 4-resevoir gravity fed system with either a mini- or micro-manifold (4-barreled 100 μm tip) for bath or focal application, respectively (BPS-4 system, ALA Systems).

Data analysis and inclusion criteria

Data analysis was conducted using PulseFit (HEKA) and Igor (Wavemetrics) software. A requirement for data inclusion was stability in resting membrane potential ($\Delta < \pm$ 5mV) and input resistance ($\Delta < \pm$15%) for current-clamp recordings or holding current, input resistance ($\Delta < \pm$15%) and series resistance ($\Delta < \pm$15%) for voltage-clamp. Data for three sweeps collected per minute were averaged and normalized to the 5 minute baseline. Group data are reported as mean $\pm$ SEM. For statistical analysis, one- and two-way ANOVAs were followed by planned t-tests (SPSS, Excel).

Results

CRF suppresses the Purkinje cell AHP and complex spike components

Somatic injection of depolarising currents (500 ms; 200 to 600 pA) results in spike activity in PCs and, following current offset, a slow AHP (see Figure 1A). Focal application of CRF for five minutes significantly reduced this AHP to 83 ± 5.5 % of baseline values (n=10; P<0.05), while having no significant effect upon the resting membrane potential (-70.1 ± 1.5 mV at t=5 min, -69.6 ± 1.8 mV at t=10 min). Switching micropressure barrels from saline to an identical saline did not affect PC responses at the pressures used. On average, AHP suppression reaches saturation within 5 minutes of CRF application, is maintained until drug cessation and, at that time, shows reversal for some cells. These data are consistent with previous results obtained by bath application of CRF onto cultured PCs (Fox and Gruol, 1993).

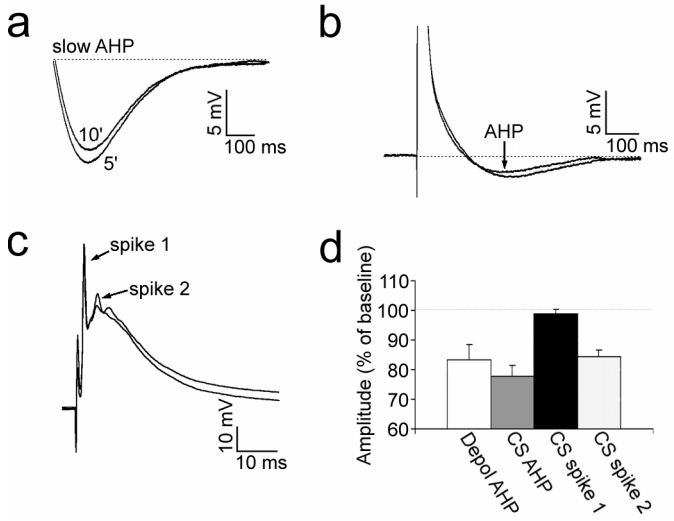

Figure 1: CRF attenuates the Purkinje cell AHP and second complex spike component. Purkinje cell responses to somatic current injection or climbing fiber stimulation before (min 5) and after (min 10) CRF application. **A**: offset of a square wave depolarising somatic current injection (inset) results in a slow PC afterhyperpolarisation (Depol AHP) which is attenuated by focal application of CRF (1.0-1.5 μM). **B:** and **C:** climbing fiber stimulation under current-clamp conditions resulted in complex spikes characterized by 2-6 fast spikes followed by a slow AHP. Focal application of CRF (1.0-1.5 μM) attenuates the complex spike AHP (B) and second component (C) while leaving the first component unaffected (n = 3). **D:** histogram demonstrating the effect of five minutes CRF upon Depol AHP and the complex spike components.

CRF applied via bath perfusion also suppresses the slow AHP following complex spikes in PCs in cerebellar slices (Miyata et al., 1999). Similarly, focal application of CRF for five minutes to a single PC significantly attenuated the complex spike AHP (77.6 ± 3.8%; *n*=3; *P<0.05*; Figure 1B). We find that the complex spike second component is simultaneously reduced by CRF (84.3 ± 2.4 %; *P*<0.05) while the first component is unaffected (99 ± 1.3 %)(Figure 1C and D). Evidence suggests that modification of the complex spike following CF-LTD induction is the direct result of AMPA receptor modification and/or internalisation at the CF-PC synapse. If CRF application acts upon the complex spike via the same mechanism we would expect to see an impact of CRF on the CF-PC EPSC.

CRF attenuates the climbing fiber-Purkinje cell EPSC

Climbing fiber-evoked EPSCs were recorded from PCs in voltage-clamp mode. The holding potential was selected to optimise cellular stability (typically -30 to -5 mV). In the control condition, the CF-EPSC amplitude remained constant for the duration of the recording (101 ± 3.3 %; *t*=25 min; *n*=6). As shown in Figure 2, addition of CRF (1.0 μM) to the perfusion media for 10 minutes reduced the CF-EPSC amplitude by half (52 ± 11.6 %; *t*=16 min; *n*=7; *P*<0.05). The EPSC suppression was, on average, reversed by a 15 minute washout period (96 ± 10.0 %; *t*=30 min; *n*=5) indicating that CRF was not toxic in nature. The PPD ratio was not affected by CRF (Figure 2D; 0.68 ± 0.03 at *t*=5 min vs 0.67 ± 0.04 at *t*=16 min; *n*=7; *P*>0.05) suggesting a postsynaptic mechanism for CRF action upon EPSC amplitude.

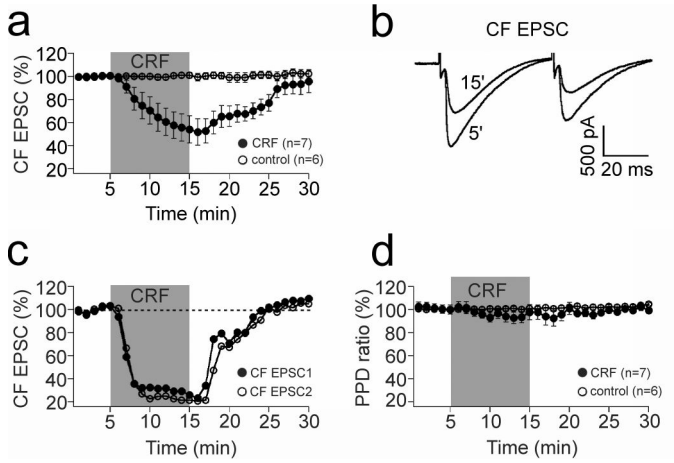

Figure 2: CRF reduces the climbing fiber-Purkinje cell EPSC by half. **A:** bath application of CRF (1.0 μM) reduces the climbing fiber-evoked PC excitatory postsynaptic current. Washout leads to a near complete recovery. **B:** representative CF-EPSCs just before CRF application (min 5) and washout (min 15). **C:** responses of an individual cell plotted across time show that the CRF-induced reduction of the CF-EPSC was often swift and dramatic. **D:** the paired-pulse depression (PPD) ratio was not significantly affected by CRF application.

CRF antagonist blocks CF-LTD induction

Bath application of the high-affinity CRF receptor antagonist astressin (0.2 μM) for 10 minutes had no effect on the CF-EPSC (100 ± 1.3 %; *t*=15 min; *n*=4) but completely blocked the effects of co-applied 1.0 μM CRF (97 ± 1.1 %; *t*=25 min; Figure 3A). Under normal saline conditions, CF tetanization (5 Hz, 30 sec) reduced the CF-EPSC within several minutes and this reduction reached a maximum within 15-20 minutes after tetanization (82 ± 3.5 %; *t*=25 min; *n*=9; *P*<0.05; Figure 3B). Bath application of astressin (0.2 μM) for 15 minutes, beginning 10 minutes before CF tetanization, blocked the induction of CF-LTD at early and late (95 ± 1.8 %; *t*=25 min; *n*=13; *P*<0.05) time points (Figure 3B). The induction of CF-LTD was considered successful when a cell demonstrated >10% reduction 20-25 minutes after CF tetanization. CF-LTD was induced in 7 of 9 cells in the control condition but in only 1 of 6 cells in the astressin condition (Figure 3C).

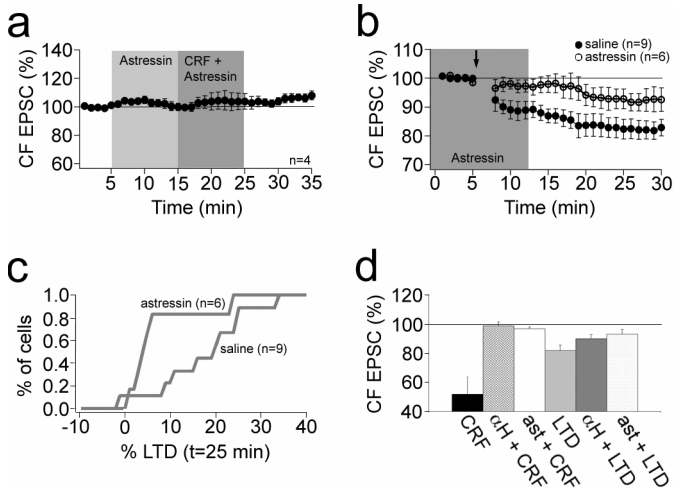

Figure 3: CRF receptor antagonists impair climbing fiber-Purkinje cell LTD. **A:** CRF receptor antagonist astressin (0.2 μM) had no impact upon the CF-evoked Purkinje cell EPSC but completely blocked the effect of bath-applied CRF (1.0 μM; *n* = 4). **B:** application of astressin beginning 10 minutes prior to CF tetanization (5 Hz, 30 sec; arrow) blocked LTD induction. **C:** cumulative probability distribution plotting the % of cells showing a given % of EPSC reduction at *t* = 25 min. The probability of LTD induction is greatly reduced in the CRF antagonist condition. **D:** summary histogram showing that CRF antagonists (αH-CRF or astressin) were sufficient to block the effects of 10 min CRF (1.0 μM) application and sufficient to attenuate CF-LTD (min 25).

Similar to astressin, bath application of the low-affinity CRF receptor antagonist αh-CRF (1.0 μM) for 10 minutes had little or no effect upon the CF-EPSC (95 ± 6.0 %; *n*=4) but blocked the effects of 1.0 μM CRF, measured 10 minutes after co-application (99 ± 3.4 %; *n*=4). Bath application of αh-CRF (1.0 μM) for 15 minutes, beginning 10 minutes before CF tetanization, had only a moderate impact on LTD measured at later time points (89 ± 4.0 %; *t*=25 min; *n*=9) compared to control (Figure 3D).

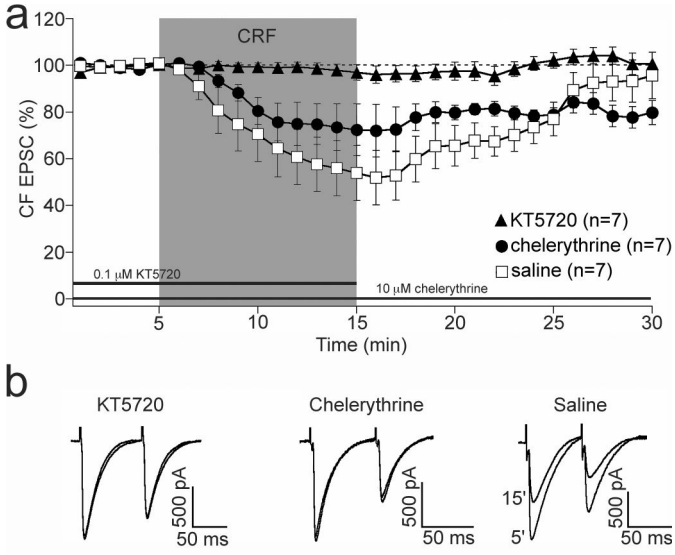

Figure 4: CRF effect upon the climbing fiber-Purkinje cell EPSC are protein kinase mediated **A:** inhibitors of PKC (chelerythrine) or PKA (KT5720) impair the effect of CRF (1.0 μM) upon the CF-evoked Purkinje cell EPSC. **B:** example traces of EPSCs at min 5 and min 15. While the PKC inhibitor reduced the CRF effect by only half on average, in several cases such as the example shown here the block was complete.

Kinase inhibitors block the impact of CRF upon the CF-PC EPSC

CRF receptors are G-protein bound and are reported to act through PKA and PKC (Blank et al., 2003). Thus, we examined the effects of kinase inhibitors upon the CRF-mediated suppression of the CF-PC EPSC. The PKC inhibitor chelerythrine (10 μM) was bath-applied for 25-35 minutes prior to, and during, bath application of CRF (1 μM). The PKA inhibitor KT5720 (0.1 μM) was bath-applied for 10 minutes prior to, and 10 minutes during, CRF application. As shown in Figure 4, antagonism of PKC activity reduced the effects of CRF by approximately half compared to the CRF alone condition (72 ± 11.2 %; t = 16 min; n = 7; P=0.05), while antagonism of PKA activity completely blocked the effects of co-applied CRF (96 ± 3.6 %; t = 16 min; n = 7; P<0.05).

Discussion

Here, we show for the first time that CRF, a neuropeptide that is released from CF terminals under high-activity conditions, postsynaptically reduces CF-EPSCs and is required for LTD induction at CF synapses.

CRF regulates CF-PC synaptic efficacy

Endogenous CRF is supplied to the cerebellar cortex by both mossy fibers and climbing fibers (Palkovits et al., 1987; Van den Dungen et al., 1988) and PCs express type 1, and possibly type 2, CRF receptors (Bishop et al., 2000; Swinny et al., 2003). The ultrastructure is clearly available for CRF to influence PC physiology and

plasticity. Here, we find that focally applied exogenous CRF suppresses the PC slow AHP following either somatic current injection or climbing fiber activation (Figure 1). In addition, we find that exogenous CRF suppresses component 2 of the complex spike while component 1 remains unaffected. Thus, three separate features of the PC complex spike are modified by the presence of CRF in exactly the same manner as they are by CF-LTD induction (Hansel and Linden, 2000; Schmolesky et al., 2005). CRF might exert its influence on the complex spike through the same mechanism posited for CF-LTD: by reducing AMPA receptor-mediated currents. To test this prediction we bath-applied exogenous CRF and observed its effect upon the CF-EPSC.

The application of CRF caused a dramatic, yet reversible, reduction in CF-EPSCs (Figure 2) that was blocked by co-application of the CRF receptor antagonists αh-CRF or astressin (Figure 3). The application of either antagonist alone had no effect upon the CF-EPSC. Taken together, these results make three points. First, basal endogenous [CRF] does not regulate CF-PC synaptic efficacy in the cerebellar slice. If it did we would expect CRF-R antagonists to influence the CF-EPSC, which they did not. Second, moderate concentrations of CRF (such as the 1.0 μM applied here) are capable of temporarily reducing CF-PC synaptic efficacy by half. Thus, activity-driven release of higher concentrations of CRF could have a significant, if transient, impact upon glutamatergic transmission at the CF-PC synapse. Third, it appears likely that the effects of CRF upon the complex spike are, in some part, the direct result of an attenuated CF-EPSC. This supposition is based upon three facts: a) pharmacologically suppressing the CF-EPSC with NBQX causes impaired CF-evoked PC dendritic Ca^{2+} transients; b) the complex spike AHP is Ca^{2+}-mediated; and c) reduced CF-evoked Ca^{2+} transients are associated with an attenuation of the complex spike AHP and second component (Schmolesky et al., 2002; 2005; Weber et al., 2003). That said, CRF also impairs the slow AHP evoked by somatic current injection (Figure 1; Fox and Gruol, 1993), a case in which glutamatergic receptors are not involved. Thus, as suggested previously by Miyata et al. (1999), CRF might also influence K^+ channels directly. Voltage-gated Ca^{2+} channels are not a likely target of CRF since Ca^{2+} transients evoked by somatic current injection are not affected by CRF application (Miyata et al., 1999).

Postsynaptic effects of CRF

A recent report by Liu et al. (2004) demonstrates that CRF may postsynaptically influence glutamatergic transmission in both the amygdala and lateral septum. Type 1 CRF receptors in the cerebellum are expressed in the proximal PC dendrite across from PF terminals and in nonsynaptic regions, but not across from CF terminals (Swinny et al., 2003). These receptors are also found in the CF presynaptic terminal. The absence of CRF receptor expression in the PC dendritic region across from CF terminals is somewhat surprising given the prominent CRF labelling in these terminals. This absence might be explained by high rates of ligand-receptor coupling followed by CRF receptor internalisation (J.D. Swinny, personal communication; Bloch et al., 1999). Otherwise, CF-supplied CRF must act on PCs via diffusion to adjacent dendritic regions. While we cannot exclude the possibility that CRF acts presynaptically to impair CF-PC synaptic efficacy, the fact that the CF-EPSC PPD ratio was unaffected by CRF application (Figure 2) argues in favor of a postsynaptic

site of influence. We speculate that presynaptic CRF binding on the CF terminal may serve an autoregulatory function, as has been described for other neuropeptides (Merighi, 2002).

Endogenous CRF receptor binding is required for the induction of CF-LTD

The current data clearly demonstrate that exogenous CRF is capable of influencing CF-evoked sub- and supra-threshold events. These effects were transient, indicating that a moderate rise in [CRF] is, by itself, insufficient to induce CF-LTD. However, attempts to induce CF-LTD in the presence of the CRF receptor antagonists αh-CRF or astressin were impaired or failed entirely (Figure 3). Thus, concomitant with increases in mGluR1 activation, dendritic $[Ca^{2+}]_i$, and PKC activity (Hansel and Linden, 2000), endogenous ligand at some undetermined concentration must bind CRF receptors for the induction of CF-LTD to occur. The required levels of endogenous ligand could be supplied through the basal release of CRF (mossy fibers or climbing fibers), basal release of the CRF-related peptide urocortin (parallel fibers or climbing fibers; Swinny et al., 2002) or, as we believe to be most likely, activity-driven release of CRF from climbing fibers.

Potential corticotropin releasing factor signal transduction pathways

The action of CRF is exerted by binding to type 1 and/or type 2 CRF receptors. Multiple receptor splice variants exist and receptor binding may activate a wide range of coupled G-proteins (Grammatopoulos et al., 2001) and, thereby, transduction events. Reports on CRF action in diverse cell types indicate the ability of this peptide to activate the adenylyl cyclase/PKA and PKC pathways (Grammatopoulos et al., 2001; Blank et al., 2003). Studies have shown that both PF-LTD and CF-LTD induction require heightened PKC activity (Hansel and Linden, 2000; Hansel et al., 2001; Weber et al., 2003). The involvement of PKA activity in PF-LTD appears unlikely (Ito and Karachot, 1992; Storm et al., 1998) but has not yet been tested for CF-LTD.

It is clear that mGluR1 binding contributes to increased PKC activity. Logic suggests that basal rates of CRF-R binding might help set PKC tone. In addition, elevated CRF-R binding during periods of high activity could act to raise PKC levels above threshold for synaptic modification. In support of these hypotheses, biochemical assays demonstrate that CRF application significantly increases PKC activity in cerebellar slices (Miyata et al., 1999). Consistent with this observation, we find that PKC inhibition substantially reduces the effect of CRF upon the CF-PC EPSC (Figure 4).

There is no evidence that PKA acts directly upon AMPA-Rs in Purkinje cells. However, recent studies have revealed that the AMPA-R phosphorylation underlying cerebellar LTD relies not only upon the activation of kinases, but also on the inhibition of phosphatases (Eto et al., 2002; Launey et al., 2004). Thus, CRF-R activation of PKA could lead to the activation of phosphatase inhibitor proteins and, thereby, cause a transient reduction in the CF-EPSC. If true, inhibition of PKA activity

should reduce or block the affects of CRF upon the CF-EPSC, which we have in fact observed.

In conclusion, activity at the CF-PC synapse plays a central role in cerebellar function by driving the complex spike, influencing simple spike throughput, elevating dendritic Ca^{2+} levels, and acting as a necessary associative signal for heterosynaptic PF LTD. Plasticity at the CF-PC synapse is, therefore, likely to influence ongoing cerebellar processing (Schmolesky et al., 2002; 2005), neuroprotection (Weber et al., 2003), and memory formation (Coesmans et al., 2004). This study shows, for the first time, that the neuropeptide CRF could influence these neural functions by transiently suppressing CF-PC efficacy or facilitating CF-LTD.

Acknowledgements

This work was supported by an EUR fellowship (M.T.S.), the Hersenstichting Nederland (C.D.Z., M.T.S., C.H.), NWO (C.D.Z.), NWO-VIDI (C.H.) and the Royal Dutch Academy of Sciences (C.H.).

Barmack NH, Young WS. 1990. Optokinetic stimulation increases corticotropin-releasing factor mRNA in inferior olivary neurons of rabbits. J Neurosci 10:631-640.

Bishop GA. 1990. Neuromodulatory effects of corticotropin releasing factor on cerebellar Purkinje cells: an in vivo study in the cat. Neuroscience 39:251-257.

Bishop GA, King JS. 1992. Differential modulation of Purkinje cell activity by enkephalin and corticotropin releasing factor. Neuropeptides 22:167-174.

Bishop GA, Seelandt CM, King JS. 2000. Cellular localization of corticotropin releasing factor receptors in the adult mouse cerebellum. Neuroscience 101:1083-1092.

Blank T, Nijholt I, Grammatopoulos DK, Randeva HS, Hillhouse EW, Spiess J. 2003. Corticotropin-releasing factor receptors couple to multiple G-proteins to activate diverse intracellular signaling pathways in mouse hippocampus: role in neuronal excitability and associative learning. J Neurosci 23:700-707.

Bloch B, Dumartin B, Bernard V. 1999. In vivo regulation of interneuronal trafficking of G protein-coupled receptors for neurotransmitters. Trends Pharmacol Sci 20: 315-319.

Coesmans M, Weber JT, De Zeeuw CI, Hansel C. 2004. Bidirectional parallel fiber plasticity in the cerebellum under climbing fiber control. Neuron 44:691-700.

Crepel F, Mariani J, Delhaye-Bouchaud N. 1976. Evidence for a multiple innervation of Purkinje cells by climbing fibers in the immature rat cerebellum. J Neurobiol 7:567-578.

Eto M, Bock R, Brautigan DL, Linden DJ. 2002. Cerebellar long-term synaptic depression requires PKC-mediated activation of CPI-17, a myosin/moesin phosph-atase inhbitor. Neuron 36:1145-1158.

Fox EA, Gruol DL. 1993. Corticotropin-releasing factor suppresses the after-hyperpolarization in cerebellar Purkinje neurons. Neurosci Lett 149:103-107.

Grammatopoulos DK, Randeva HS, Levine MA, Kanellopoulou KA, Hillhouse EW. 2001. Rat cerebral cortex corticotropin-releasing hormone receptors: evidence for receptor coupling to multiple G-proteins. J Neurochem 76:509-519.

Hansel C, Linden DJ, D'Angelo E. 2001. Beyond parallel fiber LTD: the diversity of synaptic and non-synaptic plasticity in the cerebellum. Nat Neurosci 4:467-75.

Hansel C, Linden DJ. 2000. Long-term depression of the cerebellar climbing fiber--Purkinje neuron synapse. Neuron 26:473-482.

Ito M, Karachot L. 1992. Protein kinases and phosphatase inhibitors mediating long-term desensitization in cerebellar Purkinje cells. Neurosci Res 14:27-38.

Launey T, Endo S, Sakai R, Harano J, Ito M. 2004. Protein phosphatase 2A inhibition induces cerebellar long-term depression and declustering of synaptic AMPA receptor. Proc Natl Acad Sci 101:676-81.

Liu J, Yu B, Neugebauer V, Grigoriadis DE, Rivier J, Vale WW et al. 2004. Corticotropin-releasing factor and Urocortin I modulate excitatory glutamatergic synaptic transmission. J Neurosci 24:4020-4029.

Merighi A. 2002. Costorage and coexistence of neuropeptides in the mammalian CNS. Prog Neurobiol 66:161-190.

Miyata M, Okada D, Hashimoto K, Kano M, Ito M. 1999. Corticotropin-releasing factor plays a permissive role in cerebellar long-term depression. Neuron 22:763-775.

Miyata M, Finch EA, Khiroug L, Hashimoto K, Hayasaka S, Oda SI et al. 2000. Local calcium release in dendritic spines required for long-term synaptic depression. Neuron 28:233-244.

Palkovits M, Leranth C, Gorcs T, Young WS. 1987. Corticotropin-releasing factor in the olivocerebellar tract of rats: demonstration by light- and electron-microscopic immunohistochemistry and in situ hybridization histochemistry. Proc Natl Acad Sci 84:3911-3915.

Schmolesky MT, Weber JT, De Zeeuw CI, Hansel C. 2002. The making of a complex spike: ionic composition and plasticity. Ann N Y Acad Sci 978:359-390.

Schmolesky MT, De Zeeuw CI, Hansel C. 2005. Climbing fiber synaptic plasticity and modifications in Purkinje cell excitability. Prog Brain Res 148:81-94.

Shen Y, Hansel C, Linden DJ. 2002. Glutamate release during LTD at cerebellar climbing fiber-Purkinje cell synapses. Nat Neurosci 5:725-726.

Storm DR, Hansel C, Hacker B, Parent A, Linden DJ. 1998. Impaired cerebellar long-term potentiation in type I adenylyl cyclase mutant mice. Neuron 20:1199-1210.

Strata P, Rossi F. 1998. Plasticity of the olivocerebellar pathway. Trends Neurosci 21:407-413.

Swinny JD, Kalicharan D, Gramsbergen A, Van der Want JJ. 2002. The localisation of urocortin in the adult rat cerebellum: a light and electron microscopic study. Neuroscience 114:891-903.

Swinny JD, Kalicharan D, Blaauw EH, IJkema-Paassen J, Shi F, Gramsbergen A et al. 2003. Corticotropin-releasing factor receptor types 1 and 2 are differentially expressed in pre- and post-synaptic elements in the post-natal developing rat cerebellum. Eur J Neurosci 18:549-562.

Tian JB, Bishop GA. 2003. Frequency-dependent expression of corticotropin releasing factor in the rat's cerebellum. Neuroscience 121:363-377.

Van den Dungen HM, Groenewegen HJ, Tilders FJ, Schoemaker J. 1988. Immunoreactive corticotropin releasing factor in adult and developing rat cerebellum: its presence in climbing and mossy fibers. J Chem Neuroanat 1:339-349.

Weber JT, De Zeeuw CI, Linden DJ, Hansel C. 2003. Long-term depression of climbing fiber-evoked calcium transients in Purkinje cell dendrites. Proc Natl Acad Sci 100:2878-2883.

Chapter 5

Otolith deprivation induces optokinetic compensation

CE Andreescu, MM de Ruiter, CI De Zeeuw, MTG De Jeu

Adapted from J Neurophysiol 94(5):3478-3496, 2005

Abstract

According to the multisensory integration theory vestibular, optokinetic and proprioceptive inputs act in concert to maintain a stable retinal image of the visual world. Yet, it remains elusive to what extent the otolith organs contribute to this process and whether a specific loss of otolith input is compensated for. Here we investigated the compensatory eye movements in *tilted* mice, which lack otoconia due to a mutation in otopetrin 1. *Tilted* mice showed very small displacements of the eyes in the orbit during static roll paradigms, suggesting the absence of functional otolith organs. Independent of head position with respect to gravity, the gain and phase lead of angular vestibulo-ocular reflex of *tilted* mice were decreased and increased, respectively (frequencies 0.2 to 1 Hz and peak accelerations 8 to 197 deg/sec^2, respectively). Furthermore, lack of otolith input increases the dependency of the vestibular system on stimulus frequency. In contrast, the gain of optokinetic reflex in *tilted* mice was significantly higher in the low frequency range than in control mice, regardless of the position of the mice in space or the plane of the eye movements. To explain these results, a simple model was used in which a multisensory integration unit was embedded. With this model, we were able to simulate all the behaviours observed. Thus our data and the model support the presence of the multisensory integration system and revealed a compensatory enhanced optokinetic reflex in *tilted* mice, indicating an adaptive synergism in the processing of otolith and visually-driven signals.

Introduction

To maintain a stable retinal image one needs access to information provided by sensory systems controlling the vestibulo-ocular reflex (VOR), optokinetic reflex (OKR) and cervico-ocular reflex. Moreover, the control systems of these individual reflexes need to be sufficiently integrated in the central nervous system in order to weigh the impact and need of the different components under a wide variety of physical circumstances (Raphan et al., 1979; Merfeld and Zupan, 2002; Mergner et al., 2003; Angelaki et al., 2004). Otolith organs provide a specific contribution to this multisensory system. Electrical stimulation of otolith organs (Fluur and Mellstrom, 1971) or otolith nerves (Suzuki et al., 1969) demonstrated that otoliths control eye movements. The otolith signals are conveyed via primary otolith afferents (Fernandez and Goldberg, 1976a, b) to the vestibular nuclei (Bush et al., 1993). These signals are able to generate an angular maculo-ocular reflex, which operates as a low-pass-filtered response (rabbits: Barmack, 1981; Van der Steen and Collewijn, 1984; rats: Brettler et al., 2000; mice: Harrod and Baker, 2003; cats: Rude and Baker, 1988; Tomko et al., 1988; monkeys: Paige and Tomko, 1991; Angelaki and Hess, 1996). In addition, information provided by the otolith organs influences the orientation of the eyes with regard to gravity and linear acceleration (Baarsma and Collewijn, 1975; Cohen et al., 2001). This information must be combined with input from semicircular canals to obtain proper compensatory eye movements (Angelaki et al., 2004). Moreover, converged otolith-canal neural activity significantly changes its modulation in different behavioral contexts such as active and passive head movements (McCrea and Luan, 2003). In some of these situations the otolith information may be used to transform primary semicircular canal signals into space-reference angular motion (Angelaki and Hess, 1995). Thus, several lines of evidence suggest that the

otolith organs control eye movements via vestibular and oculomotor nuclei that are also used by the semicircular canal system.

According to the multisensory integration theory, one expects not only that deficits in the otoliths can cause a variety of problems in the canal-driven system, but also that compensation must take place. Yet, at present it is not clear whether dysfunctional otoliths can be compensated for, and if so, how and under which circumstances such compensations can occur. Eye movement recordings of primates under microgravity in space have not been conclusive due to small sample sizes, limited experimental time and the fact that the otoliths can still sense accelerations in this situation (Dizio and Lackner, 1992; Clement et al., 1993; Correia, 1998; Moore et al., 2003). Moreover investigations on this topic have been hampered by the inability to mechanically lesion the otolith organs or nerves without affecting the input from the semicircular canals or without the loss of afferent fibers that will induce a reactive synaptogenesis (Goto et al., 2002).

To investigate potential vestibular compensatory processes, unilateral stimulation experiments on patients with unilateral vestibular nerve dissections (Clarke and Engelhorn, 1998) and gravity-aligned/misaligned rotation experiments on patients with vestibular neuritis were performed (Schmid-Priscoveanu et al., 2004). However, these pathological circumstances were not specific enough to elucidate the compensatory mechanism induced by dysfunctional otoliths.

In the present study, we investigated potential mechanisms for compensation using *tilted* mice, which lack otoconia due to a spontaneous recessive mutation in otopetrin 1 gene (Otop 1) located on chromosome 5 (Hurle et al., 2003). Although their vestibular ganglion does develop relatively slowly (Smith et al., 2003), the projections from the otolith organs to the vestibular nuclei seems to be at least grossly normal in these mutant mice (Crapon de Caprona et al., 2004). Furthermore, *tilted* mice do not show any permanent abnormal phenotype in organ systems other than the otoliths (Ornitz et al., 1998). The linear vestibular evoked potential (linear VsEPs) is absent in *tilted* mice (Jones et al., 2004), as a consequence of the absence of otoconia. Apart from confirming their deficiency in gravito-inertial information by determining their eye position following static roll paradigms, we investigated their angular vestibulo-ocular reflex in the dark (aVOR) and the light (angular visually enhanced VOR or aVVOR) as well as their optokinetic reflex (OKR) over a wide range of stimulus parameters. The lack of otoconia decreases the gains and increases the phase errors not only during “otolith-mediated” aVOR but also during “canal-mediated” aVOR and increases the vestibular system dependency on frequency, especially at stimulus frequencies smaller than 1 Hz. We demonstrate that a frequency dependent enhancement of the optokinetic system can be used as a compensatory mechanism for a lack of functional otoliths. Furthermore, a simple model structure was explored in order to interpret the experimental data, to formulate a possible physiological template of how the canal, otolith and visual signals share centrally processing and to obtain insight in the consequences of otolithic dysfunction.

Materials and methods

In this study, we used eighteen homozygous *tilted* mice (Otop 1^{tlt}) and twenty-two heterozygous control littermates (age: 12 - 20 weeks; The Jackson Laboratory). The recessive *tlt* mutation arose spontaneously in 1983 on the STOCK p^{6H}/p^{d} and was backcrossed onto the C57BL/6J background. The mutant mice were not deaf or blind (Ornitz et al., 1998). They were housed on a 12 hour light/dark cycle with food and water available *ad libitum*. All animal procedures described were in accordance with the guidelines of the ethical committee of Erasmus MC, Rotterdam.

Phenotype assessment

The homozygous *tilted* mice were easily identified by their inability to swim when they were dropped from at least 20 cm height into a deep tank of water. *Tilted* mice cannot find the surface of the water and need rescuing to prevent drowning. Heterozygous control littermates mice can find the surface of the water and swim easily (Ornitz et al. 1998).

Surgical procedures

An acrylic pedestal was formed on the animal's skull under general anesthesia of a mixture of isofluoran (Isofloran 1-1.5%; Rhodia Organique Fine Ltd), nitrous oxide and oxygen. The pedestal construction was made as follows: a midline incision was made to expose the dorsal cranial surface and four stainless steel screws (1x1.5mm) were implanted in the calvarium and then embedded in dental acrylic. A pre-fabricated piece equipped with two nuts was attached to the pedestal in order to fixate the mouse in the restrainer device.

Video eye movement recording apparatus

After a recovery period (3 days), each mouse was handled daily for 2 days. During the experiment it was placed in an acrylic tube, with their head secured. The tube was inserted into the setup via a carrier that allowed orientation of the mouse (from mouse upright to mouse with its nose up or down; ±90 degree). The carrier on which the mouse was fixed also permitted translation of the mouse in the left-right direction and near-far direction from the camera. The purpose of these translations was to position the mouse's eyeball on the rotation axis of the video camera, which ran through the center of the table (Stahl et al., 2000).

A cylindrical screen (diameter 63 cm) with a random-dotted pattern (each element 2^{o}) surrounded the turntable (diameter 60 cm). Both the surrounding screen and the turntable were driven independently by an AC servo-motor (Harmonic Drive AG, The Netherlands). The table and drum position signal were measured by potentiometers, filtered (cut-off frequency 20 Hz), digitized (CED Limited, Cambridge, UK) and stored on a computer.

Three infrared emitters (maximum output 600 mW, dispersion angle 7^o, peak wavelength 880 nm) illuminated the eye during the recording. The camera and two infrared emitters were fixed to the turntable. The third infrared emitter was connected to the camera and aligned horizontally with the camera's optical axis. This third emitter produced the tracked corneal reflection (CR).

The eye movements were recorded using the eye-tracking device of Chronos Vision. The images of the eye were captured using an infrared sensitive CMOS camera (frame rate 50 Hz) and were relayed to a personal computer equipped with acquisition software from Chronos Vision (IRIS).

Behavioral testing

A head-fixed coordinate frame was defined as follows: the yaw (z) axis was the ventro-dorsal axis, the roll (x) axis was naso-occipital and the pitch (y) axis was interaural. Four different approaches were used to test the eye movement performance. First, the eye movement counterroll performances were measured during different static horizontal roll stimuli. Mice in upright stance (naso-occipital axis along an earth-horizontal plane) were positioned at different roll angles between ± 20^o. The mice were rotated very slowly (5^o/s) around their naso-occipital axis from one to another position. All tilt positions of the mouse were held at least for 20 sec or until the eye position was stable. Second, the optokinetic eye movements (OKR), the angular vestibulo-ocular eye movements (aVOR) and the angular visually-enhanced vestibulo-ocular eye movements (aVVOR) were measured during different paradigms. The amplitude was kept at 5^o while the frequency of the sinusoidal stimulus ranged from 0.2 to 1 Hz (generating a peak velocity between 6 deg/sec and 31 deg/sec, and a peak acceleration between 8 deg/sec^2 and 197 deg/sec^2) during the following paradigms:

1. Dynamic horizontal yaw (Yh): mice upright (naso-occipital axis along the earth-horizontal plane), rotation around ventro-dorsal axis;
2. Dynamic vertical roll (Rv): mice nose up (naso-occipital axis along the earth-vertical plane), rotation around naso-occipital axis;
3. Dynamic horizontal roll (Rh): mice upright (naso-occipital axis along the earth-horizontal plane), rotation around naso-occipital axis.

Third, aVOR was tested at constant peak velocities (8 deg/sec and 30 deg/sec) while the frequency varied between 0.1 and 1.6 Hz. Fourth, aVOR was tested at constant peak acceleration (18 deg/sec^2) while the frequency varied between 0.1 and 1.6 Hz. The constant peak velocity and acceleration were tested using the dynamic horizontal yaw paradigm (Yh).

Each paradigm was presented to the mice at least for three days, but not all the paradigms were delivered on the same day. Each animal was recorded no more than once a day. Before aVOR recordings, pilocarpine 4% (Laboratories Chauvin, France) was used to limit the pupil dilatation in darkness.

Data analysis

A calibration was made before any of the recordings were started. The camera was rotated several times by ± 10^{o} around the earth-vertical axis passing through the center of the table. The positions of the pupil (P) and corneal reflection (CR) recorded at the extreme positions of the camera rotation were used to calculate Rp, the radius of rotation of the pupil (Stahl et al., 2000).

The gain and the phase of the eye movements were calculated by using a custom-made Matlab programme (Mathworks Inc., Natick, USA). The eye position (E) was calculated using the CR and P positions from the recorded file and the Rp value was computed from the calibration (Stahl et al., 2000).

$$E = \arcsin[(CR-P)/Rp]$$

To obtain slow-phase eye velocity the eye-position data (E) was differentiated. The quick phases were identified using a velocity-threshold filter. The trace parts containing the quick phase (0.02 sec before the saccades and 0.08 sec after the saccades) were removed from the eye velocity data. To obtain stimulus velocity, the stimulus (table or drum) trace was also differentiated. Both eye and stimulus velocity signals were filtered by a Butterworth low pass filter with a cut off frequency of 40 Hz, before they were fitted by a sine wave function using a least-squares method. Gain was computed as the ratio of eye velocity to stimulus velocity whereas phase was expressed as the difference (in degrees) between the eye velocity and stimulus velocity traces. In the static roll paradigm, gain was computed as a ratio of eye position (degrees) to head position (degrees), whereas the sensitivity was computed as a ratio of eye position (degrees) to the sine of the head roll angle, which is equal with the linear acceleration along the interaural axis (head y axis) in unit of g = 981 cm/s^2 (Maruta et al., 2001).

Model description and simulation

The model is a feedback model (Figure 6A) for roll aVORs and OKRs and represents an extension of that proposed by Green and Galiana (1998). The boxes in the model represent dynamic element and circles represent summing junctions. The first order approximations of semicircular canals $C(s)=1/(T_c s+1)$, otolith organs $O(s)=1/(T_o s+1)$, neural feedback filter $F(s)=1/(T_f s+1)$, eye plant $P(s)=1/(T_p s+1)$ and retinal slip integrator $R(s)=1/s$ were implemented with T_c= 3 sec (Jones and Spells,1963; Curthoys, 1982: rat), T_o= 0.016 sec, and T_f= T_p= 0.24 sec (Fernández and Goldberg, 1976c; Robinson, 1981; Galiana and Outerbridge, 1984; Green and Galiana, 1998). The retinal slip velocity signal was saturated before it entered the model (saturation threshold 2 degr./s), because of the limited sensitivity of the retinal ganglion cells (Oyster et al., 1972; Collewijn, 1972). Model parameters associated with the gains of different pathways (see Figure 6A: a, b, c and d) were chosen to satisfy the following criteria: 1) first, weight *a* (vestibular nuclei projection) was chosen to reproduce experimentally observed horizontal roll aVOR gains of tilted mice (*a*=0.28); 2) then projection weight *b* (otoliths afferent projection) was chosen to fit the static otolith sensitivity of 26 ^{o}/g of control mice (*b*=0.121); 3) the remaining projection weights *c*

(retina projection) and *d* (cerebellar projection) were chosen to reproduce the OKR in control mice (*c*=0.10 and *d*=6.5).

The model was implemented using Matlab simulation toolbox Simulink (Mathworks, Natick, MA). Model simulations were performed using a fixed-step Runge-Kutta integration routine (ode45) with time steps of 0.01 s. Model predictions were compared to experimental data.

Statistics

To compute the session average, gain and phase values were combined per trial. Session averages from at least three days were used to calculate the final gain and phase value per mouse. Data were presented as mean ± SD. For statistical comparisons we used the two-way ANOVA for repeated measures and the standard *t*-test. Statistical analysis was performed using the commercial software package SPSS 11.0 (SPSS Inc.).

Results

Otolithic function during static roll

Tilted mice lack otoconia in both otolith organs (Ornitz et al., 1998). To test the function of the otolith organs, mice were subjected to static horizontal roll. Mice were rotated very slowly (5°/s) towards the end-point roll angle where they were held at least for 20 sec or until the eye position was stable. Head roll angles around an earth horizontal axis varied between ± 20° generating a projection of the gravity vector along the interaural axis ranging from -0.34 g to +0.34 g. Sensitivity and gain of the eye counterroll in *tilted* mice were 3 ± 3 °/g and 0.06 ± 0.005 (n = 7), respectively (Figure 1A-B).

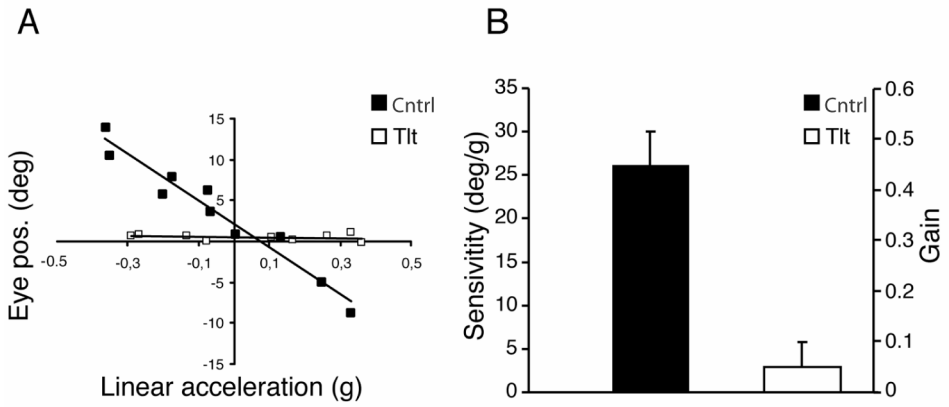

Figure 1: Static contribution of otolith organs to compensatory eye movement in normal and *tilted* mice. In **A:** one example is given for how the sensitivity was calculated: the eye position was plotted against the sine of the roll angle (the linear acceleration along the interaural axis) for a control mouse (filled squares) and a *tilted* mouse (open squares). **B:** Eye positions recorded during different static roll angles showed smaller sensitivity and gain values in *tilted* mice. Data present the mean + SD.

Both values were significantly lower than those in control mice (n = 7; sensitivity 26 ± 4°/g, p < 0.001, t-test; gain 0.45 ± 0.07, p < 0.001, t-test; Figure 1A-B). In control mice, but not in *tilted* mice, there was a linear relationship (r^2 = 0.79) between eye position and linear acceleration along the interaural axis. *Tilted* mice did not show any relationship between the eye position and the head roll angle (r^2 = 0.002). Together, these data indicate that the static contribution of the otoliths to compensatory eye movements is negligible in otoconia-deficient mice.

Contribution of otoliths to the VOR

If the static contribution of otoliths to the eye position is affected in the mutants, one expects that the dynamic contribution of otoliths to the VOR is also affected. We therefore subjected control and *tilted* mice to horizontal roll (Rh), which activates conjunctively the vertical semicircular canals and otolith organs (Figure 2A). The vertical roll (Rv; Figure 2B) and horizontal yaw (Yh; Figure 2C) paradigms were used to dynamically stimulate the vertical semicircular canals or the horizontal semicircular canals, respectively. An eye movement recording from each stimulus paradigm is shown in Figure 2.

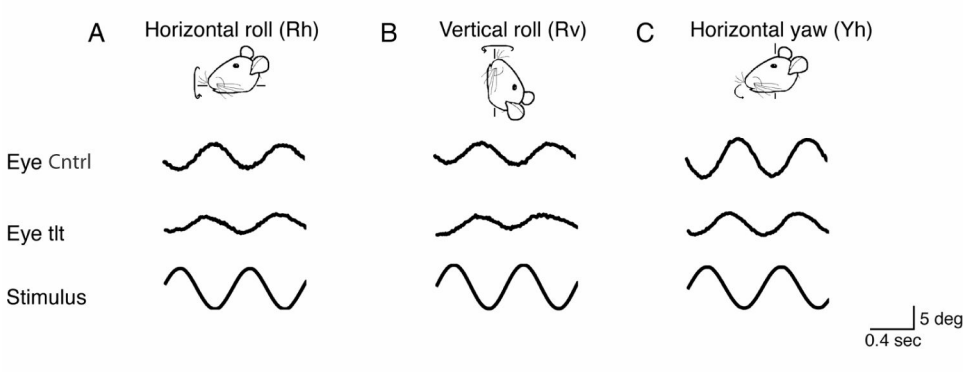

Figure 2: Example of compensatory eye movements during sinusoidal rotation in dark at 0.6 Hz and 5 degree. Vertical eye movements measured during horizontal roll aVOR (Rh; **A:**) and vertical roll aVOR (Rv; **B:**) and horizontal eye movements during yaw aVOR (Yh; **C:**) are shown. Inset: 5 degree amplitude (vertical) and 0.4 sec (horizontal).

In control mice (n = 8) the gains of the horizontal roll (Rh) aVOR varied from 0.38 ± 0.11 at 0.2 Hz to 0.59 ± 0.1 at 1.0 Hz, while their phase leads were relatively fixed around 10 degrees at all frequencies (Figure 3A). *Tilted* mice (n = 7) had significantly lower gains (varying from 0.14 ± 0.08 at 0.2 Hz to 0.44 ± 0.12 at 1 Hz; p < 0.005, ANOVA) and significantly higher phase leads (varying from 93.00 ± 19.8° at 0.2 Hz to 33.6 ± 4.9° at 1 Hz; p < 0.001, ANOVA) at all frequencies. Both the gain and phase differences between mutants and control mice decreased as the frequency increased. The finding that the eye movement performance during horizontal roll is severely affected in *tilted* mice does not necessarily mean that the eye movement performance during vertical roll and horizontal yaw stimuli are also impaired, because these are more selectively driven by the vertical and horizontal semicircular canals,

respectively. On the other hand, these types of reflexes may also be impaired in *tilted* mice, if otolith information is needed for the central integration process preceding these compensatory eye movements. We therefore investigated the aVOR during vertical roll and horizontal yaw. Although the differences between mutants (n = 9) and control mice (n = 7) were less prominent than during horizontal roll, vertical roll paradigm showed lower gains and higher phase leads in *tilted* mice (Figure 3B; for gain and phase values p = 0.08 and p < 0.01 (ANOVA), respectively).

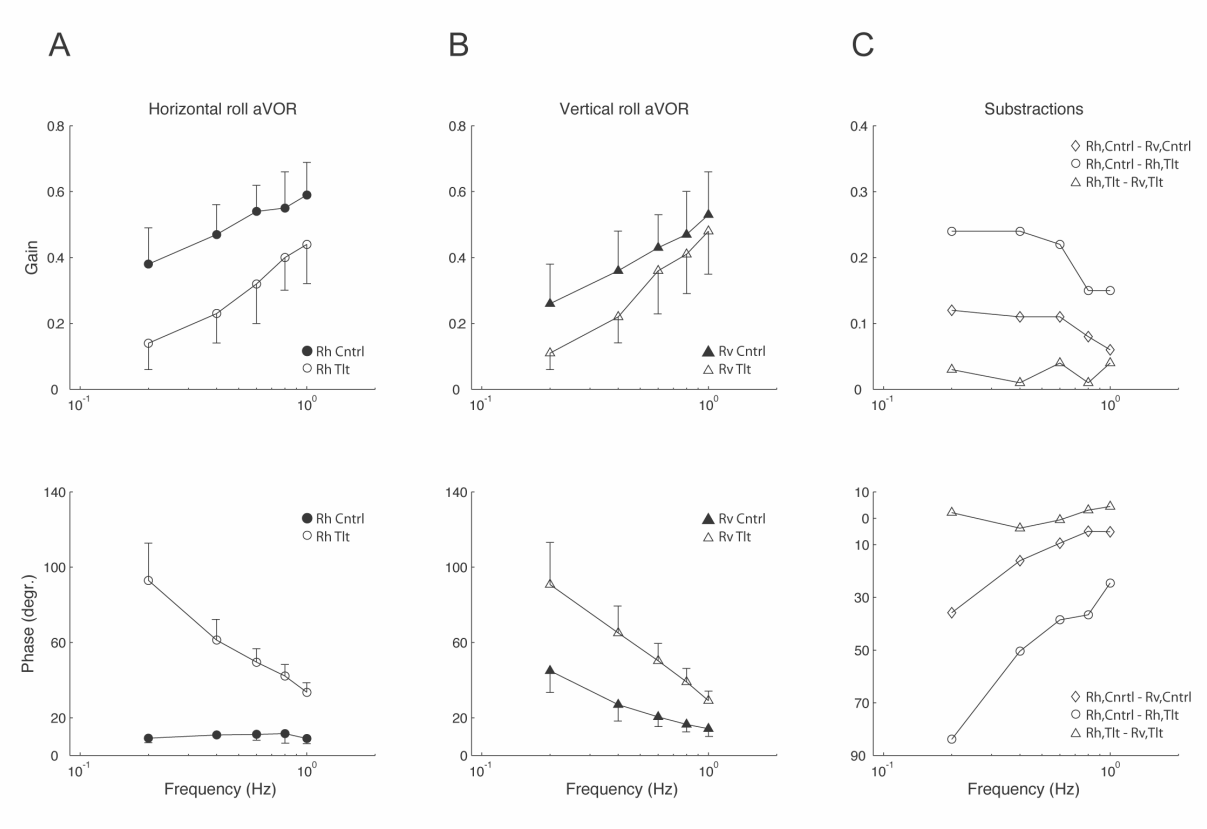

Figure 3: *Tilted* mice show deficits during roll aVOR. **A:** During horizontal roll at which both the semicircular canals and otoliths are stimulated both gain and phase values of *tilted* mice (open circles) are severely affected. **B:** During vertical roll at which only the vertical canals are directly stimulated both gain and phase values of *tilted* mice (open triangles) are moderately affected. **C:** Subtractions of the vertical roll from horizontal roll eye responses in control mice (diamonds) and *tilted* mice (triangles), as well as subtractions of the horizontal roll eye responses in *tilted* mice from horizontal roll eye responses in control mice (circles) are shown. Dynamic stimulation of otolith organs increases the gain values and decreases the phase leads of the aVOR in a frequency dependent manner (diamonds) less than the combined dynamic-static stimulation of the otolith organs (circles). In *tilted* mice there is no difference between canals only and canals-otolith mediated aVOR (triangles). Rh and Rv indicate horizontal roll and vertical roll, respectively. Data present the mean + or - SD.

The otolith input contribution to the aVOR can be determined by subtracting the vertical roll from horizontal roll eye responses in control mice or by subtracting the horizontal roll responses in *tilted* mice from the horizontal roll responses in control mice. Figure 3C shows that these two subtractions do not lead to the same outcome in terms of gain or phase. It appears unlikely that this difference is due to some

interaction between the horizontal and vertical canals, because subtraction of the eye movement performance during vertical roll in *tilted* mice from that during horizontal roll in *tilted* mice renders an outcome of approximately zero (Figure 3C). Thus, it is likely that a static-otolith driven component combined with a dynamic-otolith-canals driven component lead to higher gains and lower phases in control mice during horizontal roll aVOR as compare to *tilted* mice during vertical roll aVOR and horizontal roll aVOR.

Because the aVORs over the studied frequency range depend on peak acceleration (Van Alphen et al., 2001), we tested the horizontal yaw aVOR not only during constant amplitude (5 degrees) but also during constant peak velocity and constant peak acceleration paradigms. In control mice (n = 8) the gains of the horizontal yaw (Yh) aVOR at constant amplitude stimulation varied from 0.43 ± 0.11 at 0.2 Hz to 0.77 ± 0.11 at 1 Hz, whereas their phase leads decreased from 27.9 ± 10.2^{o} at 0.2 Hz to 6.1 ± 2.6^{o} at 1 Hz (Figure 4A).

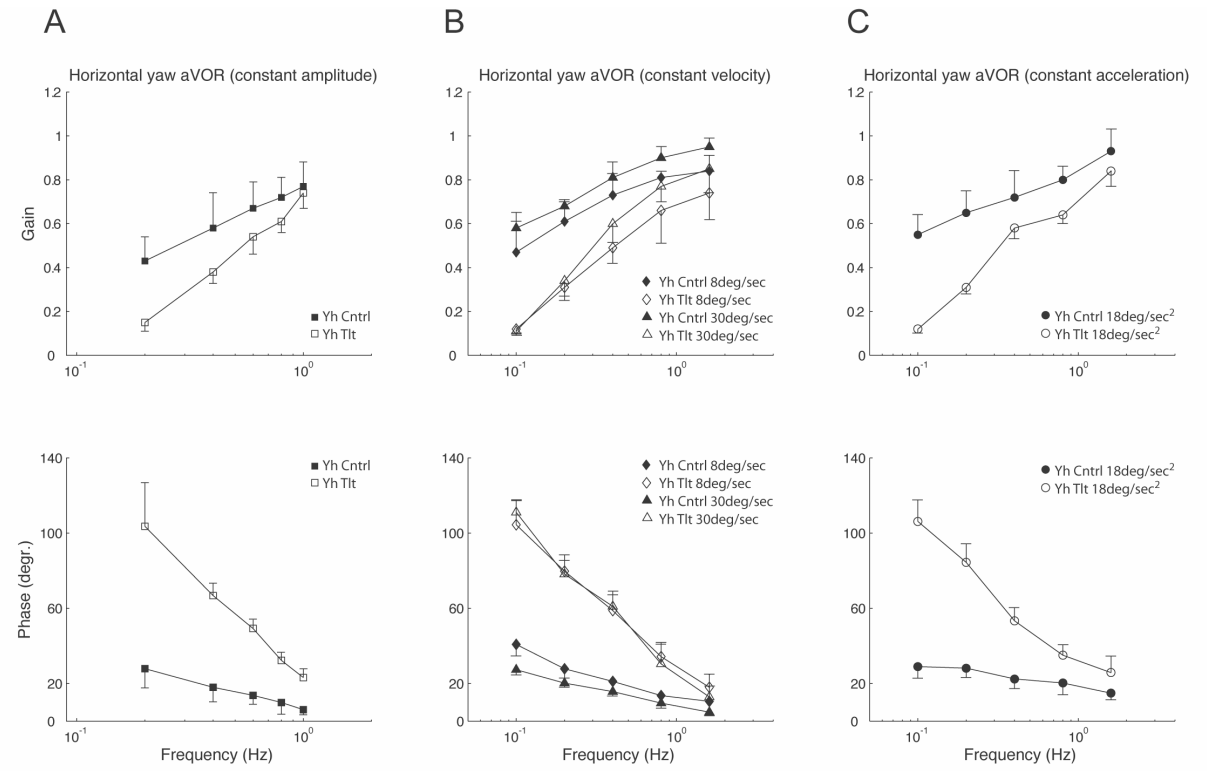

Figure 4: *Tilted* mice show deficits during yaw aVOR. During horizontal yaw in which only the horizontal canal is directly stimulated both gain and phase values of *tilted* mice are moderately affected in all tested conditions: **A:** constant amplitude (5 degree), **B:** constant velocities (8 deg/sec and 30 deg/sec) and **C:** constant acceleration (18 deg/sec/sec). Data present the mean + or - SD.

Tilted mice (n = 7) had significantly lower gains (varying from 0.15 ± 0.04 at 0.2 Hz to 0.44 ± 0.07 at 1 Hz; $p < 0.005$, ANOVA) and significantly higher phase leads (varying from 103.6 ± 23.2^{o} at 0.2 Hz to 23.2 ± 4.7^{o} at 1 Hz; $p < 0.001$, ANOVA). When the performance of the horizontal yaw (Yh) aVOR was tested during constant peak

velocity (8 deg/sec and 30 deg/sec; Figure 4B) and constant peak acceleration (18 deg/sec^2; Figure 4C), *tilted* mice (n=5) showed again significantly lower gains and significantly higher phase leads than control mice (for all gain and phase values $p < 0.001$ (ANOVA)). The aVOR gains and phases in control mice were dependent not only on frequency but also on acceleration of the stimulus (Figure 4C), increasing and decreasing, respectively, as the acceleration increased. If in *tilted* mice the aVOR gains and phases had been also dependent on amplitude and/or acceleration of the stimulus, then separate curves should have emerged in Figure 4B. In *tilted* mice aVOR gains do not depend on amplitude and/or acceleration at low frequencies (0.1 and 0.2 Hz), but depend only on the frequency of the stimulus, whereas aVOR phases depend only on stimulus frequency over the studied frequency range.

These data indicate that inputs from the otolith organs improve the eye movement performance during aVOR especially at the lower frequencies. In the absence of the otolith input, at low frequencies, the vestibular system of the mouse converts from a system dependent on frequency, peak velocity and peak acceleration of the stimulus to a system primarily dependent on the frequency of the stimulus.

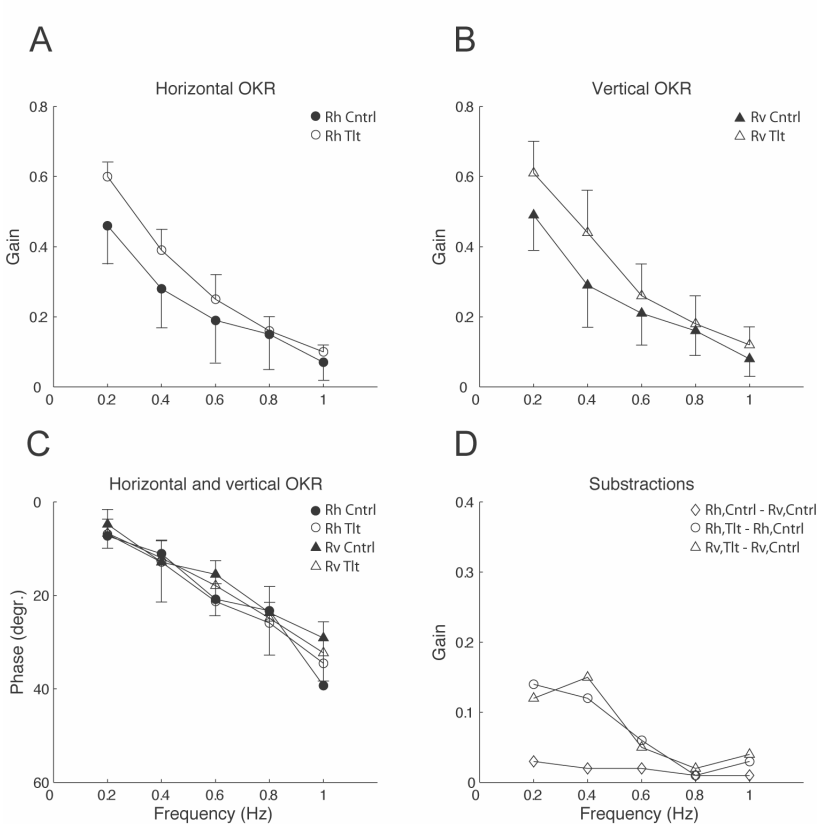

Figure 5: Low-frequency OKR compensation due to otolith dysfunction. **A-C:** *Tilted* mice show higher gains during horizontal roll OKR (A) and vertical roll OKR (B) at the lower frequencies, while their phase values are normal at all frequencies (C). **D:** The position of the mouse does not influence the compensatory OKR gains (circles and triangles). Rh and Rv indicate horizontal roll and vertical roll, respectively. Data present the mean + or - SD.

OKR compensation

The data described above showed that the otolith organs can improve both via static and dynamic mechanisms the eye movement performance during aVOR around different axes in space. This contribution is most prominent at lower frequencies. These findings raise the question whether the deficits that occur in otoconia-deficient mice during aVOR can be compensated by a secondary enhanced OKR, which can particularly dominate oculomotor performance at the lower frequency range (Collewijn and Grootendorst, 1979). We therefore tested the OKR under the same set of body orientations and frequencies that were used for the experiments described above. For the vertical eye movement OKR, i.e. that of the horizontal roll and vertical roll, the gain values of the OKR of *tilted* mice (n = 11) were significantly higher than those of control mice (n = 10) at the two lowest frequencies of 0.2 Hz and 0.4 Hz which correspond to velocities 6 deg/sec and 8 deg/sec but not at the higher frequencies (Figure 5A-B). In control mice (n = 8) the gains of the horizontal yaw OKR varied from 0.69 ± 0.08 at 0.2 Hz to 0.15 ± 0.04 at 1 Hz whereas *tilted* mice (n = 7) had significantly higher gains (varying from 0.80 ± 0.05 at 0.2 Hz to 0.26 ± 0.08 at 1 Hz; data not shown). The significance levels varied from $p < 0.05$ in vertical roll position to $p < 0.001$ in yaw position (ANOVA). In contrast, no significant differences were observed in the phase values of the OKR among the mutants and controls (p-levels varied from 0.54 in horizontal roll to 0.98 in vertical roll; ANOVA). The subtraction of the OKR gain values of control mice in horizontal roll position from those of *tilted* mice in the same position did not differ from the same subtraction in vertical roll position (Figure 5D). Thus, the position of the mouse does not influence the gains of the vertical eye movement OKR. Although the optokinetic compensation was significant and robust in all body positions in *tilted* mice, it was not sufficient to obtain a normal gain of the VVOR (Table I). For example, the VVOR gains during yaw movements were significantly higher in control mice (n = 9; 0.88 ± 0.06) than in *tilted* mice (n = 8; 0.80 ± 0.06); ($p < 0.01$, ANOVA).

Model simulations

The dynamic behaviours of the horizontal and vertical roll aVOR and OKR of control and tilted mice were simulated by the model shown in Figure 6A. To simulate the horizontal roll aVOR of control mice, vestibular nuclei projection weight *a* was set to 0.28, otoliths projection weight *b* was set to 0.121, retina projection weight *c* and cerebellar projection weight *d* were set to zero. In order to mimic the vertical roll aVOR of control mice, the otolithic projection weight *b* was reduced. In tilted mice this projection weight *b* was set to zero.

Figure 6B shows the experimental and predicted data of the roll aVOR of control and tilted mice. The predicted frequency response of the horizontal roll aVOR of control and tilted mice are consistent with our experimental data. The vertical roll aVOR of control mice was simulated by reducing the projection weight *b* by 35%.

Simulations of the model for the optokinetic response of control and tilted mice are illustrated in Figure 6C. To simulate roll OKR of control mice, vestibular nucleus projection weight *a* was set to 0.28, otolith projection weight *b* was set to zero, retina projection weight *c* was set to 0.1 and cerebellar projection weight *d* was set to 6.5.

Increment of the cerebellar projection weight *d* from 6.5 to 8.7 mimicked the optokinetic compensation observed in tilted mice. Both the experimental data as well as the predicted data show that this compensatory mechanism is frequency-dependent.

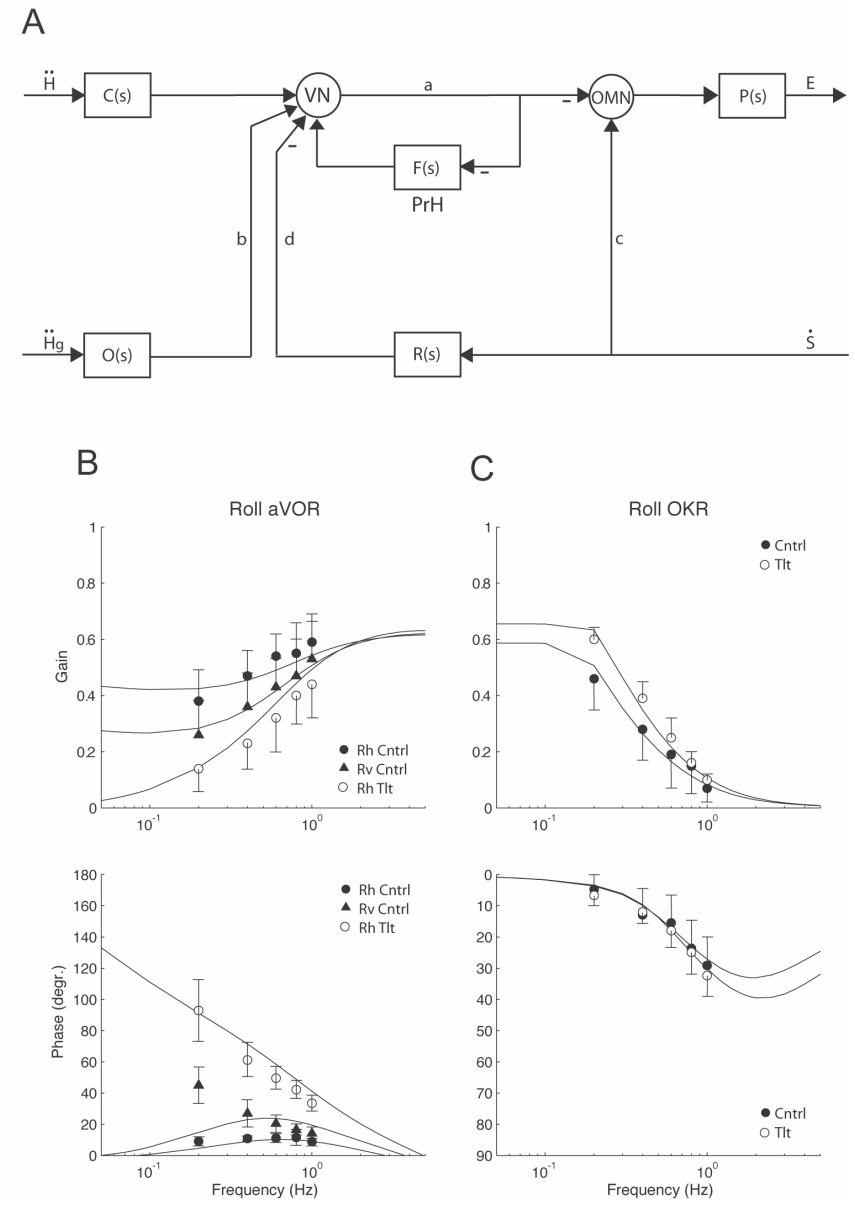

Figure 6: The proposed compensatory eye movement model with multisensory integration of otolith, canal and retina signals. **A:** Schematic representation of the model for roll aVOR and OKR in which semicircular canals C(s), otolith O(s) and retina R(s) signals are incorporated (Green and Galiana, 1998). Inputs to the model are head acceleration ($\ddot{H}$), gravity induced interaural acceleration ($\ddot{Hg}$) and retinal slip velocity ($\dot{S}$). Output of the model is eye position (E). Boxes are dynamic elements that represent a sensor [C(s), O(s) and R(s)], a motor plant [P(s)], or a neural filter [F(s)]. Circles are summing junctions used to represent particular cell populations including neurons of the vestibular nucleus (VN), neurons of the oculomotor nucleus (OMN) and neurons of the prepositus hypoglossi (PrH). The model parameters *a*, *b*, *c* and *d* associate with the projection weight of the different

pathways. Detailed description of the model parameters can be found in the material and methods section. **B:** Comparison of model predictions and experimental horizontal roll aVOR of control (filled circles; *b* = 0.121) and *tilted* mice (open circles; *b* = 0). The vertical roll aVOR of control mice was simulated by changing the projection weight *b* into 0.079. **C:** Comparison of model predictions and experimental optokinetic responses of control (filled circles; *d* = 6.5) and *tilted* mice (open circles; *d* = 8.7).

Table I: Values are mean ± SD. Gain values (eye velocity / stimulus velocity) and phase values (eye velocity - stimulus velocity in degrees) of the angular visually enhanced vestibulo-ocular reflex (aVVOR) at stimulus frequencies ranging from 0.2 to 1 Hz during horizontal roll (Rh), vertical roll (Rv) and horizontal yaw (Yh).

Gains:

Paradigm	Mice	0.2 Hz	0.4 Hz	0.6 Hz	0.8 Hz	1 Hz
Rh	Wt (n = 8)	0.78 ± 0.11	0.82 ± 0.11	0.82 ± 0.10	0.83 ± 0.13	0.82 ± 0.13
	Tlt (n = 10)	0.59 ± 0.06	0.57 ± 0.04	0.58 ± 0.05	0.63 ± 0.07	0.67 ± 0.06
Rv	Wt (n = 12)	0.70 ± 0.13	0.68 ± 0.14	0.65 ± 0.14	0.73 ± 0.15	0.72 ± 0.13
	Tlt (n = 7)	0.65 ± 0.08	0.62 ± 0.08	0.63 ± 0.08	0.67 ± 0.11	0.71 ± 0.09
Yh	Wt (n = 9)	0.85 ± 0.06	0.90 ± 0.05	0.89 ± 0.05	0.88 ± 0.06	0.88 ± 0.08
	Tlt (n = 8)	0.84 ± 0.05	0.76 ± 0.09	0.78 ± 0.04	0.81 ± 0.06	0.84 ± 0.05

Phases:

Paradigm	Mice	0.2 Hz	0.4 Hz	0.6 Hz	0.8 Hz	1 Hz
Rh	Wt (n = 8)	0.4 ± 2.8	-0.8 ± 2.4	-0.7 ± 2.9	-1.4 ± 3.0	-0.5 ± 1.5
	Tlt (n = 10)	-1.7 ± 4.4	4.2 ± 4.5	8.6 ± 5.4	5.2 ± 4.0	7.3 ± 5.0
Rv	Wt (n = 12)	3.9 ± 2.4	1.5 ± 2.3	0.8 ± 2.6	2.2 ± 2.2	2.7 ± 5.3
	Tlt (n = 7)	-0.7 ± 4.2	1.0 ± 4.9	3.8 ± 7.2	7.1 ± 4.7	4.8 ± 5.8
Yh	Wt (n = 9)	0.4 ± 1.8	0.3 ± 1.0	-0.1 ± 2.6	0.1 ± 1.3	0.7 ± 1.5
	Tlt (n = 8)	-1.1 ± 1.9	0.5 ± 3.7	3.7 ± 2.3	1.6 ± 5.1	3.5 ± 4.1

Discussion

Our data show 1) that absence of otoconia leads to dysfunctional otolith organs impairing both the static contribution to the vestibulo-ocular counterroll and the static and dynamic contribution to the angular vestibulo-ocular reflex; 2) that the deficits occur most prominently at the lower frequencies of the aVOR; 3) that the absence of functional otolith organs results in greater frequency dependence of the aVOR; 4) that in light these deficits are to a large extent compensated by an enhanced optokinetic response; and 5) that a simple model in which the vestibular nucleus was embedded as a multisensory integration unit, could simulate all eye movement behaviours observed. In conjunction, they provide supportive evidence for an adaptive multisensory integration system for stabilizing the retinal image.

VOR deficits

The lack of otoconia in *tilted* mice resulted in dysfunctional otolith organs that were virtually unable to evoke correct eye movement responses following static or dynamic displacement of the head. With regard to the static stimuli, we found that the gain and sensitivity of their eye-counterrolls were approximately 10% of those in control mice littermates. The residual counterroll eye movements in *tilted* mice might be driven by inputs from extracervical somato-sensory receptors (Krejcova, 1971; Yates et al., 2000) or by inputs from giant otoconia that are sometimes present in *tilted* mice (Ornitz et al., 1998). The sensitivity in control mice (26^{o}/g) was in between that of rabbits (17^{o}/g) (Maruta et al., 2001) and fish (30^{o}/g) (Benjamins, 1918; Cohen et al., 2001). With regard to the dynamic stimuli in *tilted* mice, we found the most prominent aberrations during horizontal roll, indicating that this paradigm evokes a relatively high activity in the otolith organs. Interestingly, comparison between control mice and *tilted* mice also revealed deficits in eye movement performance following horizontal yaw and vertical roll stimulation even though these paradigms are thought to evoke relatively little dynamic activity in the otolith organs (see also Harrod and Baker, 2003). Moreover, we showed that subtraction of the eye movement performance during horizontal roll in the mutants from that during horizontal roll in control mice is not equal to the difference between eye movement performance during vertical roll in control mice and that during horizontal roll in control mice (Figure 3C). Altogether, these results suggest the presence of an otolith component during both horizontal yaw and vertical roll stimulations and show that by placing control mice in the vertical position, the contribution of the otolith organs to aVOR is not completely removed. This possibility is confirmed by the model suggested (Figure 6A), which indicates that in vertical position the otolith organs of control mice still give a functional contribution (Figure 6B). The most obvious explanation of these unexpected otolith contributions in this situation is that the otolith organs are statically stimulated and that this static otolith signal is partially able to correct the “vertical semicircular canals aVOR” in these control mice (Figure 3B and 6B). The presence of a static otolith signal during rotation of mice in the plane of the horizontal canals will also explain the eye movement aberration found in *tilted* mice during horizontal yaw stimulations. An alternative explanation is that otolith organs were not precisely placed in the centre of rotation during stimulation. Consequently, a dynamic stimulation of the otolith organs was induced that would be large enough to contribute substantially to the aVOR. This possiblity is very unlikely, because the tangential and centripetal acceleration are under these circumstances too low (tangential acceleration = 0.002g; centripetal acceleration = 0.0002g) to elicit a response (Clarke and Engelhorn, 1998). The tilt angle of the rotation axis with respect to gravity elicits the otolith responses, therefore the facts that the macular surface of the otolith organs is curved, not planar (Flock, 1964) and that otolith organs do not lie in the plane of the semicircular canals (Curthoys et al., 1999) are also no plausible explanations for our results. Nevertheless, it remains unclear whether the mechanism suggested, is entirely responsible for this large otolith-dependent aVOR component. The possibility that otolithic deprivation in *tilted* mice altered the neuronal activity of utricular afferents still needs to be elucidated. In order to unravel this mechanism, electrophysiological measurements of either utricular afferents or vestibular nuclei neurons are necessary.

The similarities in eye movement responses evoked by horizontal linear acceleration and off-vertical axis rotation in rat led to the conclusion that utricular driven eye movement in rodents complements the semicircular canal activations in order to achieve gaze stability during horizontal roll stimulation (Hess and Dieringer, 1990, 1991). The horizontal roll aVOR can be explained by the fact that signals derived from otolith organs and semicircular canals converge at the level of vestibular neurons, which send their eye movement commands to the oculomotor nuclei (Sato et al., 2000; Zhang et al., 2001; Dickman and Angelaki, 2002; Zhang et al., 2002). The missing static otolith correction in the *tilted* mice and the convergence of the otolith and canal-driven signals might also explain our finding that the aberrations in aVOR of *tilted* mice were frequency-dependent not only during horizontal roll, but also during vertical roll and horizontal yaw. This is the first study that shows that in the absence of otolith input, the dependency of the vestibular system on the frequency of the stimulus is increased. Taken together our aVOR data support the multisensory integration theory in that the brain must combine information from semicircular canals and otolith organs in order to make proper compensatory eye movements (Harrod and Baker, 2003; Angelaki et al., 2004).

OKR compensation

We found that OKR gain values of *tilted* mice were significantly increased. Several findings support the argument that this increase reflects a mechanism that will compensate for deficits in the aVOR. First, the increases in OKR gain occurred in every position at which deficits in the aVOR were detected, i.e. that of the horizontal roll, horizontal yaw and vertical roll. Second, the increases in OKR gain occurred predominantly at the lower frequencies, which corresponds to the frequency range at which the aVOR gain values were most prominently affected. Furthermore, the VVOR gain values were not increased in *tilted* mice, suggesting that the OKR increase was not a primary effect but a secondary effect in an attempt to correct the VVOR gain values that were partly reduced.

The mechanism that underlies OKR compensation in *tilted* mice probably resembles that underlying OKR and VOR adaptation following visuo-vestibular or visual training paradigms (Collewijn and Grootendorst, 1979; Nagao, 1983; Iwashita et al., 2001). During these adaptations OKR or VOR gain values change in response to enhanced retinal slip. While a change in VOR gain depends on the direction of retinal slip in relation to the direction of the eye movement, the OKR gain always increases when there is enhanced retinal slip, independent from the direction of the slip (Collewijn and Grootendorst, 1979; De Zeeuw et al., 1998). In *tilted* mice the aVOR gains are reduced due to dysfunctional otoliths, which in turn increase the retinal slip triggering a compensatory change in the OKR. Similarly, the low-frequency aVOR can be enhanced as a mechanism to compensate for a decrease in OKR gain; this reversed process occurs in lurcher mice, which suffer from reduced OKR gain values due to a lack of floccular Purkinje cells (Van Alphen et al., 2002). Even so, it should be noted that a total blockage of the VOR such as occurs in shaker mutants, Usher Syndrome Type 1B patients or subjects after bilateral labyrinthectomy does not necessarily result in increased OKR gains (Cohen et al., 1973; Barmack et al., 1980; Sun et al., 2001). In these cases the vestibular deficits fall too much in the high frequency range and/or the increased retinal slip levels fall outside the optimal range that can drive

optokinetic signals mediating adaptation in the flocculus of the cerebellum (Simpson et al., 1996). Thus, the optokinetic system may be particularly suited to compensate for the lack of otolith-driven information necessary for a proper aVOR as both systems have similar low pass filter characteristics, while it may not be well designed to compensate for deficits in the vestibular-canal system, which dominates the higher frequencies. These observations correspond with the behaviour of our model. Alterations in the weight of cerebellar projection *d* affect the responses in a similar low-pass-filter chararacteristic way as described above (Figure 6C), suggesting that the cerebellar cortex is a suitable site for this OKR compensatory mechanism.

In conclusion, by analysing mutants with specific deficits in their otoliths we provide evidence that the otolithic input shows central cross-talk with the input of the semicircular canals and that the otolith organs provide indispensable information for the angular vestibulo-ocular reflex. The lack of otolith input increases the dependency of the vestibular system on the stimulus frequency. The optokinetic reflex can compensate for the lack of gravito-inertial perception in the low frequency range. By using a simple model, in which the vestibular nucleus was embedded as a multisensory integration unit, we were able to simulate all behaviours observed in control and in *tilted* mice. All these phenomena support the presence of an adaptive multisensory integration system that combines information from otolith organs, semicircular canals, and retina in order to make proper compensatory eye movements.

Acknowledgments

The authors gratefully acknowledge Hans van der Burg, Elize D. Haasdijk and Chronos Vision for their excellent technical support. This study was supported by NWO (ZON-MW) and NeuroBsik (Senter).

Angelaki DE, Hess BJ. 1995. Inertial representation of angular motion in the vestibular system of rhesus monkeys. II. Otolith-controlled transformation that depends on an intact cerebellar nodulus. J Neurophysiol 73:1729-1751.

Angelaki DE, Hess BJ. 1996. Three-dimensional organization of otolith-ocular reflexes in rhesus monkeys. I. Linear acceleration responses during off-vertical axis rotation. J Neurophysiol 74:2405-2424.

Angelaki DE, Shaikh AG, Green AM, Dickman JD. 2004. Neurons compute internal models of the physical laws of motion. Nature 430:560-564.

Baarsma EA, Collewijn H. 1975. Eye movements due to linear accelerations in the rabbit. J Physiol 245:227-249.

Barmack NH. 1981. A comparison of the horizontal and vertical vestibulo-ocular reflexes of the rabbit. J Physiol 314:547-564.

Barmack NH, Pettorossi VE, Erickson RG. 1980. The influence of bilateral labyrinthectomy on horizontal and vertical optokinetic reflexes in the rabbit. Brain Res 196:520-524.

Benjamins CE. 1918. Contribution á la connaissance des réflexes tonique des muscles de l'oeil. Neerlandaises de Physiologie de l'Homme et des Animaux 2:536-544.

Brettler SC, Rude SA, Quinn KJ, Killian JE, Schweitzer EC, Baker JF. 2000. The effect of gravity on the horizontal and vertical vestibulo-ocular reflex in the rat. Exp Brain Res 132:434-444.

Bush GA, Perachio AA, Angelaki DE. 1993. Encoding of head acceleration in vestibular neurons. I. Spatiotemporal response properties to linear acceleration. J Neurophysiol 69:2039-2055.

Clarke AH, Engelhorn A. 1998. Unilateral testing of utricular function. Exp Brain Res 121:457-464.

Clement G, Popov KE, Berthoz A. 1993. Effects of prolonged weightlessness on horizontal and vertical optokinetic nystagmus and optokinetic after-nystagmus in humans. Exp Brain Res 94:456-462.

Cohen B, Maruta J, Raphan T. 2001. Orientation of the eyes to gravitoinertial acceleration. Ann N Y Acad Sci 942:241-258.

Cohen B, Uemura T, Takemori S. 1973. Effects of labyrinthectomy on optokinetic nystagmus (OKN) and optokinetic after-nystagmus (OKAN). Int J Equilib Res 3:88-93.

Collewijn H. 1972. An analog model of the rabbit's optokinetic system. Brain Res 36(1):71-88.

Collewijn H, Grootendorst AF. 1979. Adaptation of optokinetic and vestibulo-ocular reflexes to modified visual input in the rabbit. Prog Brain Res 50:771-781.

Correia MJ. 1998. Neuronal plasticity: adaptation and readaptation to the environment of space. Brain Res Brain Res Rev 28:61-65.

Curthoys IS. 1982. The response of primary horizontal semicircular canal neurons in the rat and guinea pig to angular acceleration. Exp Brain Res 47(2):286-294.

Curthoys IS, Betts GA, Burgess AM, MacDougall HG, Cartwright AD, Halmagyi GM. 1999. The planes of the utricular and saccular maculae of the guinea pig. Ann N Y Acad Sci 871:27-34.

De Caprona MD, Beisel KW, Nichols DH, Fritzsch B. 2004. Partial behavioral compensation is revealed in balance tasked mutant mice lacking otoconia. Brain Res Bull 64(4):289-301.

De Zeeuw CI, Hansel C, Bian F, Koekkoek SK, Van Alphen AM, Linden DJ, Oberdick J. 1998. Expression of a protein kinase C inhibitor in Purkinje cells blocks cerebellar LTD and adaptation of the vestibulo-ocular reflex. Neuron 20:495-508.

Dickman JD, Angelaki DE. 2002. Vestibular convergence patterns in vestibular nuclei neurons of alert primates. J Neurophysiol 88:3518-3533.

Dizio P, Lackner JR. 1992. Influence of gravitoinertial force level on vestibular and visual velocity storage in yaw and pitch. Vision Res 32:111-120.

Fernandez C, Goldberg JM. 1976a. Physiology of peripheral neurons innervating otolith organs of the squirrel monkey. I. Response to static tilts and to long-duration centrifugal force. In: J Neurophysiol 39:970-984.

Fernandez C, Goldberg JM. 1976b. Physiology of peripheral neurons innervating otolith organs of the squirrel monkey. II. Directional selectivity and force-response relations. J Neurophysiol 39:985-995.

Fernandez C, Goldberg JM. 1976c. Physiology of peripheral neurons innervating otolith organs of the squirrel monkey. III. Response dynamics. J Neurophysiol 39:996-1008.

Flock A. 1964. Structure of the Macula Utriculi with Special Reference to Directional Interplay of Sensory Responses as Revealed by Morphological Polarization. J Cell Biol 22:413-431.

Fluur E, Mellstrom A. 1971. The otolith organs and their influence on oculomotor movements. Exp Neurol 30:139-147.

Galiana HL, Outerbridge JS. 1984. A bilateral model for central neural pathways in vestibuloocular reflex. J Neurophysiol 51(2):210-241.

Green AM, Galiana HL. 1998. Hypothesis for shared central processing of canal and otolith signals. J Neurophysiol 80:2222-2228.

Goto F, Straka H, Dieringer N. 2002. Gradual and reversible central vestibular reorganization in frog after selective labyrinthine nerve branch lesions. Exp Brain Res 147:374-386.

Harrod CG, Baker JF. 2003. The vestibulo ocular reflex (VOR) in otoconia deficient head tilt (het) mutant mice versus f C57BL/6 mice. Brain Res 972:75-83.

Hess BJ, Dieringer N. 1991. Spatial organization of linear vestibuloocular reflexes of the rat: responses during horizontal and vertical linear acceleration. J Neurophysiol 66:1805-1818.

Hess BJ, Dieringer N. 1990. Spatial Organization of the Maculo-Ocular Reflex of the Rat: Responses During Off-Vertical Axis Rotation. Eur J Neurosci 2:909-919.

Hurle B, Ignatova E, Massironi SM, Mashimo T, Rios X, Thalmann I, Thalmann R, Ornitz DM. 2003. Non-syndromic vestibular disorder with otoconial agenesis in tilted/mergulhador mice caused by mutations in otopetrin 1. Hum Mol Genet 12:777-789.

Iwashita M, Kanai R, Funabiki K, Matsuda K, Hirano T. 2001. Dynamic properties, interactions and adaptive modifications of vestibulo-ocular reflex and optokinetic response in mice. Neurosci Res 39:299-311.

Jones GM, Spells KE. 1963. A theoretical and comparative study of the functional dependence of the semicircular canal upon its physical dimensions. Proc R Soc Lond B Biol Sci 157:403-419.

Jones SM, Erway LC, Johnson KR, Yu H, Jones TA. 2004. Gravity receptor function in mice with graded otoconial deficiencies. Hear Res 191:34-40.

Krejcova H, Highstein S, Cohen B. 1971. Labyrinthine and extra-labyrinthine effects on ocular counter-rolling. Acta Otolaryngol 72:165-171.

Maruta J, Simpson JI, Raphan T, Cohen B. 2001. Orienting otolith-ocular reflexes in the rabbit during static and dynamic tilts and off-vertical axis rotation. Vision Res 41:3255-3270.

McCrea RA, Luan H. 2003. Signal processing of semicircular canal and otolith signals in the vestibular nuclei during passive and active head movements. Ann N Y Acad Sci 1004:169-182.

Merfeld DM, Zupan LH. 2002. Neural processing of gravitoinertial cues in humans. III. Modeling tilt and translation responses. J Neurophysiol 87:819-833.

Mergner T, Maurer C, Peterka RJ. 2003. A multisensory posture control model of human upright stance. Prog Brain Res 142:189-201.

Moore ST, Clement G, Dai M, Raphan T, Solomon D, Cohen B. 2003. Ocular and perceptual responses to linear acceleration in microgravity: alterations in otolith function on the COSMOS and Neurolab flights. J Vestib Res 13:377-393.

Nagao S. 1983. Effects of vestibulocerebellar lesions upon dynamic characteristics and adaptation of vestibulo-ocular and optokinetic responses in pigmented rabbits. Exp Brain Res 53:36-46.

Ornitz DM, Bohne BA, Thalmann I, Harding GW, Thalmann R. 1998. Otoconial agenesis in tilted mutant mice. Hear Res 122:60-70.

Oyster CW, Takahashi E, Collewijn H. 1972. Direction-selective retinal ganglion cells and control of optokinetic nystagmus in the rabbit. Vision Res 12:183-193.

Paige GD, Tomko DL. 1991. Eye movement responses to linear head motion in the squirrel monkey. I. Basic characteristics. J Neurophysiol 65:1170-1182.

Raphan T, Matsuo V, Cohen B. 1979. Velocity storage in the vestibulo-ocular reflex arc (VOR). Exp Brain Res 35:229-248.

Rude SA, Baker JF. 1988. Dynamic otolith stimulation improves the low frequency horizontal vestibulo-ocular reflex. Exp Brain Res 73:357-363.

Sato H, Imagawa M, Kushiro K, Zakir M, Uchino Y. 2000. Convergence of posterior semicircular canal and saccular inputs in single vestibular nuclei neurons in cats. Exp Brain Res 131:253-261.

Schmid-Priscoveanu A, Kori AA, Straumann D. 2004. Torsional vestibulo-ocular reflex during whole-body oscillation in the upright and the supine position: II. Responses in patients after vestibular neuritis. J Vestib Res 14:353-359.

Simpson JI, Wylie DR, De Zeeuw CI. 1996. On climbing fiber signals and their consequence(s). Beh Brain Sciences 19:380-394.

Smith M, Yuan Wang X, Wolgemuth DJ, Murashov AK. 2003. Development of the mouse vestibular system in the absence of gravity perception. Brain Res Dev Brain Res 140:133-135.

Stahl JS, van Alphen AM, De Zeeuw CI. 2000. A comparison of video and magnetic search coil recordings of mouse eye movements. J Neurosci Methods 99:101-110.

Sun JC, Van Alphen AM, Bohne BA, De Zeeuw CI. 2001. Shaker-1 mice show an optokinetic reflex but no vestibulo-ocular reflex. Ann N Y Acad Sci 942:492.

Suzuki JI, Tokumasu K, Goto K. 1969. Eye movements from single utricular nerve stimulation in the cat. Acta Otolaryngol 68:350-362.

Tomko DL, Wall CD, Robinson FR, Staab JP. 1988. Influence of gravity on cat vertical vestibulo-ocular reflex. Exp Brain Res 69:307-314.

Van Alphen AM, Schepers T, Luo C, De Zeeuw CI. 2002. Motor performance and motor learning in Lurcher mice. Ann N Y Acad Sci 978:413-424.

Van Alphen AM, Stahl JS, De Zeeuw CI. 2001. The dynamic characteristics of the mouse horizontal vestibulo-ocular and optokinetic response. Brain Res 890:296-305.

Van der Steen J, Collewijn H. 1984. Ocular stability in the horizontal, frontal and sagittal planes in the rabbit. Exp Brain Res 56:263-274.

Yates BJ, Jian BJ, Cotter LA, Cass SP. 2000. Responses of vestibular nucleus neurons to tilt following chronic bilateral removal of vestibular inputs. Exp Brain Res 130:151-158.

Zhang X, Sasaki M, Sato H, Meng H, Bai RS, Imagawa M, Uchino Y. 2002. Convergence of the anterior semicircular canal and otolith afferents on cat single vestibular neurons. Exp Brain Res 147:407-417.

Zhang X, Zakir M, Meng H, Sato H, Uchino Y. 2001. Convergence of the horizontal semicircular canal and otolith afferents on cat single vestibular neurons. Exp Brain Res 140:1-11.

Chapter 6

General discussion

The mammalian cerebellum shares its building blocks, its circuitry and even its plasticity with other areas in the brain and is, in that sense, not a unique structure. Many different brain structures in different animal groups are built according to a similar blueprint, have comparable connections and show similar forms of plasticity. Circuits such as the dorsal cochlear nucleus (Oertel and Young, 2004) and the amygdala (Medina et al., 2002) in mammals, and the central lobes and electrosensory lateral line lobe (ELL) in mormyrid electric fish (Sawtell et al., 2005), are merely examples.

A general feature of these cerebellar and cerebellum-like structures is that information conveyed by parallel fibers is used to achieve some aspect of sensorimotor coordination. Often, this involves predicting the consequences of sensory events. Examples of cerebellar computations include correcting the gain of the VOR in mammals and cancellation of the predictable components of sensory input, such as self-generated electric organ discharge (EOD) cancellation in mormyrid fish (Oertel and Young, 2004; Sawtell et al., 2005). But how is this information about the external world encoded in neural spikes and spike trains? How are these spikes transformed at successive stages of processing, for instance, in the cerebellum? How are spikes altered by experience and how are they ultimately used to guide adaptive behaviour? Studying the mammalian cerebellum alone cannot easily answer all of these questions. Therefore, analyzing comparable circuits can help to understand better the organizing principles of the cerebellum.

The mormyrid ELL, for example, forms the first stage of central electrosensory processing and receives well-understood sensory stimuli, which are easy to control experimentally. This allows specific behaviours to be traced electrophysiologically from sensory input to motor output. Furthermore, mormyrid cerebellar central lobes, in contrast to the mammalian cerebellum, lack deep cerebellar nuclei (DCN). Instead, the Purkinje neurons project onto efferent cells in their proximity in the ganglionic layer. This makes studying plasticity between Purkinje cells and the physiological-equivalent of DCN cells much more feasible than in mammals. Lastly, mormyrid Purkinje cells have unique dendritic trees, with large distances between parallel and climbing fiber innervation sites. These features of dendritic tree organization are extremely important for spike propagation and thus for the induction of synaptic gain changes at the parallel fiber-and climbing fiber-Purkinje cell synapses. Mammals and mormyrids thus posses rather different Purkinje cells in functional terms, but similar cerebellar networks. Studying both networks carefully could give valuable insights into why Purkinje cells are shaped the way they are in these systems, and what impact this has on cerebellar integrative function.

This thesis compiles research projects that differ greatly from each other at first glance but, when looked at carefully, reveal a shared goal. They individually and in combination add to the understanding of how the propagation and integration of ionic currents, and the cellular machinery activated by these currents, can induce long-term changes in Purkinje cell spike output, ultimately resulting in behavioral changes. This thesis demonstrates that mormyrid and mammalian climbing fiber responses differ in many respects. Differences in the morphology of the dendritic tree might explain these differences in the climbing fiber responses since sodium channel expression patterns and sodium currents, which are highly involved in the shaping of spike patterns, prove to be similar between these species (chapter 2).

Purkinje-like medium ganglion (MG) cells in the mormyrid ELL, which also share a similar sodium channel expression pattern, have been shown to, in contrast to mammalian Purkinje cells, display massive backpropagation of sodium spikes from the soma to the distal dendrites (Gomez et al., 2005). Anti-Hebbian plasticity in the ELL depends on the generation of these backpropagating spikes (Bell et al., 1997). Our intracellular recordings from these cells demonstrated that backpropagation is active and is sculpted by potassium currents (chapter 3).

Sodium currents, dendritic morphology, and action potential propagation thus seem to play very important roles in spike output patterns and even synaptic plasticity. Other factors, such as proteins released during synaptic stimulation, can also exert their effect on the induction, or maintenance, of long-term synaptic efficacy changes and thus on Purkinje cell spike output. Corticotropin releasing factor (CRF) is thought to be released from climbing fibers in an activity-dependent manner (Barmack and Young, 1990; Tian and Bishop, 2003). We investigated the influence of CRF on complex spike morphology and climbing fiber long-term depression (CF-LTD) induction. Application of CRF mimics the effects of CF-LTD by reducing both the second spike component and the afterhyperpolarization, and by reducing the excitatory postsynaptic current (EPSC) size (chapter 4).

Synaptic changes induced at the parallel or climbing fiber synapses during cerebellar learning tasks are known to have long-lasting effects on animal behavior (Ito, 1982; 1989). The oculomotor system is very plastic and relies heavily on cerebellar learning for its plasticity, and is therefore very well-suited to study cerebellar learning in an in vivo model. We studied the plasticity of the optokinetic reflex (OKR) and vestibule-ocular reflex (VOR) in mice that lack otoconia in their vestibular system. Our data revealed a compensatory enhanced OKR in *tilted* mice, indicating an adaptive synergism in the processing of otolith and visually-driven signals (chapter 5). In this chapter these results and their relation to each other will be discussed.

6.1 Ionic currents in spike formation

Ion channels and the currents carried by these channels are principally responsible for the anatomy of spike waveforms. They are, however, not the only factors influencing spike forms. The integration and propagation of ionic currents, mainly determined by cell morphology but also by ion channel distribution and density, also plays a crucial role (Magee et al., 1998; Stuart et al., 1997; Vetter et al., 2001). Chapters 2 and 3 of this thesis discuss the role these sodium channels and the currents carried by these channels play in the formation of spikes and the induction of plasticity. However, other important ion channels, such as calcium and potassium channels, which are known to be important for complex spike firing in rat Purkinje cells (Schmolesky et al., 2002), have not been investigated in chapter 2. Since potassium channels mainly play a role in the hyperpolarization seen at the final phase of the mammalian complex spike, it is not very likely that potassium currents are responsible for the lack of complex spikes in mormyrid Purkinje cells. However, because the distribution and density of potassium channels is not known for *Gnathonemus petersii* central lobe Purkinje cells, this idea remains speculative. For other mormyrid fish the potassium channel distribution has been elucidated for both ELL MG cells and central lobe Purkinje cells, and has been shown to be similar.

Because *Gnathonemus petersii* MG cells show a similar potassium channel distribution as these fish it is likely that central lobe Purkinje cells also display a similar potassium channel distribution (Rashid et al., 2001a+b).

Chapter 3 shows that blocking potassium currents in MG cells of the mormyrid ELL by TEA application leads to a broadening of the spikes fired by these cells. The slow climbing fiber-evoked sodium excitatory postsynaptic potential (EPSP) recorded from the mormyrid central lobe Purkinje cells can thus potentially be explained by a lower expression level of potassium channels in these fish compared to rat Purkinje cells. Calcium channels are involved in forming the plateau potential of the mammalian complex spike and might be responsible for the spikelets riding on top of this plateau (Schmolesky et al., 2002). As for potassium channels, there is only a small body of evidence showing the presence of calcium currents and thus calcium channels in the mormyrid central lobes. Plasticity in the mormyrid ELL is known to rely on calcium signals much like the plasticity seen in the mammalian cerebellum. The distribution of calcium channels over the plasma membrane of central lobe Purkinje cells is unknown. The advanced calcium signaling pathway through inositol 1,4,5-triphosphate (IP_3)-mediated internal stores seems to be highly conserved throughout evolution (Koulen et al., 2000). Whether or not this also holds true for calcium channels in the plasma membrane remains to be elucidated, but the importance of calcium for many crucial pathways in neuronal action suggests that it will be. Since calcium channels are heavily involved in shaping the mammalian complex spike, a difference in the expression pattern or distribution of calcium channels in mormyrid Purkinje cells could explain the differences in the evoked climbing fiber response. Calcium channel expression and distribution patterns therefore are an interesting subject for future studies.

Antibody labeling in chapter 2 indicated that voltage-gated sodium channel α-subunits are distributed equally over the plasma membranes of rat and mormyrid fish Purkinje cells. The channel densities also proved to be comparable between these species. The α-subunits $Na_v1.1$ and $Na_v1.6$ have been shown to be expressed in mammalian Purkinje cells (Gong et al., 1999; Schaller and Caldwell, 2003). $Na_v1.2$ expression, however, is still under debate (Black et al., 1994; Felts et al., 1997; but see Brysch et al., 1991; Gong et al., 1999). In our hands, $Na_v1.2$ sodium channels seem to be present in both rat and mormyrid Purkinje cells in both the somata and the dendrites of Purkinje neurons. Our western blot experiments confirm the presence of a protein of the appropriate size that is recognized by the antibody against $Na_v1.2$ α-subunits. The assignment of the different sodium currents to the various sodium channels is not straightforward. Therefore, we cannot conclude from the presence of particular sodium currents that a particular sodium channel is expressed. Single channels can produce different currents under different conditions, and some are even capable of producing all three sodium currents observed in mammalian Purkinje cells (e.g. $Na_v1.6$). The presence of, for instance, fast sodium currents does not prove the presence of sodium channel $Na_v1.1$. A caveat of our study is that the use of commercially-available antibodies on mormyrid tissue is not straightforward. These antibodies are usually directed against rat or mouse antigens, and have been raised in mammals. This leads to questions such as the specificity of the antibodies used in the mormyrid brain and the homology of the antigens studied, as a gene library of mormyrids is not available to answer this last question. This makes the use of a large arsenal of control studies a necessity. Furthermore,

determination of the expression density is virtually impossible. These facts only allow us to report the staining patterns we find in descriptive terms. All three sodium channels described seem to be present in the dendrites of both rat and mormyrid Purkinje cells. $Na_v1.2$ and $Na_v1.6$ labeling appears to be very dense in the dendrites. Stuart and Häusser, however, showed using patch-clamp recordings from the soma and dendrites that the amplitude of sodium current following an action potential decreased in amplitude with increasing distance into the dendrites. Outside-out patches excised from the soma and dendrites revealed that the sodium channel current density also decreased with distance from the soma (Stuart and Häusser, 1994). Their data suggests fewer sodium channels at the distal dendrites. Their initial finding can be explained, however, by active damping of the backpropagating action potential by, for instance, potassium currents. Another explanation could be that our staining only appears to be very dense in the molecular layer because of the increasing membrane to volume ratio in the dendrites versus the soma.

The electrophysiological responses we recorded from mormyrid fish, i.e. sodium currents and the CF EPSCs, were consistently about half of the size of the same response in rat Purkinje cells. Since the staining densities of sodium channels were similar, suggesting a similar channel density, a lower sodium channel expression level does not seem to explain the difference observed. The somata of mormyrid Purkinje cells are about half the size of rat Purkinje cell somata. Since the sodium currents recorded from dissociated cells also proved to display a 1:2 ratio for mormyrid fish versus rat Purkinje cells, the cell size and therefore lower capacitance of the mormyrid Purkinje cell caused the smaller currents observed, rather than a difference in channel density.

6.2 Backpropagating spikes and dendritic morphology

Chapter 3 discusses the backpropagation of sodium spikes in the dendritic tree of the MG cells in the mormyrid ELL. It studies the localization of sodium channels along the somato-dendritic axis and investigates the shaping of broad sodium currents by potassium currents and the possible involvement of γ-aminobutyric acid (GABA) in the induction of anti-Hebbian plasticity, which depends on the backpropagation of spikes. Backpropagation of sodium spikes into the dendritic tree seems to depend heavily on the shape of the dendritic tree. Long straight dendrites propagate spikes easily, whereas branching points heavily attenuate the signal (Vetter et al., 2001). Also, the expression patterns of calcium and potassium channels along the dendrite can facilitate or block backpropagation, respectively (Tsubokawa et al., 2000; Williams and Stuart, 2000).

The dendritic trees of the MG cells in the mormyrid ELL are long and straight and only branch at the very proximal dendrites. The dendritic organization of these cells is therefore highly suited for spikes to backpropagate. Indeed, MG cells show almost unrestricted backpropagation of somatic broad action potentials into the dendrites (Lemon and Turner, 2000). The dendritic trees of Purkinje cells located in the central lobes of the mormyrid “cerebellum” display a similar architecture as seen in MG cells. They have highly organized long dendrites, which run parallel to each other towards the pial surface. Therefore, it is highly possible that central lobe Purkinje cells, in contrast to mammalian Purkinje cells, display backpropagation of spikes all the way

into the very distal dendrites. The expression patterns of sodium and potassium channels play a major role in backpropagation as well, but the sodium channel densities investigated in chapter 2 and 3 are very similar for both ELL MG and central lobe Purkinje cells. In addition, the potassium channel expression patterns are likely to be similar as explained in paragraph 6.1. Since backpropagating spikes in the ELL are crucial for the generation of anti-Hebbian plasticity, it is tempting to consider the possible existence of anti-Hebbian plasticity at the parallel fiber to central lobe Purkinje cell synapse.

The physical distance between parallel fiber and climbing fiber innervation sites is very large for central lobe Purkinje cells as compared to mammalian Purkinje cells. A "golden rule" for the induction of associative synaptic gain changes is that a large calcium signal, caused by for instance climbing fiber activation, and parallel fiber activity occur within a certain time frame (Coesmans et al., 2004). The initiation site of parallel fiber plasticity is at the parallel fiber to Purkinje cell synapse, which in the mormyrid central lobes is far away from the climbing fiber innervation site. Therefore, the large depolarizing potential reaching the soma of the cell after climbing fiber activity likely needs to backpropagate to the distal dendrites to evoke voltage-gated calcium influx which, combined with NMDA receptor activation, leads to an associative depression at the parallel fiber synapse. Backpropagation is thus possibly present in central lobe Purkinje cells that resemble MG cells in features crucial for backpropagation. Moreover, they are likely to depend on backpropagation for the induction of plasticity since the synaptic input sites are so far apart. Mammalian Purkinje cells, which show heavily attenuated backpropagating spikes due to the high degree of dendritic branching (Stuart and Häusser, 1994), display a completely different innervation pattern than mormyrid central lobe Purkinje cells. The climbing fiber innervation runs up very high in the dendritic tree and is thought to innervate even rather distal dendrites. The climbing fiber innervation in mammals overlaps to a large degree with the parallel fiber innervation sites. In a system like this, where the distance between the depolarizing climbing fiber input and the (also) plastic parallel fiber input is only short, there is thus no need for backpropagating signals in the induction of plasticity.

6.3 Climbing fiber LTD and spike modulation

There are many intracellular factors involved in the induction and maintenance of rat cerebellar plasticity, such as glutamate receptors, ion channels, IP_3 stores, and the protein kinase A (PKA) and protein kinase C (PKC) pathways. Chapter 4 studied the role of the intracellular factor CRF at the rat climbing fiber terminals, which have been shown to be plastic (Hansel and Linden; 2000). We showed that CRF application mimics the effects of CF-LTD by reducing the climbing fiber EPSC, the second complex spike component and the complex spike afterhyperpolarization (AHP) in rat Purkinje neurons. CRF seems to be part of the PKA and/or PKC signaling pathway since application of PKA or PKC inhibitors attenuated the effects of CRF. The main role for CF-LTD in cerebellar learning is to change the probability for parallel fiber LTD by a reduction in the climbing fiber-evoked calcium transients (Schmolesky et al., 2002; Coesmans et al., 2004). Also, a role in preventing calcium concentrations to reach neurotoxic levels during high-frequency firing (O'Hearn and Molliver, 1997) has been postulated for CF-LTD. The influence of CRF application and CF-LTD

induction on the complex spike waveform itself is interesting because changes in complex spike morphology may lead to changes in the number of action potentials generated by the axon and changes in the duration of the “complex spike pause” in simple spike firing (Figure 1) (Schmolesky et al., 2002).

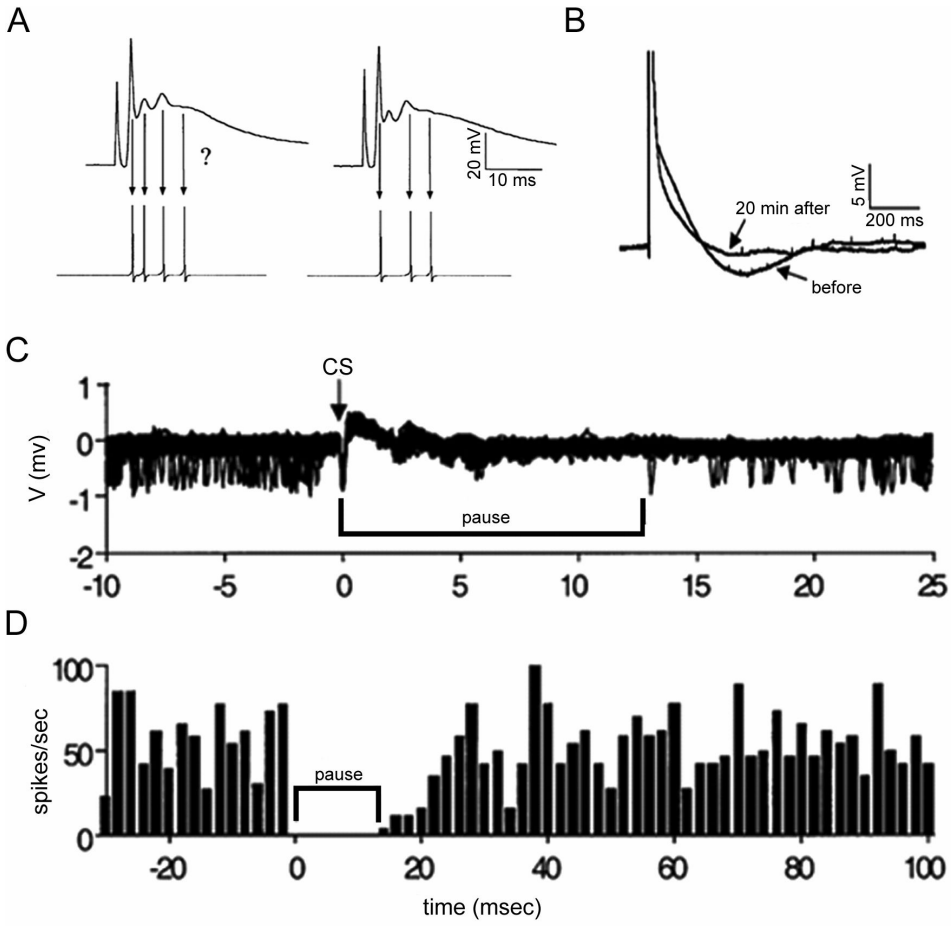

Figure 1: A: Each spike (or spikelet) component of the complex spike might activate an axonal spike. Selective attenuation of one spikelet could result in alteration of the axonal spike pattern. **B:** Climbing fiber (CF) tetanization-induced modifications of the complex spike waveform can also be associated with a reduction in the slow afterhyperpolarization. **C,D:** Extracellular recordings of spontaneous activity from a single Purkinje cell in an awake mouse reveal a high rate of simple spike firing that is interrupted by the AHP of a single complex spike. The simple spike activity before and after a complex spike is presented by overlaying 130 traces locked to complex spike generation (C:). The peri-response time histogram (2-ms bin width) generated from these data reveal an absolute pause of 13 ms (D:). This pause can potentially be modified by changes in the AHP amplitude *(adapted from Schmolesky et al., 2002).*

To date, we have limited information on the axonal spike pattern that results from a complex spike. Initial data indicate that every spikelet can activate an all-or-nothing sodium spike in the axon, but this observation was not made for every complex spike (Ito and Simpson; 1971). Also, changes in the AHP could be crucial. A spontaneous or stimulus-driven complex spike leads to a pause in ongoing high-frequency simple spike activity (Simpson et al., 1996). One standing hypothesis is that this complex

spike pause is due in part to the same calcium-activated potassium currents that generate the complex spike AHP. Since CRF application and CF-LTD both consistently attenuate the AHP, and thus also attenuate the calcium-activated potassium currents, they probably also exert their effect on the complex spike pause in simple spike firing. Furthermore, learning-associated reductions in K^+-mediated hyperpolarizations have been reported in multiple regions of the brain including the cerebellum where AHP reductions in Purkinje cells of rabbits have been observed following classical conditioning (Schreurs et al., 1998). Strikingly, we can conclude from these data that rather small changes in the complex spike waveform of rat Purkinje cells, due to depression of the climbing fiber to Purkinje cell synapse, likely have a large impact on the firing behavior of the Purkinje cell. Mormyrid central lobe Purkinje cells respond to climbing fiber activity with spikes that are far less “complex” and thus appear to be less prone to subtle modifications than the rat climbing fiber response. However, climbing fiber responses of mormyrid central lobe Purkinje cells do appear in several waveforms under conditions that need to be unraveled further. The climbing fiber response in these cells either consists of a single EPSP, a similar EPSP with small spikes on top of the slow decay phase, or a so-called “broadspike” (Han and Bell, 2003). Since small changes in spike morphology of rat Purkinje cells impose large differences in spike output, it is possible that Purkinje cells in the mormyrid central lobes respond with different patterns of axonal spikes to the different climbing fiber responses recorded at the soma. This, and the conditions underlying the climbing fiber response differences, needs to be investigated further to address these ideas.

6.4 Sensorimotor systems in rats and mormyrids

Two seemingly distinct systems are discussed in chapters 3 and 5, namely, the electrosensory system, of which the ELL forms an important part (chapter 3), and the oculomotor system (chapter 5). These systems are not as distinct, however, as they appear to be at first glance. Both systems are used to analyse sensory information, and both make use of a highly plastic “cerebellar” side loop to adjust the sensory information they receive before sending it to higher motor centers (Bell et al., 2005; Sawtell et al., 2005; Ito, 1972, 1982). There are also several differences between these systems. The mormyrid electrosensory system, for instance, receives only one type of sensory information via the electrosensory afferents projecting from electroreceptors in the skin towards the ELL (Sawtell et al., 2005). The ELL compares this sensory input with feedback, such as information about self-generated EODs, which it receives from higher motor centers. The ELL integrates this information, which it receives via parallel fiber systems, and subtracts the self-generated EOD from the electrosensory signal (Sawtell et al., 2005). The ELL, like all mormyrid cerebellar structures, is therefore specialized to receive parallel fiber information and to work as a coincidence detector (Meek, 1992). The mammalian oculomotor system receives sensory information from the eyes and the vestibular system. Visual input is received by the Purkinje cells mainly through climbing fibers. The visual information can thus be considered as an error signal when it coincides with vestibular information transmitted through the mossy fiber, parallel fiber pathway (Arnold and Robinson, 1991). The mammalian cerebellum therefore can be considered to be specialized in analyzing climbing fiber input (Meek, 1992). The

mammalian cerebellum, like the mormyrid cerebellum and ELL, also appears to work as a coincidence detector (Meek, 1992).

6.5 Future experiments

This thesis presents a large quantity of new data concerning the function of sodium channels, spike anatomy, spike propagation, spike integration, intracellular factors and otolith deprivation in cerebellar plasticity. New data is gathered to elucidate old questions, but often also poses new ones. From the experimental data presented in this thesis, the following questions arise and form new possible subjects of study.

Chapter 2 describes the role of sodium channels in shaping climbing fiber response patterns in a comparative study between rat cerebellum and the mormyrid central lobes. The role that potassium currents and especially calcium currents play in shaping climbing fiber responses in rat cerebellar Purkinje cells has been well established (see paragraphs 1.3 and 6.2). The expression patterns of the different potassium and calcium channels are unknown for the mormyrid cerebellum. It is possible that the currents carried by these channels differ between species. These channels are therefore worthwhile studying. Even though the different sodium currents studied in chapter 2 did not differ between rat and mormyrid Purkinje cells, suggesting that the sodium channels carrying these currents share similar properties, we do not know if the β-subunits that associate with the sodium channel α-subunits are also similar.

As discussed in paragraph 6.3, the waveform of rat climbing fiber responses may determine axonal spike patterns, which are sent to the DCN cells, and the complex spike interval in simple spike firing. LTD at the climbing fiber synapse likely modulates this phenomenon. This hypothesis needs to be tested for rat Purkinje cells, but similar phenomena in Purkinje cells of the mormyrid central lobes are also worthwhile studying.

Backpropagating spikes in the ELL have been shown to be crucial for the induction of anti-Hebbian plasticity at the parallel fiber to MG cell synapse (discussed in paragraphs 1.3, 3 and 6.2). Since the morphology of Purkinje cells in the central lobes resembles MG cell morphology more than it resembles Purkinje cell morphology in higher vertebrates, demonstrating backpropagation of action potentials into the dendritic tree of these cells could be the first step towards also describing anti-Hebbian plasticity at the central lobe Purkinje cells in the mormyrid brain. Furthermore, it is only a matter of time before reports about plasticity at the central lobes are published, as all cerebellar systems studied in great detail so far have been shown to be highly plastic. The role of DCN plasticity in cerebellar adaptation has recently attracted much attention (chapter 5; Aizenman et al., 1998). There are, however, no descriptions of plasticity at the “Purkinje” cell to efferent cell synapse anywhere in the mormyrid “cerebellar” structures. Since the DCN-like efferent cells are located in the same layer as the Purkinje cells, the mormyrid central lobes are highly suited to study plasticity at the Purkinje cell to efferent cell synapse in a much simpler way than possible in the mammalian cerebellum.

In chapter 4, we investigated the role of CRF in CF-LTD. CF-LTD is the only form of plasticity thus far known at this synapse. Depression of a synapse always needs to be reversed by potentiation; otherwise, the depression would become saturated and render the synapse useless. From this theoretical standpoint, there must thus also be some form of postsynaptic CF-LTP. Protocols to induce potentiation at the climbing fiber to Purkinje neuron synapse need to be developed, but what potentiation at this synapse would mean for Purkinje cell output remains speculative. An increase in the number of plateau spikelets could lead to a higher number of axonal action potentials per complex spike fired. A longer simple spike pause, due to a higher influx of calcium ions and thus a larger activation of calcium-activated potassium channels, can also be a consequence.

In chapter 5, we proposed a model that explains our finding that the OKR can compensate for the lack of gravitoinertial perception in the low-frequency range. This was done by assuming that the vestibular nucleus is the multisensory integration unit responsible for this compensation. In other words, we assume that the vestibular nucleus is plastic in this system. It would be very elegant if this model could be confirmed by blocking plasticity in the vestibular nucleus in the *tilted* mouse. This could provide us with information to what extent the vestibular nucleus is involved in OKR adaptation and what the ratio between cerebellar cortical versus vestibular nuclear adaptation is in this system.

Aizenman CD, Manis PB, Linden DJ. 1998. Polarity of long-term synaptic gain change is related to postsynaptic spike firing at a cerebellar inhibitory synapse. Neuron 21(4):827-835.

Barmack NH, Young WS. 1990. Optokinetic stimulation increases corticotropin-releasing factor mRNA in inferior olivary neurons of rabbits. J Neurosci 10:631-640.

Bell CC, Caputi A, Grant K. 1997. Physiology and plasticity of morphologically identified cells in the mormyrid electrosensory lobe. J Neurosci 17:6409-6423.

Bell CC, Meek J, Yang JY. 2005. Immunocytochemical identification of cell types in the mormyrid electrosensory lobe. J Comp Neurol 483:124-142.

Black JA, Yokoyama S, Higashida H, Ransom BR, Waxman SG. 1994. Sodium channel mRNAs I, II and III in the CNS: cell-specific expression. Brain Res Mol Brain Res 22:275-289.

Brysch W, Creutzfeldt OD, Luno K, Schlingensiepen R, Schlingensiepen KH. 1991. Regional and temporal expression of sodium channel messenger RNAs in the brain during development. Exp Brain Res 86:562-567.

Coesmans M, Weber JT, De Zeeuw CI, Hansel C. 2004. Bidirectional parallel fiber plasticity in the cerebellum under climbing fiber control. Neuron 44(4):691-700.

Felts PA, Yokoyama S, Dib-Haij S, Black JA, Waxman SG. 1997. Sodium channel α-subunit mRNAs I, II, III, NaG, Na6 and hNE (PN1): different expression patterns in developing rat nervous system. Brain Res Mol Brain Res 45:71-82.

Gomez L, Kanneworff M, Budelli R, Grant K. 2005. Dendritic spike back propagation in the electrosensory lobe of *Gnathonemus petersii*. J Exp Bio 208: 141-155.

Gong B, Rhodes KJ, Bekele-Arcuri Z, Trimmer JS. 1999. Type I and type II Na(+)channel α-subunit polypeptides exhibit distinct spatial and temporal patterning, and association with auxiliary subunits in rat brain. J Comp Neurol 412:342-352.

Han VZ, Bell CC. 2003. Physiology of cells in the central lobes of the mormyrid cerebellum. J Neurosci 23(35):11147-11157.

Hansel C, Linden DJ. 2000. Long-term depression of the cerebellar climbing fiber Purkinje neuron synapse. Neuron 26:473-482.

Ito M, Simpson JI. 1971. Discharges in Purkinje cell axons during climbing fiber activation. Brain Res 31:215-219.

Ito M. 1972. Neural design of the cerebellar motor control system. Brain Res 40(1):81-84.

Ito M. 1982. Cerebellar control of the vestibulo-ocular reflex around the flocculus hypothesis. Annu Rev Neurosci 5:275-296.

Ito M. 1989. Long-term depression. Annu Rev Neurosci 12:85-102.

Koulen P, Janowitz T, Johnston LD, Ehrlich BF. 2000. Conservation of localization patterns of IP(3) receptor type 1 in cerebellar Purkinje cells across vertebrate species. J Neurosci Res 61(5):493-499.

Lemon N, Turner RW. 2000. Conditional spike backpropagation generates burst discharge in a sensory neuron. J Neurophysiol 84(3):1519-1530.

Magee J, Hoffman D, Colbert C, Johnston D. 1998. Electrical and calcium signaling in dendrites of hippocampal pyramidal neurons. Annu Rev Physiol 60:327-346.

Medina JF, Repa JC, Mauk MD, LeDoux JE. 2002. Parallels between cerebellum and amygdala dependent conditioning. Nat Rev 3:122-131.

Meek J. 1992. Comparative aspects of cerebellar organization; From mormyrids to mammals. Eur J Morph 30:37-51.

Oertel D, Young ED. 2004. What's a cerebellar circuit doing in the auditory system? TINS 27(2):104-110.

O'Hearn E, Molliver ME. 1997. The olivocerebellar projection mediates ibogaine-induced degeneration of Purkinje cells: a model of indirect, trans-synaptic excitotoxicity. J Neurosci 15:8828-8841.

Rashid AJ, Dunn RJ, Turner RW. 2001a. A prominent soma-dendritic distribution of $K_v3.3$ K+ channels in electrosensory and cerebellar neurons. J Comp Neurol 441:234-247.

Rashid AJ, Morales E, Turner RW. 2001b. The contribution of dendritic K_v3 K+ channels to burst threshold in a sensory neuron. J Neurosci 21:125-135.

Sawtell NB, Mohr C, Bell CC. 2005. Recurrent feedback in the mormyrid electrosensory system: Cells of the preeminential and lateral toral nuclei. J Neurophys 93:2090-2103.

Sawtell NB, Williams A, Bell CC. 2005. From sparks to spikes: information processing in the electrosensory systems of fish. Cur Opin Neurobiol 15:437-443.

Schaller KL, Caldwell JH. 2003. Expression and distribution of voltage-gated sodium channels in the cerebellum. The Cerebellum 2:2-9.

Schreurs BG, Gusev PA, Tomsic D, et al. 1998. Intracellular correlates of acquisition and long-term memory of classical conditioning in Purkinje cell dendrites in slices of rabbit cerebellar lobule HVI. J Neurosci 18:5498-5507.

Schmolesky MT, Weber JT, De Zeeuw CI, Hansel C. 2002. The making of a complex spike: ionic composition and plasticity. Ann NY Acad Sci 978:359-390.

Simpson JI, Wylie DR, De Zeeuw CI. 1996. On climbing fiber signals and their consequence(s). Behav Brain Sci 19:384-398.

Stuart G, Häusser M. 1994. Initiation and spread of sodium action potentials in cerebellar Purkinje cells. Neuron 13:703-712.

Stuart G, Spruston N, Sakmann B, Häusser M. 1997. Action potential initiation and backpropagation in neurons of the mammalian CNS. Trends Neurosci 20:125-131.

Tian JB, Bishop GA. 2003. Frequency-dependant expression of corticotropin releasing factor in the rat's cerebellum. Neuroscience 121:363-377.

Tsubokawa H, Offermans S, Simon M, Kano M. 2000. Calcium-dependant persistent facilitation of spike backpropagation in the CA1 pyramidal neurons. J Neurosci 20(13):4878-4884.

Vetter P, Roth A, Häusser M. 2001. Propagation of action potentials in dendrites depends on dendritic morphology. J Neurophysiol 85:926-937.

Williams SR, Stuart GJ. 2000. Action potential backpropagation and somato-dendritic distribution of ion channels in thalamocortical neurons. J Neurosci 20(4):1307-1317.

Summary

The cerebellum controls the motor system by analyzing differences between intention and action, and by adjusting the actions of motor centers in the spinal cord and cerebral cortex accordingly. There are strong indications for a cerebellar role in the recalibration and adaptive adjustment of movements, learning of motor skills and associative learning. Disease of the human cerebellum leads to abnormalities that can be fitted into three main categories: hypotonia, ataxia and intention tremors.

The principal cell type in the mammalian cerebellum is the Purkinje cell which forms the sole output of the cerebellar cortex. Purkinje cells receive input from excitatory parallel fibers and climbing fibers. The signals Purkinje cells compute from these inputs are sent via the deep cerebellar nuclei to higher motor centers. The cerebellum and cerebellar-like structures of mormyrid fish are grossly organized the same way. They also contain Purkinje or Purkinje-like cells and receive input from parallel fibers and, in some structures, climbing fibers. The cerebellar output is, however, sent to efferent cells located in the ganglionic layer instead of deep nuclei.
On a single-cell level the differences between mammalian and mormyrid Purkinje cells are striking. Mormyrid Purkinje cell dendrites are straight and long, and branch sparsely only at the most proximal dendrites, whereas mammalian Purkinje cells display branching throughout their dendritic trees. Another large difference is the physical distance between parallel fiber and climbing fiber innervation sites, which are rather distant from each other in the mormyrid cerebellum, but overlap considerably in the mammalian cerebellum.

Climbing fiber stimulation of mammalian Purkinje cells leads to an all-or-none climbing fiber response called the “complex spike”. Sodium channels are likely to play an important role in shaping the complex spike. Mormyrid fish, however, respond to climbing fiber stimulation with a slow all-or-none excitatory postsynaptic potential (EPSP) lacking the characteristic spike components of the complex spike. Purkinje-like cells in the mormyrid electrosensory lateral line lobe (ELL) are known to backpropagate sodium spikes elicited in the soma towards the distal parts of their dendritic tree. In contrast, mammalian Purkinje cells do not backpropagate sodium spikes.

Connections in the mammalian cerebellar cortex are highly plastic. Plastic changes have been described at the parallel fiber-Purkinje cell synapse, where presynaptic long-term potentiation (LTP) and postsynaptic LTP and long-term depression (LTD) have been described, and at the climbing fiber-Purkinje cell synapse, where postsynaptic LTD has been noted. The mormyrid ELL is plastic at the parallel fiber-Purkinje cell synapse where anti-Hebbian plasticity has been described. This form of plasticity relies heavily on backpropagating spikes.

The mammalian oculomotor system is highly suitable to study cerebellar function and thus cerebellar plasticity in vivo. This system compares and controls the vestibulo-ocular reflex (VOR), optokinetic reflex (OKR) and cervicoocular reflex to reduce retinal slip. The cerebellum and vestibular nucleus play a central role in this system.

Chapter 2 begins with a description of rat and mormyrid climbing fiber responses which differ markedly between these species. Sodium channels and dendritic branching patterns are known to play an important role in shaping the climbing fiber response. We thus investigated the localization of sodium channel α-subunits in the mormyrid central lobes and the rat cerebellum. We found that $Na_v1.1$, $Na_v1.2$ and $Na_v1.6$ α-subunits are distributed equally over the plasma membrane of the Purkinje cells in these structures. We then described the currents carried by the sodium channels studied, since differences in these currents could potentially explain the difference in climbing fiber response. We found, however, that the sodium currents recorded from rats and mormyrid fish shared their kinetic properties both in acutely isolated Purkinje cell somata and in intact Purkinje cells in slices. We therefore concluded that our study provides a first description of the sodium channel distribution in the mormyrid central lobes and confirms the presence of $Na_v1.2$ in the rat cerebellum. The differences found in climbing fiber response patterns cannot, however, be attributed to differences in sodium channel distribution. These differences are more likely caused by the completely different branching characteristics of the Purkinje cell dendritic trees of these animals. A contribution of calcium and potassium currents also cannot be excluded.

Chapter 3 describes the localization of tetrodotoxin (TTX) sensitive voltage-gated sodium channels over the somato-dendritic axis of cells in the ELL. Purkinje-like medium ganglion (MG) cells are shown to highly express voltage-gated sodium channels ($Na_v1.1$, 1.2 and 1.6). We also demonstrated the presence of dendritic and somatic action potentials in MG cells. Dendritic spikes can propagate both in a retrograde and anterograde fashion. Backpropagation proves to be active over at least the inner half of the molecular layer. These sodium action potentials are shown to be sculpted by potassium currents. Backpropagating spikes are crucial for the induction of anti-Hebbian plasticity at the parallel fiber-MG cell synapse. The suggested role of γ-aminobutyric acid (GABA) as a retrograde messenger in the formation of this form of plasticity was also investigated. Even though MG cells contain high concentrations of GABA in their dendrites, dendritic release of GABA is not essential for the observed plasticity.

In chapter 4 the role of corticotrophin releasing factor (CRF) in the induction of climbing fiber LTD was investigated. CRF is released by climbing fibers under high-activity conditions. CRF application alone transiently mimics CF-LTD by causing a reduction in the CF-evoked excitatory postsynaptic current (EPSC), complex spike second component, and complex spike afterhyperpolarization. Application of CRF receptor antagonists blocked these effects of CRF. Furthermore, they reduced the expression amplitude and induction probability of CF-LTD measured at the EPSC level. These results suggest that under certain sensorimotor conditions, co-release of CRF could downregulate transmission and facilitate LTD induction at the climbing fiber-Purkinje cell synapse. The effects of CRF might be through protein kinase A (PKA) and/or protein kinase C (PKC) pathways since inhibition of either protein attenuated the effects of CRF.

Plasticity in a sensorimotor system in vivo is discussed in chapter 5. Vestibular, optokinetic and proprioceptive inputs act in concert to maintain a stable retinal image of the visual world. The contribution of the otolith organs in this system, and whether the system can compensate for the loss of otolith input, remains to be elucidated. We

investigated compensatory eye movements in mice lacking otoconia due to a mutation in otopetrin 1. These *tilted* mice show very small displacements of the eyes in the orbit during static roll paradigms, suggesting the absence of functional otolith organs. The gain of the angular VOR is decreased whereas the phase lead is increased. The dependence of the vestibular system on stimulus frequency is also increased. The gain of the OKR is significantly higher in the low-frequency range regardless of the position of the mice in space or the plane of the eye movements. We used a model in which a multisensory integration unit is embedded. This model was able to simulate all the data obtained. The data and model thus supported the existence of a multisensory integration system and revealed a compensatory enhanced OKR in *tilted* mice, indicating an adaptive synergism in the processing of otolith and visually-driven signals.

Populaire samenvatting

Achterin de schedel, net boven de hersenstam, bevinden zich de kleine hersenen (cerebellum). Het cerebellum helpt bij de besturing van het bewegingsapparaat door de verschillen tussen een door de hersenen gewenste actie en de uiteindelijk door het bewegingsapparaat gemaakte beweging te analyseren. Hierop worden de acties van de motorcentra in de hersenschors en het ruggenmerg aangepast door het cerebellum. Er zijn sterke aanwijzingen dat het cerebellum een belangrijke rol speelt in het aanpassen van bewegingen, maar ook in het leren van complexe bewegingen en zelfs associatief leren (conditioneren).

Verschillende ziekten kunnen het cerebellum aantasten. Dit leidt vaak tot abnormale verschijnselen in de bewegingspatronen. Over het algemeen betreft het hier problemen met het voorbereiden, het beginnen en het coördineren van bewegingen.

Het voornaamste celtype in het cerebellum is de Purkinjecel. De Purkinjecel is de enige cel die informatie vanuit de cerebellaire schors naar andere hersengebieden stuurt. Dit gebeurt via de diepe cerebellaire kernen. Purkinjecellen ontvangen de informatie over bewegingen van parallelvezels en klimvezels. De parallelvezels lopen zoals de naam al suggereert parallel aan de Purkinjecellaag. De klimvezels klimmen als het ware in de uitlopers, de dendrieten, van de Purkinjecel. De signalen die de Purkinjecellen van deze beide vezels ontvangen, worden door de Purkinjecellen bewerkt. Vervolgens worden deze signalen naar de diepe kernen van het cerebellum gestuurd. Vanuit de diepe kernen gaan de signalen naar de motorcentra's in de hersenschors.

Het onderzoek beschreven in dit proefschrift is voor een deel gebaseerd op studies waarbij de kleine hersenen van de olifantvis vergeleken werden met de kleine hersenen van de rat. De olifantvis behoort tot de groep van *mormyridea* en leeft in midden Afrika.

Het cerebellum van deze olifantvissen is grotendeels hetzelfde opgebouwd als het cerebellum van zoogdieren. Ook in deze dieren vinden we Purkinjecellen en cellen die daar sterk op lijken. Net als bij zoogdieren ontvangen deze cellen signalen van parallelvezels en klimvezels. Klimvezels komen bij deze vis echter niet in alle cerebellum-gelijkende structuren voor. De gegevens die de Purkinjecellen versturen worden niet, zoals bij zoogdieren, naar diepe kernen gestuurd, maar naar cellen die zich in dezelfde laag als de Purkinjecellen bevinden. Op celniveau zijn de verschillen tussen de Purkinjecellen van zoogdieren en mormyride Purkinjecellen overduidelijk. De dendrieten van mormyride Purkinjecellen zijn recht en lang en vertakken slechts sporadisch en dichtbij het cellichaam van de Purkinjecel. De dendrieten van zoogdier Purkinjecellen vertakken daarentegen vele malen vaker en over de gehele lengte van de dendrietboom.

Een ander groot verschil tussen deze diergroepen is de fysieke afstand tussen de plaatsen waar de parallelvezels en klimvezels contact maken met de dendrietboom. Bij de mormyride Purkinjecel maken de vezels contact op relatief grote afstand van elkaar, terwijl deze vezels in de dendrietboom van zoogdieren over een groot gebied met elkaar overlappen.

In het cerebellum van zoogdieren leidt klimvezelactiviteit tot een “alles of niets” reactie van de Purkinjecel, de zogenaamde “complex spike”. De complex spike is een actiepotentiaal die is opgebouwd uit meerdere componenten. Natriumkanalen spelen waarschijnlijk een belangrijke rol in de vormgeving van deze actiepotentialen. De Purkinjecellen van olifantvissen reageren echter heel anders op klimvezelactiviteit. Zij reageren met een actiepotentiaal met maar één enkele piek, zonder dat daarop de voor de complex spike zo karakteristieke extra spike componenten volgen. Natriumstromen, opgewekt in het cellichaam van sterk op Purkinjecellen lijkende cellen in het electrosensorische laterale zijlijn lobje (ELL) van olifantvissen kunnen teruggestuurd worden naar de toppen van de dendrietboom van deze cellen. Purkinjecellen van zoogdieren zijn hiertoe niet in staat.

In het cerebellum van zoogdieren zijn de verbindingen tussen de cellen erg plastisch; ze veranderen voortdurend. Plasticiteit in de cerebellaire schors is al beschreven tussen parallelvezels en Purkinjecellen, en tussen klimvezels en Purkinjecellen. In het mormyride ELL lobje is ook plasticiteit waargenomen tussen de parallelvezels en de sterk op Purkinjecellen lijkende cellen. Deze vorm van plasticiteit is sterk afhankelijk van de eerder genoemde teruggestuurde natriumstromen.

Het oogbewegingsysteem van zoogdieren kan ons veel leren over het functioneren van het cerebellum en zijn plasticiteit in het intacte dier. Het oogbewegingsysteem vergelijkt en beheerst de vestibulaire (van het evenwichtsorgaan) oculaire reflex, de optokinetische (van het oog) reflex en de cervicooculaire (vanuit nekspieren) reflex. De functie van dit systeem is het reduceren van retinale slip. Retinale slip is het ongewenst verschuiven van het omgevingsbeeld over het netvlies. Het cerebellum en de vestibulaire kern (één van de diepe kernen) spelen een centrale rol in dit systeem.

Hoofdstuk 2 begint met een beschrijving van de klimvezelrespons van ratten en olifantvissen. Deze blijken erg veel van elkaar te verschillen. Natriumkanalen en de manier waarop de dendrietboom vertakt, spelen een grote rol in de vorming van de klimvezelrespons. Om die reden hebben we de aanwezigheid en de verdeling van natriumkanalen in het cerebellum van ratten en vissen onderzocht. De natriumkanalen $Na_v1.1$, $Na_v1.2$ en $Na_v1.6$ bleken allemaal aanwezig en ongeveer gelijk verdeeld te zijn over het cerebellum van deze dieren.

Vervolgens hebben we de natriumstromen die door de beschreven kanalen lopen nader bestudeerd. Verschillen in deze natriumstromen tussen ratten en olifantvissen kunnen mogelijk het verschil in klimvezelrespons tussen deze diersoorten verklaren. In zowel geïsoleerde cellichamen als in intacte Purkinjecellen van ratten en vissen bleken deze natriumstromen vrijwel gelijk te zijn. Zodoende concluderen we dat onze studie een goede eerste beschrijving is van de natriumkanaalverdeling en de natriumstromen in het cerebellum van olifantvissen.

Onze studie bevestigt ook de al vermoede aanwezigheid van $Na_v1.2$ natriumkanalen in het cerebellum van ratten. De gevonden verschillen in klimvezelrespons kunnen echter niet verklaard worden door een verschil in de natriumkanalen of natriumstromen. Deze verschillen worden waarschijnlijk veroorzaakt door de compleet verschillende patronen van dendrietvertakking die we hebben waargenomen bij de Purkinjecellen van deze dieren. De verschillen in de onderzochte responspatronen kunnen ook nog veroorzaakt worden door andere

ionen zoals kalium en calcium. Meer onderzoek in deze richting is nodig om dit te bevestigen of uit te sluiten.

Hoofdstuk 3 beschrijft de lokalisatie van tetrodotoxine (TTX)-gevoelige natriumkanalen over het cellichaam en de dendrietboom van de sterk op Purkinjecellen lijkende cellen in het ELL lobje. Wij tonen aan dat deze zogenaamde medium ganglion (MG) cellen dezelfde natriumkanalen bevatten als de Purkinjecellen in het cerebellum. Ook laten we de aanwezigheid van actiepotentialen in de cellichamen en dendrieten van MG cellen zien. Actiepotentialen in de dendrieten van deze cellen blijken zich zowel retrograad (terug) als anterograad (vooruit) te kunnen bewegen. Het terugstromen van actiepotentialen kan in ieder geval plaatsvinden in de binnenste helft van de moleculaire laag. Deze actiepotentialen kunnen worden vervormd door kaliumstromen. Terugstromende actiepotentialen zijn cruciaal voor het induceren van plasticiteit in de synaps tussen parallelvezels en MG cellen.

Er wordt verondersteld dat γ-aminoboterzuur (GABA) (een belangrijke boodschapperstof) optreedt als retrograde boodschapper in de vorming van deze vorm van plasticiteit. Deze mogelijkheid hebben wij verder onderzocht. Ondanks het feit dat er in de dendrietboom van MG cellen hoge concentraties GABA liggen opgeslagen, blijkt het vrijgeven van GABA uit de dendrieten niet essentieel te zijn voor de beschreven plasticiteit.

Hoofdstuk 4 is een uiteenzetting van de manier waarop we de invloed van de corticotropine releasing factor (CRF) op de inductie van plasticiteit in de synaps tussen klimvezel en Purkinjecel in het cerebellum van de rat hebben bestudeerd. Hoge activiteit van de klimvezel zorgt voor het vrijmaken van CRF uit deze klimvezel. De extracellulaire toediening van CRF laat effecten zien die sterk lijken op de effecten zoals die zijn beschreven na depressie van de klimvezel-Purkinjecel synaps door klimvezelstimulatie. CRF toediening verkleint de klimvezelrespons, verkleint de tweede spike component van de complex spike en verkleint de hyperpolarisatie die na de complex spike volgt. Toediening van CRF receptor-antagonisten, die de receptor voor CRF op de Purkinjecel blokkeren, blokkeren bovengenoemde effecten van CRF op de Purkinjecel. Daarbij reduceren ze ook het effect van, en de kans op, door hoogfrequente stimulatie geïnduceerde klimvezel-depressie. Deze resultaten suggereren dat het vrijkomen van CRF onder bepaalde condities kan zorgen voor een verlaagde synaptische transmissie en een versterking van de depressie van de synaps tussen klimvezel en Purkinjecel. De effecten van CRF op de Purkinjecel kunnen verlopen via PKA en/of PKC routes, aangezien de inhibitie van deze eiwitkinasen het effect van CRF teniet doet.

De plasticiteit van een intact sensorimotorsysteem wordt besproken in hoofdstuk 5. In dit systeem werken vestibulaire (van het evenwichtsorgaan), optokinetische (van het oog) en proprioceptische (vanuit spieren) signalen samen om te zorgen dat er een stabiel beeld van de buitenwereld op het netvlies ontstaat. De exacte bijdrage van de otolith evenwichtsorganen in dit systeem, en de mate waarin dit systeem in staat is te compenseren voor het verlies van otolith informatie, is tot op heden niet duidelijk.

Wij onderzochten de compensatoire oogbewegingen van muizen zonder otolith organen. Deze zogenaamde "*tilted*" muizen moeten het stellen zonder steentjes in hun otolith organen. Dit is veroorzaakt door een mutatie in het otopetrin 1 gen. *Tilted*

muizen blijken maar hele kleine verplaatsingen van hun ogen te hebben gedurende testen waarbij ze werden blootgesteld aan een statische rolbeweging. Dit suggereert, zoals eerder al vermoed uit het anatomische beeld, de afwezigheid van functionele otolith organen. De versterking van de vestibulaire oculaire reflex is ook sterk verminderd in deze dieren, terwijl de fase juist weer sterker voorliep. De afhankelijkheid van het vestibulaire systeem van de stimulatie frequentie nam ook toe. In de lage frequentiegebieden nam de versterking van de optokinetische reflex significant toe, ongeacht de positie van de muis in de ruimte of het vlak van de oogbeweging.

Hoofdstuk 5 wordt afgesloten met een model waarin een multisensorische integratie-eenheid is opgenomen. Dit model is in staat de verkregen data te simuleren. Onze data en het model steunen zodoende het bestaan van een multisensorisch intergratie-eenheid en onthullen een door compensatie versterkte optokinetische respons in *tilted* muizen. Dit is indicatief voor plasticiteit in de verwerking van otolithische en visuele signalen in dit systeem.

List of publications

MM de Ruiter, CI De Zeeuw, C Hansel. Voltage-gated sodium channels in cerebellar Purkinje cells of mormyrid fish (submitted).

J Engelmann, E van den Burg, J Bacelo, MM de Ruiter, C Hansel, K Grant, Y Sugawara. Analysis of backpropagation in interneurons of the Mormyrid ELL (to be submitted).

MT Schmolesky, MM de Ruiter, CI De Zeeuw, C Hansel. The neuropeptide corticotropin releasing factor regulates transmission and plasticity at the climbing fiber-Purkinje cell synapse (submitted).

CE Andreescu, MM de Ruiter, CI De Zeeuw, MTG De Jeu. 2005. Otolith deprivation induces optokinetic compensation. J Neurophysiol 94(5):3487-3496.

JH Kamphoven, MM de Ruiter, LP Winkel, HM van der Hout, J Bijman, CI De Zeeuw, HL Hoeve, BA van Zanten, AT van der Ploeg, AJ Reuser. 2004. Hearing loss in infantile Pompe's disease and determination of underlying pathology in the knockout mouse. Neurobiol Dis 16(1):14-20.

J van der Wees*, MA van Looij*, MM de Ruiter*, H Elias, H van der Burg, S Liem, D Kurek, JD Engel, A Karis, BG van Zanten, CI De Zeeuw, FG Grosveld, JH van Doorninck. 2004. Hearing loss following Gata3 haploinsufficiency is caused by cochlear disorder. Neurobiol Dis 16(1):169-178.

MA van Looij, H van der Burg, RS van der Giessen, MM de Ruiter, J van der Wees, JH van Doorninck, CI De Zeeuw, GA van Zanten. 2005. Gata3 haploinsufficiency causes a rapid deterioration of distortion product otoacoustic emissions (DPOAEs) in mice. Neurobiol Dis 20(3):890-897.

* Contributed equally

Curriculum vitae

(door Ralda van den Berg - de Ruiter)

Dertig jaar geleden, op 18 januari 1976, werd in ‘s-Gravenzande, een kleine kustplaats in het Westland, een jongetje geboren, Markus Martijn de Ruiter. Hij woonde daar zelfs een tijdje in dezelfde straat als Erica Terpstra. Toen hij drie was, besloten zijn ouders te verhuizen naar Vlaardingen. In Vlaardingen ging hij naar basisschool ‘t Ambacht. Martijn had het niet zo op leren. Tafels leren, waar had je het voor nodig? Lezen en schrijven, mensen begrijpen me heus wel! Hij verstopte zijn schriften om onder z’n huiswerk uit te komen. Martijn was geen studiebol. Hij bleef op de basisschool zelfs een keer zitten! Hij speelde dan ook liever buiten met z’n buurjongens of badminton bij Refoba, waar hij diverse keren clubkampioen werd.

Toch moest Martijn verder in z’n schoolcarrière en dus ging hij naar de Sint Jozef Mavo in Vlaardingen. Daar won hij een keer een verkleedwedstrijd in het kader van de boekenweek. Op het laatste moment had zijn moeder van jute Sinterklaaszakken een creatie in elkaar gezet. Met deze ‘zwerver-look’ won hij het boek ‘Kruistocht in Spijkerbroek’ van Thea Beckman. Af en toe lijkt hij nog terug te verlangen naar deze tijd, als hij zijn baard laat staan en het verkeerde t-shirt op de verkeerde broek aantrekt…

Martijn had inmiddels in zijn sportcarrière een overstap gemaakt naar de atletiek. Z’n specialiteit was de 800 meter. Hij was goed en trainde hard en erg veel. Er was dus weinig tijd voor andere dingen zoals meisjes en uitgaan. Af en toe passeerde er een leuk meisje, maar voordat hij doorhad dat hij in de smaak viel, was haar liefde alweer bekoeld. Het uitgaan miste hij niet en is ook nooit zijn hobby geworden.

Ook op de Mavo waren wiskunde en Nederlands zijn grote struikelblokken. Maar na vier jaar zwoegen slaagde hij met zulke goede cijfers dat hij naar de Havo mocht. Martijn ging in 1993 naar scholengemeenschap Spieringshoek in Schiedam.

Toen hij zeventien was, besloten zijn ouders te verhuizen naar een andere straat in Vlaardingen. In diezelfde tijd besloten mijn ouders ook naar die straat in Vlaardingen te verhuizen. Ik werd het buurmeisje van Martijn. Eerst eigenlijk van Annemieke, zijn zusje, die ik af en toe wel eens tegenkwam bij het uitgaan en op feestjes. Martijn kwam pas een jaar later in beeld, op een nieuwjaarsborrel van één van onze buren. Martijn was een beetje ‘alto’. Hij slofte op Dr. Martens (omdat hij z’n veters niet vastmaakte) en luisterde naar Nirvana en Pearl Jam. Ik kocht ook Dr. Martens (paarse, maar maakte wel m’n veters vast). Twee weken na die borrel, op 14 januari 1995, gingen we voor het eerst samen uit en was onze verkering officieel.

Martijn haalde dat jaar zijn Havo-diploma en begon in september op het HLO in Delft. Ondertussen had hij zijn spikes aan de wilgen gehangen en was hij gestart met een voetbal- en wielercarrière. Ook werd hij steeds vaker gespot bij het uitgaan en op feestjes (hij deed het voor mij).

Het laboratoriumonderwijs (inmiddels verhuisd naar Rotterdam) paste helemaal in het straatje van Martijn, alleen die stomme wiskunde zat hem weer eens dwars. Hij

koos voor de biomedische richting en na vijf jaar werd hij ingenieur in de biomedische wetenschappen.

Op zijn stageplek bij de afdeling anatomie van de Erasmus Universiteit kreeg hij van professor De Zeeuw toen een baan aangeboden als AIO. In augustus 2000 begon hij met z'n baan als AIO en deed (toen nog) gehooronderzoek. Na 2 jaar gepriegel met muizenoren is Martijn overgestapt naar de kleine hersenen van ratten en olifantvissen. Wat hij daar allemaal mee gedaan heeft, kan elders in dit proefschrift gevonden worden. En anders legt hij het u nog wel een keer, met veel geduld, uit.

Martijn is in de tussentijd ook weer veranderd van sportcarrière. Hij heeft z'n voetbalschoenen verruild voor hockeyschoenen, maar dat beviel ook niet echt. Z'n laatste passie is mountainbiken. De racefiets is verruild voor een supersonische mountainbike met twee wielsets, een geweldige Fox F80 RL voorvork, een Thomson Elite zadelpen en een duur zadel.

Z'n buurmeisje is sinds 29 augustus 2002 zijn vrouw en hij is op 18 november 2005 de trotse vader geworden van Meine.

Ralda van den Berg- de Ruiter

Markus Martijn de Ruiter

Geboren	18 januari 1976 te 's-Gravenzande
1995	HAVO; Scholengemeenschap Spieringshoek te Schiedam
1995 - 2000	HLO biomedisch; Hogeschool Rotterdam en Omstreken
Nov 1999	Werkbezoek, Department of Otolaryngology, Washington University Med. School, St. Louis, MO, U.S.A
2000 - 2006	AIO aanstelling; afd. neurowetenschappen, Erasmus MC
2006	Post-doc aanstelling; afd. neurowetenschappen, Erasmus MC

Dankwoord

Het is een van mijn eerste “papa-vrijdagen”. Ralda heeft nog steeds zwangerschapsverlof en heeft Meine meegenomen naar een vriendin. Niet zoveel om handen dus. Een mooi moment om eens rustig al die mensen te bedanken die de afgelopen jaren voor mij, op welke wijze dan ook, het schrijven van dit boekje, en het onderzoek dat daaraan ten grondslag ligt, mogelijk hebben gemaakt.

In chronologische volgorde wil ik graag de volgende mensen bedanken:

Chris, mijn promotor, bedankt dat je, toen ik meer dan 6 jaar geleden alweer, als HLO stagiair op jouw afdeling rond kwam kijken gelijk volop enthousiast was over het werk dat ik deed. De mogelijkheid om in het begin van mijn stage al gelijk een maand naar St. Louis te mogen was uniek. Dat ik na mijn stage kon aanblijven als AIO heeft mijn carrière onomstotelijk in een stroomversnelling gebracht.

Barbara Bohne, thank you very much for the time you let me spend in your lab in November 1999. In that month you and Gary taught me tons about the anatomy of the inner ear, its dissection and hearing research in general. I hope you will be pleased to read in my publication list that all this effort from your side resulted in three nice papers after all. Even though my thesis and current research are not involving the inner ear, I still hope to return to that field in the future.

Jan Bijman, direct na mijn verblijf in Amerika heb ik de resterende 7 maanden van mijn stage en het eerste jaar van mijn promotie in jouw lab doorgebracht. In deze periode hebben we samen verwoede pogingen gedaan om whole cell patch-clamp afleidingen te maken van de haarcellen in het binnenoor. Helaas is ons dit nooit echt gelukt, waarna we het meer in de ABR en histologie hoek zijn gaan zoeken. Het artikel over gehoorschade bij de ziekte van Pompe, met Arnold Reuser en Joep Kamphoven, was er zonder jouw bemoeienissen nooit gekomen. Naast je wetenschappelijke input heb ik altijd erg genoten van “de mens” Jan. Iedere dag hadden we wel weer een leuke grap in het vooruitzicht, maar ook de serieuze discussies over de meest uiteenlopende zaken waren altijd waardevol. Vooral je genuanceerde manier van denken, je liefde voor mensen, en je grote kennis op vele terreinen, van wetenschap tot politiek, spreken mij aan. Weet je nog, ons werkbezoek aan Tubingen!

Susan Liem, mevrouw Van Looij, Helineth Elias, samen met jullie heb ik veel meet- en priegelwerk gedaan aan het oor van de muis. Susan heeft veel pionierwerk verricht met de ABR opstelling. Met Marjolein en Helineth heb ik vele uren ABRs gemeten en (pogingen) tot uitprepareren van binnenoren gedaan. Daarnaast natuurlijk ook een hoop plezier gemaakt, o.a. in Florida.

Ook alle andere “gehoormensen” hartelijk dank. Zonder Zjak, Hikke, Bert, en Carla zouden een hoop experimenten, kleuringen, ijkingen enz. niet goed gegaan zijn.

Joep en Arnold, bedankt dat jullie mij hebben betrokken bij het Pompe project. Het resulterende paper is stiekem het artikel waarop ik het meest trots ben.

Christian Hansel, mijn copromotor. Nadat het gehooronderzoek beëindigd was, kon ik onder jouw bezielende leiding verder met mijn promotie en zijn we een andere richting opgegaan. Het projectje waarmee ik jouw lab binnenkwam zou een paar maandjes duren. Gewoon een leuk project met olifantvissen. Uiteindelijk duurde dit project, met wat tussenpozen, zo'n vier jaar. In jouw lab heb ik veel geleerd over het cerebellum, Purkinjecellen, plasticiteit en patch-clamp technieken. Maar ook heb ik leren honkballen, hebben we veel slechte grappen gemaakt en vooral ook veel lol gehad. Een echte baas ben je eigenlijk niet, een fijn mens om voor te werken wel.

John, wij zijn eigenlijk al vrienden vanaf het moment dat ik mijn kamer in kwam lopen na een zomervakantie van drie weken en jou achter je nieuwe bureau zag zitten. Dat mijn bureau, dat naast het jouwe stond, helemaal leeg was gehaald, had je wel zien gebeuren, maar jij wist ook niet dat degene die die computer et cetera gebruikte nog terug zou komen. Ja, dat is ook de afdeling Neurowetenschappen! Ach, drie weken vakantie is ook gewoon te lang ☺. Dan is het logisch dat al je spullen weg zijn! Vanaf die tijd hebben we vaak geluncht in het park, politieke ideeën uitgewisseld, rondgereden tussen Gouda en Rotterdam en Gouda en Schiphol, en hoeveel verhuizingen gedaan??? Natuurlijk hebben we ook veel samengewerkt in het Hansel lab. Jouw beroemde gekreun vanuit "the tent" blijft legendarisch en zal me nog altijd doen glimlachen als ik er weer eens aan denk. Bedankt dat je me hebt aangenomen als postdoc dit jaar. Ik hoop dat het een vruchtbare samenwerking zal zijn.

Jenn, ook jij bedankt voor alle lunches, wandelingen, fijne gesprekken en etentjes die we gehad hebben in de laatste 5 jaar. En natuurlijk voor alle tips over computer programma's, lay-out, formulieren voor reisdeclaraties, het verbeteren van mijn proefschrift tijdens je vakantie enzovoorts. Altijd handig om goed georganiseerde vrienden te hebben. Ik wens jullie heel veel succes en plezier in Canada. Ik hoop dat jullie daar een "thuis" zullen vinden.

Matthew, you were always in for a joke but you are also a very driven and serious scientist. There are two things that directly come to mind from our days in the Hansel lab. 1st) The time that Boeke was just coming to the lab and you were trying to pronounce his name in a Dutch way. This resulted in something that sounded as "foeke". Everybody just acted like we did not hear it until Boeke was gone. I think it was John who then asked you: "Did you just call him fucker?!". 2nd) The hilarious episode that our stay in the gay-inn in New Orleans was. The bed we shared there was really only a 1.5 person bed! Seeing you naked also still causes nightmares.

Coesmans, leuk dat je nog af en toe eens langskomt om het lijden op het lab gade te slaan! Altijd erg gezellig om je uit te horen over je co-schappen. We hebben veel samengewerkt en veel samen gemopperd op experimenten die niet wilden lukken en op de soms slechte kwaliteit van de plakjes. Kortom, goede tijden!

Boeke, jouw lekkere nonchalante houding bevalt mij altijd uitermate goed. Qua veel dingen zitten we redelijk op één lijn en onze vaak dwaze gesprekken tijdens de metingen hebben me veel plezier bezorgd. Dankzij jou heb ik ook veel leuke nieuwe CD's mogen ontdekken. Die slechte techno van je went alleen nooit ben ik bang! Leuk ook dat je de tijd kon vinden, tussen je co-schappen door, om mij bij te staan als paranimf.

Lieve Susan, in de korte tijd die je op de afdeling neurowetenschappen hebt doorgebracht, ben je al snel een hele goede vriendin geworden. Onze appelpauzes waren een oase van rust in, voor ons beiden, niet de makkelijkste periode in onze carrière. Dankzij jou waren de laatste loodjes niet zo heel erg zwaar. Ook het onderricht, in de kinetiek van natriumkanalen, dat ik van je mocht ontvangen was uitermate nuttig. Bedankt ook voor je zeer nuttige, uitgebreide, en nauwgezette kritiek op dit boekje. Zonder jou had het er stuk minder netjes uitgezien. Geniet van de komende tijd wanneer met z'n tweetjes, met z'n drietjes wordt!

Raghu, after some "getting used to each other time" I really enjoyed your company in the lab. The new insights I received through your Indian wisdom, the music you play in the lab, (it's at least better than ABBA) and your attempts to teach me some Kannada have broadened my view. I hope all turns out well for you, so you can stay in the department for the years to come.

Amor heeee. "Really man, why am I so stupid? I don't know!" These are the often heard things we say to each other. Anyway, I can write whatever I want about you since you won't be able to understand it anyway! Mon ami, je t'aime!

Dan blijven er nog een heleboel mensen over die op de een of andere manier ook een steentje hebben bijgedragen aan dit proefschrift en/of de gezelligheid op het lab.

Hans, Elize, Erika, Mandy hartelijk dank voor jullie technische assistentie bij het solderen, bouwen, monteren, perfuseren, inbedden, coupes snijden, kleuringen doen, etc.

Sara, Bogdan, Freek, it was always a pleasure to have you guys come into our lab to pull pipettes and make solutions etc.

Corina, every day we all waited for you to enter the lab and brighten our day with your beautiful smile. Also many thanks to you and Marcel for still putting my name on the paper even though my data was ditched long before the final version.

Jacob, thank you for inviting me to share my ELL staining data with you and for the weekend I spent with you in the lab in Gif. It was very enjoyable to present my data there and I learned a lot from that trip. Also many thanks for your efforts to come up with a revised version of the manuscript just before the deadline of this thesis.

Eddie, bedankt voor je computer en foto ondersteuning. Het aanhoren van je laatste politieke beschouwingen was ook altijd de moeite waard.

Edith en Loes, hartelijk dank voor alle hulp bij de administratieve rompslomp. Waar moet deze brief ook alweer in? Welke koerier is het beste voor dit pakje? Hoe werkt de fax? Zijn er nog van dit soort enveloppen? Dat soort dingen.

Annette en crew, bedankt voor al jullie bestelwerk.

Ongetwijfeld ben ik mensen vergeten die ook hun steentje hebben bijgedragen. Wees niet teleurgesteld, ik waardeer jullie ten zeerste!

Naast de mensen die op de werkvloer, als collega's, betrokken zijn bij je onderzoek is het thuisfront minstens net zo belangrijk.

Lieve Ralda, tja waar moet ik beginnen. Dit dankwoord moet natuurlijk niet honderden pagina's in beslag gaan nemen maar die heb ik wel nodig om met taal te beschrijven wat je voor me betekent. Bedankt dat je in me gelooft. Dat je er altijd voor me bent. Je bent een zeer liefdevol en genuanceerd mens. Ik hou ontzettend veel van je. Natuurlijk ook bedankt voor je hulp bij de lay-out van dit boekje en het nakijken en verbeteren van verschillende hoofdstukken. En natuurlijk voor de grappige CV die je voor me geschreven hebt. Ik hoop dat we heel oud worden samen en dat we dan nog net zo van elkaar en ons(ze) kind(eren) genieten als we nu doen.

Meine, je bent nog zo'n klein hummeltje. Net twee maanden oud maar zo belangrijk voor mama en mij. Ik geniet elke minuut van de dag van je. Jouw bijdrage aan dit proefschrift is eigenlijk een averechtse. Je hebt het boekje nog weer een heel stuk relatiever gemaakt dan het al was ☺.

Mijn ouders, Guus en Eveline, jullie hebben altijd achter me gestaan en geprobeerd mij in mezelf en mijn capaciteiten te laten geloven. Tot op de dag van vandaag gaat dat nog steeds met vallen en opstaan maar ik ben toch een aardig eindje gekomen na mijn MAVO diploma. Wij zijn erg blij dat we altijd bij jullie aan kunnen kloppen voor advies en gezelligheid. Je denkt er nooit over na, omdat het voor ons zo gewoon is, maar je hoort helaas wel eens anders.

Mijn zusje, Annemieke, en Mark. Gezellig eten op zondag op de kade. Horen wat jullie allemaal uitspoken op je werk. Werelden met elkaar vergelijken eigenlijk. Altijd erg gezellig.

John en Annette, het is een cliché maar waar, ik had geen leukere schoonouders kunnen wensen. We kunnen altijd bij jullie terecht voor leuke en minder leuke dingen. Gelukkig lachen we het vaakst! Eten op zondagavond, een "opa Berg actie" opvoeren, lekker op vakantie met z'n allen. Bedankt.

Marnix en Eva, meer dan alleen maar het broertje van mijn vrouw. Je zou van vriendschap kunnen spreken. Het nadeel is, als ik dat doe, moet ik weer helpen verhuizen binnenkort! Ook met jullie is het altijd erg gezellig als we met z'n allen op de kade zijn. Hopelijk vinden jullie snel een leuk huis.

Robert en Annemiek, ook in dit dankwoord zijn jullie weer de enige vrienden die ik wil noemen. Begint wel een beetje eng te worden hè! Waar moet ik jullie allemaal voor bedanken? Allereerst, en bovenal, bedankt dat jullie van die goede vrienden zijn. Ten tweede, jullie hebben me aan de drank geholpen, ook geen misselijk feit! Natuurlijk ook hartelijk dank dat je mijn paranimf wilt zijn Robert. Ik hoop dat we in de toekomst nog veel plezier zullen hebben met z'n zevenen.

Martijn de Ruiter